Understanding and Modelling Extreme Multi-hazard Events

Aloïs Tilloy

Thesis submitted for the degree of Doctor of Philosophy

Department of Geography, King's College London

24 March 2021

Funded by an EDF R&D Studentship

Abstract

The study of natural hazard interrelations exposes the complexity of extreme climatological, geophysical and hydrological processes and poses new science challenges. This PhD thesis is located at the confluence of multivariate statistics, climatology and natural hazard modelling and aims to provide new approaches to model and quantify natural hazard interrelations. **Chapter 2** consists of a critical literature review of 146 sources. From these, the historical context for quantitative single-hazard and multi-hazard assessment is discussed, and 19 different modelling methods to model multi-hazard interrelations are identified and organized into three broad approaches (empirical, stochastic, mechanistic). **Chapter 3** examines the multi-hazard landscape of the European Atlantic Region (EAR) but has global relevance in its application. A total of 16 relevant natural hazards for the EAR region are identified on three main criteria: (i) frequency of occurrence, (ii) spatial relevance, (iii) potential to impact energy infrastructures. Based on the knowledge of hazard interrelations and physical drivers, natural hazards are grouped into five multi-hazard networks. Through a review of 32 single hazard catalogues, 50 historic major multi-hazard events in the EAR are pinpointed for each network. Within each network, the prevalence of each hazard interrelation is discussed. After identifying the main modelling approaches and dominant hazard interrelations in the EAR, the abilities of a group of modelling method for multi-hazard modelling is assessed. **Chapter 4** evaluates the efficacy of bivariate extreme modelling approaches for multi-hazard scenarios. Six bivariate extreme models are evaluated and compared by using each model's fitting capabilities to 60 synthetic datasets. The properties of the synthetic datasets are matching bivariate time series of environmental variables. The systematic framework contrasts model strengths (model flexibility) and weaknesses (poorer fits to the data). The benefits of this framework are highlighted with two applications to natural hazard interrelation modelling. Using the findings of **Chapter 3,** two pairs of natural hazard are selected: extreme hot temperature–wildfire; extreme wind–extreme rainfall. **Chapter 5** analyses the spatiotemporal features of hazard interrelations using climate reanalysis data for two hazards (extreme wind and extreme rainfall) for 1979–2019 within a region including Great Britain and the British channel. A clustering algorithm is used to create hazard clusters with extreme values (above the 99% quantile) of hourly precipitation and wind gust. A total of 4555 compound wind-rainfall clusters are detected for 1979–2019 by assessing the spatiotemporal overlap of the two hazards. The characteristics (e.g., size, duration, season, intensity) of created clusters are confronted with observations and analysed. One of the bivariate modelling methods assessed in **Chapter 4** is used to estimate return periods of compound hazard events. The relationship between the return period of compound hazard events and the spatial and temporal attributes of compound hazards events is then analysed. Throughout the thesis, the following main aspects of a quantitative multi-hazard approach are addressed: interrelation characterisation, multivariate modelling, physical drivers, spatiotemporal overlap, data. Robust solutions to identify, discriminate and model hazard interrelations at different spatial and temporal scales are offered.

Acknowledgements

First, I would like to thank Prof Lindsay Beevers and Dr Martin Widmann, who accepted to examine my thesis and for their insightful comments and conversation during the Viva on January 21st 2021.

When I arrived in London in January 2017, I was far from imagining what I was about to encounter. I first met Prof Bruce Malamud, my primary supervisor, and I want to thank him, for his patience and unwavering support. Through the years, I learned so much and realized how privilege I was to work with such an outstanding academic and a caring supervisor. I was also lucky to have two supervisors at EDF R&D UK centre: Dr Hugo Winter and Dr Amelie Joly-Laugel. They show great interest in my work and have always been available when I needed them. Their input was vital in the process of writing this thesis. Working with these three persons, between the two institutions of KCL and EDF, made this PhD challenging but also truly interdisciplinary and intellectually exciting. Thanks to the three of you, it was an immense pleasure to have you on board.

I also encountered a vibrant and friendly working environment in the Department of Geography, King's College London. I want to thank the persons there that helped me to develop my projects, solve my problems and offered me opportunities during my time at King's: Dr Faith Taylor, Dr Andreas Baas, Dr Mark Mulligan, Dr Margaret Kadiri, Dr Ana Turbelin, Dr Mark de Jong and Uldis Zandovskis. I am also extremely grateful to have encountered amazing friends from all around the globe in the PhD room, "La Familia": Alex, Pratik, Alejandro, Alejandra, Seungwon, Brandon, Shreyasi, Claudia, Roxana, Nirali, Viviane, Dimi, Sam, Peter. These people changed my life in so many ways, expanded my horizons through deep and passionate conversations, took care of me when I had difficult times. Thank you guys for so many unforgettable moments.

EDF fully funded this thesis, I therefore thank the EDF company as a whole, for offering me the opportunity to join King's College London and for supporting me continuously during this PhD. I want to especially thank Tiphaine Le Morvan, coordinator of the MADONNE3 project under which my PhD is funded, for her support and her enthusiasm toward my work. I am also grateful to the persons that worked with me and helped me in Croydon and in Paris. Alexis for all his insightful advice, Angus, Tara, Megan, Ionel, Esteve, Sylvie, Roberto, Marc and others.

I am thankful to those who supported me in the early stages of this adventure. Pietro Bernardara, who was the manager of the Natural hazard team at EDF and put me on track. My professors at Polytech Nice Sophia: Pierre Brigode and Olivier Delestre, who trained me and convinced me I was capable of pursuing a PhD in London. Thank you also to Arnaud Belleville, who recommended me for the position.

During three years, I had the opportunity to travel around Europe for workshops and conferences. I am indebted to the King's Geography Department, who funded a significant part of these trips and allowed me to expand my network in the academic world. I want to thank the persons I met at these conferences, for the insightful conversations and for being inclusive with me: Stefano, Anaïs, Silvia, Anna.

I thank my family, who always supported me whatever my decisions were. I hope they will be proud of this achievement. A big thank to my French friends who participated in this experience: Guillaume, Malo, Gwénolé, Théo. Thank you also to Kevin Richards for your comments on my work.

Finally, I am grateful to the person who accompanied me through most of this journey, who had to put up with my terrible temper, my humour, my arrogance, my frenchitude. Nathalie, my partner, my love, who also went through the process of writing a PhD. She shared her experience with me, but more importantly, taught me about myself. I will always admire her sensitivity and her prodigious inner strength.

Table of Contents

List of Figures

Chapter 1:

Chapter 2:

Chapter 3:

Chapter 4:

Chapter 6:

List of Tables

Glossary and nomenclature

Glossary

Term	Definition	Chapter
Clustering	The process of grouping data by their similarities.	5
Compound event	"The combination of multiple drivers and/or hazards that contributes to societal and environmental risk" (Zscheischler *et al.*, 2018, p.471).	1, 2, 3, 4, 5
Conceptual model	A model that uses simplified conceptualization of a system to represent different components of a process.	2
Copula	A joint distribution function which defines the dependence between two variables independently from the marginal distributions of these variables (Nelsen, 2006).	2, 4
Disaster	"A serious disruption of the functioning of a community or a society at any scale due to hazardous events interacting with conditions of exposure, vulnerability and capacity, leading to one or more of the following: human, material, economic and environmental losses and impacts" (UNDRR, 2017, p.13).	1, 2, 3
Exposure	"The situation of people, infrastructure, housing, production capacities and other tangible human assets located in hazard-prone areas" (UNDRR, 2017, p.18).	1
Extremal dependence	Dependence between two variables in the asymptotic (extreme) domain.	2, 4
Extreme event	"The occurrence of a value of a hazard variable above (or below) a threshold value near the upper (or lower) ends of the range of observed values of the variable" (Seneviratne *et al.*, 2012, p.557)	1, 2, 3, 4, 5
Extreme value analysis	A statistical approach for modelling rare (or extreme) events using the extreme value theory	2, 4
Hazard (natural)	"Natural process or phenomenon that may cause loss of life, injury or other health impacts, property damage, loss of livelihoods and services, social and economic disruption, or environmental damage" (UNISDR, 2009, p.17)	
Hazard interrelation	Any type of relationship linking one hazard to another from a statistical or physical perspective	1, 2, 3, 4, 5
Impact	"The effects on natural and human systems of physical events, of disasters, and of climate change" (IPCC, 2012, p.561)	1

Term	Definition	Chapter
Intensity (hazard)	A measure of the extremeness of a variable	1, 2, 3, 4, 5
Level curve	Isoline corresponding to a probability of exceedance (or quantile) for a bivariate dataset	2, 4
Magnitude (hazard)	Variable characterizing the maximum severity of an event	1, 2, 3, 5
Marginal distribution	Univariate distribution of variables in a multivariate context	4
Multi-hazard	"The selection of multiple major hazards that the country faces, and the specific contexts where hazardous events may occur simultaneously, cascadingly, or cumulatively over time, and taking into account the potential interrelated effects" (UNDRR, 2017, p.19).	1, 2, 3, 4, 5, 6
Physical model	Model that aims to simulate the behaviour of different systems such as the atmosphere, the ocean, the climate, hydrological and geophysical systems	2
Regression (statistical)	A statistical method to measure changes in a dependent variable in response to changes in one or several independent variables	2
Risk	"The potential for adverse consequences for human or ecological systems, recognising the diversity of values and objectives associated with such systems" (IPCC, 2019, p. 696)	1, 2, 6
Statistical dependence	A condition in which two random variables are not independent	1, 2, 3, 4
Vulnerability	"The conditions determined by physical, social, economic and environmental factors or processes which increase the susceptibility of an individual, a community, assets or systems to the impacts of hazards" (UNDRR, 2017, p.24)	1

Table of abbreviations

Abbreviation	Meaning	Page Introduced
AD	Asymptotic Dependence	127
AI	Asymptotic Independence	127
AIC	Akaike Information Criterion	125
ASAMPSA_E	Advanced Safety Assessment Methodologies: Extended PSA	23
BGS	British Geological Survey	69
BIC	Bayesian Information Criterion	125
BN	Bayesian Network	187
CC	Compound Cold	97
CCR	Caisse Central de Réassurance	33
CD	Compound Dry	97
CH	Compound Hazard	39
CHCI	Compound Hazard Cluster Identification	146
Cond-Ex	Conditional Extremes model	108
CRED	Centre for Research on the Epidemiology of Disasters	44
CS	Convective Storm	97
Cv	Coefficient of variation	122
DBSCAN	Density-Based Spatial Clustering of Applications with Noise	146
DEFRA	Department for Environment Food and Rural Affairs	82
EAR	European Atlantic Region	69
ECMWF	European Centre for Medium range Weather Forecast	99
EDF	Electricité De France	22
EEA	European Environment Agency	70
EFFIS	European Forest Fire Information System	82
EM-DAT	Emergency Events Database	44
E-OBS	Daily gridded observational dataset for precipitation, temperature and sea level pressure in Europe	108
ERA5	Fifth generation of ECMWF atmospheric reanalyses of the global climate	30
ESPON	European Spatial Planning Observation Network	75

Abbreviation	Meaning	Page Introduced
ETC	Extratropical Cyclone	73
ETI	Energy Technologies Institute	76
EVT	Extreme Value Theory	110
FGM	Farlie-Gumbel-Morgenstern	108
GM	Ground Motion	97
GPD	Generalized Pareto Distribution	114
I.i.d	independent and identically distributed	111
IEA	International Energy Agency	22
IPCC	Intergovernmental Panel on Climate Change	21
IRDR	Integrated Research on Disaster Risk	78
JT-KDE	Joint Tail Kernel Density Estimator model	108
KDE	Kernel Density Estimator	117
LMF	Likelihood Multiplication Factor	167
LWT	Lamb Weather Type	191
MCS	Mesoscale Convective System	85
MH	Multi-Hazard	39
MHRA	Multi-Hazard Risk Assessment	23
NARSIS	New Approach to Reactor Safety ImprovementS	23
NASA	National Aeronautics and Space Administration	100
NPBN	Non Parametric Bayesian Network	188
NUTS	Nomenclature of Territorial Units for Statistics	75
PCC	Pair Copula Construction	66
PSA	Probabilistic Safety Analysis	40
SREX	Special report on managing the risks of extreme events and disasters to advance climate change adaptation	21
SSI	Storm Severity Index	89
UNDRR	United Nations Disaster Risk Reduction	20
wd	Weighted Euclidean distance	128
WMO	World Meteorological Organization	108

Chapter 1: Introduction

Planet Earth includes many complex, interconnected and interacting processes. The outcomes of these processes can be destructive for humans and the environment and lead to disasters (AghaKouchak *et al.*, 2018). Some of these destructive outcomes are called natural hazards, such as floods, earthquakes, landslides, and wildfires (Alexander, 1993; Eden, 2008). Natural hazards are far from independent, as has been shown in previous studies (e.g., Hewitt and Burton, 1971; Gill and Malamud, 2014). This thesis examines interrelations between natural hazards and develops methodologies to quantify the dependence between natural hazards and extreme events. This introduction is organized as follows: First, the terms extreme events, natural hazards and associated concepts will be defined and discussed in **Section 1.1**. The different approaches developed to analyse hazard interrelations are introduced in **Section 1.2**. **Section 1.3** outlines the motivations to study natural hazards in a multi-hazard context from industry and academic perspectives. Aims and objectives are presented and discussed in **Section 1.4**. Finally, an outline of the thesis is provided in **Section 1.5.**

1.1 Extreme events, natural hazards and risk

In the thesis forward matter (pp. 15–16) is given a glossary of 22 terms used commonly throughout this thesis. In this section, I discuss several of these terms surrounding the concepts of extreme events, natural hazards and risk.

In this thesis, the term *natural hazard* (hereafter referred to as a 'hazard') will follow the definition of UNISDR (2009), as a natural process or phenomenon that may have negative impacts on society. An *impact* can be defined as the effects (e.g., consequences, losses) on natural and human systems of extreme events or natural hazards (IPCC, 2012). Although this thesis is not focusing on impact, potential negative impacts and damages of extreme events or natural hazards to energy infrastructure are its drivers. Potential damaging impacts are often related to the magnitude of the hazard or extreme event (Merz *et al.*, 2020). In the hydro-climatological (Della-Marta *et al.*, 2009; Mazas and Hamm, 2017) and solid-earth (Geist and Parsons, 2006; McGuire, 2008) sciences, the magnitude of hazards are often quantified in terms of probability or return frequency and therefore associated with extreme events. An *extreme event* is defined as the occurrence of a value of an environmental variable above (or below) a threshold value near the upper (or lower) ends ('tails') of the range of observed values of the variable (Seneviratne *et al.*, 2012).

Extreme events and natural hazards often but not always negatively impact society (Lavell *et al.*, 2012). *Disasters* (i.e., severe disruption of the functioning of a community or a society) (UNDRR, 2017) are the result of the interaction of the hazard with two other components of risk (exposure and vulnerability) (UNDRR, 2017). A risk can be defined as "the potential for adverse consequences for human or ecological systems" (IPCC, 2019, p.696). **Figure 1.1** displays these three key concepts that make up risk: hazard, vulnerability and exposure (See **Glossary**). The need to enlarge this risk framework (**Figure 1.1**) has been stressed by the United Nation Sendai Framework (UNDRR, 2015) and recent literature (Gallina *et al.*, 2016; Terzi *et al.*, 2019). In particular, expanding the traditional risk components into multi-hazard, exposure, and multi-vulnerability is necessary to represent complex multi-risk interactions (Terzi *et al.*, 2019). Therefore, the contribution of this work to disaster risk reduction is confined to the hazard component and in particular, to interrelations between hazards. The interest around interrelated hazard and extremes has been increasing over the last decade (e.g. Kappes *et al.*, 2010; Marzocchi *et al.*, 2012) and is now aggregated under two main concepts: multi-hazard (Gill and Malamud, 2014) and compound events (Leonard *et al.*, 2014).

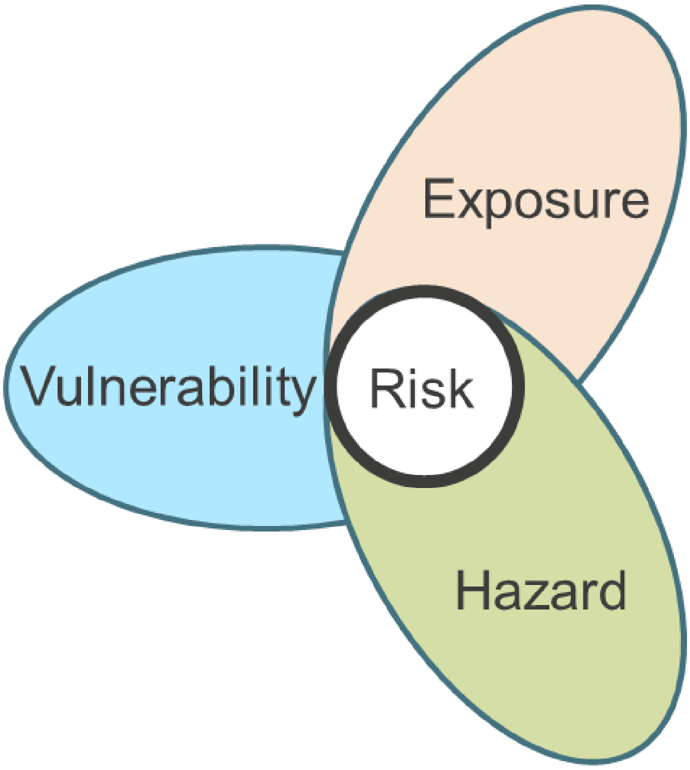

Figure 1.1: Key concepts involved in disaster risk management (modified from Lavell *et al.*, 2012)

1.2 Multi-hazard and compound events

When there is more than one hazard at a time, the term *multi-hazard* is often used (Kappes *et al.*, 2010). A multi-hazard approach accounts for different probabilities and intensities of multiple hazards (Eshrati *et al.*, 2015). Different intergovernmental organisations have emphasized the need for multi-hazard approaches. The Sendai Framework defined a multi-hazard approach as (UNDRR, 2017, p.19) "the selection of multiple major hazards that the country faces, and the specific contexts where hazardous events may occur simultaneously, cascadingly, or cumulatively over time, and taking into account the potential interrelated effects". When two hazards occur in a cascade, the primary and the secondary hazard can cause different impacts or consequences to human or natural systems. The hazard interrelations can also lead to a combined impact that is different from the sum of each hazard's impacts separately. We note that in this thesis, given a primary hazard triggering a secondary natural hazard (e.g., an earthquake triggering landslides), the secondary hazard is not considered an impact of the primary hazard.

In the Intergovernmental Panel on Climate Change (IPCC) special report on managing the risks of extreme events and disasters to advance climate change adaptation (SREX) (Seneviratne *et al.*, 2012), the combination of multiple physical processes was termed as a *compound event*. The definition of these compound events is relatively similar to the one of multi-hazard. SREX (Seneviratne *et al.*, 2012, p.118) defined compound events as: "(i) two or more extreme events occurring simultaneously or successively, (ii) combinations of extreme events with underlying conditions that amplify the impact of the events, or (iii) combinations of events that are not themselves extremes but lead to an extreme event or impact when combined. The contributing events can be of similar (clustered multiple events) or different type(s)".

The terms *multi-hazard* and *compound event* bring together much of the literature on hazard interrelations. We note that although this work is built on these concepts, definitions provided in this thesis, in particular in **Chapter 2** can differ from the ones proposed by other scholars. For example, this thesis confines *compound hazard* to the interrelation between statistically dependent hazards as the result of a common primary event or large-scale processes. The definition of *compound events* by SREX encompass more interrelation types (see **Chapter 2**). In a recent article by Zscheischler *et al.* (2020), a typology of compound weather and climate events that can be related to the classification done in **Chapter 2** is proposed.

Although Hewitt and Burton (1971) advocated almost 50 years ago for an "all-hazard-at-a-place" framework (Gill, 2016), the field of multi-hazard remains relatively new and fragmented. Multi-hazard research is by nature multidisciplinary; it includes, among others, statisticians, physical and social geographers, earth scientists, civil engineers. The consequence is a range of research that reports this hybridity by adopting different methods, approaches, vocabulary, and different spatial scales (e.g., a country, a region, a building) **(See Chapter 2).** The variety of approaches can be explained by the variety of possible impacts caused by natural hazards, which can differ widely depending on the scale and sector one is interested in (e.g., agricultural crops vs transport network). This thesis testifies to this plurality and intends to capture the multiple facets of multi-hazard research at the interface between statistics, climate science, geoscience and disaster risk reduction.

1.3 Motivation

This section outlines the motivation to study natural hazards in a multi-hazard context from industry and academic perspectives. Challenges associated with multi-hazards are discussed, and the approach proposed in this thesis is presented.

Recent disasters and the constantly increasing threat of climate disruption draw the attention of various industrial sectors toward multi-hazard challenges (Ciurean *et al.*, 2018). Among these, the energy sector, particularly the nuclear industry, is firmly aiming to lead the way. This work has been done in collaboration with research engineers from EDF (Electricité de France). EDF is the biggest electricity supplier in Europe and the 5th globally, with an installed capacity of 130 GW in 2017, of which 56% is nuclear (IEA, 2018). Most EDF assets are located in France and the United Kingdom. EDF activities and assets (dams, wind turbines, electric grid) have always required the most advanced methods in natural hazard understanding and risk assessment to ensure the safety of the infrastructures and the quality of its service. Although the methodologies developed in this doctoral work aim to be widely applicable in terms of geographical location, these methodologies are applied within a region that is hosting a fair amount of EDF infrastructures (**Chapter 3**).

On March 11 2011, the Great North East Japan earthquake of magnitude 9 triggered a devastating tsunami (waves exceeding 10 m) and landslides (Miyagi *et al.*, 2011; Poljansek *et al.*, 2017). The tsunami wave was higher than planned in the protection of the Fukushima nuclear power plant (Mignan *et al.*, 2016). This event led to heavy casualties, enormous property losses and a major nuclear accident (Norio *et al.*, 2011). After the Fukushima nuclear disaster, the nuclear industry reacted by adjusting its safety requirements. Several projects were launched (ASAMPSA_E, Narsis) aiming to "identify some lessons learned from the Fukushima Dai-ichi accident" (Kumar *et al.*, 2016, p.2) and "better understand and estimate the likelihood of the most causes prone to initiate nuclear accidents and to identify the most critical elements of the systems" (Narsis, 2020). The need to adopt a multi-hazard approach was identified as one of the main lessons to be learnt from this catastrophe. The characterisation of hazard interrelations was the first step toward a multi-hazard approach (Decker and Brinkman, 2015; Narsis, 2020). This thesis is to be viewed in this context. It aims to develop a quantitative multi-hazard approach and bridge some existing gaps in academic literature.

In the last decade, multi-hazards risk assessment (MHRA) studies highlighted the need for a "common language" between hazards of different nature and different origins (Kappes *et al.*, 2010; Schmidt *et al.*, 2011; Marzocchi *et al.*, 2012; Orencio and Fujii, 2013). One primary way to deal with multiple hazards is to study each hazard for a given area separately. Spatial and temporal dynamics play an essential role in hazard interrelations, leading to compound hazard or hazard cascades (Sutanto *et al.*, 2020; Zscheischler *et al.*, 2020). The impact of each hazard could be compared collectively (with losses as impact variable; see **Figure 1.2**) depending on their intensity/magnitude through risk curves or hazard maps (Schmidt-Thomé and Kallio, 2006; Schmidt *et al.*, 2011; Kappes *et al.*, 2012a; Orencio and Fujii, 2013). A limitation of the approach illustrated in **Figure 1.2** is that interrelations between hazards are not considered. This has been described as a "multilayer single hazard" approach by Gill and Malamud (2014). Indeed, the combined impact of several natural hazards may be different than the sum of their parts and leads to increased impacts (Tarvainen *et al.*, 2006; Gill and Malamud, 2014; de Ruiter *et al.*, 2020). As an example, during storm Xynthia in 2010, the combination of extreme wind gusts, high tides and a skew surge modified the vulnerability of flood protection infrastructures (dikes) and led to their failure (Liberato *et al.*, 2013).

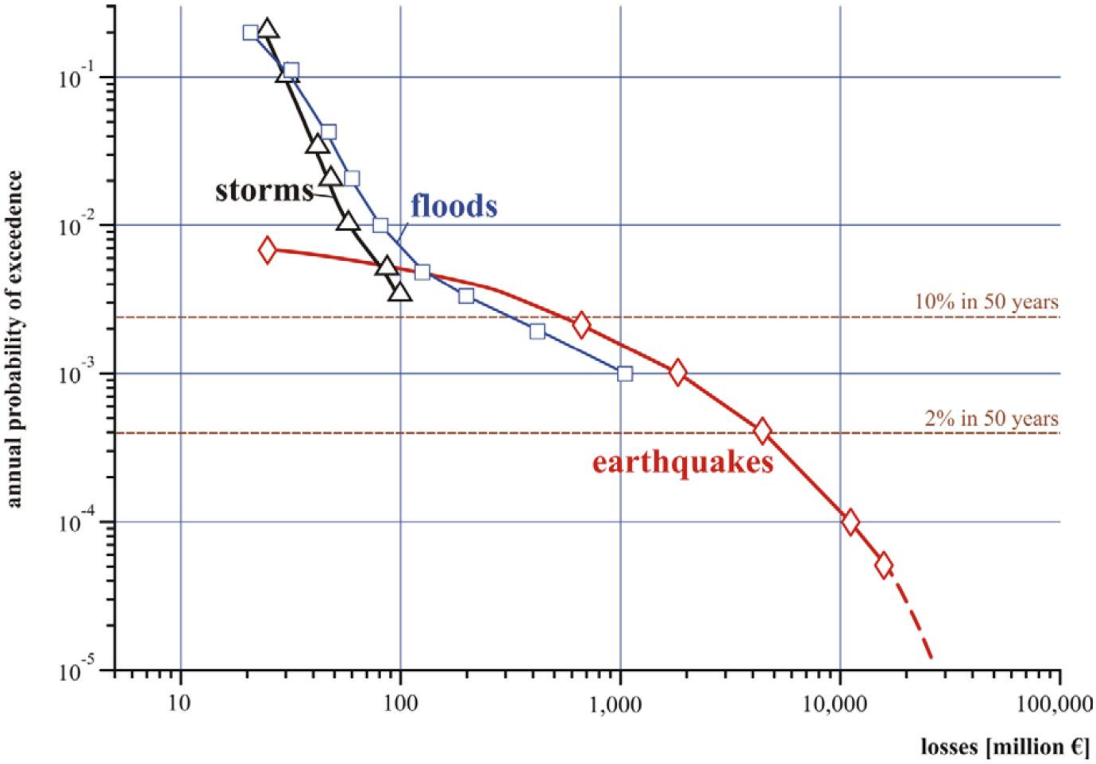

Figure 1.2: Example of risk curves (probability of exceedance as a function of loss) of windstorms, floods and earthquakes for the city of Cologne, Germany. Losses include buildings and contents in the sector's private housing, commerce and industry. Figure from Grunthal *et al.* (2006).

Several semi-quantitative approaches have been developed to display and examine hazard interrelation. Matrices have been developed to display and qualify natural hazards interrelations (e.g., Kappes *et al.*, 2010; Mignan *et al.*, 2014; Gill and Malamud, 2014) with an example given in **Figure 1.3**. These matrices provide information about interrelations between pairs of hazards (e.g., interrelation type, the plausibility of the interrelation). When dealing with more than two hazards, qualitative network diagrams, with nodes (e.g. hazards/processes) and connectors (relationships types) to generate a diagram of possible multi-hazard relationships have been used in different contexts (Ciurean *et al.*, 2018). Such approaches have been used to visualize interrelations between natural hazards and drivers in mountainous (van Westen *et al.*, 2014) or coastal (Leonard *et al.*, 2014) environments. A variety of quantitative methods and models exist for the analysis of hazard interrelations (Hao and Singh, 2016; Sadegh *et al.*, 2018). Nonetheless, the selection of suitable models for a given hazard interrelation remains challenging. Model outputs also need to be translated into relevant metrics for practitioners.

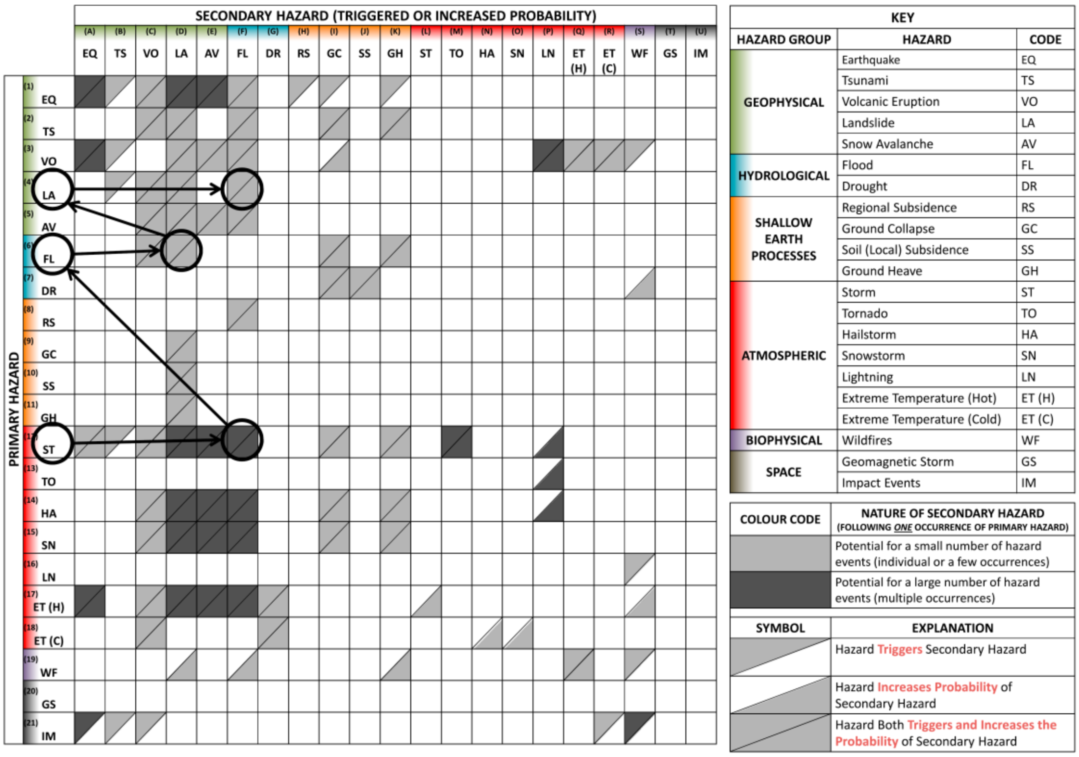

Footnotes
[1A,D,E; 3A,P; 12D-F,M,P; 13P; 14D-F,P; 15D-F; 17A,D-F; 21A] The secondary hazards in these cases are all accepted to most likely occur as large numbers of events, and are thus analysed in this way.
[1C] There is disagreement in the literature about the nature of this relationship .
[2,6,12,14,15C] Water input triggers or increases the probability of a phreatic/phreatomagmatic eruption.
[3I] Volcanism increases the acidity of rain, promoting dissolution of carbonate material.
[12A] Low pressure systems have been shown to trigger or increase the probability of slow earthquakes on faults that are already close to failure (Liu *et al.,* 2009).
[17A,C-F] Secondary hazards triggered or have an increased probability over a range of time-scales, through snow and glacial melting.
[18C] Long term reductions in temperature can increase glaciation and thus decrease sea-levels. This reduction in sea-levels can reduce confining pressures, promoting volcanic eruptions.

Figure 1.3: An example of a matrix of interrelated hazards A 21 × 21 matrix with primary natural hazards on the vertical axis and secondary hazards on the horizontal axis. These hazards are coded, as explained in the key. This matrix can be used to present an example of a scenario. In this example, a storm event (ST) triggers flooding (FL), which then triggers landslides (LA). These landslides (LA) may then trigger or increase the probability of further flooding (FL) through the blocking of a river or the increase of sediment within the fluvial system. Figure from Gill and Malamud (2014)

The identification of all spatially relevant hazards to a place along with the review of natural hazard interactions and their relation to different environments are essential steps toward adopting a multi-hazard approach. This thesis advances the development of a full multi-hazard assessment by establishing a quantitative multi-hazard approach that accounts for and quantifies relationships between hazards. The quantitative multi-hazard approach developed through this thesis is articulated around five interlinked axes: (i) *classify hazard interrelations* (ii) *assess modelling methods for hazard interrelations*, (iii) *catalogue datasets suitable multi-hazard assessment.*, (iv) *consider spatiotemporal scales of hazard interrelations* and (v) *identify physical processes behind multi-hazard.* These five areas of work are displayed in **Figure 1.4** and are key concepts while defining the aim and objectives of this thesis.

Figure 1.4: Graphical representation of the five interlinked work domains around a quantitative multi-hazard approach as defined in this thesis.

1.4 Aim and objectives

Research aim: This thesis aims to develop a quantitative multi-hazard approach by (i) increasing the understanding of hazard interrelations, (ii) evaluating and developing methods to quantify natural hazard interrelations in time and space.

The main research objectives (O) and research questions (Q) are the following (colours are defined further below):

O1: To systematically identify and classify approaches to quantify specific hazard interrelations.

Q1.1: What methods have been used in the literature for a quantitative multi-hazard assessment?

Q1.2: How does one create a general classification for natural hazard interrelation models?

Q1.3: How does one quantitively model the relationship within different natural hazards pairs?

Q1.4: What quantitative model(s) is(are) the most suitable for a given natural hazard interrelation?

O2: To design multi-hazard scenarios in a given region with as a case study Western Europe

Q2.1: Which natural hazards and hazards interrelations are relevant to Western Europe?

Q2.2: Which hazards are more likely to occur within the same multi-hazard event in Western Europe?

Q2.3: How does one prioritize which natural hazard interrelations should be studied?

O3: To apply quantitative models to diverse hazard interrelations

Q3.1: *How does one systematically select the most suitable quantitative model for a given hazard interrelation?*

Q3.2: How does one translate hazard interrelation types into probability types?

Q3.3: *What are the different types of numerical data available to study hazard interrelations in Western Europe?*

O4: To analyse spatiotemporal features of hazard interrelations with gridded data

Q4.1: *How does one identify occurrences of natural hazards with climate reanalysis data?*

Q4.2: *How does one define hazard interrelations in space and time?*

Q4.3: *What is the influence of the intensity of natural hazards on the spatiotemporal features of compound hazards?*

Each research question is associated with one of the five aspects of a quantitative multi-hazard approach displayed in **Figure 1.4**. The following colours are used.

- ***Orange***: hazard interrelations classification
- ***Grey***: quantitative hazard interrelations modelling
- ***Brown***: numerical data for multi-hazard
- ***Blue***: spatiotemporal scales of hazard interrelations
- ***Green***: identify physical processes and drivers behind multi-hazard.

1.5 Outline of the thesis

Figure 1.5 displays each chapter's main aims and connects these aims with the five aspects of a quantitative multi-hazard approach. **Figure 1.5** highlights the four research chapter's complementarity in covering and every aspect of a quantitative multi-hazard approach.

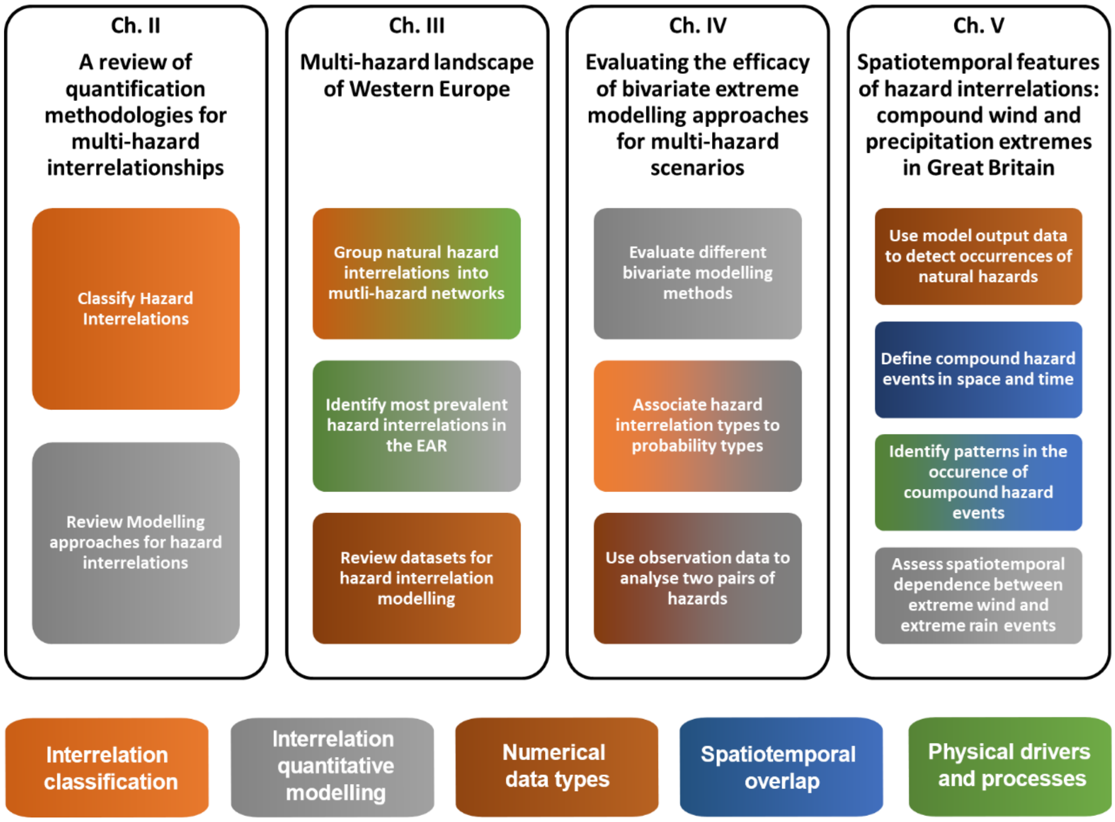

Figure 1.5: Main aims of each of the four research chapters of the thesis. The aims are linked by their colour to the five key aspects of the quantitative multi-hazard approach displayed in Figure 1.4.

This PhD thesis is organized into four research chapters, as follows.

Chapter 2: A review of quantification methodologies for multi-hazard interrelationships.

This review chapter uses grey- and peer-review literature to identify and compare current research available to quantify hazard interrelations. It provides a historical context for quantitative single hazard and multi-hazard assessment. It identifies 19 different modelling methods to quantify natural hazard interrelationships which are clustered into three broad modelling approaches: stochastic, empirical, and mechanistic. Examples of applications for each of the three quantitative modelling approaches are provided. This chapter was published in September 2019 as Tilloy *et al.* (2019) (Tilloy A, Malamud BD, Winter H and Joly-Laugel A "A review of quantification methodologies for multi-hazard interrelationships" in *Earth-Science Reviews*). All authors discussed the whole plan of this article. I reviewed the literature, designed the different databases and finished the draft, including all figures in the article. Bruce Malamud, Hugo Winter and Amélie Joly-Laugel revised the article. Bruce Malamud provided support for the systematic and critical literature review methodology.

Chapter 3: Multi-hazard landscape of Western Europe

This research chapter identifies relevant hazards and hazard interrelations for the European Atlantic Region using blended sources of evidence and reviews data available in the public domain to study multiple natural hazards and quantitatively model their interrelations. A total of

16 interrelated hazards are grouped into five multi-hazard networks based on physical drivers (e.g., meteorological, geophysical) and prior knowledge on interrelations between hazards. A multi-hazard network is composed of a set of interrelated hazards occurring in a given space-time frame. A catalogue of 50 multi-hazards events (10 per network) is provided to illustrate the approach. Based on this catalogue, spatiotemporal characteristics of each network as well as the prevalence of each hazard and hazard interrelation in each network are discussed. Modelling multiple hazard interrelations requires data for different natural hazards with compatible characteristics (e.g., resolution). Indeed, 35 freely available datasets to study and model hazard interrelations were reviewed and classified.

Chapter 4: Evaluating the efficacy of bivariate extreme modelling approaches for multi-hazard scenarios

This research chapter evaluates the efficacy of six distinct bivariate extreme models through their fitting capabilities to 60 synthetic datasets. The properties of the synthetic datasets (marginal distributions, tail dependence structure) are chosen to match bivariate time series of environmental variables. The systematic framework developed contrasts the model strengths (model flexibility) and weaknesses (poorer fits to the data). To highlight the benefits of the systematic modelling framework developed, two pairs of hazards are considered with the following environmental data: (i) observed daily precipitation and maximum wind gusts for 1971 to 2018 in London, UK; (ii) observed daily mean temperature and wildfire numbers for 1980 to 2005 in Porto district, Portugal. This chapter was published in August 2020 as Tilloy *et al.* (2020) (Tilloy A, Malamud BD, Winter H and Joly-Laugel A: "Evaluating the efficacy of bivariate extreme modelling approaches for multi-hazard scenarios" in *Natural Hazards and Earth System Sciences*). All authors discussed the plan of this article. I designed and implemented all the experiments, prepared all the data, and finished the draft, including all figures in the article. Bruce Malamud, Hugo Winter and Amélie Joly-Laugel revised the article. Hugo Winter provided support on the statistical modelling methods and theory.

Chapter 5: Spatiotemporal features of hazard interrelations: compound wind and precipitation extremes in Great Britain

This research chapter uses climate reanalysis data (ERA5) to measure and analyse temporal and spatial features of natural hazards and their interrelations by using a spatiotemporal clustering technique. The chapter focuses on the interrelation between extreme precipitation and extreme wind gust during 1979–2019 within a region including Great Britain and North-West France. The Density-Based Spatial Clustering of Applications with Noise (DBSCAN) algorithm is used to create hazard clusters with extreme values (above the 99% quantile) of precipitation and wind gust. The characteristics (e.g., size, duration, season, intensity) of the created clusters are confronted with observations and analysed. Bivariate modelling is used to estimate return periods of compound hazards events and discuss the influence of the intensity of extreme rainfall and extreme wind on the spatial and temporal scales of compound hazards events.

Chapter 6: Summary, conclusion and future research directions provides a summary of the contributions and proposes future research directions.

Chapter 2: A Review of Quantification Methodologies for Multi-Hazard Interrelationships

Summary:

Globally and yearly, individual hazards and hazard interrelations have the potential to result in socio-economic losses. Here, in this critical review, we use grey- and peer-review literature to identify and compare current research available for the quantification of hazard interrelations, focussing on 14 different natural hazards. We first provide a historical context for quantitative single-hazard and multi-hazard assessment. We then construct a literature database with 146 references related to multi-hazard interrelations. We use our literature database to identify trends for hazard interrelation and multi-hazard and from these group hazard interrelations into five types: triggering, change condition, compound, independence and mutually exclusive. Our critical review identifies 19 different modelling methods to quantify natural hazard interrelationships which we cluster into three broad modelling approaches: stochastic, empirical, and mechanistic. We then synthesize results of our classification of quantification methods for hazard interrelationships and using two matrices illustrate this in practice for 24 different interrelations between 14 natural hazards (out of 196 possible interrelations), one for cascading hazards (temporal order in the multi-hazard event) and one for compound hazards (two or more hazards acting together). Finally, we provide examples of applications for each of the three quantitative modelling approaches defined. We believe that this review will lead to a better understanding of quantification methodologies for hazard interrelations between different sub-disciplines that focus on natural hazards, thus aiding cross-disciplinary approaches for better understanding potential risk related to multi-hazard events.

***Published in *Earth-Science Reviews* in September 2019.** Minor edits have been made to ensure consistency in reference style and language with the rest of the thesis. The substance of the chapter remains unchanged from the originally published paper, except for the addition of an afterwards.

Tilloy, A., Malamud, B. D., Winter, H. and Joly-Laugel, A.: A review of quantification methodologies for multi-hazard interrelationships, Earth-Science Rev., 196, 102881, 2019. doi: 10.1016/j.earscirev.2019.10288.

2.1 Introduction

In this chapter, we review quantification methodologies for the interrelations between different natural hazards. Here, the term hazard will follow the definition by UNDRR (2017), which refers to a natural hazard (hereafter referred to as a 'hazard') as a natural process or phenomenon that may have negative impacts on society. The magnitude of the hazard is one component of risk (hazard, exposure and vulnerability) (UNDRR, 2017). When a high intensity of a natural hazard is encountered, the word extreme is often used to describe these events. The limitations of single hazard studies have been highlighted in the past decade (e.g., Kappes *et al.*, 2012a; Gill and Malamud, 2014; Terzi *et al.*, 2019). Indeed, the interaction of different hazards can lead to an impact that is greater than the sum of the single hazard effects (Terzi *et al.*, 2019). When dealing with more than one hazard at a time the terms multi-hazard and compound hazard (or compound event), the focus of this review, are often used (Kappes *et al.*, 2012b; Seneviratne *et al.*, 2012; Leonard *et al.*, 2014). The term compound hazard is sometimes encompassed within multi-hazard (e.g., UNDRR, 2017); moreover, the term compound hazard is also frequently used for weather and climate-related hazards (Seneviratne *et al.*, 2012; Zscheischler and Seneviratne, 2017).

When considering natural hazards (e.g., landslides, earthquakes, tsunami), each hazard can be linked to other hazards or processes, resulting in the phrase 'multi-hazard', which has a strong link with the term multi-risk in numerous studies (e.g., Greiving *et al.*, 2006; Kappes *et al.*, 2012a, 2012b; Marzocchi *et al.*, 2012; Gallina *et al.*, 2016; Terzi *et al.*, 2019). Gill and Malamud (2014) considered four steps of a multi-hazard framework, in which the first step is a multi-layer hazards approach (Gill and Malamud, 2014), where interrelations are not really considered, and hazards are superposed in a region. Other examples of a multi-layer hazards approach in a region include Grünthal *et al.* (2006), Tarvainen *et al.* (2006) and Orencio and Fujii (2014). The other three steps of the multi-hazard framework of Gill and Malamud (2014) go further to include hazard interactions (interrelationships), coincident hazards and hazard vulnerabilities, with their work focussing on hazard interactions in a multi-hazard framework context. In this review, we will focus specifically on hazard interrelations within the broader context of multi-hazard frameworks.

As shown later in this review, the interest around events that include multiple natural hazards (or multi-hazard events) has been growing since the beginning of the 21st century. The methods and approaches to tackle multi-hazard vary between different natural hazard communities (e.g., geophysical vs. hydrological vs. atmospheric hazard communities). A comprehensive multi-hazard approach could also enhance other disciplines such as forecasting and early warning or climate change studies. There are several challenges associated with quantifying multi-hazard interrelationships which this work aims to tackle, including the following:

(i) *Fragmentation of literature in the field*, with a challenge that a wide variety of terms are used to define hazard interrelationships (e.g., cascade, interaction, compound) (Pescaroli and Alexander, 2018).

(ii) *Gaps in the multi-hazard approaches taken by different institutions* (e.g., single hazards layered without considering interrelationships vs. holistic multi-hazard approaches which include interrelationships and dynamic vulnerability) (Gill and Malamud, 2014, 2016).

(iii) *The complexity of multi-hazard events* and how to address a deterministic equation-based (theoretical) understanding which might apply to 'all' events that are similar vs. a case study based empirical understanding which might be applicable just to a given scenario of a specific event (Geist *et al.*, 2009; Catane *et al.*, 2012; Bout *et al.*, 2018; Kumbier *et al.*, 2018).

We believe there is a need to not only study case studies inclusive of multi-hazard interrelationships but to generalize to more inclusive frameworks that apply to a broad range of hazards and locations. In this chapter, we propose what we consider is a more general and inclusive framework based on a systematic review of quantitative methods and terminology in the broader multi-hazard literature. We believe this will be useful for those responsible for hazards in given regions to put into context methods being used more generally globally. This can be done by applying methods that are not yet applied to certain hazard interrelations or by studying interrelations that have not yet been quantified. This review is focused on reviewing modelling methods for quantifying hazard interrelations; whereas, previous studies have focussed on either documenting qualitative interrelationship between natural hazards or the modelling methods alone (Kappes *et al.*, 2012a; Gill and Malamud, 2014; Hao and Singh, 2016; Hao *et al.*, 2018; Terzi *et al.*, 2019). The different classifications and hazard interrelations matrices developed in this review, combined with an extensive literature database (see **Appendix A**) offer tools and keys to understand the main challenges of quantifying natural hazards interrelations.

Many regions in the world are prone to events that include more than one natural hazard, with interrelationships between the hazards that occur over the same location during the same period (Gill and Malamud, 2014; Leonard *et al.*, 2014). We call these events multi-hazard events. These are usually based on physical phenomena (e.g., thunderstorm, mid-latitude cyclone). Examples of these include the following:

(iv) In 2010, storm Xynthia hit the west coast of France. The storm itself was not particularly extreme for the season but the coincidence of extreme wind, high tides, storm surge and the fact that the soils were already saturated led to huge damage (CCR, 2017).

(v) In winter 2014, the UK experienced a succession of major storms that led to severe damage due to wind, flooding and avalanches in Scotland (Met Office, 2015).

(vi) In 2011, the Great North East Japan earthquake and resultant tsunami had devastating consequences (Davis, 2016; Kumasaki *et al.*, 2016).

(vii) In 2018, Wildfires in California increased the severity of flash floods (AghaKouchak *et al.*, 2018).

These four multi-hazard events all include multiple natural hazards that are interrelated (in different ways), with the events developing on a given region within a period.

In this critical review, we used as evidence a hazard interrelationship literature database consisting of 146 references from the peer- and grey-literature. This review aims to be representative of the current state of modelling interrelationships between natural hazards. In addition to discussing strengths, weaknesses, and commonalities of multi-hazard quantification approaches, we include background on selected diverse modelling methods that are used for multi-hazard modelling. Although we believe our review is representative of the broader literature on multi-hazard, it is not intended to be inclusive of every work or every quantitative approach relating to multi-hazard from the 1980s to when this chapter is written.

This critical review article is organized as follows. We first (**Section 2**) present a literature database built in the context of this review and three subgroups of this database: (i) terminology around multi-hazard and compound events, (ii) interrelationship types for natural hazards, (iii) natural hazards interrelationships. We then present (**Section 3**) different models used in the scientific community to quantify relationships between two and three natural hazards, including some practical examples. We finish (**Section 4**) with discussion and conclusions.

2.2 Construction of a hazard interrelationship literature database

We first created a multi-hazard interrelationship literature database with three main objectives:

(i) To encompass the broadest possible number of terms and approaches for multi-hazard assessments.

(ii) To understand different possible interrelations between natural hazards

(iii) To focus on quantitative methods for hazard interrelations.

To construct this database, we searched for relevant peer-reviewed references in the Web of Science™ online platform and Google Scholar™ using keywords and Boolean search criteria. We also considered in Google Scholar™ conference proceedings, grey literature (e.g., government, technical, and project reports), and PhD dissertations. After a preliminary iterative approach of a couple of dozen references to decide on keywords, we used the following keywords (with appropriate inclusion of plural and other derivatives where appropriate): "multi-hazard", "compound", "hazard", "dependence", "cascade", "multi-risk", "model", "probability". The keyword searches we did were not systematic but rather used combinations of these keywords, combined with some searches that added specific terms for natural hazards (see **Section 2.2.3**), to gain a representative sample of papers in the literature that addressed the three objectives given above.

Our final literature database consisted of 146 references from 83 sources for a 38-year period (1980–2018). Amongst the 146 references, 84% are peer-reviewed scientific journal articles, 6% are reports from projects or institutions, 5% are books, 4% are conference proceedings and 1% are PhD theses. This database is the material for our analysis and is available in **Table A1**. In **Figure 2.1**, violin plots are used to display the distribution of articles over time for those nine journals in the multi-hazard database with ≥3 articles.

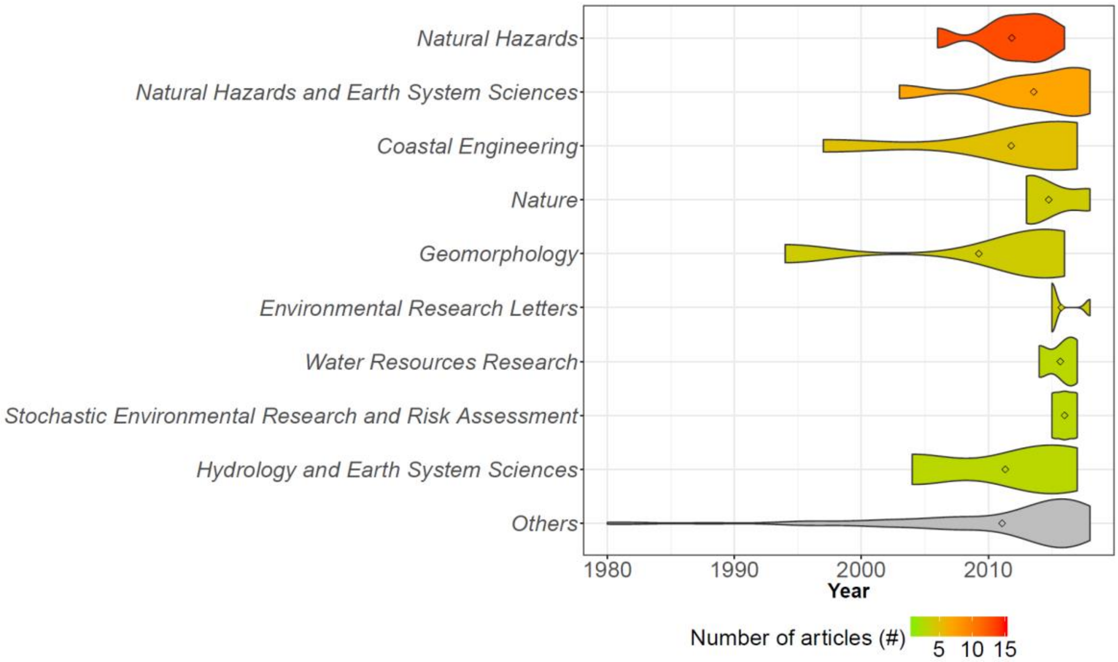

Figure 2.1: Journals in terms of the number of articles listed in our multi-hazard literature database of 146 references and as a function of year. Shown are the 9 journals (out of 83 in the database) which have 3–13 articles, ranked from most articles (journal *Natural Hazards* with 13 articles) to fewest articles (*Hydrology and Earth System Sciences* with 3 articles). Each journal is represented by a violin plot showing the smoothed number of publication per year, 1980 to 2018. The green to red colour (legend) within bars shows the number of articles for that journal. A category for 'Others' references is displayed as the bottom-most violin plot, in grey, and is comprised of 10 sources with 2 references each and 64 sources with 1 reference each (84 references from 74 sources). Small circles within each violin plot represent the mean year of publication for each source.

In our literature review database, those journals the most represented include *Natural Hazards* (*n* = 13), *Natural Hazards and Earth System Sciences* (*n* = 6), *Coastal Engineering* (*n* = 5), *Nature* (*n* = 4), *and Geomorphology* (*n* = 4). One can speculate that the variety of hazards studied in these journals might also require a variety of methods to quantify their interrelations. We can also note the growing interest in fields related to multi-hazard from the late 1990s.

As we are interested in terminology around multi-hazard, hazard interrelations and methodologies for quantifying these interrelations, this database is divided into three interrelated subgroups which we illustrate in:

(iv) *Terminology* subgroup comprises those 85 references that contain terms related to multi-hazard: {(multi-hazard*) OR [compound AND (event* OR flooding OR extreme*)]}. This subgroup will be used to analyse the terminology around multi-hazard in **Section 2.2.1**.

(v) *Interrelation type* subgroup comprises 4 references that classify different types of interrelations between natural hazards and we will use in **Section 2.2.2** to define five types of interrelations between hazards that will be used in this chapter.

(vi) *Models* subgroup, comprises 70 references that examine interrelations between natural hazards in a quantitative way, focusing on possible interrelations between 14 natural hazards that we selected following different criteria. This is discussed further in **Section 2.2.3**.

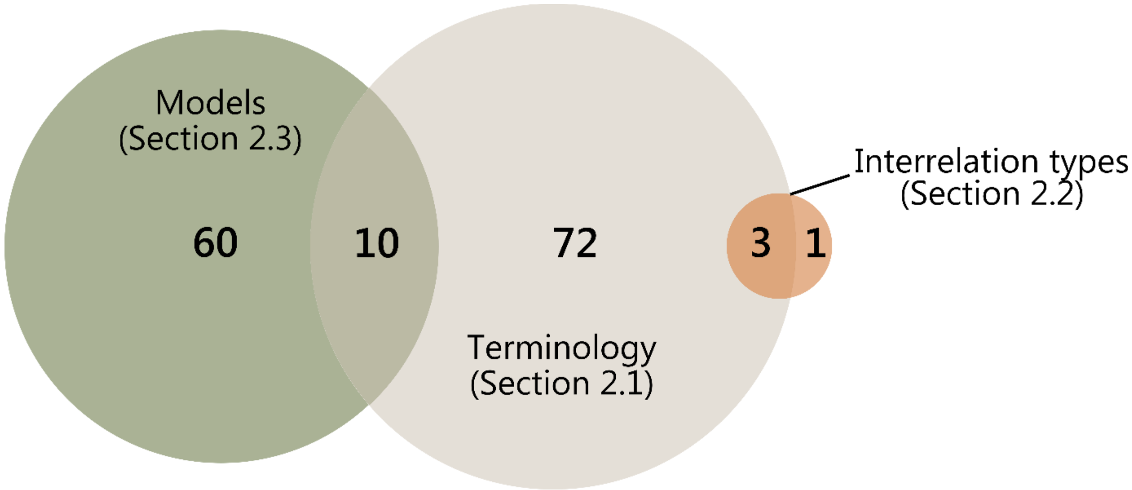

Figure 2.2: The 146 references in our multi-hazard literature database divided into three subgroups of literature (and their overlaps) which we will discuss in Section 2.1 (Terminology), Section 2.2 (Interrelation types) and Section 2.3 (Models). Numbers and size of circles correspond to the number of references.

2.2.1 Terminology in the context of multi-hazard, compound hazard, and hazard interrelations

Multiple hazards have been studied in different contexts and by different research communities (e.g., Kappes *et al.*, 2012b; Leonard *et al.*, 2014; Hao *et al.*, 2018). In the introduction, we referred to some sources that are widely used (e.g., UNDRR, 2017) that define compound hazard as a sub-group of the term 'multi-hazard'. However, as we explored our literature from **Figure 2.2**, two broad streams of studies were found: those using the word multi-hazard and others using the word compound hazard (with some overlap). There was a loose correlation of study foci with the words used, with multi-hazard tending towards those studies to do with solid earth and surface process hazards, and compound hazard to do with those hazard related studies in hydrometeorology. We will below develop the terminology around these approaches, focussing on these two streams, multi-hazard and compound hazard.

The terms multi-hazard and compound hazard have a broad range of interlinked and overlapping definitions, of which we give a couple of examples here. For example, a multi-hazard approach accounts for different probabilities and intensities of multiple hazards (Eshrati *et al.*, 2015). A general definition for a compound hazard events has been given by the IPCC SREX (Seneviratne *et al.*, 2012) and also given and discussed by Leonard *et al.* (2014, p. 115) as "an extreme impact that depends on multiple statistically dependent variables or events". Eshrati *et al.* (2014) distinguished between compound hazard and multi-hazard, stating the following (p. 79):

> *"While compound hazards are characterized as 'several elements acting together above their respective damage threshold', multi-hazard are characterized as 'elements of quite*

different kinds coinciding accidentally, or more often, following one another with damaging force' ".

Hewitt and Burton (1971) and more recently Kappes *et al.* (2012) and Eshrati *et al.* (2014) highlighted that the terms multi-hazard and compound hazard correspond to the two main mechanisms to characterize hazard interrelations.

Previous studies have highlighted the abundance of terms to qualify hazard interrelations (e.g., Kappes *et al.*, 2012b; van Westen and Greiving, 2017). The profusion of terminologies and definitions makes it hard to find a generally accepted definition of a multi-hazard. Moreover, some terms are linked and part of the same conceptual framework. Here we did an extensive review of the available literature to find patterns in the use of particular terms to define hazard interrelations within the context of multi-hazard and compound hazard.

To offer a better understanding of the terminology around multi-hazard and compound hazard, we first listed terms that are used to represent hazard interrelations. To do this, we relied on previous reviews on multi-hazard which already gathered terms to describe relations between hazards (Kappes *et al.*, 2012b; Gill and Malamud, 2014; Leonard *et al.*, 2014; van Westen and Greiving, 2017; Pescaroli and Alexander, 2018). Selected terms are displayed in **Figure 2.3**.

For the 146 references in our literature database, we searched each of the documents for those containing the keywords {(multi-hazard*) OR [compound AND (hazard* OR extreme* OR event* OR risk*)]}. We performed this selection using the software Mendeley™ which performs word searches within the entire PDF file of each reference. Among the 146 sources in our database, 85 (59%) fulfilled these conditions. By doing this selection we include different sources aiming to deal with the broad issue of multi-hazard. Amongst these 85 sources, 66 (77%) contain the word "multi-hazard" and 29 (35%) the word "compound" (of these 66 and 29 sources, ten of them contain both terms). The term multi-hazard is more frequently used than compound hazard. In our literature database, the term "compound AND (event OR extreme OR hazard)" was first mentioned in 2012 (Lavell *et al.*, 2012), while the use of the term "multi-hazard" is more established (first mention in 2002) (van Westen *et al.*, 2002). Moreover, as was discussed above, these terms are complementary to defining hazard interrelationships.

Our next step was to study the distribution of terms used to define hazard interrelations among these two terminology streams (multi-hazard and compound hazard). Terms we looked for in both streams include the following: cascade, chain, interaction, interrelation, dependence, combination, multivariate, domino, trigger, coincidence, amplification. As discussed in the introduction to **Section 2.2.1**, these words were selected from previous works on multiple hazards (Kappes *et al.*, 2012b; van Westen and Greiving, 2017; Pescaroli and Alexander, 2018) and were considered the most relevant. **Figure 2.3** displays the results of this analysis in a treemap, with the green (left) representing percentage results of those interrelationship terms within multi-hazard (MH) and orange (right) those within the compound hazard (CH).

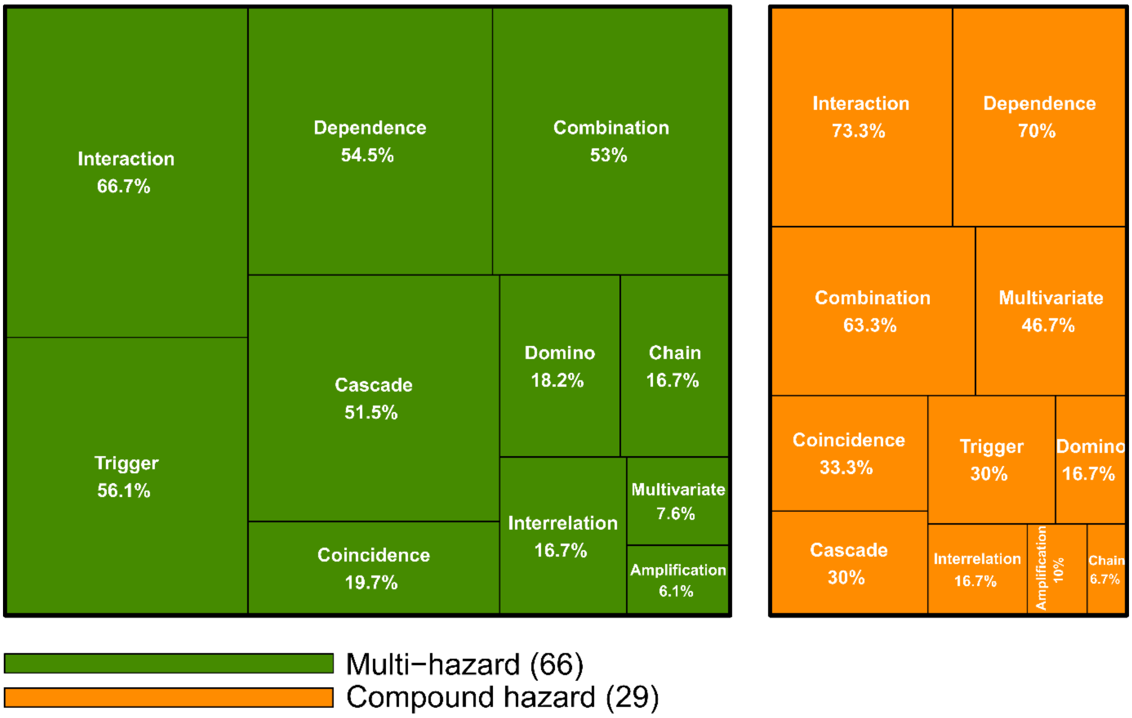

Figure 2.3: Treemap of multi-hazard and compound hazard terminology used in 85 sources to describe and quantify hazard relationships. This treemap chart shows the proportion of use of terminology used in our multi-hazard literature database. Terms are grouped in two literature streams which correspond to "multi-hazard" (green, 66 references) and "compound hazard" (orange, 29 references), noting that ten of the references have both words so are included (repeated) in the green and orange parts. Each of the 85 sources within the two terminology streams of multi-hazard and compound hazard was examined for word use, within some cases a given reference using greater than one of the words (sum of all values is >100%).

From **Figure 2.3** we can see that the terms "interaction", "dependence" and "combination" are the most widely used in both frameworks (each term is used in 53–73% of all references in the MH or CH frameworks). The terms "trigger" and "cascade" are more often used within the MH framework (trigger: 56% in MH vs. 30% in CH; cascade 52% in MH vs 30% in CH). This contrasts with the terms "multivariate" and "coincidence" which are more associated with the CH terminology stream (multivariate: 8% MH vs 47% CH; coincidence: 20% MH vs 33% CH). This highlights the differences between the multi-hazard (MH) and compound hazard (CH) streams, and how they do not refer to the same physical processes. Differences in terminology have to do with disciplines and the modelling methods to quantify interrelations as will be shown in **Section 2.3**.

Figure 2.3 also shows that the term "interrelation" is equally used (17%, i.e. one in six references) for both MH and CH. We consider interrelation to be a neutral term, equally used in both MH and CH. This analysis of the terminology shows that (i) some authors refer to compound hazard events as distinct from multi-hazard, and that (ii) authors who refer to compound hazard events do not always choose the same terms to define hazard interrelations.

2.2.2 Interrelationships between hazards

After defining two different terminology streams (multi-hazard and compound hazard) and analysing the terminology around hazard interrelations (**Section 2.1**), in this section we review different ways of classifying hazard interrelations, using the terminology previously presented.

Some authors classify hazard interrelations for different purposes. Gill and Malamud (2014) defined four interrelation types which they built on a critical review of >200 references, including many case studies. Decker and Brinkman (2015) defined three different interrelation types between natural and human-made hazards in the context of the project ASAMPSA_E (Advanced Safety Assessment Methodologies: Extended PSA) focusing on hazards posing potential threats to nuclear installations and their possible correlations. Liu *et al.* (2016) did a systemic classification of hazard interrelations based on characteristics of the hazard-forming environment defining four different types which they expressed in probabilistic terms. Finally, van Westen and Greiving (2017) consider four types of hazard relationships based on previous research. The interrelation types within each of the four references are given in **Table 2.1**.

Table 2.1: Four different interrelation classifications for natural hazards from different sources. Each reference has a letter (A, B, C, D) and each interrelation type has a number (1, 2, 3, 4).

Article	Interrelation type
A. Gill and Malamud (2014)	***(A1) Interactions where a hazard is triggered***: One hazard triggers one (or more) other hazard(s). ***(A2) Interactions where the probability of a hazard is increased***: One hazard changes environmental parameters that move towards an increase in the likelihood of another hazard. ***(A3) Interactions where the probability of a hazard is decreased***: One hazard changes environmental parameters that move towards a decrease in the likelihood of another hazard. ***(A4) Events involving the spatial and temporal coincidence of natural hazards***: Two hazards are independent and occur simultaneously by coincidence.
B. Decker and Brinkman (2015)	***(B1) Causally connected hazards:*** When one hazard may cause another hazard; or when one hazard is a prerequisite for a correlated hazard. ***(B2) Associated hazards:*** Hazards which are probable to occur at the same time due to common root causes. ***(B3) Combinations of independent phenomena***: Two hazards are independent.
C. Liu *et al.* (2016)	***(C1) Independent relationship***: Two hazards are independent. ***(C2) Mutex relationship***: Two hazards cannot occur together; their trigger factors are mutually exclusive. ***(C3) Parallel relationship***: Two hazards depend on the same trigger factors. ***(C4) Series relationship***: One hazard triggers another hazard.
D. van Westen and Greiving (2017)	***(D1) Independent events***: Two hazards are independent. ***(D2) Coupled events***: Two hazards are triggered by the same triggering event. ***(D3) One hazard changes the conditions for the next***. ***(D4) Domino or cascading hazard***: One hazard causes the next.

In these four references that examined interrelationship classifications (**Table 2.1**), the same processes are described in different ways with different terms. Moreover, it is possible to find bridges in-between these classifications. For example, *triggering interaction* **(A1)** is equivalent to *causally connected hazard* **(B1)**, *series relationship* **(C4)** and *cascading hazard* **(D4)**. From these different classifications we can highlight five different interrelation types: *independence, triggering, change conditions, compound hazard, mutual exclusion*. These are summarized in **Table 2.2** along with the reference and interrelation type from **Table 2.1**.

Table 2.2: Five interrelation types as synthesized from the four references (A to D) presented in Table 2.1 and used in this review.

Interrelation type	*A. Gill and Malamud (2014)*	*B. Decker and Brinkman (2015)*	*C. Liu et al. (2016)*	*D. van Westen and Greiving (2017)*
I. Independence	✓	✓	✓	✓
II. Triggering	✓	✓	✓	✓
III. Change condition	✓			✓
IV. Compound hazard		✓	✓	✓
V. Mutual exclusion	✓		✓	

Here we described in detail each of these five interrelation types, along with case-study examples of each interrelation type:

– **I. Independence (A4, B3, C1, D1)**: Coincidence between hazards can occur. It implies a spatial and temporal overlapping of two (or more) hazards without any dependence or triggering relationship. It is equivalent to the independent relationship in Liu *et al.* (2016) and van Westen and Grieving (2017) and the spatial-temporal coincidence in Gill and Malamud (2014). An example is the 2010, Pacaya volcanic eruption and tropical storm Agatha which hit the Pacific coastline of Guatemala almost simultaneously, leading to exacerbated damages due to ash blocking drainage system of rainfall triggering lahars (Gill and Malamud, 2014). We also include in this category cases where two (or more) hazards develop over the same area, independently, at different times (e.g., cyclone occurring a few weeks after an earthquake).

– **II. Triggering** (Cascading) **(A1, B1, C4, D4):** Implies a primary and a secondary hazard. As explained by Gill and Malamud (2014), any natural hazard might trigger zero, one or more secondary natural hazards (Tarvainen *et al.*, 2006; De Pippo *et al.*, 2008; Kappes *et al.*, 2012b; Marzocchi *et al.*, 2012). The secondary natural hazard might be identical or different from the primary hazard. As an example, an earthquake might trigger landslides, which may create a natural dam on rivers. The breaking of landslide dams can trigger a flood, resulting in a hazard cascade (Catane *et al.*, 2012).

– **III. Change conditions (A2, D3):** This relates to one hazard altering the disposition of a second hazard by changing environmental conditions. This phenomenon has been discussed in previous papers (Kappes *et al.*, 2010; Catane *et al.*, 2012). One of the reasons is its variable temporal scale, for example, a wildfire might denude an area of vegetation and harden the soil thus amplifying the strength of floods through increasing over ground flow and result in a debris flow (Canon *et al.*, 2007). A wildfire can have a non-negligible influence on soil infiltration up to one year after its occurrence (Shakesby and Doerr, 2005). For example, in Las Conchas in New Mexico in 2011, a wildfire charred more than 150 000 acres leading to an increased flood one month later (FEMA, 2012). There is a similar issue with river flooding amplified by landslides (Costa and Schuster, 1988).

- **IV. Compound hazard** (association) **(B2, C3, D2):** In this interrelation, different hazards are the result of the same "primary event", or large scale processes (Mazas and Hamm, 2017) which are not necessarily hazards. In this case, there is not a primary and a secondary hazard as the different hazards occur simultaneously. As an example, the co-occurrence of river flooding and sea surge could be the result of the same large-scale process (tropical cyclone, mid-latitude cyclone) (Bevacqua *et al.*, 2017; Dowdy and Catto, 2017). The two hazards are considered as dependent and form a multi-hazard event called compound flooding (Klerk *et al.*, 2015; van den Hurk *et al.*, 2015; Wahl *et al.*, 2015; Moftakhari *et al.*, 2017). Depending on the scale we focus on this dependence can be almost instantaneous or lagged. Therefore, Klerk *et al.* (2015) found a statistical dependence between extreme discharge on the Rhine river and extreme sea level at its outlet into the North Sea, but with a 6 days lag time. This can be explained by the size of the Rhine catchment. Moreover, some other dependencies are spatially and temporally closer, such as the dependency between lightning activity and hail occurrence (Lang and Rutledge, 2002; Carey *et al.*, 2003).
- **V. Mutual exclusion** (negative dependence) **(A3, C2):** Two natural hazards can also exhibit negative dependence or be mutually exclusive. There is limited literature because a negative dependence of two hazards does not lead to an increased impact, which is the case for positive dependence. There are many examples of hazards that show negative dependence, often hydrometeorological (e.g., heavy rain and fire). However, such negative dependence is often on a particular spatial and/or temporal scale. For example, within a tropical cyclone, both extreme wind and lightning are likely to occur but Molinari *et al.* (1999) shown that the extremes of these two hazards occur in different parts of the cyclone. On the scale of the whole cyclone, those two hazards are positively dependent, but on a narrower scale, they appear to not occur in an extreme way together.

We will use these five interrelation types (independence, triggering, change condition, compound hazard, mutual exclusion) in the rest of this chapter. Moreover, a focus has been put on triggering (type II), change condition (type III) and compound hazard (type IV) in **Section 4.2** as these interrelations are of greater interest compared to independence and mutual exclusion (Kappes *et al.*, 2012a; Gill and Malamud, 2014; Decker and Brinkman, 2015; Mignan *et al.*, 2016).

2.2.3 Natural hazard interrelations models database

To select relevant hazards for our analysis we first referred to previous reviews on hazard interrelationships (Gill and Malamud, 2014; Decker and Brinkman, 2015) where they give qualitative information about natural hazard interrelations with matrices. Gill and Malamud (2014) present a matrix of potential interactions between 21 different natural hazards while the one realized for the ASAMPSA_E project by Deker and Brinkman (2015) contains 70 natural hazards (many sub-categories of those given by Gill and Malamud, 2014).

We use three selection criteria for the natural hazards we choose to focus on, such that they would be a diverse and representative range. These selection criteria loosely informed our list of 14 natural hazards and were as follows: (i) those hazards that caused past recorded impact (disasters) in Europe; (ii) hazards prone to have interrelations with at least one other natural hazard; (iii) hazards that can be quantified with one (or a small set) of environmental variables. The hazards and categories we use further below are not exclusive, and other studies might choose other hazards to focus on, or classify a given hazard type into two different (more relevant) types.

Our first criteria that helped to loosely inform our final list of diverse hazard types is past recorded impact to Europe. To do this we used the Emergency Events Database (EM-DAT) a record of disasters maintained by the Centre for Research on the Epidemiology of Disasters (CRED, 2018). EM-DAT contains data on the occurrence and effect of over 14,600 disasters (as of 2018) in the world from 1900 to present. There are several criteria for a disaster to be included in the dataset, including ≥ 10 people died or ≥100 people affected or declaration of a state of emergency or a call for international assistance (CRED, 2018) Despite its recognition, the quality of this disaster database faces biases (e.g., threshold biases, spatial aggregations) discussed by Jonkman (2005) and Gall *et al.* (2009).

With these biases in mind, we extracted disaster profiles in Europe from EM-DAT (CRED, 2018) over the period 1900 to 2018. The distribution of natural disasters from this database is displayed in **Figure 2.4.** The corresponding natural hazards that resulted in these disasters include earthquakes, hazards related to convective storms (lightning, extreme wind, hail, extreme rainfall, river flooding), extra-tropical cyclones (sea surge, extreme waves, coastal flooding, extreme wind, extreme rainfall), extreme temperature (heatwave, cold wave), drought, forest fires and snow avalanches.

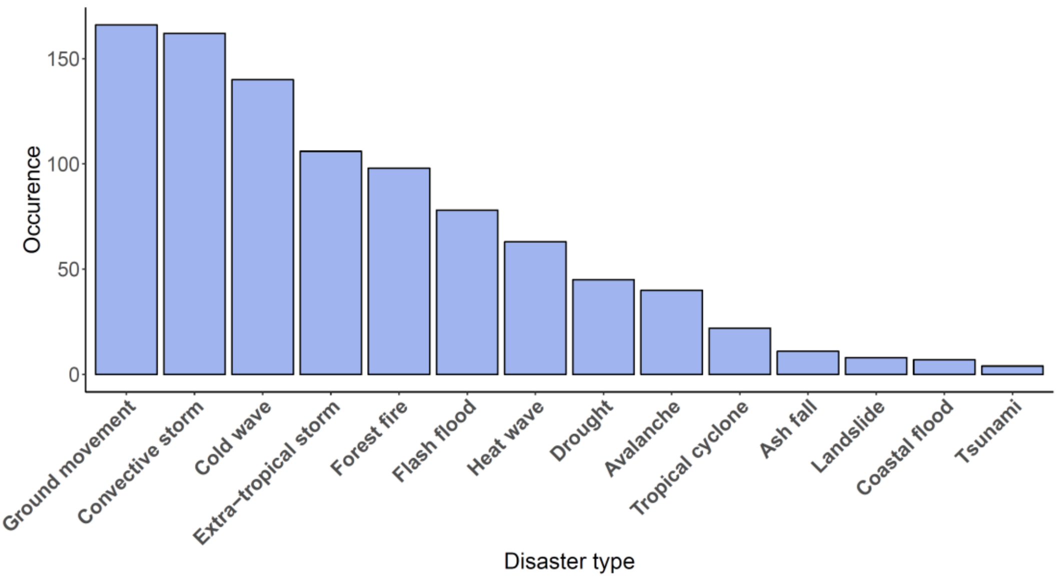

Figure 2.4: Occurrences of 14 disaster types in Europe in the period 1900-2018. Data from CRED (2018).

Most of the hazards resulting in the disasters shown in **Figure 2.4** can be expressed with environmental variables and, as it will be shown in **Section 3**, are suitable for modelling. Two hazards from **Figure 2.4** we do not include are snow avalanches and wildfires. Snow avalanches, despite their destructive power and their relevance for Europe, are difficult to model regarding their interrelations with other hazards. Wildfires have a complex link with other hazards such as drought, extreme temperature, lightning and floods (Myers and Van Lear, 1998; Littell *et al.*, 2016; AghaKouchak *et al.*, 2018). However, the multiplicity of possible combinations leading to a fire outbreak are beyond the scope of this study focusing on interrelations between two hazards, so they are also excluded. From the natural disasters in **Figure 2.4** and our selection criteria, we selected 14 natural hazards (**Table 2.3**).

Table 2.3: A list of 14 single natural hazards considered in this chapter broken up into geophysical, atmospheric and hydrologic natural hazard categories

1. GEOPHYSICAL	*2. ATMOSPHERIC*	*3. HYDROLOGICAL*
1.1 Earthquake	*2.1 Lightning*	*3.1 Sea surge*
1.2 Landslide	*2.2 Extreme rainfall*	*3.2 Extreme waves*
1.3 Volcanic eruption	*2.3 Extreme wind*	*3.3 River Flood*
	2.4 Extreme temperature	*3.4 Tsunami*
	2.5 Hail	*3.5 Drought*
	2.6 Tornado	

Based on 14 natural hazards from **Table 2.3**, there are 196 interrelationship pairs possible, if each hazard can potentially interact with another hazard of the same type. For example, an earthquake might trigger a landslide, but also an earthquake can increase the probability of another earthquake occurring. In our multi-hazard literature database, 70 of the references are to do with interrelationship case studies relevant to the hazards given in **Table 2.3**. Note that there was an iterative process in our methodology for those references included in the final literature database, in that after the database was initially compiled, the hazards to be studied were decided upon (above) and then additional references to do specifically with those hazards given in **Table 2.3** were added.

We will now use the 70 references from our multi-hazard literature database in combination with the 14 natural hazards given in **Section 2.3** to examine in detail different methodologies for the quantification of hazard interrelationships.

2.3 Methodologies for quantifying hazards interrelations

This section focuses on hazard interrelation modelling and quantification, particularly for pairs of hazards. In this section, we are interested in (i) how different disciplines quantify hazard interrelations and (ii) creating a grouping of these different methods into an overall framework. Literature is used here as evidence for this task and includes 70 references (See **Figure 2.2** and **Appendix B Table B1**) which each have an aspect of quantification between two given hazards. In **Section 2.3.1** we give a representation of current knowledge related to hazard interrelation modelling through two matrices. In **Section 2.3.2**, the main models for quantifying hazard interrelationships are presented with examples of applications to natural hazard interrelations. Finally, in **Section 3.3**, the applicability of the modelling approaches to different types of hazard interrelations and categories of natural hazards are discussed.

2.3.1 Natural hazard interrelations matrices

We now use the 14 hazards selected in **Section 2.3** and displayed in **Table 2.3**, combined with evidence from our natural hazard interrelations models database (**Appendix B Table B1)**, to create two hazard interrelations matrices (see **Table 2.2** and **Section 2.2.1** for further discussion of terminology):

(i) *cascading hazards* (**Figure 2.5**): two hazards that occur sequentially in time where one hazard *triggers* or *changes the conditions* of another secondary hazard;

(ii) *compound hazards* (**Figure 2.6**): two statistically dependent hazards occurring simultaneously at the same location.

(iii) These matrices (**Figures 2.5** and **2.6**) display the types of interrelation between hazards (**Section 2.2.2**), and the category of model used in the literature to quantify the interrelations (we have divided these broadly into stochastic **S**, empirical **E** and mechanistic **M**). For example, extreme rainfall triggers or changes conditions for landslide and this interrelation has been modelled with empirical and mechanistic models. We will later (**Section 2.3.2**) give a much more detailed view and classification of the different interrelation modelling approaches.

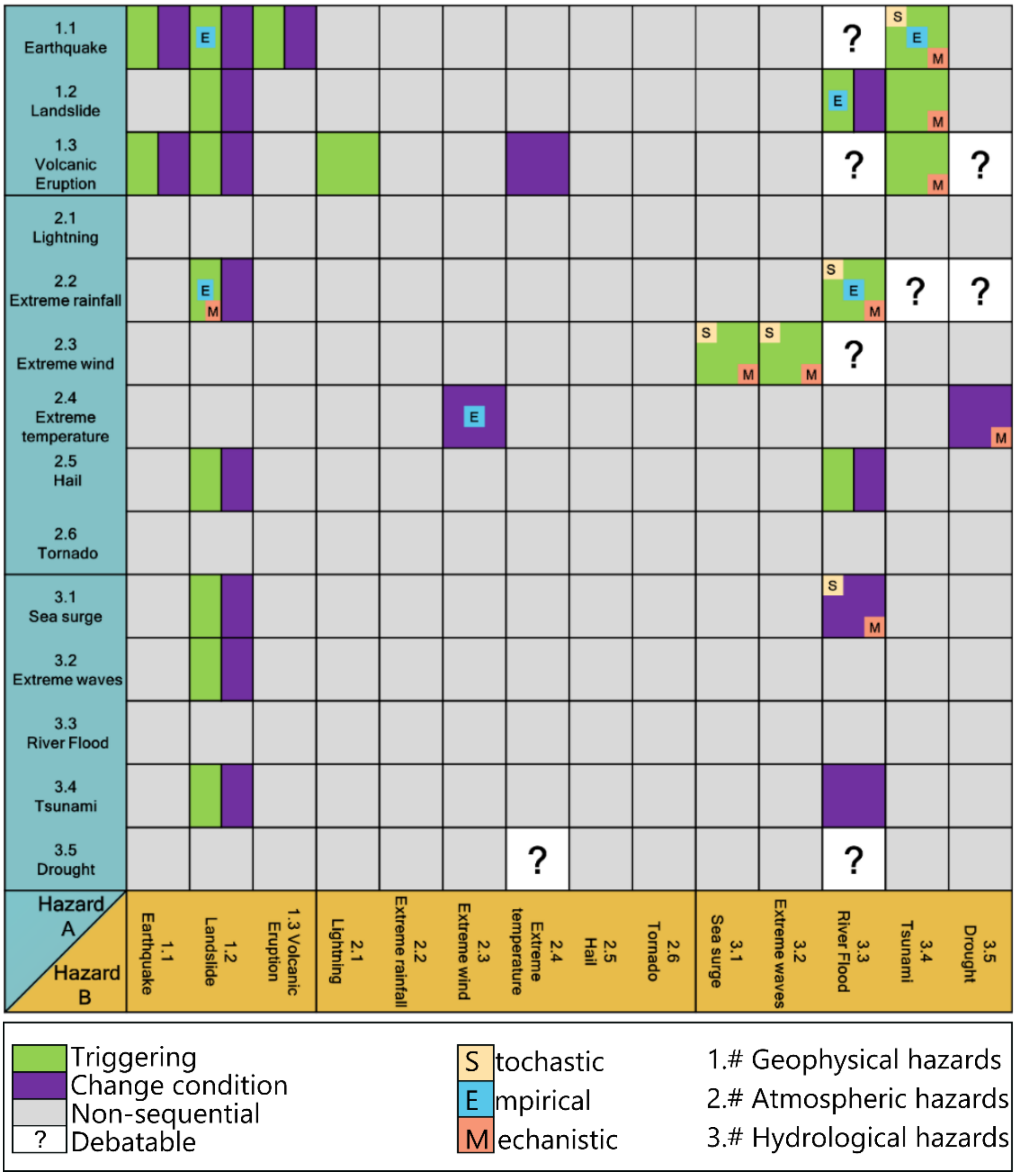

Figure 2.5: Cascading hazard interrelation matrix for the considered hazards in this study. Matrix-based on 70 references and the modelling approach applied. This figure shows the type of interrelations between hazards when there is a sequential effect – from hazard A to hazard B – and the modelling methods which are used for each pair of hazards. The colours of the cells represent the interrelation types: green for triggering, purple for amplification; cells in grey represent non-sequential interrelations (see Figure 2.6) and white cells (with '?') represent interrelations with debatable nature. The letters represent the interrelation type: S for stochastic, E for empirical and M for mechanistic. The numbers refer to the natural hazard category: 1.# for geophysical; 2.# for atmospheric and 3.# for hydrological.

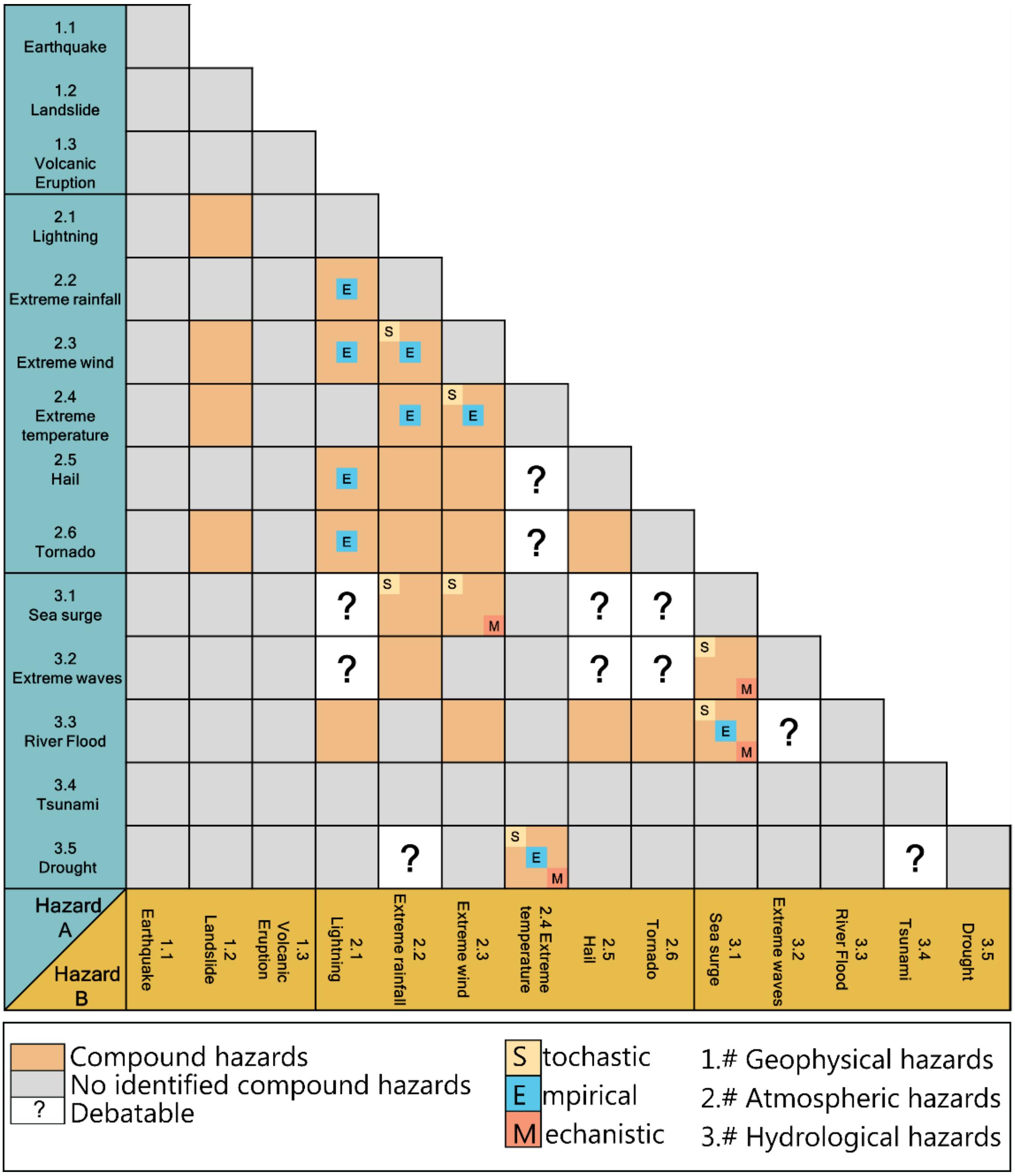

Figure 2.6: Compound interrelation matrix for the considered hazards in this study. Matrix-based on 70 references and the modelling approach applied. This figure shows the type of interrelations between hazards when there is a known association between hazards (compound hazards) and the modelling methods which are used for each pair of hazards. The colours of the cells represent the interrelation types: beige for known compound, light grey for no identified compound hazards (see Figure 2.5 for identified cascading hazards); and white cells represent interrelations with debatable nature. The letters represent the interrelation model: S for stochastic, E for empirical and M for mechanistic. The numbers refer to the natural hazard category: 1.# for geophysical; 2.# for atmospheric and 3.# for hydrological.

The cascading hazards matrix presented in **Figure 2.5** displays relationships when one hazard triggers another (e.g., earthquake triggers a landslide) or when one hazard changes the conditions for another (e.g., earthquake increase the probability of landslide by reducing the soil cohesion). Both interrelation types imply one primary (earthquake) and one secondary hazard (landslide) as they were defined by Gill and Malamud (2014) in a matrix they constructed. In **Figure 2.5**, the matrix hazard A is always prior (in time) to hazard B. Hazard interrelations that are not sequential are not considered and some interrelations are still debatable according to the literature. For example, the relationship between earthquake and flood is still not clear. From the (14 ×14) = 196 interrelationship pairs possible in the **Figure 2.5** matrix, we have indicated 33 where there is a potential cascading relationship, of which 13 are both triggering & change condition (purple & green), 7 triggering (green), 5 change condition (purple), and 8 'debatable' (white). These were identified from the work of Gill and Malamud (2014), Decker and Brinkman (2015) and Mignan *et al.* (2016). We then looked for quantification relationships (an iterative process within the construction of our natural hazard interrelations model database) and for 12 of the cells in **Figure 2.5** we found quantification studies relating one hazard with another (indicated by **S**, **E**, **M** in the matrix), which we will discuss in greater depth in **Section 3.3.3**.

The same 14 hazards as in **Figure 2.5** are presented in **Figure 2.6**, but in this case, there is no temporal or causal relationship between hazards, therefore only 105 interrelationships (cells) are possible. Every hazard might be associated with another hazard (compound hazard), but in the literature, some compound interrelationships are more likely to occur. In **Figure 2.6**, cells are identified that are: (i) (26 cells) compound (where a statistically significant dependent relationship has been identified in the literature), (ii) (11 cells) where the relationship is debatable in the literature. The remaining 68 cells (grey) have not been identified as having a definite compound hazard relationship in the literature. Although a compound hazard relationship might not exist (**Figure 2.6**), a cascading hazard might exist (**Figure 2.5**). Of the compound cells identified, 12 have been marked (using our interrelationship database) with a specific model approach using letters **S**, **E**, or **M**. When natural hazards are compound (associated or statistically dependent), they are likely to occur together because they depend on the same precursory factors. Liu *et al.* (2016) defined trigger factors that induce hazards and control the frequency and magnitude of hazards. Because of the statistical dependence of compound hazards (e.g., extreme wave and sea surges), they have been widely studied with stochastic models (see **Section 2.3.2**) (Hawkes *et al.*, 2002; Dong *et al.*, 2015; Rueda *et al.*, 2016; Petroliagkis, 2018). Moreover, lack of data and the short time range of available records have limited the use of stochastic methods for interrelations with hazards such as lightning or hail. Empirical methods are more commonly used to acknowledge or quantify relationships (Lang and Rutledge, 2002; Price and Federmesser, 2006; Schultz *et al.*, 2011; Iordanidou *et al.*, 2016).

2.3.2 **Models and classification**

In this section, we present three hazard interrelation modelling approaches (stochastic, empirical, mechanistic, indicated by **S**, **E**, **M** in the matrices in **Figures 2.5** and 2.**6**) which covers the14 hazards we selected **(Table 2.3)**. Here, by models, we mean statistical or numerical tools used to quantify hazard relationships. The idea behind this classification is to build a framework to clarify different quantification methods to deal with a range of hazard interrelations.

In **Figure 2.7** we present these three different categories of models to quantify interrelations between natural hazards and their subcategories. This categorisation was built using the 70 studies in our natural hazard interrelations model database (**Appendix B Table B1**). For each of the 70 studies, we pulled out the main modelling method(s) used to quantify hazard interrelationships and the types of hazards (where appropriate). We then used the overall evidence and categorized these. Our categorizations were inspired by classifications already made for hydrological models (Devia *et al.*, 2015), dependence modelling in hydrology (Hao and Singh, 2016; Hao *et al.*, 2018), landslide susceptibility models (Reichenbach *et al.*, 2018) and more general overview on models in science (Frigg and Hartmann, 2012).

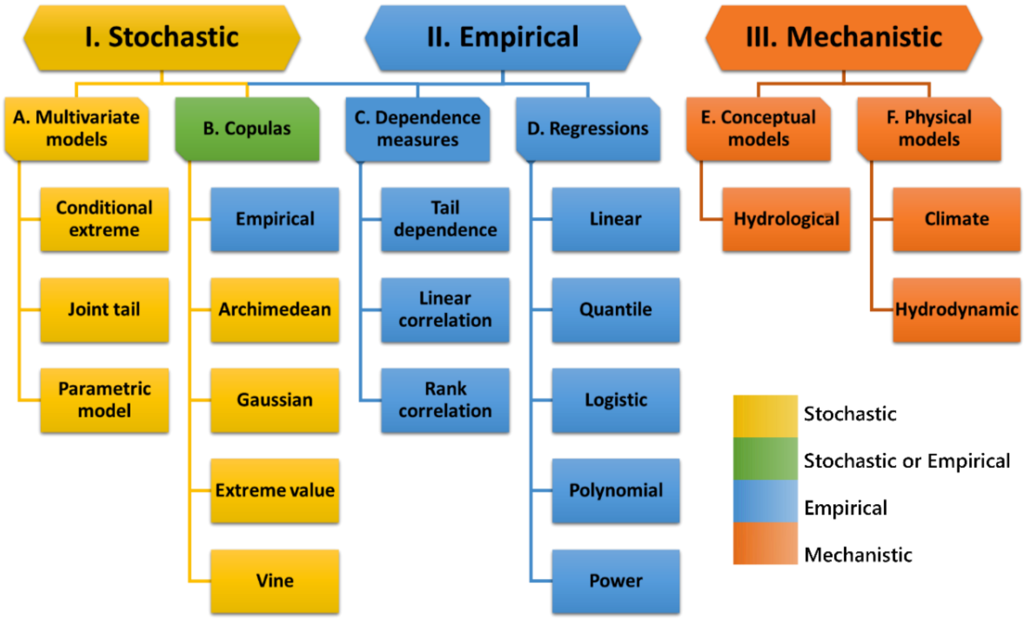

Figure 2.7: Natural hazard interrelationship models: three different modelling approaches (I. stochastic, II. empirical, and III. mechanistic), six families (A. multivariate, B. copula, C. dependence measures, D. regressions, E. conceptual models and F. physical models) and 19 modelling methods. This classification is based on a review of 70 references from 1980 to 2018 (see Appendix B Table B1).

Figure 2.7 gives an overview of the main modelling methods available for different types of interrelations. Three different modelling approaches are highlighted, within which there are model families (two for each modelling approach) which are subdivided into modelling methods. In total, for the 70 references (73 pairs of natural hazards) in our database, we recorded 79 unique uses of 19 different modelling methods, of which the stochastic modelling approach had 27 (34%) uses, empirical had 31 (39%) uses, and mechanistic 21 (27%) uses. For the stochastic approach, there are two families (A. multivariate and B. copula) and 7 modelling methods. For the empirical approach, there are three families (B. copula—shared with stochastic, C. dependence measures, D. regressions) and 9 methods. Finally, for the mechanistic approach, there are two families (E. conceptual models, F. physical models) and 3 methods. Later in **Section 3.3,** we give the number of uses (out of 79) for each modelling method.

We shall now define the three main modelling approaches (stochastic, empirical, mechanistic). Because of the vast literature for each method, here we provide a concise explanation for each of the six model families in **Figure 2.7** with relevant linked literature and illustrate four methods with case studies.

2.3.2.1 Approach I: Stochastic models

We define stochastic models as models based on samples of different variables with random behaviour (Cox and Miller, 1965). In this category, we include all the methods with the generation of random data from statistical distributions. In **Section 2.2.2** we presented different types of interrelationships between natural hazards, in case of compound events, there is usually a statistical dependency between different natural hazards. Stochastic models can model this statistical dependency between extreme environmental variables (e.g. extreme wind, extreme rainfall) (Ledford and Tawn, 1997; Yang and Zhang, 2013; Zheng *et al.*, 2014; Ming *et al.*, 2015). Methods presented in this category come from multivariate statistics and extreme value statistics (Tawn, 1988, 1990; Coles and Tawn, 1991, 1994; Nelsen, 2006; Gudendorf and Segers, 2010). One of the main strengths of these models is that they allow for extrapolation beyond the range of available data. Among stochastic models, we distinguish two model families: (i) copulas (which can also be empirical) and (ii) multivariate models (**Figure 2.7**). The main difference between these two families is that multivariate models include marginal modelling (i.e., modelling the distribution of each separate variable) while copulas solely focus on modelling the dependence structure (Hao and Singh, 2016). Stochastic models have been particularly used to model compound hazards (**Figure 2.6**) as they provide the joint probabilities of two hazard occurring at the same time. Conditional probability has also been used to model causal relationships (Liu *et al.*, 2018). Stochastic models permit the estimation of joint probabilities of exceedance and return periods; these quantities are commonly required by engineers and decision-makers.

2.3.2.1.1 Copulas

In a bivariate case, a copula is a joint distribution function which defines the dependence between two variables independently from the marginal distributions of these variables (Heffernan, 2001; Favre *et al.*, 2004; Nelsen, 2006; Hao and Singh, 2016). See (Genest and Favre, 2007) for a good introduction to copulas. For two variables X and Y, any bivariate distribution function with marginal distribution functions $F_X(x)$ and $F_Y(y)$ and the joint cumulative distribution function $F_{X,Y}(x,y)$ can be expressed as a copula in the following form (Nelsen, 2006):

$$F_{X,Y}(x,y) = C\{F_X(x), F_Y(y)\} \tag{2.1}$$

where C is the copula function. Copulas are not limited to two variables and therefore equation (1) can be extended to higher dimensions. Several classes of copula with different properties are available (Joe, 1997; Favre *et al.*, 2004; Nelsen, 2006). Copulae used in our literature database belong to one of the three following classes: Archimedean copulas, Gaussian copulas and extreme value copulas. Copulae are parametric models; indeed, each copula is suitable within a given range of dependence structures. Without prior knowledge of the studied hazards, several copulae with different levels of complexity need to be fitted to the data and compared (Sadegh *et al.*, 2017). Using a copula which does not capture adequately the dependence structure between two variables can lead to either underestimation or overestimation of the joint probability of these two variables (Ledford and Tawn, 1997; Mazas and Hamm, 2017).

2.3.2.1.2 Multivariate models

Despite their theoretical relation to copulas (Tawn, 1990; Heffernan, 2001), multivariate models differ from copulas as they include margins in the modelling process (i.e. marginal distributions are usually fixed for a given model). Multivariate models are usually parametric (Ledford and Tawn, 1997) or semi-parametric (Heffernan and Tawn, 2004; Hao and Singh, 2016). Among multivariate models, parametric models developed for the characterization of bivariate extreme value distributions have been the most used to investigate hazard interrelations (Gumbel, 1961; Yue, 2000; Zheng *et al.*, 2013). The conditional extreme model (Heffernan and Tawn, 2004) has the particularity of estimating the dependence structure between two variables conditioned on one being extreme. A joint tail model requires all variables to become large at the same rate; this can be problematic when looking at compound events where not all the variables are extreme (Leonard *et al.*, 2014; Liu *et al.*, 2018). Parametric multivariate models have the same limitations as copula models as they can typically handle only one form of extremal dependence. However, semi-parametric models such as the conditional extremes model are more data-driven, offering more flexibility at the price of a higher sensitivity (e.g. leading to different results with different datasets even when modelling the same processes) (Winter, 2016).

2.3.2.1.3 Example of stochastic approach: Estimation of the joint probability of extreme rainfall and sea surge

The interrelation between extreme rainfall and sea level is of primary interest when studying coastal flooding. Indeed, high sea levels prevent the flow of excess water due to extreme precipitations toward the open sea (Zheng *et al.*, 2013; Klerk *et al.*, 2015; van den Hurk *et al.*, 2015). The quantification of the interrelations between these two hazards has previously been done using stochastic models (**Figure 2.6**). As both hazards are related to stormy weather conditions (e.g., cyclonic systems) (Zheng *et al.*, 2013) this interrelation has been quantified through the estimation of joint probabilities of occurrence (Lian *et al.*, 2013; K. Xu *et al.*, 2014; Zheng *et al.*, 2014; Klerk *et al.*, 2015). Lian *et al.* (2013) looked at the joint probability of extreme rainfall and sea surge in Fuzhou City, China for the years 1952 to 2008. The dependence structure, and therefore the joint probability of rainfall and sea level exceeding extreme levels was assessed using the Gumbel copula, from the class of extreme value copulas (**Figure 2.7**).

Lian *et al.* (2013) found that for their study area, 24 hours extreme rainfall and high sea level were positively dependent. This implies that these two hazards are compound hazards. **Figure 2.8** shows the joint probability of having an event associated with different 24 hours extreme rainfall return periods (5 to 50 yr) and tidal level (5 to 50 yr) established with a Gumbel copula.

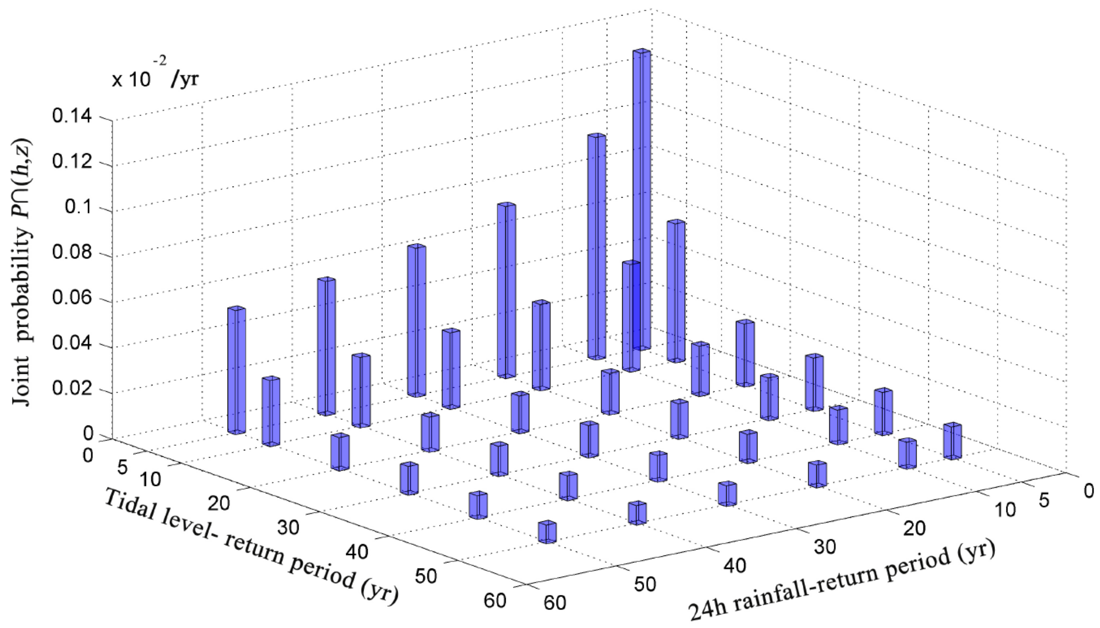

Figure 2.8: Bar graph of the joint probability of tidal level (sea level) and 24 hours rainfall as a function of their respective return periods (figure from Lian *et al.* 2013).

In coastal engineering, the joint probability of extreme waves and sea surges has also been widely studied with different classes of copulas (Masina *et al.*, 2015; Rueda *et al.*, 2016; Mazas and Hamm, 2017) or multivariate models (Coles and Tawn, 1994; Hawkes, 2008; Dong *et al.*, 2015).

2.3.2.2 Approach II: Empirical models

Empirical models are based on measurements and are observation oriented. In empirical models, empirical distributions are fitted directly to the observed data. Among empirical models, we defined two families: dependence measures and regressions. The main drawback of empirical models in comparison to stochastic and mechanistic models is the impossibility to extrapolate beyond the range of the data (Zou *et al.*, 2003).

2.3.2.2.1 Dependence measures

While looking at hazard relationship, a popular method is to compute dependence measure (Zheng *et al.*, 2013; Klerk *et al.*, 2015; Petroliagkis, 2018; Ward *et al.*, 2018). Dependence measures aim to describe how two (or more) variables are correlated. Several dependence measures including linear correlation (Pearson) or rank correlation (Spearman, Kendall) can be used to measure the strength of the association between variables (Hashemi *et al.*, 2015; Hao and Singh, 2016). The most popular dependence measure to quantify the dependence between two hazards is the Pearson linear correlation coefficient □ (Zou *et al.*, 2003):

$$\rho = \frac{\mathrm{cov}(x,y)}{\sigma_x \sigma_y} \qquad (2.2)$$

Where cov(x,y) the covariance of the two variables x and y, with associated standard deviations (respectively) σ_x and σ_y.

For an estimation of the dependence in the tails or extreme parts of the distributions, dependence measures previously presented might not be accurate and other dependence measures are more appropriate (Hao and Singh, 2016). Dependence between variables in the joint tail domain has been widely studied in the statistics literature (e.g., Coles and Tawn, 1991; Ledford and Tawn, 1997; Coles *et al.*, 2000; Heffernan, 2001; Heffernan and Tawn, 2004; Keef *et al.*, 2013; Zheng *et al.*, 2014). The dependence between variables in the tails can be classified as asymptotic dependence (or asymptotic independence) and the different diagnostics and measures developed are summarized in Heffernan (2001). Two variables can therefore be asymptotically independent but also have dependence at sub-asymptotic level. Dependence measures are often used as a first estimate of the potential relationship between two hazards and also support the selection process of an appropriate stochastic model (**Section 2.3.2.1**).

2.3.2.2.2 Regression

Regressions have been widely used to quantify interrelations between natural hazards (Costa and Schuster, 1988; Keefer, 2002; Koutroulis *et al.*, 2012; Suppasri *et al.*, 2012; Meng and Shen, 2014; Iordanidou *et al.*, 2016). Regression is a statistical method to measure changes in a dependent variable in response to changes in one or several independent variables (Chen *et al.*, 2014). There are many different types of regression models such as linear regressions, power regressions, logistic regressions or quantile regressions (Zou *et al.*, 2003; Nelder and Baker, 2006; Chen *et al.*, 2014; Hao *et al.*, 2018). Linear regressions are the most commonly used to estimate relationships between natural hazards (Caine, 1980; Keefer, 2002; Koutroulis *et al.*, 2012; Iordanidou *et al.*, 2016; Petroliagkis, 2018) and is often associated with the Pearson linear correlation coefficient (Eq. 2). The generalized linear model framework encompasses more sophisticated types of regressions such as the logistic regressions (appropriate when the dependent variable is dichotomous) (Nelder and Baker, 2006). In situations where we are more interested in high (or low) levels for hazards (e.g. an extreme quantile as opposed to the median), quantile regression provides a better approach than linear regression (Chen *et al.*, 2014; Hao *et al.*, 2018). Regressions have been particularly used for cascading hazards (**Figure 2.5**) as they include independent (primary hazard(s)) and independent (secondary hazard(s)) variables.

2.3.2.2.3 Example of empirical approach: two examples

Here we give two examples of empirical approaches. Our first is the *tail dependence between river flow and sea surge*. For hazard interrelation quantification, one often wants to focus on the extremes (Svensson and Jones, 2004; Dutfoy *et al.*, 2014). Svensson and Jones (2004) used the extremal dependence measures χ and $\bar{\chi}$ introduced by Coles *et al.* (1999) to study the extremal dependence between sea surge, river flow and precipitation in south and west Britain (**Figure 2.9**). These coefficients aim to measure the extremal dependence for bivariate random variables (X, Y) and assume initially that the marginal distributions of x and y are identical. The dependence measure χ is the probability of one variable being extreme given the other is extreme. The extremal dependence coefficient varies in the range [0;1] with a value of 0.0 meaning that the two variables are asymptotically independent and a value of 1.0 that they are asymptotically perfectly dependent. The dependence measure $\bar{\chi}$ estimates the level of dependence in the particular case of asymptotically independent variables.

Svensson and Jones (2004) highlighted statistically significant asymptotic dependence between river flow and daily maximum sea surge, two hazards that combine to form a compound hazard (**Figure 2.6**). In their study, this dependence is associated with overarching meteorological events (i.e., mid latitude cyclones). These events may cause both sea surge and high river flow (via precipitation). The characteristics of the studied catchment such as size can influence the results. For large catchment areas, time lags can become increasingly important, which can be used to capture the interrelations between sea surge and river flooding (Svensson and Jones, 2004; Zheng *et al.*, 2013; Klerk *et al.*, 2015; van den Hurk *et al.*, 2015).

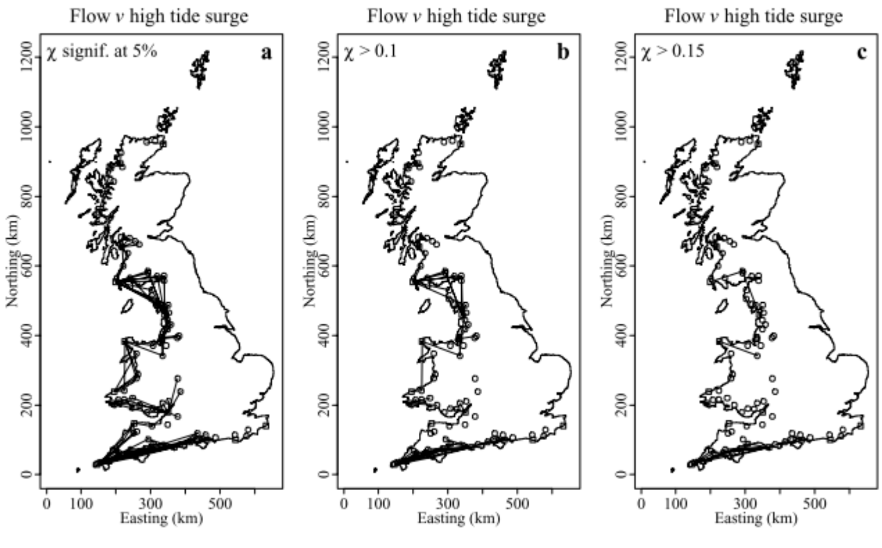

Figure 2.9: Example of an empirical approach: dependence river flow and daily maximum sea surge occurring at high tide around the coastline of the UK. Lines connect neighbouring station-pairs with χ exceeding (a) the 95% significance level, (b) 0.10, and (c) 0.15 (figure from Svensson and Jones. 2004)

Our second empirical approach example is one that is widely studied in terms of interrelations between hazards, *extreme rainfall and landslides* (e.g., Caine, 1980; Glade, 2000; Guzzetti *et al.*, 2007). According to our review, the quantification of rainfall-triggered landslides (triggering relationship, **Section 2.3**) has been mostly done through empirical models (**Figure 2.5**). Guzzetti *et al.* (2007) (amongst others) expressed this interrelation through a regression between rainfall intensity I (mm h^{-1}) and rainfall duration D (h) which gives a threshold for landslide triggering. This relationship is of the form of (Glade, 2000):

$$I = C \times D^{\alpha} \tag{2.3}$$

with, C and α constants.

As shown in **Figure 2.10**, this relationship varies depending on the region concerned, one of the main limitation of this approach. The triggering threshold also depends on other parameters such as the history of landslide occurrence, soil type, slope, and antecedent conditions. This last aspect has been addressed by Glade (2000) in New Zealand.

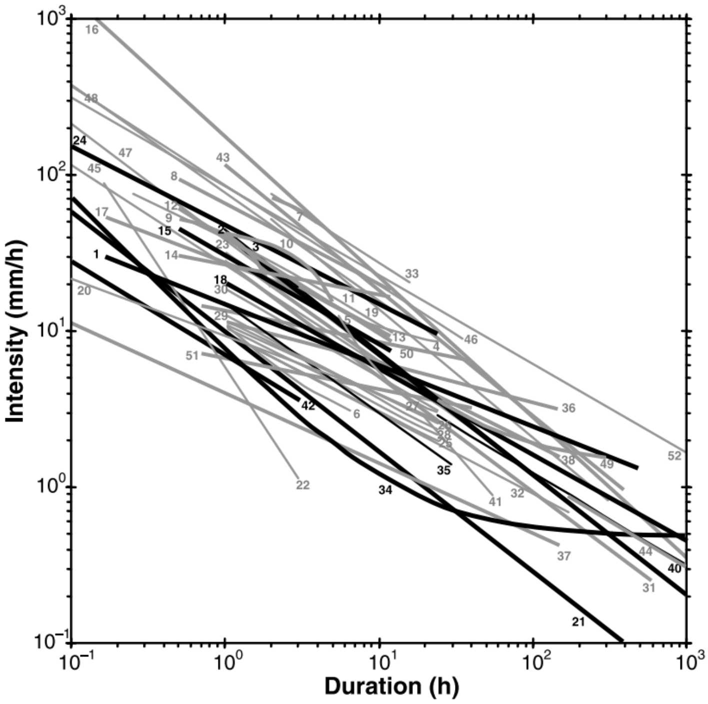

Figure 2.10: Intensity-duration relationship for landslide triggering in New Zealand (from Guzzetti *et al.* 2007)

2.3.2.3 Approach III. Mechanistic models

Mechanistic models are mathematically idealized representation of real phenomena (Devia *et al.*, 2015). They are based upon physical processes and mechanisms that rule the considered system operations. Usually, mechanistic models are applied on water bodies (Booij *et al.*, 1996; Geist *et al.*, 2009; Luger and Harris, 2010; Dutykh *et al.*, 2011), as the equations coming from fluid mechanics can be used. Mechanistic models are divided into two families: conceptual models and physical models.

2.3.2.3.1 Conceptual models

Conceptual models are widely used in hydrology (Nash and Sutcliffe, 1970; Devia *et al.,* 2015). In hydrology, conceptual models aim to describe all the components of hydrological processes with various interconnected reservoirs which represent the components of the flow of a river (e.g., infiltration, runoff, snowpack). Conceptual models need a large amount of input data (usually rainfall and temperature records) to assess different parameters through calibration. Examples of hydrological conceptual models include GR (Coron *et al.*, 2017), HBV, TOPMODEL and MORDOR (Devia *et al.*, 2015).

2.3.2.3.2 Physical models

Physical models aim to simulate the behaviour of different systems such as the atmosphere (Tinti *et al.*, 2003), the ocean (Klerk *et al.*, 2015), the climate (Kašpar *et al.*, 2017) and hydrological systems (Devia *et al.*, 2015; Bout *et al.*, 2018). Based on our literature database, physical models tend to use fluid mechanics, heat transfer equations or thermodynamic laws. In hydrology, the processes of water movement are represented by finite difference equations (Silvestro *et al.*, 2016). To model mechanistically extreme hydrological events, an extensive amount of data (e.g., soil moisture content, initial water depth, topography, topology, dimensions of river network) is required (Dietrich *et al.*, 2010; Bout *et al.*, 2018). This massive need for data is the main drawback of physically-based hydrological models compared to conceptual models (Devia *et al.*, 2015). Hydrodynamic models are based on the shallow water equation and are usually 1D or 2D with the modelled domain often represented with triangular meshes (Tinti *et al.*, 2003; Wang *et al.*, 2012; Silva-Araya *et al.*, 2018). This modelled domain can be discretized by numerical methods such as finite elements or finite volumes (Geist *et al.*, 2009). Physical models can overcome many weaknesses of the empirical or stochastic models because they use parameters which have physical meaning. However, they are often computationally intensive (Geist *et al.*, 2009; Luger and Harris, 2010; Borgonovo *et al.*, 2012).

2.3.2.3.3 Example of Mechanistic approach: Volcanic eruption triggering a Tsunami

Here we give an example of a mechanistic approach, that of a volcanic eruption triggering a tsunami. Hydrodynamic or hydraulic models based on shallow water equations are suitable to model hazard interrelations within bodies of water (sea, lake and river) (e.g., Pelinovsky and Poplavsky, 1996; Kumbier *et al.*, 2018). Tsunami characteristics allow the use of shallow-water equations to model the propagation and intensity of a tsunami wave given the characteristics of an earthquake or a submarine landslide (Geist *et al.*, 2009; Luger and Harris, 2010). Various studies have been conducted to develop operational code for the numerical modelling of tsunamis (e.g., Pelinovsky and Poplavsky, 1996; Dutykh *et al.*, 2011). Numerical models are also used to assess the effect of tsunamis generated by continental slope slides on particular shorelines (Geist *et al.*, 2009) or to better understand the effect of past tsunamis on particular areas (Power *et al.*, 2017).

Tinti *et al.* (2003) provide a thorough example of the mechanistic approach, using a hydrodynamic model to assess the interrelation between a volcanic eruption (here a pyroclastic flow) and tsunamis in the Gulf of Naples. From historical eruptions, Vesuvius can produce explosive eruptions with a large volume of pyroclastic flows. Tinti *et al.* (2003) considered two processes that could trigger a tsunami from pyroclastic flows: (i) the penetration of dense flows into the water, which is comparable to a landslide-induced tsunami; (ii) the overpressure pulse generated by light pyroclastic flow travelling on the sea surface over long distances. To estimate the influence of a pyroclastic flow, Tinti *et al.* (2003) estimated the pressure pulse that could be produced by a large Vesuvian eruption and propagated it over the whole Gulf of Napoli (**Figure 2.11**). Using the non-linear shallow water equations they found that the potential amplitude of a tsunami triggered by pyroclastic flows in the Gulf of Naples remains small (with the largest waves having an amplitude around 70 cm on the coastline), even including uncertainties around the set of parameters.

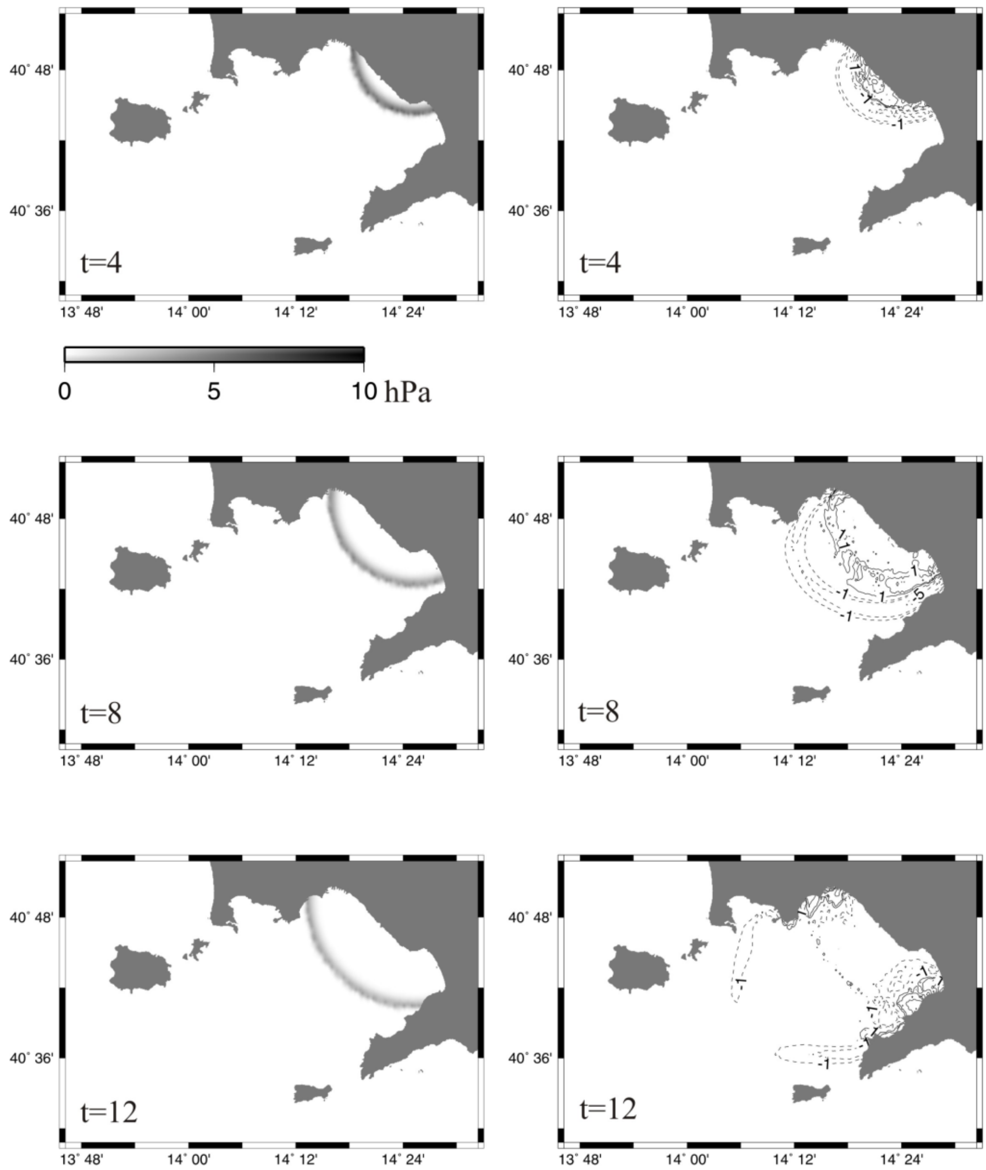

Figure 2.11: Pressure pulse-field (on the left) computed at different times, given in minutes. Water elevation fields (on the right) computed at the same instant. Time is measured from tsunami origin time and not from the beginning of the eruption. Contour lines labels are in cm. Positive/negative elevation curves are solid/dashed lines (figure from Tinti *et al.* 2003)

2.3.3 Hazards, models and interrelations

In **Section 3.2** we defined three different modelling approaches for hazard interrelations quantification (stochastic, empirical, mechanistic) along with associated modelling families and methods. We will now focus on the links between these modelling approaches/families/methods with the previously defined hazard categories (atmospheric, geophysical, hydrological) and three of the five interrelation types (change condition, compound, triggering). Within the three modelling approaches presented in **Section 2.3.2**, some modelling methods are more popular for hazard interrelation studies (i.e., they occurred more frequently in our hazard interrelationship model database, **Appendix B Table B1**).

Figure 2.12a shows the number of uses of modelling methods amongst the 70 natural hazard interrelations studies (79 uses overall: stochastic 27 uses; empirical 31 uses; mechanistic 21 uses), with 6 of our 70 references using more than one modelling methods. There are different reasons for a given reference having more than one use: (i) the same modelling method has been applied to different hazard combinations (Carey *et al.*, 2003; van den Hurk *et al.*, 2015); (ii) different modelling methods are compared using the same hazard combination (Zheng *et al.*, 2014; Sadegh *et al.*, 2017); (iii) different modelling methods are combined for a given hazard combination (Dietrich *et al.*, 2010; van den Hurk *et al.*, 2015; Petroliagkis, 2018).

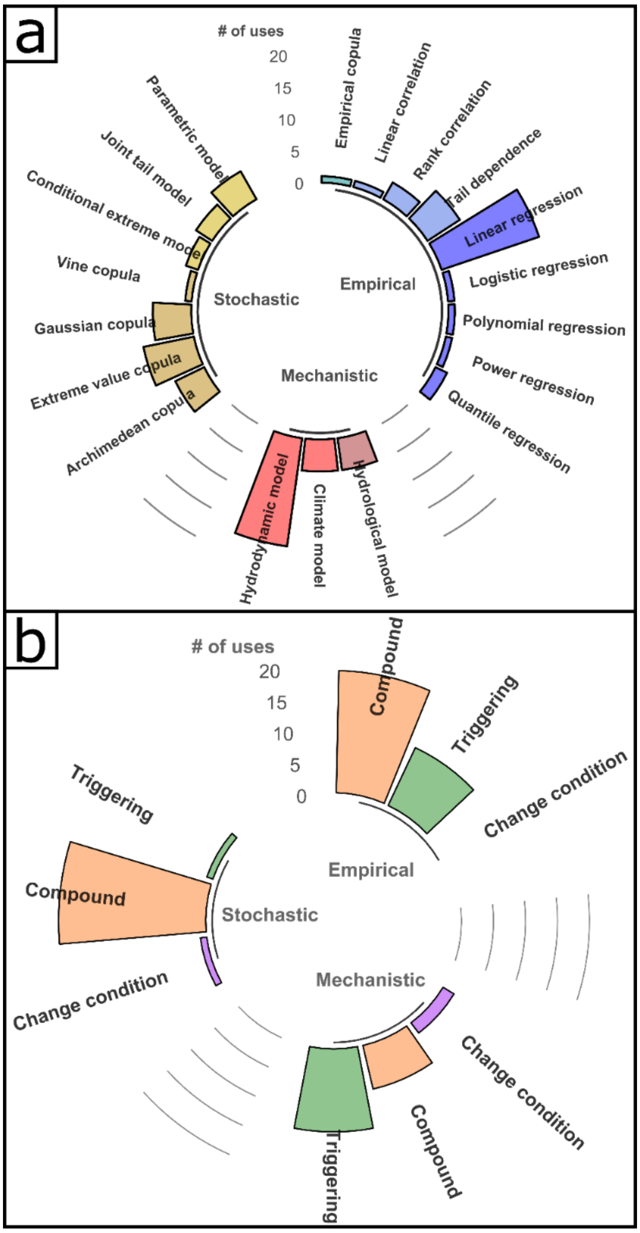

Figure 2.12: Circular barplot for each of the three modelling approaches (stochastic, empirical, and mechanistic): (a) the modelling method number of uses from Figure 2.7 (out of 79 model method uses); (b) three interrelation types frequency (triggering, compound, change condition). Data based on our interrelationship database (Appendix B Table B1). Colour groupings used approximate those given in Figures 2.5 to 2.7.

Figure 2.12a shows that amongst the 70 references (79 uses) for hazard interrelationship modelling:

- Stochastic modelling approach: *extreme copulas* method are the most prevalent (30% of stochastic modelling uses, 8 occurrences out of 27. This is explained by the fact that among the 14 hazards selected in this review, several are the extreme occurrence of environmental variables (e.g. extreme temperature).
- Empirical modelling approach: *linear regressions* methods are the most prevalent (51% of empirical modelling uses, 16 occurrences out of 31). This is probably due to their relative ease of use and interpretation.
- Mechanistic modelling approach: *hydrodynamic models* are the most prevalent (81% of mechanistic modelling uses, 17 occurrences out of 21). Hydrodynamic models are relevant in describing many different types of hazard interrelations (e.g., river flooding, coastal flooding, compound flooding, tsunami).

Figure 2.12b shows the frequency of the three interrelation types (triggering, compound, change condition) (total of 77 uses in our hazard interrelationship database) as a function of the three modelling approaches (stochastic, empirical, mechanistic). The reason for one reference having more than one use is analogous to the ones mentioned above. We find from **Figure 2.12b**:

- Stochastic modelling approach: the *compound* interrelation type is by far the most prevalent (22 out of 25 uses, 90%). Stochastic models presented in this study do not capture temporal effects or feedback loops, even if the use of lag times or conditional probabilities can overcome this limitation (van den Hurk *et al.*, 2015; Liu *et al.*, 2018). However, as compound hazards are two (or more) hazards that act together on a given region and time (**Section 2.2.2**), stochastic models are particularly relevant for these as can be seen in **Figure 2.12b.**
- Empirical modelling approach: the *compound* interrelation type (20 out of 30 uses, 67%) is twice as prevalent as the *triggering* interrelation type (10 out of 30, 33%). The relative simplicity of empirical models offers a way to obtain a quantitative assessment of a hazard interrelation when mechanistic models (next) cannot be applied.
- Mechanistic modelling approach: the *triggering* interrelation type (13 out of 22 uses, 59%) is more prevalent than *compound* (7 out of 22) and *change condition* (2 out of 22) types. The complexity and level of precision of mechanistic models allow one to represent a broad range of interrelations including amplification or triggering effects.

Within our three modelling approaches, we defined six families, two for the stochastic and mechanistic approaches and three for the empirical approach (one of which is shared with the stochastic approach). In **Figure 2.13,** we consider the modelling family as a function of the category of hazard studied (atmospheric, geophysical, hydrological). We start with the 70 references in our interrelationship database. Of these, 68 references have one pair of hazards discussed, and two sources have 3 (Carey *et al.*, 2003) and 2 (van den Hurk *et al.*, 2015) different hazard combinations. For the 73 hazard combinations in our database, we then paired each natural hazard with the model family used in the reference. For example, Bout *et al.* (2018) examine the interaction of rainfall (atmospheric natural hazard category) and landslides (geophysical hazard category) using a hydrodynamic model (physical model family) and Bevacqua *et al.* (2017) examine sea surge (hydrological hazard category) and river flooding (also hydrological hazard category) using vine copulas (copula model family). Therefore, we would count 1 x physical model in the atmospheric hazard category, 1 x physical model family in the geophysical hazard category, and 2 x copula model family in the hydrological hazard category. In **Figure 2.13**, there are 56 instances for atmospheric, 22 for geophysical and 89 for hydrological natural hazard categories. We then count the percentage of instances within each natural hazard category as a function of the six model families on a radar chart.

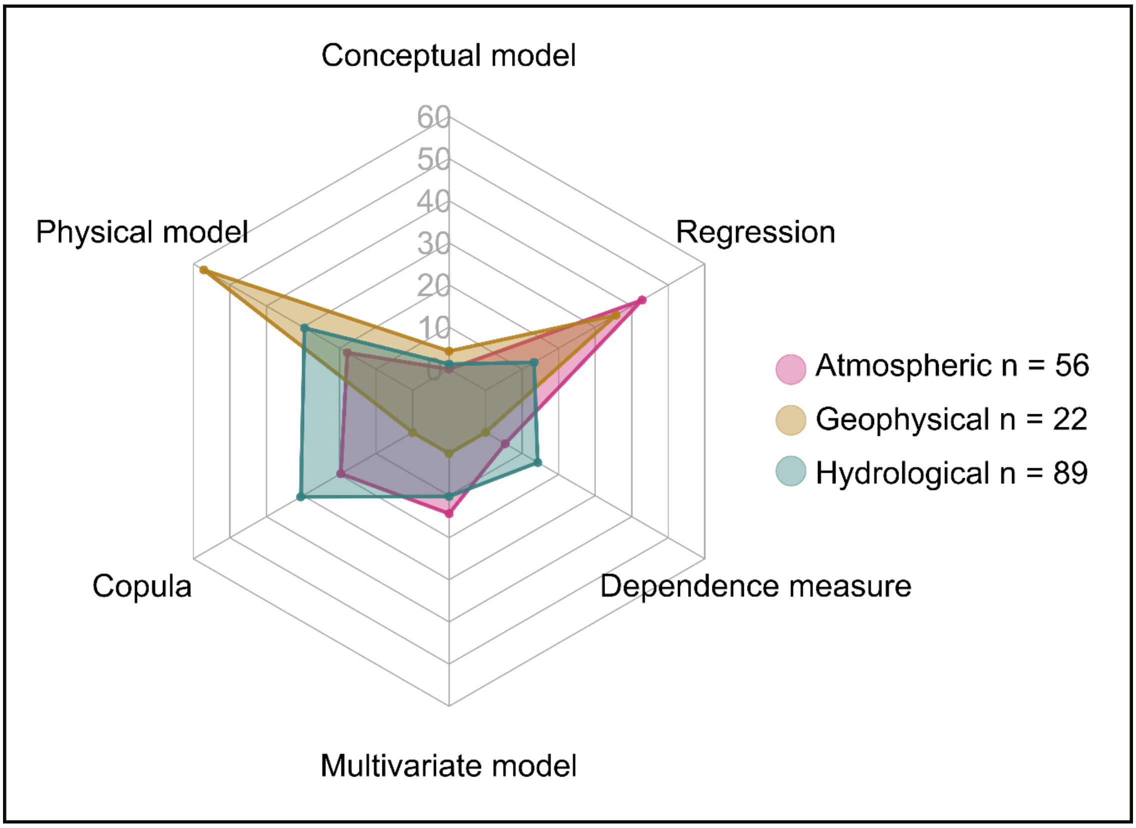

Figure 2.13: Radar chart of the use (in %) within each model family by hazard groups. Percentages are out of the number of instances within each natural hazard category (given in legend).

From **Figure 2.13** we find:

- For atmospheric hazards, the regression modelling family is largely dominant (43%) in our interrelation database. This can be explained by the complexity of modelling interrelations between atmospheric hazards such as hail, lightning or wind and the lack of robust or large enough datasets for some of these hazards (Webb, 2016).
- Geophysical hazards are predominantly either physical models (57%) or regression model (36%). Physical models are favoured when the resources are sufficient (data

quantity, computational power) but regressions can be applied with lower quantities of data.

- Hydrological hazards have been studied with every model family in this review. Copulas (31%) and physical models (30%) are the most popular as they can provide results from a wide range of scenarios and extrapolate beyond the observations.

In **Section 2.3**, we reviewed the use of 19 different modelling methods for the quantification of interrelations between 14 different natural hazards. We will now discuss some of the results presented in **Section 2.2** and **Section 2.3**.

2.4 Discussion and conclusions

The study of multi-hazard is a relatively new field (Kappes *et al.*, 2012b; Gill and Malamud, 2014; Pescaroli and Alexander, 2018; Terzi *et al.*, 2019) and still not unified in its terminologies and approaches. This critical review article has aimed to use grey- and peer-review literature to critically identify and compare current research in quantifying (natural) hazard interrelations. In this critical review article we aspire to add to others in the multi-hazard community who have reviewed and identified relevant modelling approaches to quantify different kinds of interrelations between hazards and risks (e.g., Liu *et al.*, 2015; Gallina *et al.*, 2016; Hao and Singh, 2016; Terzi *et al.*, 2019). By doing an extensive review, including a broad range of natural hazards involving different time and space scales, we have aimed to contribute to a better understanding on the state-of-the-art regarding hazard interrelations quantification and offer a clear view on weaknesses and strength of several methods in different contexts. For this purpose, a natural hazard interrelationship literature database of 146 sources (**Appendix A**) was created and used to explore the following: (**Section 2.2.1**) *terminology* surrounding multi-hazard interrelations; (**Section 2.2.3**) *quantification models* for interrelations between hazards. This section will discuss the five following themes: (a) the diversity of modelling methods for quantifying hazard interrelations; (b) some of the main drivers in modelling method selection for hazard interrelations quantification; (c) limitations (uncertainties) of the modelling methods; (d) limitations of the present review; (e) perspectives for extending this interrelationship classification to more than two hazards.

The diversity of modelling methods for quantifying hazard interrelations: In this chapter, we have focussed on the quantification of interrelations between two (vs. three or more) hazards, for 14 different natural hazards. We used matrices (**Figures 2.5** and **2.6**) to display our findings, similar to other studies (e.g., Gill and Malamud, 2014; Decker and Brinkman, 2015). We used these matrices to display the use of different modelling approaches (stochastic, empirical, mechanistic) for hazard interrelations quantification. The wide variety of modelling approaches reviewed highlights the lack of a unified framework for multi-hazard quantification. Indeed, this variety is not surprising, given the range of natural hazards considered in this study (**Table 2.1**) across geophysical, atmospheric and hydrological categories. Different types of hazard interrelations that extend across varying spatial and temporal scales require a panoply of modelling methods, and a coupling between these models (Leonard *et al.*, 2014). The difficulty to model all hazard interrelations in the same manner is highlighted in **Section 2.3**, where two matrices are displayed (for 14 natural hazards) to present (i) cascading hazards (**Figure 2.5**) and (ii) compound hazards (**Figure 2.6**). Later, we summarize (**Figure 2.7** and **2.12**) the 19 modelling methods that are most prominently used in the literature across 14 natural hazards for quantifying the interrelationships between these hazards. The figures and database (**Appendices A** and **B**) are a resource that can be consulted by the reader to be more aware of (i) those modelling methods (including reference to specific literature) currently directly being done for a given hazard interrelationship pair, (ii) other potential modelling methods that are being applied across all hazards studied here. For example, the interrelation between drought and extreme temperature have been studied with empirical (quantile regression) and stochastic methods (Gaussian copula) (Meng and Shen, 2014; Serinaldi, 2016), but it might also be studied using other methods in the database such as conditional extreme models or other types of regression depending on the needs.

Some of the main drivers in modelling method selection for hazard interrelations quantification. It is not the purpose of this study to rank modelling methods in general. Nevertheless, we can argue from **Section 3.3** that some approaches or even models seem more applicable to given interrelation types or hazard categories and hazard types. Indeed, relationships where one hazard triggers or changes the conditions for another imply causality, which is not undertaken by the stochastic models reviewed in this work. Similarly, interrelations between compound (associated) hazards cannot be modelled with regression models which imply that one parameter (hazard) is influencing the other (causality). For example, interrelations of any geophysical hazard with any hazard category (geophysical, atmospheric, hydrological) are mostly quantified with physical models or regressions while interrelations of a hydrological hazard with any hazard category are mostly studied with copulas or physical models. As most of the hazard interrelations studies in our database are case studies, model choice is conditioned by the studied area, the hazards studied or the quality of the data available. But the choice of a quantification method when studying interrelations between hazards goes beyond the previously cited constraints; the context and the purpose of the study play an important role. For example, a study with engineering purposes might be more prone to use multivariate model to extrapolate beyond the range of observations while a study focusing on the impact of a particular hazard interrelation might favour a physical model.

Limitations (uncertainties) of the modelling methods. There are many limitations for the 19 modelling methods discussed here, with one of the major ones being data quality. Empirical models are more sensitive to data quality because they are data-driven. In stochastic modelling approaches, additional uncertainties come from the different assumption made (e.g., statistical distribution choice, dependence model selection). In the case of mechanistic models, data are also central to calibrate and validate the model, and other uncertainties arise from some assumptions and simplifications inherent to the model.

Limitations of the present review. One of the limitations of the model classification presented in this review is that it is designed for interrelations between two hazards. Multi-hazard modelling becomes effectively more complicated when going to higher dimensions (i.e., more than two). Empirical models such as regression accept multiple parameters. This can be useful to create a hazard index or indicators for multiple hazard risk (Marzocchi *et al.*, 2012; Nadim *et al.*, 2013; Westen *et al.*, 2017). Mechanistic models can represent the behaviour of several environmental variables. But, their scales often do not correspond to the needs of a multi-hazard study (Leonard *et al.*, 2014).

Regarding stochastic models, most of the parametric copulas in use for bivariate hazard models lack flexibility when going to higher dimensionality (Bevacqua *et al.*, 2017; Hao *et al.*, 2018). Besides, the variability of the dependencies among the different pairs of hazards makes it harder to model (Bevacqua *et al.*, 2017). A multivariate extreme model such as the conditional extreme model is suitable for high-dimension (Heffernan and Tawn, 2004); although, this model has not been tested for high dimensional multi-hazard modelling yet. The present review does not cover all the possible methods for quantifying natural hazard interrelations. Methods such as agent-based modelling or event trees could have been included, but these latter are weak in addressing uncertainties (Terzi *et al.*, 2019) and their relevance is limited when dealing with a low number of variables. The physical phenomena behind natural hazards can offer better insight or better characterisation of the interrelation, particularly for meteorological hazards. These events have been sketched in the literature and are mostly considered as predictors or triggering factors (Liu *et al.*, 2016; Bevacqua *et al.*, 2017). Other limitations of this review include those inherent in any critical and systematic review (e.g., see discussion in Gill and Malamud, 2014; Reichenbach *et al.* 2018, for inherent weaknesses), such as potentially not having covered all relevant literature to 'capture' the current use of models relevant for quantifying hazard interrelations. We believe, though, that our review methodology (**Section 2.2**) is robust enough to capture not all literature, but the majority of modelling methods and approaches currently in use for the 14 hazards we explored in this review chapter.

Perspectives for extending this interrelationship classification to more than two hazards. To address the challenge of extending our classification to a high number of variables, recent research conducted suggests pair-copula construction (PCC) (Bevacqua *et al.*, 2017, Lui *et al.*, 2018) and network approaches (Nadim *et al.*, 2013; Leonard *et al.*, 2014; Gill and Malamud, 2016; Liu *et al.*, 2017) to model multi-hazard events. PCC is also called vine copula (Bedford and Cooke, 2002; Hashemi *et al.*, 2016; Bevacqua *et al.*, 2017, Lui *et al.*, 2018). The decomposition which the vine copula framework allows one to select different bivariate copulas for each pair of variables, providing great flexibility in dependence modelling (Brechmann and Schepsmeier, 2013; Hao and Singh, 2016). Among the network approaches, Bayesian networks are very promising with an increasing use not only in multi-hazard risk assessment studies but also in dependability analysis, risk analysis and maintenance studies (Gutierrez *et al.*, 2011; Duval *et al.*, 2012; Weber *et al.*, 2012; Poelhekke *et al.*, 2016; Kwag and Gupta, 2017; Sperotto *et al.*, 2017). Bayesian networks have lots of benefits when dealing with a great number of variables, particularly their versatility and their capacity to model both dependability and causality relationships (Weber *et al.*, 2012). Moreover, Bayesian networks are not originally designed to deal with continuous variables (Sperotto *et al.*, 2017) and that is why these were not discussed in **Section 2.3**. Non-parametric Bayesian networks which associate the structure of Bayesian network and copulas (Hanea, 2010; Hanea *et al.*, 2010, 2015) represent one way to overcome this limitation. For example, this method has been used to study multiple dependence between river discharge and storm surge in the USA during a hurricane (Couasnon *et al.*, 2018). The association of copulas and Bayesian networks is a dynamic area of study and different approaches have already been developed with very few applications to natural hazards (Hanea, 2010; Elidan, 2010; Bauer and Czado, 2016; Pircalabelu *et al.*, 2017).

In conclusion, we have used our literature database composed of 146 references to identify trends for hazard interrelation. We first highlight trends in terminology to define hazard interrelations from these group hazard interrelations into five hazard interrelationship types: triggering, change condition, compound, independence and mutually exclusive. Our critical review focuses on 14 different natural hazards from three hazard categories (atmospheric, geophysical, hydrological) and the possible interrelations that can occur between these. From the 14×14 possible hazard interrelation couples within our set of hazards, we find quantification methods applications to 24 different interrelations. Two matrices are created to illustrate this in practice, one for cascading hazards (temporal order in the multi-hazard event) and one for compound hazards (two or more hazards acting together). We then identify three modelling approaches (stochastic, empirical, mechanistic) including 19 modelling methods to quantify hazard interrelations between two hazards for 14 hazards. We then synthesize the results of our classification of quantification methods for hazard interrelationships and propose an outlook on the modelling approaches used regarding the category of the hazards studied and the type of the interrelation between these latter. In this context, using an appropriate modelling method combined with a better understanding of physical phenomena leading to hazards interrelations (multi-hazard events) might be one of the keys toward efficient hazard interrelation quantifications.

Afterwords:

This afterwards is written after the publication of Tilloy *et al.* (2019) and included here as part of this thesis, as further discussion points on the usefulness and limitations of the approach described in this chapter.

The classification of hazard interrelations made in this chapter uses a mix of statistical criteria and process-based criteria. Both criteria are useful to characterize hazard interrelations. Process-based criteria are more related to causal interactions while statistical connections are particularly useful when processes are not fully understood or not modellable. Two classifications (with bridges) could then be useful and associated with statistical (stochastic/empirical) or mechanistic models.

The categorisation of models done in this chapter and displayed in **Figure 2.8** can be subject to discussions and readjustments. Although it was designed through a rigorous literature review on hazard interrelations (**Appendicies A** and **B**), this classification does not include all possible methods to model hazard interrelations. The categorisation includes 19 different modelling methods and is intended to capture a map of the main work on hazard interrelation modelling as of 2019. The three modelling approaches defined in **Section 2.3.2** may not be the most meaningful for the set of methods reviewed. While mechanistic models represent an unambiguous category, the boundary between stochastic and empirical models is more porous as copulas and regressions both depend on observational data and have stochastic aspects.

A distinction between stochastic models which would include copulas, regressions and dependence measures could be more meaningful than the one currently displayed in **Figure 2.7**. Copulas are multivariate models; therefore, the separation of stochastic models between parametric (copula) from non or semi-parametric (Joint tail model, conditional extremes) could also be more relevant than the current partition. Another meaningful categorisation within stochastic models could separate distribution models (copula, multivariate extreme models), which model a whole distribution from expectation models (regressions) which model the expected value of an outcome variable from one or several input variables. Some methods presented in **Figure 2.7** are also fundamentally interlinked (e.g., tail dependence measure used as parameters for extreme value copula) or can be combined (e.g. copula regression, Masarotto and Varin, 2017). Despite these shortcomings, the author believes that this classification, and more importantly, the 19 modelling methods reviewed in this chapter, remain meaningful in the context of hazard interrelation modelling.

Chapter 3: The multi-hazard landscape of Western Europe

Summary:

Natural hazards can be associated with geophysical or meteorological processes. In that context, understanding potential drivers and processes leading to hazard interrelations is of prior interest. This chapter aims to go beyond the study of pairs of hazards and to examine the multi-hazard landscape of the European Atlantic Region (EAR). A total of 16 natural hazards were selected to characterize the multi-hazard landscape of the EAR. These 16 natural hazards are grouped based on physical drivers (e.g., meteorological, geophysical) and prior knowledge on interrelations between hazards. Five sets of interrelated hazards occurring in a given space-time frame named multi-hazard networks are created: Ground movements, convective storms, extratropical cyclones, compound dry hazards and compound cold hazards. A range of sources has been reviewed to create these networks and find evidence of past occurrences of these networks, called multi-hazard events. This catalogue also aims to bring together different sources and databases of single hazard events. Sources are of the following types: (i) Single hazards catalogues (e.g., BGS Tsunami, SurgeWatch); (ii) Catalogue of reported hydrometeorological events (e.g., Met Office, Infoclimat); (iii) Disaster databases (e.g., EM-DAT); (iv) Peer review articles. A catalogue of 50 events (10 per network) is constructed to illustrate the approach. Based on this catalogue, spatial and temporal scales, as well as dominant hazard and hazard interrelations of each of the five multi-hazard networks, are assessed semi-quantitatively. Finally, 34 freely available datasets to quantify hazard interrelations within multi-hazard networks are reviewed. The strengths and weaknesses of different types of datasets are assessed along with their applicability to different multi-hazard networks. Information about spatial and temporal scales, dominant hazards and datasets provide support for hazard interrelation modelling.

3.1 Introduction

The interdependence between different hydrological, climatological or geophysical extreme events and hazards has been highlighted in **Chapter 2** and recent literature (Sadegh *et al.*, 2017; Liu *et al.*, 2018). The classification of natural hazard interrelations provided in **Chapter 2** is part of a general effort to increase our understanding of connected hazards and extreme events (Gill and Malamud, 2014; Liu *et al.*, 2016; Zscheischler *et al.*, 2020). Recent studies have grouped interrelated hazards into events and analysed their potential drivers (Hillier *et al.*, 2020; Zscheischler *et al.*, 2020). Past notable events have been analysed through pathway schemes to improve the understanding of processes leading to compound or multi-hazard events (Schauwecker *et al.*, 2019). Climatic and geophysical characteristics of a region play an important role in the development of natural hazards and natural hazard interrelations (Terzi *et al.*, 2019). The aim of this chapter is to go beyond the study of pairs of hazard and to understand the multi-hazard landscape of a given region (i.e. the relevant single natural hazards and the processes by which they may interrelate to generate combinations or cascades of hazards) (Gill *et al.*, 2020). Regional studies of potential hazard interactions have been undertaken in several parts of the world (Tarvainen *et al.*, 2006; Kappes *et al.*, 2012a; Gill *et al.*, 2020).

This chapter is tailored to be relevant to western Europe and in particular, to France and the United Kingdom (see **Chapter 1**). The definition of the boundaries of a region to study can be related to various factors (e.g., political, physiographical, geological, climatic, biological) which influence the multi-hazard landscape. In that context, for western Europe, the concept of a biogeographical region is relevant. A biogeographical region is an area of similar character in terms of the biota (fauna & flora) present in it (EEA, 2020). The extent and boundaries of each region have been determined by changes in climate and the movement of continents, and accompanying changes in the physical and climatic barriers to migration (Calow, 1999). This relative homogeneity in term of biota is the justification for the definition of the boundaries of the region to study. The European Union delineated nine biogeographical regions for Europe (EEA, 2002). Among these is the European Atlantic Region (EAR) which includes the whole of United Kingdom and the western part of France; the two countries account for more than 60% of the Atlantic region, and the region studied in this chapter.

This chapter is structured as follows: in **Sect. 3.2**, the characteristics of the EAR are discussed, including the climate to which the region is exposed is presented (**Sect. 3.2.1**) and relevant natural hazards for the EAR are identified using blended sources of evidence (**Sect. 3.2.2**). In **Sect. 3.3**, interrelated hazards are grouped into distinct multi-hazard networks. Multi-hazard networks construction is based on physical drivers (e.g., meteorological, geophysical) and prior knowledge on interrelations between hazards. Five multi-hazards networks relevant for the EAR are designed and presented in **Sect. 3.3**. In **Sect. 3.4**, A catalogue of 50 multi-hazards events (10 per network) is constructed to illustrate the approach (**Sect. 3.4.1**). Based on this multi-hazard event catalogue, the prevalence of each hazard and hazard interrelation in each group is studied (**Sect. 3.4.2**). Finally, an overview of freely available numerical data to quantitatively study multi-hazard events from the five previously defined group is provided (**Sect. 3.4.3**).

3.2 The European Atlantic Region (EAR)

To understand the multi-hazard landscape of a given region, its climatic and physiographic characteristics are investigated. **Figure 3.1** is a physiographic map displaying the European Atlantic region (EAR) and highlighting the general low elevation of the region, in particular in coastal areas. The EAR has an area of 830,000 km^2 and includes territories of 10 countries with France and the UK representing respectively 32% and 30% of the total area (European Environment Agency, 2003). From **Figure 3.1,** we see that the region has a significant proportion of lowlands in coastal areas, particularly in the Netherlands, West Britain and in the Bay of Biscay. Mountain ranges of the British Islands and Britany are of ancient origin and therefore relatively modest in height due to erosion (Ager, 1975; Clayton, 1996) (≤ 1200m above sea level). Higher mountains (≥ 1200m above sea level) in Spain and Portugal are the result of more recent geological processes associated with the Genesis of the Alpes and the Pyrenees (Ager, 1975). Major active faults in the region are situated in the Iberic peninsula and Belgium (Giardini *et al.*, 2014).

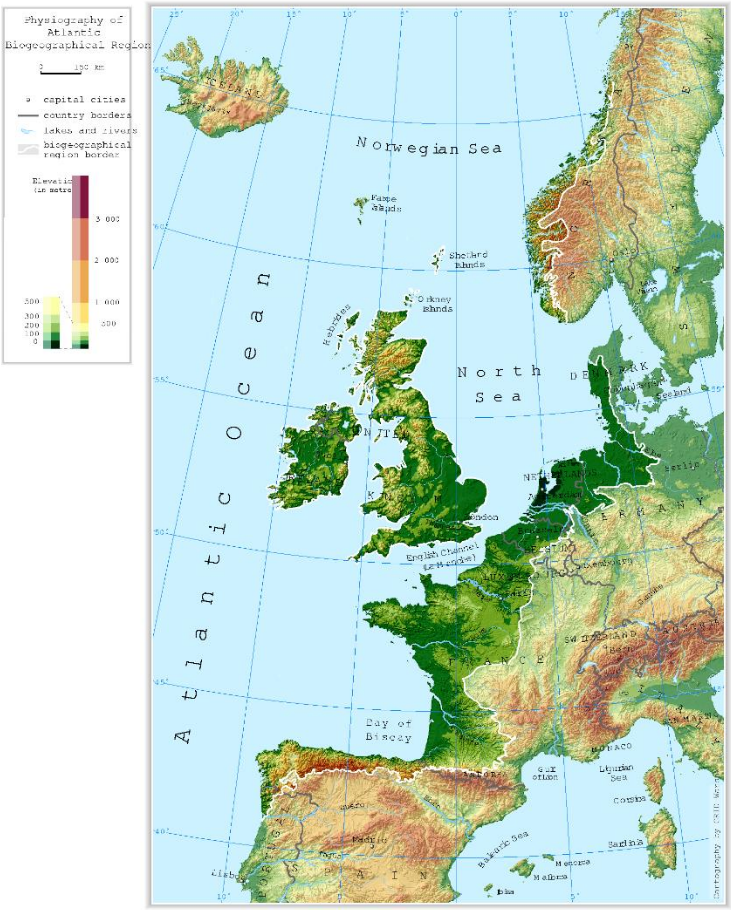

Figure 3.1: Physiographic map of Western Europe. The European Atlantic Biogeographical region is highlighted with a white line and is inclusive of all or parts of ten countries, of which the UK and western France account for 62% of the EAR total area. Figure from EEA (2003).

3.2.1 The climate of the European Atlantic Region

To better understand the climate of the EAR (and its potential driving influence for natural hazards), the Köppen-Geiger climate classification was used. This classification was developed in the late 19th century (Köppen, 1884) and is still widely used today to, for example, assess impacts of climate change (Mahlstein *et al.*, 2013). The Köppen-Geiger system classifies climate into five main classes and 30 sub-types. The classification is based on the seasonality of monthly air temperature and precipitation (Beck *et al.*, 2018b). **Figure 3.2** represents the Köppen-Geiger classification map for Europe for the period 1980–2016 at 1 km resolution. This map was developed by Beck *et al.* (2018b). Despite small variations, the EAR has on overall a temperate (no dry season, warm summer) climate (Cfb) highlighted in light green in **Figure 3.2**. The relative climatic homogeneity of the region follows its biogeographical characteristics, as different climates in a similar class share common vegetation characteristics (Beck *et al.*, 2018b). The climate is highly influenced by the Atlantic, which provides precipitation throughout the year to the region (Hulme and Barrow, 1997). However, there are significant disparities between the northern part of the region (e.g., British Islands) and the Southern part, which is bordered by drier regions of Portugal and Spain (**Figure 3.2**).

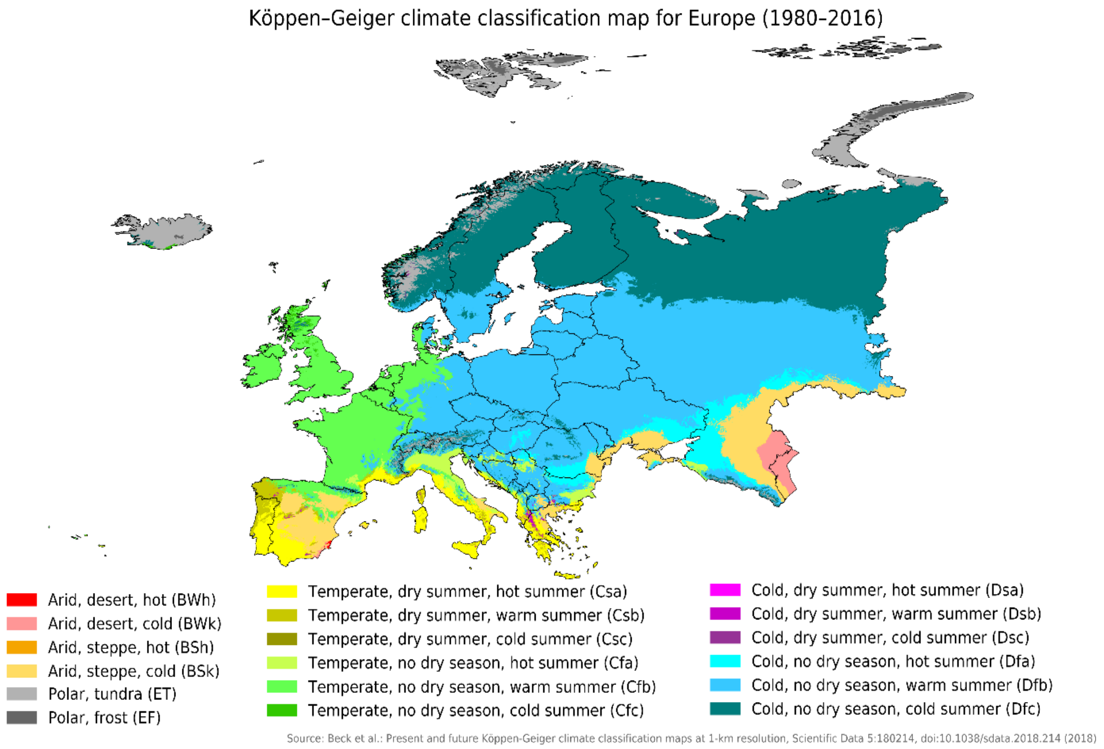

Figure 3.2: Köppen-Geiger climate classification of Europe. From (Beck *et al.*, 2018b)**.**

In the winter months, the EAR is exposed to storms and extra-tropical cyclones (ETCs), which account for over 70% of total precipitation in some areas (Hawcroft *et al.*, 2012). ETCs can also bring strong wind, high waves and storm surges (Ulbrich *et al.*, 2009; Brönnimann and Martius, 2013). Despite not having a dry season, the Atlantic region has been hit by severe drought and heatwaves in the past decades during the summer (Fink *et al.*, 2004; Barriopedro *et al.*, 2011). Hot and dry summers often lead to wildfire outbreaks (Sutanto *et al.*, 2020). However, the occurrence of drought and heatwaves is expected to increase in the 21st century due to anthropogenic climate change (Baldwin *et al.*, 2019). Even if convective storms are not as prevailing in the Atlantic region as they are around the Mediterranean sea (Drobinski *et al.*, 2014), severe thunderstorms occur in the summer and autumn, often leading to flash floods (Acreman, 1989; Anderson and Klugmann, 2014; Webb and Elsom, 2016).

3.2.2 **Natural hazards in the European Atlantic Region**

Every year, the EAR is exposed to a wide variety of natural hazards, such as floods, extreme wind, wildfires (Lung *et al.*, 2013; Roberts *et al.*, 2014). The particular hazards in a given sub-region of the EAR vary depending on that sub-region's climate, geology or topography (Schmidt-Thomé and Kallio, 2006). From **Section 3.2.1**, it is possible to identify physiographic and climatic preconditions for natural hazards in the EAR. This approach is a standard process while screening natural hazards relevant to an area (Liu *et al.*, 2016; Gill *et al.*, 2020). For example, while coastal lowlands are more vulnerable to extra-tropical cyclones (Thorne, 2014; Van Den Hurk *et al.*, 2015), mountainous areas are more prone to landslides (Van Den Eeckhaut *et al.*, 2012;

Valenzuela *et al.*, 2019). Southern parts (Spain, Portugal, France) of the EAR can see significant wildfire outbreaks in summer (Pereira *et al.*, 2011), while floodplains of northern France and the Rhine valley often experience riverine floods (Disse and Engel, 2001). The identification of relevant natural hazards for the EAR is performed on three main criteria: (i) frequency of occurrence, (ii) spatial relevance, (iii) potential to impact energy infrastructures. The relevance of natural hazards regarding these three criteria is assessed using three main sources (each associated to a criteria):

(i) Frequency of occurrence. The Emergency Events Database (EM-DAT):

The Emergency Events Database (EM-DAT) is a record of disasters maintained by the Centre for Research on the Epidemiology of Disasters (CRED, 2018). EM-DAT contains data on the occurrence and effect of over 15,300 disasters (as of 2020) in the world from 1900 to present. There are several criteria for a disaster to be included in the dataset (CRED, 2018):

- ≥ 10 people died or
- ≥100 people affected or
- declaration of a state of emergency or a call for international assistance.

Despite the international use and recognition of EM-DAT, the quality of this disaster database faces biases (e.g., threshold biases, spatial aggregations) discussed by Jonkman (2005) and Gall *et al.* (2009) and geographic information are provided at the country level. Disaster profiles for the 10 countries which are part of the EAR were extracted (France, UK, Germany, Portugal, Denmark, Netherlands, Belgium, Spain, Norway, Ireland) from EM-DAT (CRED, 2018) over the period 1900–2018. The EAR covers approximately 36% of the aggregated area of these 10 countries, meaning that some disasters retrieved and displayed in **Figure 3.3** might not have occurred within the EAR. The occurrence distribution of natural disasters from this database is displayed in **Figure 3.3**. It offers an estimate of the frequency of occurrence of different natural hazards to which the EAR is exposed. However, the small number of coastal floods recorded might be an artefact of the dataset.

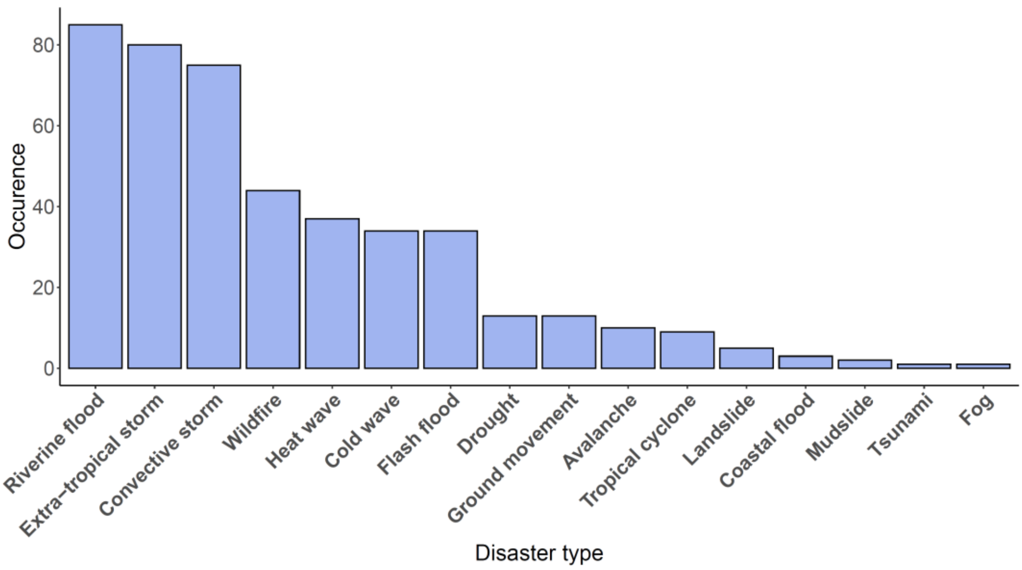

Figure 3.3: Occurrences of the 16 most frequent natural disaster subtypes in Europe in the period 1900–2020. Data from CRED (2020).

(ii) Spatial relevance. The Spatial Effects and Management of Natural and Technological Hazards in Europe - ESPON 1.3.1:

To assess the spatial relevance of natural hazards to the EAR, the main source used is the report ESPON 1.2.3.1. The ESPON (European Spatial Planning Observation Network) program finances and monitors research project on the territorial effects of major spatial developments in Europe (ESPON, 2006). Under the ESPON 2006 program, one thematic project addressed "Spatial effects of natural and technological hazards". The main aim of this project is to represent the spatial patterns of natural and technological hazards in administrative regions of the ESPON space (i.e., Europe). As part of this program, 11 natural hazards relevant to Europe were selected based on several indicators including:

– their probability of occurrence,
– the potential damage they produce,
– their spatial relevance and
– their relation to the climates of Europe.

As a result, Schmidt-Thomé and Kallio (2006) produced hazard maps showing the spatial relevance of the 11 natural hazards to Europe (avalanches, drought, earthquakes, extreme temperatures, floods, forest fires, landslides, storm surges, tsunamis, volcanic eruptions, winter and tropical storms) at a sub-national level (NUTS (Nomenclature of Territorial Units for Statistics) 3). This spatial resolution allows one to pull out the most relevant hazards for the EAR from these maps:

– drought (Spain and Portugal),
– floods (UK, France, Netherlands),
– forest fires (Spain and Portugal),

- landslides (UK, Spain, Norway),
- storm surges (UK, Netherlands, Denmark) and
- winter and tropical storms (all EAR).

Maps displaying the spatial distribution of seismic hazards (Giardini *et al.*, 2014), landslides (Van Den Eeckhaut *et al.*, 2012), lightning (Anderson and Klugmann, 2014), and hail (Punge and Kunz, 2016), have also been consulted to assess the spatial relevance of these hazards.

(iii) **Impact on energy infrastructures.** The Energy Technologies Institute (ETI) Natural Hazards Project:

The ETI Natural Hazards Project (ETI, 2018) is an initiative funded by the Energy Technologies Institute and delivered by EDF Energy, the Met Office and Mott Macdonald. This project aimed to summarise the state of the art on natural hazard characterisation for a variety of natural hazards. It focuses on natural hazards that may negatively impact energy infrastructures in the UK and is mainly aimed toward engineers of the energy sector. Natural hazards considered in the project were selected based on criteria such as the spatial relevance to the UK, potential to damage energy infrastructures and gaps in hazard characterisation. The 10 natural hazards "classes" were characterized: extreme temperatures, extreme wind, extreme precipitation, river flooding, coastal flooding, seismic volcanic and geological hazards, lightning, hail, space weather, marine biological fooling. Among these 10 hazards classes, 6 were identified as representing important hazards that can impact infrastructure across the UK (ETI, 2018): extreme temperatures, extreme wind, extreme precipitation, river flooding, coastal flooding, seismic volcanic and geological hazards. This information was used to identify hazards that have the potential to impact the energy sector and its infrastructures.

There is reasonable accordance between the disasters from EM-DAT displayed in **Figure 3.3** and those hazard selected in the two other projects (Schmidt-Thomé and Kallio; 2006, ETI, 2018). Moreover, the EM-DAT classification offers hints to group natural hazards into multi-hazard networks. For each criterion, the relevance of each natural hazard is assessed with a semi-quantitative score on three levels: (-) not mentioned, (*) mentioned, (**) mentioned and important. By combining the relevance scores on each of these three criteria**,** 16 natural hazards were selected to characterize the multi-hazard landscape of the EAR. The 16 natural hazards are associated with at least one of the EM-DAT disasters displayed in **Figure 3.3** and have an overall relevance score of at least ***.

The 16 hazards retained, their abbreviations and relevance regarding each criterion are listed in **Table 3.1**. Natural hazards with very high impact and very low probability (e.g., extreme solar eruption), low impact and high probability (e.g., fog), low spatial relevance (e.g., volcanic eruption) and not directly threatening energy infrastructures (e.g., avalanches) were ruled out during the screening process. Soil moisture excess and landslide were retained despite having a potentially low impact on energy infrastructure (**Figure 3.1**) because they play an important role in hazard cascades and flood generation (Gill and Malamud, 2014; Berghuijs *et al.*, 2019). There are some differences between the hazards selected in this chapter, and the ones used in **Chapter 2**; hazard categories are however identical to the ones presented in **Chapter 2.** Even if these are not equally threatening different parts of the Atlantic region, the 16 hazards selected are believed to be relevant to define the multi-hazard landscape of the European Atlantic region.

Table 3.1: The 16 hazards relevant to the EAR considered in this chapter broken up into four natural hazard categories: (1) geophysical, (2) atmospheric, (3) hydrological, (4) biophysical. Relevance scores are displayed for (i) frequency of occurrence; (ii) spatial relevance; (iii) impact on energy infrastructure. The overall relevance is the sum of the 3 relevance scores.

Hazard categories	Hazards	Abbreviation	(i)	(ii)	(iii)	Overall relevance
Geophysical	*1.1 Earthquake*	**EQ**	*	*	**	****
	1.2 Landslide	**LS**	*	**	-	***
Atmospheric	*2.1 Lightning*	**LI**	**	*	*	****
	2.2 Extreme rainfall	**RA**	**	**	**	******
	2.3 Extreme wind	**WI**	**	**	*	*****
	2.4 Extreme hot temperature	**EH**	**	*	**	*****
	2.5 Extreme cold temperature	**EC**	**	*	**	*****
	2.6 Hail	**HA**	**	*	*	****
	2.7 Extreme snowfall	**SN**	*	*	*	***
Hydrologic	*3.1 Storm surge*	**SS**	*	**	**	*****
	3.2 Extreme waves	**WA**	*	*	*	***
	3.3 Riverine Flood	**FL**	**	**	**	******
	3.4 Tsunami	**TS**	*	**	**	*****
	3.5 Drought	**DR**	*	**	*	****
	3.6 Soil moisture excess	**SO**	*	**	-	***
Biophysical	*4.1 Wildfire*	**WF**	**	**	*	*****

3.3 Multi-hazard networks in the European Atlantic Region

In **Chapter 2**, interrelations between 14 natural hazard types have been considered in pairs. In this chapter, the aim is to define events that include different natural hazards that are interrelated, i.e. multi-hazard networks. Multi-hazard networks are based on (i) physical drivers of the single hazards or the hazard interrelations (e.g., meteorological, geophysical) and (ii) the interrelations between those hazard types (see **Chapter 2**). A multi-hazard network is therefore composed of a set of interrelated hazards prone to be triggered by the same underlying processes and occurring in given space-time frame. In a univariate study of extreme events, the need for independent extremes is often motivated by the development of methods to identify and characterize independent events. For example, Bernardara *et al.* (2014) developed a framework to identify independent physical events such as storms, floods, and heatwaves (Bernardara *et al.*, 2014; Mazas and Hamm, 2017). This present work aims to enlarge this framework to the multi-hazard cases. In this section, the procedure used to create multi-hazard networks is presented (**Section 3.4.1**). Then, the five multi-hazard networks developed for the EAR are presented (**Section 3.4.2**). Finally, these multi-hazard networks are illustrated with a database of past occurrences of major multi-hazard events in the EAR (**Section 3.4.3**). Multi-hazard events are past occurrences of multi-hazard networks (even partial).

3.3.1 Defining multi-hazard networks

To sketch different multi-hazard networks, physical drivers that influence the occurrence of different single natural hazard types were examined. Depending on the hazards considered in this chapter (**Table 3.1**), physical drivers for multi-hazard networks can be linked to (i) hydrometeorological conditions, (i) geophysical conditions, (iii) both hydrometeorological and geophysical conditions. Multi-hazard networks as defined in this thesis can be related to concepts developed over the last two decades:

- *Predictors* (e.g., precipitation, sea level pressure): to model compound flooding event (Bevacqua *et al.* 2017).
- *Trigger factors*: to estimate both the frequency and magnitude of multiple natural hazards (Liu *et al.* 2016).
- *Scenarios*: to analyse volcanic eruptions (Selva *et al.*, 2019), tsunamis (Tinti *et al.*, 2003), or earthquakes (Schmidt *et al.*, 2011).
- *Physical events*: to sample independent extreme events (Mazas and Hamm, 2017)
- *Generic events*: The Integrated Research on Disaster Risk (IRDR) Data Report on Perils Classification and Hazards Glossary is the result of a global effort to classify natural hazards on different levels and to group hazards or perils into sets of generic events (IRDR, 2014).

From the IRDR (2014) data report and **Figures 3.1–3.3**, it is possible to identify the following multi-hazard networks:

- Extratropical cyclone (hydrometeorological)
- Convective storm (hydrometeorological)
- Ground motion (geophysical)

Extratropical cyclones and convective storm are two distinct storm systems, which can be distinguished from one another by their mechanism of development (growth), their structure, their spatial scale and their typical lifetime (Frame *et al.*, 2017). Another way to identify multi-hazard networks is to examine the relationships between natural hazards (See **Chapter 2**). For example, heatwaves and drought are interrelated with a compound interrelation and change conditions for wildfires (Tilloy *et al.*, 2019; Sutanto *et al.*, 2020). Following this approach, it is, therefore, possible to derive two more multi-hazard networks:

- Compound dry hazards (hydrometeorological)
- Compound cold hazards (hydrometeorological)

Every hazard listed in **Table 3.1** belongs to one (or more) of the five multi-hazard networks defined previously. The five multi-hazard networks used in this thesis and the natural hazards that these include are summarized in **Figure 3.4**.

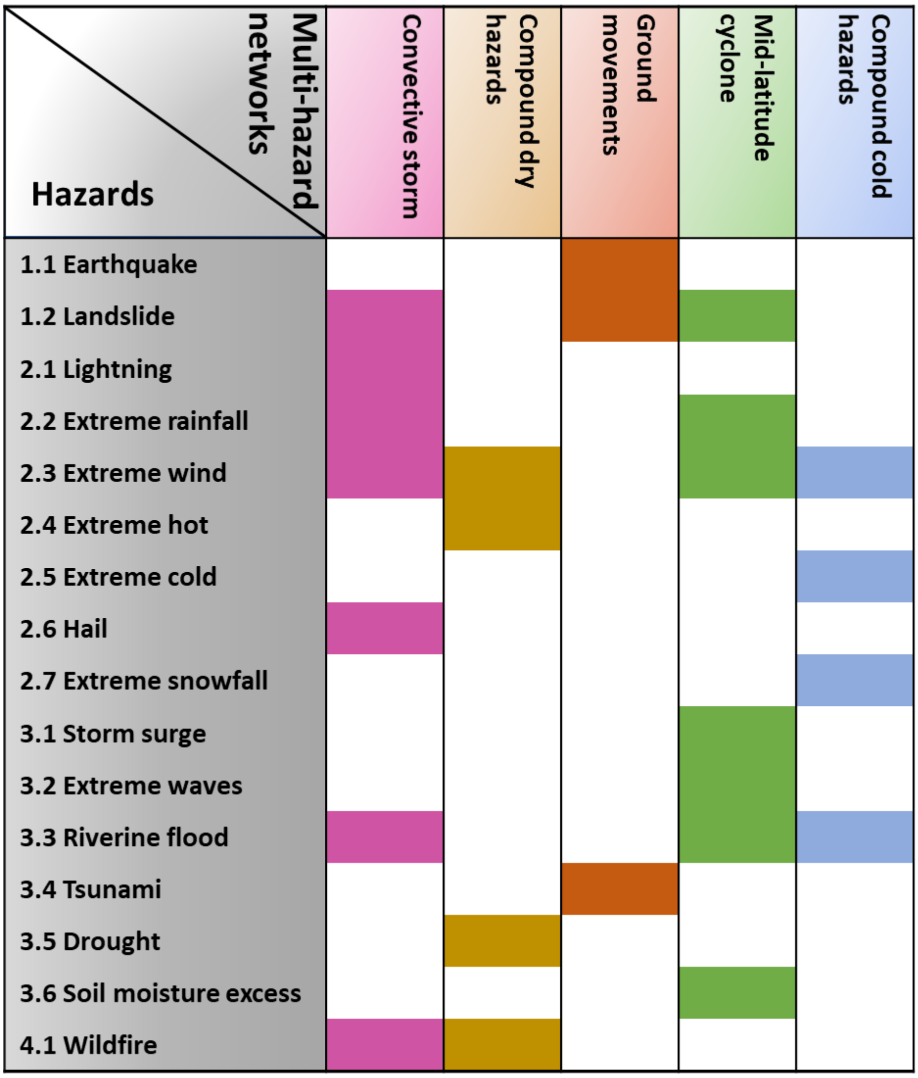

Figure 3.4: The five multi-hazard networks discussed in Chapter 3 (convective storm, compound and dry hazards, ground movement, mid-latitude cyclone, compound cold hazards) and associated hazards broken up into four natural hazard categories: (1) geophysical, (2) atmospheric, (3) hydrological, (4) biophysical.

The allocation of each natural hazard to a multi-hazard network is based on both prior knowledge of hazard interrelations (Gill and Malamud, 2014; Tilloy *et al.*, 2019) and on theoretical knowledge about the attributes of defined multi-hazard networks (e.g., convective storm are often associated with lightning and/or extreme precipitation). Justification of this classification and evidence of its relevance are provided in **Section 3.2.2** and **Section 3.4.1**. It is important to note that some natural hazards belong to several multi-hazard events; for example, extreme rainfall and extreme wind are both part of mid-latitude cyclones and convective storms. The relationship between those two hazards differs regarding the multi-hazard networks to which they belong.

Once multi-hazards networks and their associated hazards are defined, one can focus on the nature of the interrelations between the hazards and the interrelations network. Networks have often been used to represent multiple interrelations between natural hazards and other risk factors (Liu *et al.*, 2015; van Westen and Greiving, 2017; Terzi *et al.*, 2019). Here, the results and evidence from **Chapter 2** are used to develop interrelation networks for each of the five multi-hazard events.

These networks include the three main types of interrelations discussed in **Chapter 2**: (i) triggering, (ii) change condition and (iii) compound. Networks also provide useful support for the design of multi-hazard scenarios or pathways (Schauwecker *et al.*, 2019).

3.3.2 Multi-hazard Networks

In this section, an overview of the causes, dynamics and seasonality of the five multi-hazards networks is provided, along with conceptual hazard interrelation networks. Primary assumptions about hazard interrelations within each multi-hazard networks are mainly based on previous work from Gill and Malamud (2014) and results from **Chapter 2**. Detailed descriptions of each hazard interrelation are backed with evidence from the literature. Sources used to design networks of natural hazards associated with each of the five multi-hazard networks presented in **Figure 3.4** are displayed in **Table 3.2**.

Table 3.2: Supporting literature used in the design of the five multi-hazard networks. Sources are mostly peer-review articles and reports from organisations.

Multi-hazard networks	**Supporting Literature**
Ground Motion	Rodríguez *et al.* (1999); Keefer (2002); Malamud *et al.* (2004); Gill and Malamud (2014); Deker and Brinkman (2014); Geist and Parsons (2006); Suppasri *et al.* (2012); ETI (2019); Geist *et al.* (2009); Clague and Stead (2012); DEFRA (2005); Chester (2001); Fritsche and Fäh (2009); Dutykh *et al.* (2011); Fan *et al.* (2019)
Convective Storm	Gill and Malamud (2014); Decker and Brinkman (2015); Price and Federmesser (2006); Simon *et al.* (2017); Piepgrass *et al.* (1982); Carey *et al.* (2003); Schultz *et al.* (2011); Anderson and Klugmann (2014); Iordanidou *et al.* (2016); Gatlin and Goodman (2010); Lang and Rutledge (2002); Koutroulis *et al.* (2012); Houze and Hobbs (1982); Jebson (2007); Dotzek *et al.* (2009); Poljansek el al. (2017)
Extratropical Cyclone	Gill and Malamud (2014); Deroche *et al.* (2014); Roberts *et al.* (2014); Dowdy and Catto (2017); Sharkey (2018); Priestley *et al.* (2018); Ulbrich *et al.* (2009); Hawcroft *et al.* (2012); Schoenenwald (2013); Weiss (2014); Haigh *et al.* (2016); Bogaard *et al.* (2013); CCR,2020, Eden (2008), Poljansek el al. (2017)
Compound Dry hazards	Sutanto *et al.* (2020); Zscheischler and Seneviratne (2017); Vogel *et al.* (2020); Radovanovic *et al.* (2019); Perkins (2015); Alexander (2011); EFFIS (2020); Tedim *et al.* (2018); Pereira *et al.* (2011); Ganteaume *et al.* (2013); Stefanon *et al.* (2012); Ruffault *et al.* (2020); Turco *et al.* (2019), Poljansek el al. (2017), Manning *et al.* (2018, 2019)
Compound Cold Hazards	Twardosz and Kossowska-Cezak (2016); Añel *et al.* (2017); Hulme and Barrow (1997); Hall and Blöschl (2018); Berghuijs *et al.* (2019); Booth (2007); Schauwecker *et al.* (2019); Eden (2008); Hillier *et al.* (2020); Gill and Malamud (2014)

In this section, the five multi-hazard systems presented in **Figure 3.4** will be examined in detail. For each multi-hazard system, four different aspects will be discussed as follows:

- A definition of the system is provided;
- Hazard interrelations within the system are described;
- The spatial extent of the event is discussed;
- Seasonality (when applicable) and temporal extent of the multi-hazard network are evaluated.

3.3.2.1 Ground movements

Definition

Ground movements are events where substantial quantities of material (soil or water bodies) are displaced by geomorphic phenomenon. Such events are generally associated with earthquakes. Earthquakes are the ground shaking due to the movement of the Earth's tectonic plates at a fault zone (Alexander, 1993). Earthquake magnitude and depth are the main factors of landscape disturbance and play a major role in landslide distribution (Fan *et al.*, 2019). However, ground movements can occur without being directly associated with an earthquake (e.g., the 1979 Nice Tsunami) (Dan *et al.*, 2007).

Hazard interrelations

Hazards from **Table 3.1** associated with a *ground motion* multi-hazard network are earthquakes, landslides and tsunamis. Besides triggering other earthquakes (aftershocks), the ground motion induced by an earthquake can either trigger or increase the probability of landslide by reducing soil cohesion. The relationship between earthquake and landslides is now well documented (Rodríguez *et al.*, 1999; Keefer, 2002; Malamud *et al.*, 2004), but it is still hard to quantify due to the complexity and the number of factors involved (e.g., earthquake magnitude, earthquake depth, geology, slope gradient). The primary triggers of tsunamis are earthquakes (Geist and Parsons, 2006; Suppasri *et al.*, 2012), land and submarine landslides (Geist *et al.*, 2009), although these can also be triggered by impact events (Pierazzo and Artemieva, 2012). However, tsunamis also trigger landslides when reaching the coastline (Clague and Stead, 2012). Landslides have the potential to trigger and change the conditions for other landslides (Gill and Malamud, 2014). Moreover, earthquakes, landslides and tsunamis can also damage human infrastructures, such as dam breaking or watercourse containment failure, and the failure of bridges. The network of natural hazard interrelations corresponding to a ground movement multi-hazard network is displayed in **Figure 3.5.** The relationships between those hazards were assessed qualitatively according to the reviewed literature.

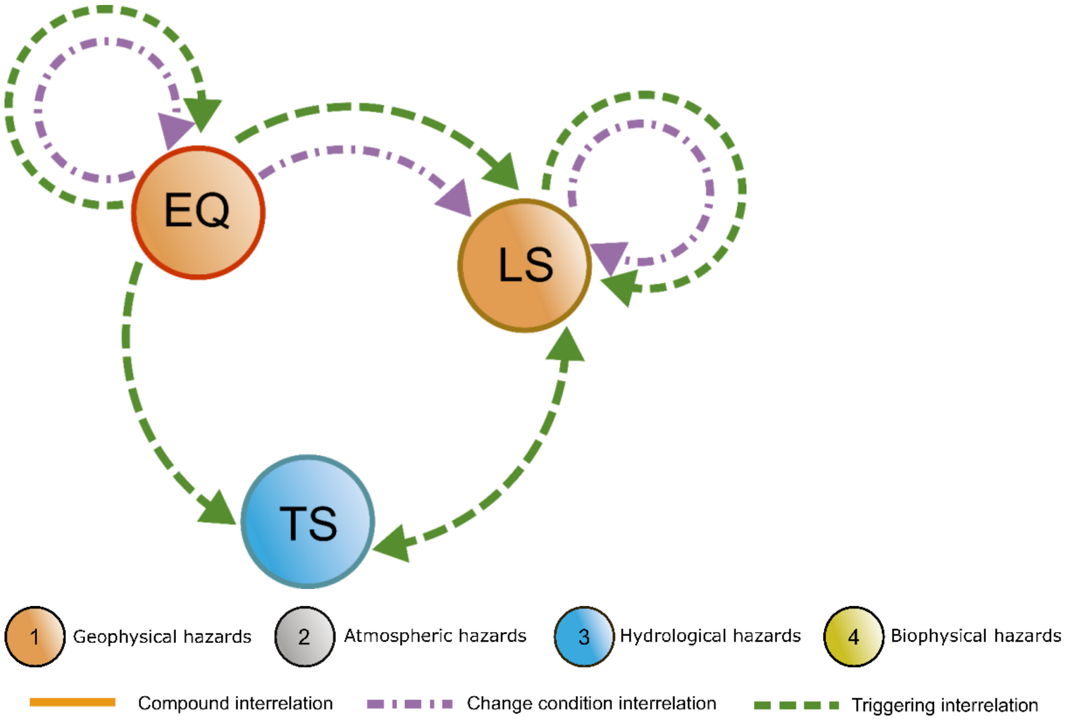

Figure 3.5: Network of natural hazards associated with a ground movement multi-hazard networks with their interrelation types. The associated hazards include EQ (earthquakes), LS (landslides) and TS (tsunamis). Arrows (see legend) indicate compound, change condition and triggering interrelations between the hazards. Built according to hazard matrices developed in Chapter 2, Gill and Malamud (2014) and literature in Table 3.2.

Spatial extent

Ground movement events develop over variable areas. The level of shaking during an earthquake is related to the distance from the epicentre, the magnitude but also the ground conditions (ETI (Energy Technologies Institute), 2018). The total area of all landslides triggered by earthquake scales with the earthquake magnitude (Malamud *et al.*, 2004; Meunier *et al.*, 2007). The spatial extent of the earthquakes and the aerial region over which subsequent landslides occur also depends on the magnitude of the earthquake. Tsunamis pose a threat to European coasts (Chester, 2001); however, the potential spatial extent of a tsunami generated by an earthquake or a landslide is believed to be relatively local (DEFRA, 2005; Lambert and Pedreros, 2012).

Temporal extent & seasonality

Ground movements associated with the direct energy of earthquakes are usually short-duration events. Nonetheless, significant earthquakes are often followed by aftershocks (Fritsche and Fäh, 2009) which modify the temporal frame of such events. Earthquake-triggered landslides generally occur in the minutes to hours after the ground shaking (Fan *et al.*, 2019). However, the consequences of large continental earthquakes can be observed years to centuries after they occur (Fan *et al.*, 2019). The arrival time of a tsunami on a coast mostly depends on the distance from the origin of the tsunami (DEFRA, 2005; Dutykh *et al.*, 2011).

3.3.2.2 Convective storms

Definition

A convective storm is a meteorological event, primarily controlled by moisture, temperature, and upward wind (Dotzek *et al.*, 2009). Also called thunderstorms, those events develop when warm air is trapped underneath much colder air. The warm, containing more humid, air rises, water vapour condenses in small droplets and clouds called cumulonimbus are formed (Jebson, 2007). Mostly occurring during the summer season, or warm times of the year, convective storms can be divided into different types (Houze and Hobbs, 1982; IRDR, 2014):

- *Multi-cell storms*: A system composed of several convective cells.
- *Squall line*: A group of storms arranged in a line.
- *Supercell*: A system composed of one massive convective cell, which can last more than one hour.
- *Mesoscale Convective System* (MCS): A collection of thunderstorms that can cover a wide area and last several hours.
- *Derecho*: A long-period windstorm associated with thunderstorms.

Hazard interrelations

A prevailing natural hazard within a convective storm is lightning. Indeed, the electrical activity at the origin of lightning results from convective processes. Lightning can be used as a proxy for thunderstorms (e.g., Price and Federmesser, 2006; Simon *et al.*, 2017) and has been used to track thunderstorms (Strauss *et al.*, 2013), to identify them (Gatlin and Goodman, 2010), or for nowcasting (Schultz *et al.*, 2011). Lightning has the potential to initiate wildfires during dry thunderstorms (García-Ortega *et al.*, 2011). Convective storms can also be marked by heavy precipitation. The relationship between extreme rainfall and lightning has been analysed using linear regressions (Piepgrass *et al.*, 1982), or the squared Pearson correlation coefficient (Iordanidou *et al.*, 2016) with different spatial scales, temporal windows and time lags. Heavy precipitation can trigger river flooding or landslides (Jaroszweski *et al.*, 2015; Schauwecker *et al.*, 2019). During a convective storm, extreme wind can also occur, these wind are usually called downburst (Dotzek and Friedrich, 2009). A downburst was defined as a strong downdraft that induces an outburst of damaging winds on or near the ground (Fujita, 1978). Downbursts usually have small spatial and temporal scales; however, the wind speed in those wind event can reach greater than 200 km h^{-1} (Fujita, 1990). Hail also frequently occurs during thunderstorms (Punge and Kunz, 2016). Despite not systematically co-occurring, these hazards are all associated with convective storms. **Figure 3.6** represents a synthetic network of the natural hazards involved in a convective storm. The relationships between those hazards were assessed qualitatively.

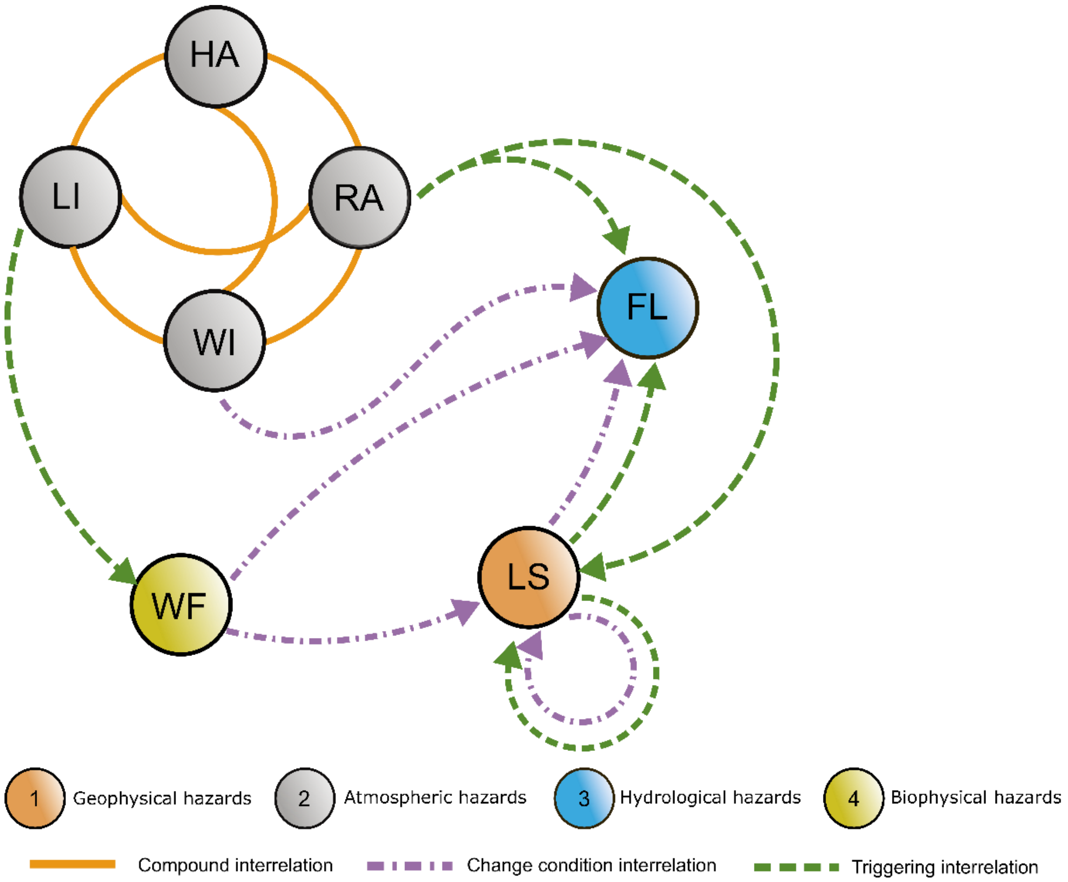

Figure 3.6: Network of natural hazards associated with a convective storm with their interrelation types. Arrows and arcs (see legend), indicate compound, change condition and triggering interrelations between the hazards Built according to hazard matrices developed in Chapter 2, Gill and Malamud (2014) and literature in Table 3.2.

Spatial extent

Depending on the type of convective event, thunderstorms could be localized (multi-cell storm) or extend up to hundreds to thousands of square kilometres (mesoscale) (Hand *et al.*, 2004; Frame *et al.*, 2017).

Temporal extent & seasonality

It has been shown that a ''typical'' convective event lasts approximately 1 h (Lang and Rutledge, 2002). Piepgrass (1982) found an average duration of 107 minutes for a convective event. However, thunderstorms do not always occur in isolation and can be grouped in mesoscale complexes. It has been shown (Morel and Senesi, 2002) that in Europe, Mesoscale Convective Systems last on average 5.5 hours and can last up to more than 20 hours. Convective storms are more likely to occur during the warm season as they are related to the convection process. In the UK, it corresponds to the summer months and the beginning of autumn (Anderson and Klugmann, 2014).

3.3.2.3 Extratropical cyclone

Definition

Extratropical cyclones (also called mid-latitude storms) are meteorological features occurring in the midlatitudes of the earth (Catto, 2016). Midlatitudes are between latitude 23° and 66° in both the northern hemisphere and southern hemisphere. In Europe, these events mainly occur during the "extended" winter (ONDJFM) (Ulbrich *et al.*, 2009; Deroche *et al.*, 2014; Roberts *et al.*, 2014). Extra-tropical cyclones are low-pressure systems that usually form at the interface between warm and cold air masses (Catto, 2016). This interface, a front, then develops into a wave shape (Dowdy and Catto, 2017; Sharkey, 2018). Extra-tropical cyclones have historically brought widespread damages to western Europe, because of their associated hazards but also because they tend to occur in series (Frame *et al.*, 2017; Priestley *et al.*, 2018).

Hazard interrelations

The passage of extratropical cyclones is usually associated with strong winds and heavy precipitation (Ulbrich *et al.*, 2009; Frame *et al.*, 2017). Indeed, in many parts of western Europe, over 70% of total precipitation is associated with extratropical cyclones (Hawcroft *et al.*, 2012). Heavy precipitation during extra-tropical cyclones, which often occur on already saturated soils in winter (e.g., winter 2020 in Great Britain), triggers floods and landslides in mountainous areas (e.g. Storm Klaus, 2009). However, the intensity of extra-tropical cyclones and their impacts have historically been measured with its associated wind speed (Schoenenwald, 2013). In the ocean, extreme wind trigger waves that can cause severe damages to coastlines (Weiss, 2014; Haigh *et al.*, 2016). Storm surges, partly due to the low atmospheric pressure over a broad area of the ocean and the wind of the storm pushing the subsequent higher level of water in the ocean, can result in extreme waves to cause coastal flooding and landslides (Bogaard *et al.*, 2013). In 1999, after storms Lothar and Martin, numerous natural dams composed of unrooted trees were reported in South-west France, increasing the risk of river flooding (CCR,2020). On some occasions, flashes of lightning may also occur in the frontal regions associated with extratropical cyclones (Frame *et al.*, 2017). **Figure 3.7** represents a synthetic network of the natural hazards involved in an extratropical cyclone. The relationships between those hazards were assessed qualitatively.

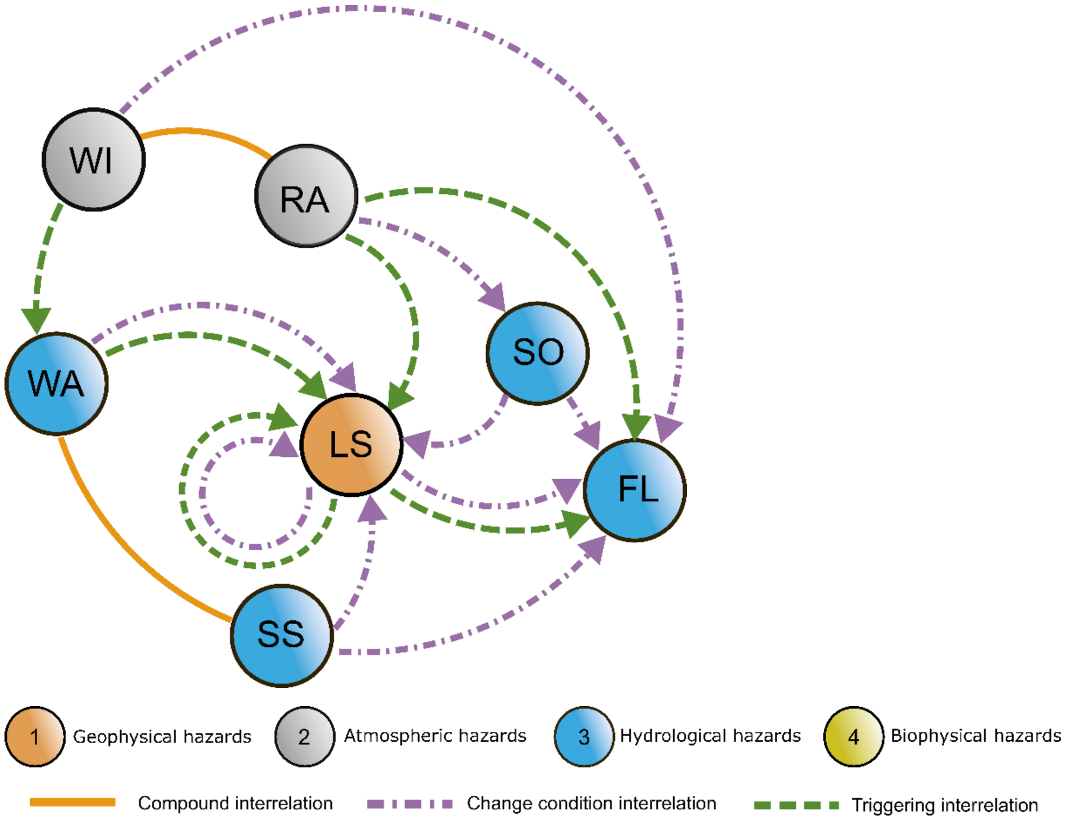

Figure 3.7 Network of natural hazards associated with an extratropical cyclone with their interrelation types. Arrow and arcs (see legend), indicate compound, change condition and triggering interrelations between the hazards Built according to hazard matrices developed in Chapter 2, Gill and Malamud (2014) and literature in Table 3.2.

Spatial extent

In meteorology, extra-tropical cyclones form and develop on a synoptic scale (≈ 1000km in diameter) (Catto, 2016). Nevertheless, the spatial extent of such events can vary. The severity of an extratropical cyclone can be measured with the Storm Severity Index (SSI), which depends on the extent, duration and intensity of the extreme wind (Leckebusch *et al.*, 2008; Soubeyroux *et al.*, 2017). Extra-tropical cyclone can lead to widespread damage from multiple hazards (e.g., storm surge, river flooding) at different places (Met Office, 2015; Catto, 2016; Hendry *et al.*, 2019). The spatial extent is, therefore a significant component for storm severity. The spatial extent of the impact of a mid-latitude cyclone also depends on its trajectory (Merz *et al.*, 2020) (e.g., a track crossing France and Germany vs. a track passing north of Scotland) .

Temporal Extent and seasonality

It usually takes an extratropical cyclone one to five days to cross western Europe (Schoenenwald, 2013; Roberts *et al.*, 2014). The duration of those events also influences storm severity. As stated above, extra-tropical cyclones mostly occur during an extended winter season and are often called winter storms.

3.3.2.4 Compound dry hazards

Definition

A compound dry hazards event is a hydrometeorological feature that involves several dry hazards (Sutanto *et al.*, 2020). This multi-hazard network is a threat to most parts of the world. However, its prevalence in Western Europe is likely to increase in a warming world (Zscheischler and Seneviratne, 2017; Vogel *et al.*, 2020). In Europe, compound dry hazards events usually occur during the summer season. Hazards involved in a compound dry hazards event can have different drivers (e.g., long term precipitation deficit, anticyclonic conditions), but their interrelations are of prior interest to assess the severity of the event (Manning *et al.*, 2018, 2019; Hao *et al.*, 2020).

Hazard interrelations

Hazards associated with a compound dry hazards event are often extreme hot temperature (heat waves), drought and wildfire. In some regions, extreme winds are sometimes associated with dry hazards events (Radovanovic *et al.*, 2019). In the summer months, dry conditions (low air moisture) are often associated with high air temperature. Sustained hot air temperatures for several days are called heat waves (Perkins, 2015). The severity of a heatwave can partly be explained by pre-existing dry soils (Alexander, 2011), while extreme hot temperatures exacerbate drought (Perkins, 2015; Manning *et al.*, 2018). Hot and dry conditions set the scene for wildfires in many parts of Europe, with severely hot and dry summers coinciding with devastating wildfire seasons (EFFIS, 2020). The wind is also a key driver for wildfire propagation (Tedim *et al.*, 2018) and can be associated with hot and dry conditions (e.g., Foehn wind). The synthetic network of hazard interrelations for a compound dry event is displayed in **Figure 3.8**.

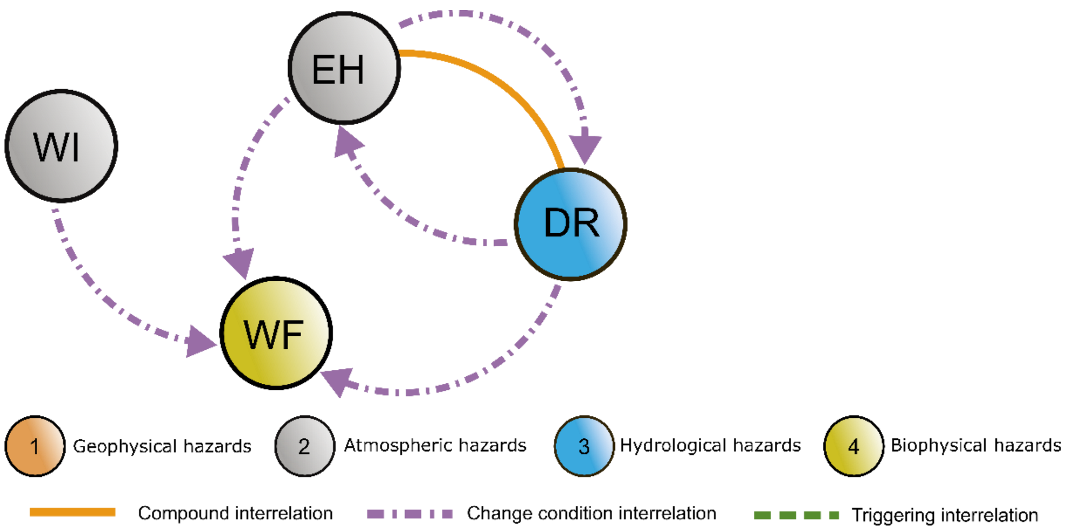

Figure 3.8 Network of natural hazards associated with a compound dry event with their interrelation types. Arrows and arcs (see legend), indicate compound, change condition and triggering interrelations between the hazards. Built according to hazard matrices developed in Chapter 2, Gill and Malamud (2014) and literature in Table 3.2.

Spatial extent

The spatial extent of compound dry hazard events highly varies, similarly to the spatial extent of its associated hazards. Drought and heatwaves can spread on vast areas (>10^6 km^2), with the most severe ones developing over the entire Atlantic region (e.g., 2003) (Rebetez *et al.*, 2009; Corzo Perez *et al.*, 2011; Spinoni *et al.*, 2019). A single wildfire can devastate up to hundreds of km^2 (Pereira *et al.*, 2011).

Temporal extent and seasonality

Compound dry hazards events usually last at least several days and up to years (Perkins, 2015; Manning *et al.*, 2019; Spinoni *et al.*, 2019). In the EAR, periods of extreme hot temperature can occur successively during the summer, between May and September, exacerbating an underlying drought (Fink *et al.*, 2004; Miralles *et al.*, 2014). Drought, particularly in the Iberian peninsula, can last up to several years (Stefanon *et al.*, 2012). The duration of a wildfire highly depends on its location, other natural hazards and human factors (Pereira *et al.*, 2011; Ganteaume *et al.*, 2013).

3.3.2.5 Compound Cold hazards

Definition

A compound cold hazards event is a hydrometeorological feature that involves several winter hazards. This multi-hazard event is usually initiated by a period of unusually cold weather. During the European winter, a typical pattern of atmospheric circulation, leading to very cold winters is an inflow of cold air from the north or east (Twardosz and Kossowska-Cezak, 2016). However, these prolonged cold conditions and their associated hazards cause multiple threat to critical sectors of society, such as energy production of transportation (Añel *et al.*, 2017).

Hazard interrelations

Hazards associated with compound cold hazards are extreme cold temperature (cold wave), extreme snowfall, extreme wind and sometimes widespread riverine flood (Eden, 2008). Extreme cold temperature and continuous periods of frost create the conditions for snow to fall and stick. The snow can be brought by different weather systems and often associated with strong winds, bringing the apparent temperature down due to the wind-chill effect (Hulme and Barrow, 1997). However, strong winds can also be associated with anticyclonic dry conditions in some regions (e.g., Mistral in the Rhone Valley) (Blanchet, 1990; Petroliagkis, 2018). The accumulation of snow over large areas can trigger thaw floods as snowmelts is a primary flood-generating mechanism (Hall and Blöschl, 2018; Berghuijs *et al.*, 2019). The synthetic network associated with compound cold events is displayed in **Figure 3.9.**

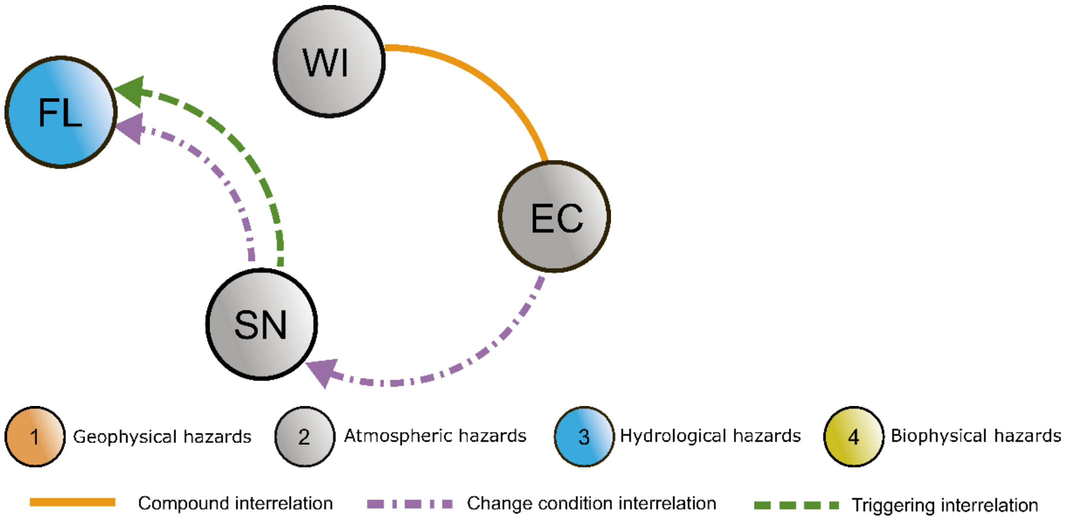

Figure 3.9 Network of natural hazards associated with a compound cold event with their interrelation types. Arrows and arcs (see legend), indicate compound, change condition and triggering interrelations between the hazards. Built according to hazard matrices developed in Chapter 2, Gill and Malamud (2014) and literature in Table 3.2.

Spatial extent

The spatial extent of a compound cold hazards event generally depends on synoptic-scale weather processes. Similarly to heatwaves, cold waves can develop over vast areas (>10^6 km^2), with the most severe ones developing over the entire Atlantic region (e.g., winter 1962–1963) (Lhotka and Kyselý, 2015). While more localized, heavy snowfall and consequent flooding can also occur on a relatively large scale with variable severity (Eden, 2008).

Temporal Extent

Compound cold hazards events can last from days to months, depending on synoptic weather conditions. This group of multi-hazard networks is often characterized by a succession of "short" events bringing snow and wind within an underlying long-lasting cold wave (Eden, 2008). The duration of such events has a significant role in their severity. Indeed, the accumulation and perseverance of snow and extremely cold temperature over time can significantly impact many aspects of society (Booth, 2007; Añel *et al.*, 2017). Nevertheless, compound cold hazards events can cause widespread disruption and damage in a very short period (e.g., Catalonia, March 2010) (Schauwecker *et al.*, 2019).

3.4 Characterising multi-hazard events

To illustrate the event-based approach and characterize more precisely the five multi-hazard networks presented in **Section 3.3**, I search for past occurrences of natural hazards presented in **Table 3.1** in the EAR and directly surrounding regions during the period 1755 to 2019. A catalogue of historic multi-hazard events is then developed (**Section 3.4.1**). Blended sources of information such as catalogues providing qualitative (hazards associated, area impacted) and semi-quantitative (duration, the magnitude of the event) information about past occurrences of natural hazards are used to create this catalogue. Features of multi-hazard events presented in the catalogue are then discussed; dominant hazards and dominant hazard interrelations are identified within the five multi-hazard networks (**Section 3.4.2**). Information about the spatial and temporal scales of multi-hazard events are also compiled and analysed. Building on this semi-quantitative knowledge, an overview of available free datasets that can be used to analyse MH events is provided in **Section 3.4.3**. These datasets are divided into three types: (i) In-situ Observations (**Section 3.4.3.1**), (ii) Model outputs (**Section 3.4.3.2**) and (iii) Satellite observations (**Section 3.4.3.3**). The relevance of each type of data to study multi-hazard is then examined.

3.4.1 Historic multi-hazard events catalogue

To provide evidence for the conceptual multi-hazard networks presented in **Section 3.3**, a catalogue of historic multi-hazard events containing a total of 50 events (10 for each of the five multi-hazard networks previously presented) is created. This catalogue also aims to bring together different sources and databases of single hazard events. To build this catalogue, I used a variety of sources for each natural hazard refined with country names and the words “database” or “catalogue”. Most of the sources reviewed account for single hazards or simply mention the occurrence of other hazards. Evidence used to build the historic major multi-hazard events catalogue comes from a range of source types and are accessible in **Appendix Table C2** and **Appendix Table C3**:

(i) Single hazards catalogues (e.g., tsunami (BGS, 2018), storm surge (Haigh *et al.*, 2015)
(ii) Catalogue of reported hydrometeorological events (e.g., Met Office (2020), Infoclimat (2020))
(iii) Disaster databases (e.g., EM-DAT (2018))
(iv) Peer review articles and books

A total of 32 catalogues providing reports on time, location and magnitude of hazards presented in **Table 3.1** are reviewed and accessible in **Appendix Table C2**. These catalogues spatially range from national to global and temporally range from 4000 years (NOAA Tsunami database) to 13 years (Floodlist). To create the multi-hazard catalogue, high magnitude single hazard events which have the potential to be multi-hazard events (e.g., flash flood) are identified. To do this, I also consider peer review articles focusing on one high impact hazard events (e.g., the great storm of 1987 in the United Kingdom). By crossing different sources, evidence supporting the occurrence of several hazards during the same event are assembled (e.g., extreme wind, extreme rainfall and river flooding for the great storm of 1987). The discrimination criterion for an event to be part of the catalogue is that it is mentioned in either:

(i) at least two of the 32 catalogues;
(ii) in one catalogue and one peer review articles on high impact hazard event.

For each of the five multi-hazard networks discussed in **Section 3.4.2**, ten major historical events are identified with the method mentioned above. Additionally, the hazards, the interrelations that might have occurred, the spatial extent, and the duration of each multi-hazard event are identified. I consider that the multi-hazard events presented in the catalogue (**Table C1)** are representative of a broad range of possible hazard interrelations within each of the five multi-hazard networks. In addition to the time and location of occurrence of the event, hazards and interrelations involved (e.g., change condition) (from **Section 4.2**), are identified. Estimations of the spatial and temporal scales of the events are also reported. The spatial scale corresponds here to the total footprint of the event, which is represented by the total area with reported impact in the sources reviewed. The spatial footprint is reported on a semi-quantitative scale including four categories: local (5×10^0 to 5×10^3 km^2), regional (5×10^3 to 5×10^4 km^2), multi-regional (5×10^4 to 5×10^5 km^2) and continental (5×10^5 to 5×10^6 km^2). The duration of events is also extracted from the reviewed literature, is expressed in days and is also associated with the duration of reported impacts. For short events such as convective storms or earthquakes, the duration is set to 1 day when no explicit duration is reported. For large scale moving systems such as large-scale extratropical cyclones, the duration represents the time during which different hazard occurred over the EAR, but not the whole lifespan of the storm.

Most of the 50 events displayed in **Appendix Table C1** had been recorded as “single” hazard events in reviewed catalogues (**Appendix Table C2**). In some cases, they can be justified by the predominant influence of one of the hazards on the damages caused (e.g., wind in Storm Martin). Each multi-hazard event displayed in **Table C1** does not include the same number of hazards or interrelation. For example, the number of hazards associated with an extratropical cyclone varies between two and six within the catalogue. The number of interrelations within events is also variable. Among the 50 events in the multi-hazard catalogue (**Table C1**), 44 occurred within the EAR and 47 in one of the ten countries over which the EAR is distributed. The three events which did not occur in one of these 10 countries occurred in neighbouring countries (Switzerland, Italy) and are ground movement events that are relatively rare in the EAR. However, these three events illustrate the approach taken here.

3.4.2 Hazard interrelations and attributes of multi-hazard networks

From **Appendix Table C1,** I analyse hazard interrelations to identify dominant hazards and dominant hazard interrelations within the five multi-hazard networks. Dominant hazard and dominant hazard interrelations are defined as follows: A dominant hazard is the most likely to occur and the most interconnected hazard within a multi-hazard network. A dominant hazard interrelation is the most likely to occur within a multi-hazard network.

Figure 3.11 displays interrelations within the 10 convective storm events from the catalogue **(Appendix Table C1**) with a chord diagram. Chord diagrams show the interrelationship between entities (here natural hazards). Nodes representing entities are arranged along a circle. The relationship between each node is represented with arcs within the circle. The importance of each connection is represented proportionally by the size of each arc. Usually, chord diagrams are used to visualize the flow of connection between one half of the circle and the other half. In **Figure 3.10**, it is not the case as the circle circumference is filled with hazards (sorted by hazard categories) which composes the convective storm multi-hazard network. Therefore, the values on the circumference of each chord diagram represent double of the cumulative number of hazard interrelations that occurred. The types of interrelations are displayed by the colour of the arcs between two nodes. The size of the arcs is proportional to the importance of the connection in the multi-hazard events catalogue. When two hazards can be interrelated with two different interrelation types (e.g., a landslide can either trigger *or* change conditions for river flood), the filling and the outside line are from two different colours. Arrows are used to represent the direction of the "hazard cascade" when relevant (i.e., triggering and change conditions interrelations).

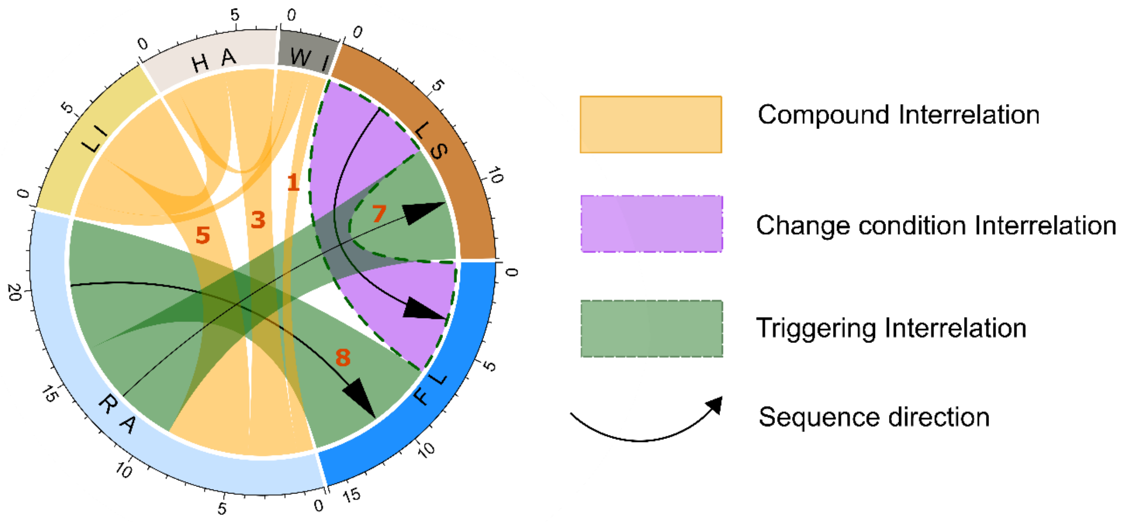

Figure 3.10 Chord diagram of hazard interrelations within a convective storm multi-hazard network using the multi-hazard events catalogue.

For example, in **Figure 3.10**, extreme rainfall (RA) is interrelated to other hazards 24 times within the ten convective storms in the catalogue displayed in **Appendix Table C1.** Extreme rainfall triggers river flooding (FL) on eight occasions and landslides (LS) seven times. Extreme rainfall also has compound interrelations with lightning (five occurrences), hail (three occurrences) and extreme wind (one occurrence). Hazard interrelations during the 10 events of each multi-hazard network are mapped using chord diagrams displayed in Figure 3.11, similar to **Figure 3.10**.

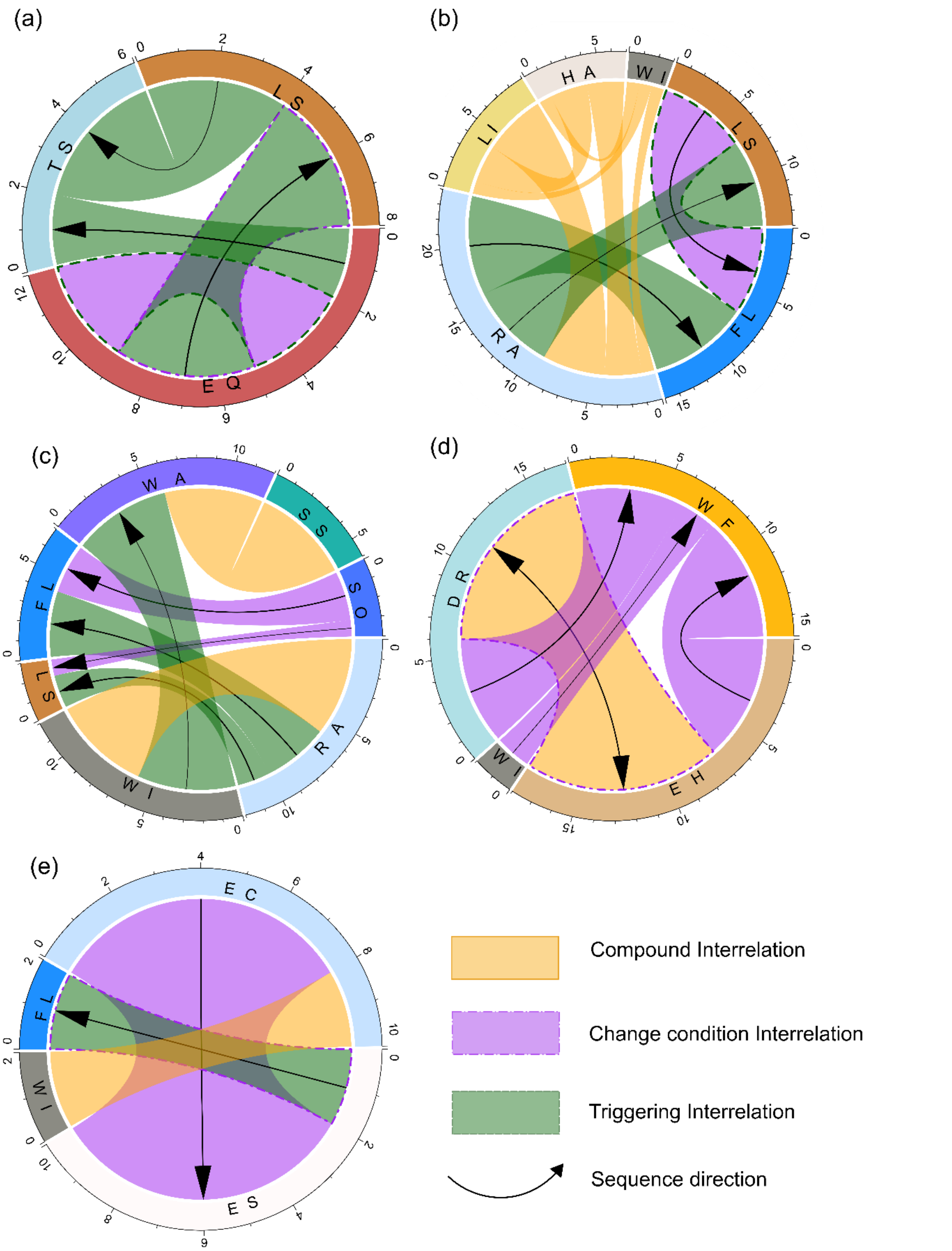

Figure 3.11: The number of hazard interrelations within the multi-hazard events catalogue for each category using chord diagrams. (a) Ground motion, (b) Convective storm, (c) Extra-tropical cyclone and (d) Compound dry and (e) Compound cold. Abbreviations for natural hazards are given in Table 1. Earthquake (EQ), landslide (LS), tsunami (TS), extreme rainfall (RA), extreme wind (WI), hail (HA), lightning (LI), river flooding (FL), extreme waves (WA), storm surge (SS), soil moisture excess (SO), extreme hot temperature (EH), wildfire (WF), drought (DR), extreme cold temperature (EC), extreme snowfall (ES).

From **Appendix Table C1**and **Figure 3.11**, one can observe the following:

– Ground motion events can include up to three different hazards. Earthquake is the dominant hazard as it triggers tsunamis, landslides and other earthquakes and is involved in 75% (12/16) of the interrelations. The remaining 25% (4) of the interrelations are landslide triggering tsunamis. For that network, hazards only occur by pairs in our catalogue (EQ-LS, LS-TS, EQ-TS) and there are only cascading interrelations (i.e., triggering, change condition).

- Convective storms can include up to six interrelated hazards. The dominant hazard in the set of events (**Table C1**) is extreme rainfall (involved in 67% (24/36) of the hazard interrelations) which is the only hazard having at least one interrelation with all other hazards of the network and is making the link between two unrelated groups of hazard within a convective storm: a “compound” network (LI, HA, WI) and a “cascade” network (FL, LS). There is no event including the six hazards in the 10 events in our catalogue, but rather different combinations.
- Extratropical cyclones can include up to seven different natural hazards. Extreme rainfall, extreme waves and extreme wind are dominant hazards in such events. These three hazards account for 86% (24/28) of the hazard interrelations recorded in the catalogue for extratropical cyclones. All 10 events in the catalogue include either extreme wind or extreme rainfall and six include both. Similarly to extreme rainfall in convective storms, extreme wind makes the link between two groups of hazards in **Figure 3.11.c** “coastal” hazards (SS, WA) and “land” hazards (RA, LS, FL, SO) and is therefore the dominant hazard of the network. The combined occurrence of these two groups of hazards can result in compound flooding (Hendry *et al.*, 2019).
- In compound dry hazards events, the interrelation between extreme hot temperature and drought is prevalent as in accounts for 42% (11/26) of hazard interrelations and these two hazards are involved in 92% (24/26) of recorded interrelations in the catalogue. It is hard to distinguish a dominant hazard for this network, but one can rather acknowledge the influence of both extreme hot temperature and drought on the dynamic of compound dry hazard events. Among the 14 interrelations with wildfires, 2 are with wind, 7 with extreme hot temperature and 5 with drought, confirming the hypothesis that a combination of these three hazards rather than one might lead to wildfires.
- In compound cold hazard events, extreme cold temperature is involved in 83% of hazard interrelations and is therefore the dominant hazard (10/12 interrelations). Extreme cold temperature sets the condition for extreme snowfall to occur (8/12 interrelations). In our catalogue, extreme cold temperature rarely occurs with extreme wind while extreme snowfall trigger river flooding on two occasions.

Figure 3.11 provides semi-quantitative estimates of the interdependencies of different natural hazards within the five multi-hazard networks designed in **Section 3.2**. Dominant hazards and hazards interrelations of each multi-hazard networks are extracted from **Figure 3.11** and **Table C1** and are listed in **Table 3.3**.

Table 3.3: Dominant natural hazard and hazard interrelations for each of the five multi-hazard networks (EQ = Earthquake; LS = Landslide; TS = Tsunami; RA = Extreme rainfall; FL = River flooding; WI = Extreme wind; EH = Extreme hot temperature; DR = Drought; EC = Extreme cold temperature; ES = Extreme snow).

Multi-hazard network	Dominant hazard(s)	Dominant interrelation(s)
Ground movement	Earthquake	EQ – LS, LS – TS [Triggering]
Convective storm	Extreme rainfall	RA – FL [Triggering]
Extratropical cyclone	Extreme wind	RA – WI [Compound]
Compound dry	Extreme hot temperature, drought	EH – DR [Compound, Change condition]
Compound cold	Extreme cold temperature	EC – ES [Change condition]

From **Appendix Table C1**, I analysed the spatial and temporal scales of each MH event groups. The spatial and temporal properties of multi-hazard events are displayed in **Figure 3.12**. Each multi-hazard network is represented by its symbol and colour. The spatial scale of multi-hazard events can take four discrete values: local, regional, multi-regional, continental, while duration is expressed in days. To prevent overplotting, data points obtained from **Table C1** are jittered (offset) in both space and time. **Figure 3.12** provides semi-quantitative information about the duration and spatial extent of the different multi-hazard networks. Scatter plots of each MH network are encircled, highlighting the inter-group variability in both duration and extend.

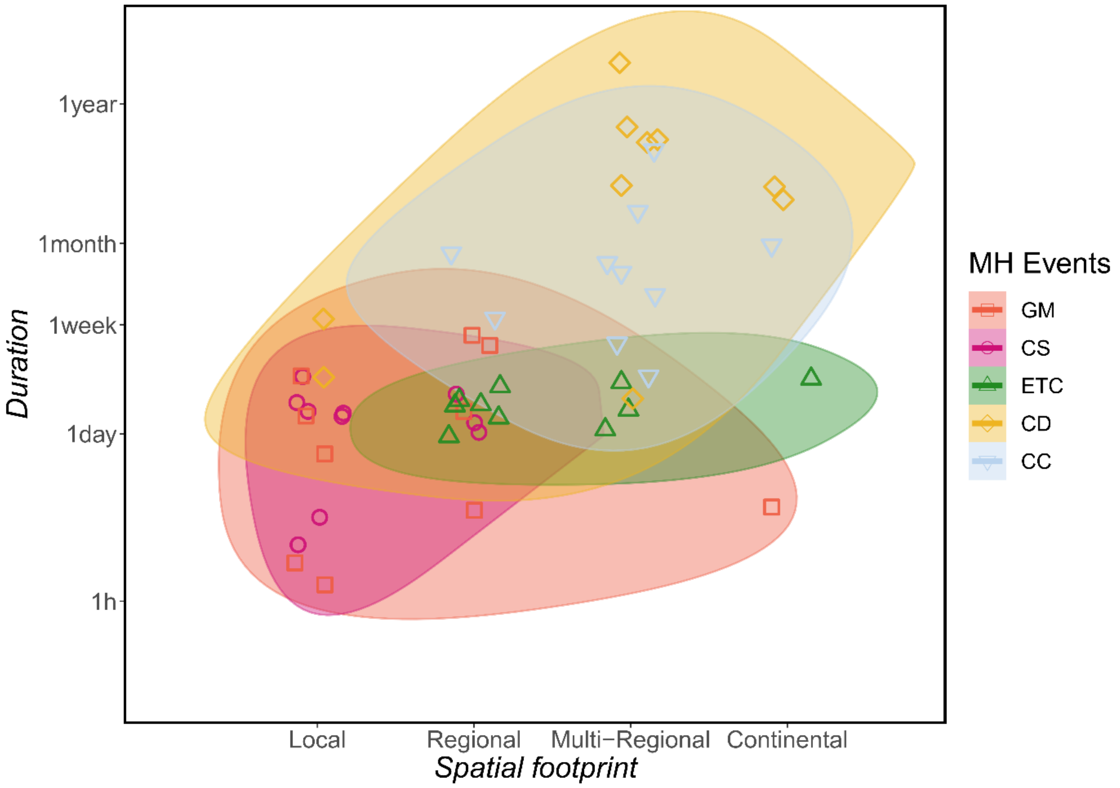

Figure 3.12 Spatial and temporal scales of 50 multi-hazard events divided into five networks by colour: Ground Motion (GM), Convective Storm (CS), Extratropical Cyclone (ETC), Compound Dry (CD) and Compound Cold (CC). Shown on logarithmic axes are the spatial and temporal scales over which the 50 multi-hazard events. Here spatial footprint refers to the area that the hazard influences and temporal scale to the timescale that the single hazard acts upon the natural environment. To prevent overplotting, data points are jittered (offset) in both axes.

Convective storms and ground motion events are generally rapid events lasting less than a day (**Figure 3.12**), even if the impact to society or the environment caused by the hazards can last much longer (de Ruiter *et al.*, 2020). While convective storms are limited to small areas, ground motion events generally occur on local to regional scales but can also affect large areas, particularly when tsunamis are involved. Extratropical cyclones reported in the MH catalogue develop over periods ranging from 1 to 3 days and generally occur over large areas and sometimes across several countries. The spatial extent of an extratropical cyclone depends on several features such as its central pressure or its track (Catto, 2016).

Finally, compound cold and dry events are more slow-onset or long-lasting events and last from days to several months. Compound dry events, and particularly drought can influence large areas, but can also be more localized when extreme heat, drought and strong wind collide to trigger and fuel wildfires (San-Miguel-Ayanz *et al.*, 2013; Tedim *et al.*, 2018; Radovanovic *et al.*, 2019). Spatial and temporal scales of compound cold and dry events are partly governed by atmospheric blocking pattern (Amraoui *et al.*, 2015; Twardosz and Kossowska-Cezak, 2016; Dizerens *et al.*, 2017; Manning *et al.*, 2019). The spatial and temporal scales of natural hazard interrelations will be further discussed in **Chapter 5.**

3.4.3 Numerical Data for multi-hazard modelling

In previous sections, hazards have been grouped in multi-hazard networks according to physical consideration and prior knowledge on natural hazard interrelations. Five networks have been defined and described (**Section 3.3**). Characteristics of events from each network have been analysed from a catalogue of 50 historic multi-hazard events (**Section 3.4.1**). Dominant hazards and hazard interrelations have been identified for each multi-hazard network, and spatial and temporal scales of such events have been discussed (**Section 3.4.2**).To quantitatively model the interrelations between different natural hazards, numerical data are necessary. However, the choice of datasets to analyse and quantify hazard interrelations is governed by various, and sometimes contradictory, factors including:

(i) The availability of data for different hazards in a given region;
(ii) The homogeneity in spatial and temporal resolutions between different hazard data;
(iii) The need for spatial and temporal resolutions that can capture as accurately as possible the interrelation between hazard.

In this section, 34 freely available datasets to study and model the five multi-hazard networks presented **in Section 3.3** are reviewed (**Appendix D**). A focus is given on datasets relevant to the EAR and in particular to the two countries occupying the most of its area: France and the United Kingdom (both of which are the focus area of research in other chapters of this PhD). The aim of this review is not to identify every available dataset to study one of the 16 hazards in **Table 3.1**, but rather to provide a general overview of the different kinds of data available to study hazard interrelations within the five multi-hazard events groups presented in **Section 5.4** along with 50 case study events. For example, climate reanalysis data (See **Section 5.3.3**) produced by the ECMWF (European Centre for Medium range Weather Forecast) is reviewed while similar datasets generated from American (USA) and Japanese agencies are not. For more exhaustive overviews, the reader can refer to, for example, Beck *et al.* (2017) for precipitation datasets and Dorigo *et al.* (2017) for soil moisture datasets. Here we divide available data to study natural hazards into three types: in-situ observation (20 datasets), model outputs (7 datasets) and remote sensing (7 datasets). The specificities, strength and weaknesses of each type of dataset, along with their applicability to different natural hazards, are assessed. The relevance of different datasets for each multi-hazard network is also discussed.

3.4.3.1 In-situ observation datasets

In-situ observations are those made at the location of the instrument (Ehhalt, 1980). This includes sensors placed on the banks of rivers, carried on weather balloons or aeroplanes, drifting in the ocean on buoys and also encompasses data collected by citizen scientists. In-situ observation data are traditionally point observations made at a station where a sensor or instrument is located. The main advantage of in-situ observations is their ability to provide precise information at a local scale with high temporal resolution (Ehhalt, 1980). To capture data from wider areas, a high number of stations are therefore required (Donat *et al.*, 2014). To take advantage of the qualities of in-situ observations over a wide area, gridded datasets from the interpolation of station-derived meteorological observations have also been developed in recent years (Cornes *et al.*, 2018). However, instrumental observations can be problematic due to sparse and inhomogeneous coverage and lead to biases due to instrumental errors (Ledesma and Futter, 2017).

All of the natural hazards considered in this piece of work can be defined as extreme or unusual occurrences of an environmental variable (e.g., extreme hot temperature) which can be measured in-situ with instruments. In the present study 20 of the 34 numerical datasets reviewed are in-situ observation datasets. I found freely accessible datasets of in-situ observations for 15 of the 16 hazards presented in **Table 3.1** and data on earthquakes, landslides, hail and tsunami have only been recorded with in-situ observations in the 34 datasets reviewed. There are different possible scales or unit to study one natural hazard and therefore, different ways to measure their intensity. For example, one can study landslides by their area or count and even study the relationship between these two attributes (Malamud *et al.*, 2004). Precipitation observations usually correspond to the quantity of water falling (measured in height) aggregated over a period which can vary from minutes to months. The relevance of the period depends here on the duration of the event to be characterized (e.g. extratropical cyclones vs convective storms).

3.4.3.2 Remote sensing datasets

Remote sensing is the obtaining of information from a distance (NASA, 2020). This is typically done from satellites or aircraft. There are two types of remote sensors, passive and active. A passive sensor uses energy naturally reflected by or emitted from the Earth's surface; these sensors measure properties such as land and sea surface temperature, vegetation properties, cloud and aerosol properties (NASA, 2020). Active sensors provide their own energy and record the amount of incident energy returned from the imaged surface (Melet *et al.*, 2020) and include different types of radio detection and radars. These types of sensors are useful for measuring, among others, precipitation, winds and ice cover (NASA, 2020). Remote sensing (e.g., satellite observations) allows the capture of data from wide areas and are thus complementary to in-situ observations. However, satellite observations cannot always capture the level of resolutions required by users as they offer a larger picture (Melet *et al.*, 2020).

Environmental variables such as surface temperature, soil moisture and fire activity can be monitored or estimated with passive remote sensing (Sheffield *et al.*, 2018; Brugnara *et al.*, 2019; Lizundia-Loiola *et al.*, 2020). Precipitation is estimated with radar measurements, while lightning strikes are remotely measured with lightning location systems (Anderson and Klugmann, 2014).

Floods, earthquakes and landslides can also be monitored with satellites (Sheffield *et al.*, 2018; Cao *et al.*, 2019), although I did not find freely available remotely sensed datasets for these hazards. Freely accessible remote sensing datasets for 6 of the 16 hazards presented in **Table 3.1** are reviewed in **Appendix D**. Overall, remote sensing datasets have antagonistic characteristics to in-situ observations. However, these two types of data can be combined and assimilated into models to create another type of datasets: model outputs datasets.

3.4.3.3 Model outputs datasets

Major atmospheric and oceanic processes have been numerically modelled for the need for meteorological forecasting (Brönnimann *et al.*, 2018). These models can numerically estimate the state of the global climate. Climate Reanalyses are generated by combining model estimates of the state of the atmosphere, ocean cryosphere, land, and so forth, with data from a range of observing platforms (in-situ, remote sensing) by applying a method named data assimilation (Brönnimann *et al.*, 2018; Hersbach *et al.*, 2018). The advantage of climate reanalyses is that they produce environmental variables homogeneously distributed at a regional, global scale (Sutanto *et al.*, 2020). Climate reanalysis data also provides estimates of variables than can hardly be measured (e.g., Convective available potential energy) which can be used to estimate the occurrence of natural hazards such as hail (Prein and Holland, 2018). The use of a climate reanalysis product to study extreme events induces several limitations in comparison to observational data (Donat *et al.*, 2014; Angélil *et al.*, 2016). In climate reanalyses, variables are computed over a grid box, and the resulting value is an average. This often leads to a smoothing of local extreme values (Donat *et al.*, 2014). The accuracy of reanalysis data also depends on various types of observations (Hersbach *et al.*, 2019). Similarly to climate reanalyses, hydrological reanalyses has been produced as an output of hydrological models, providing homogeneous data for river discharge and soil moisture regionally (Alfieri *et al.*, 2014) and globally (Alfieri *et al.*, 2020).

Many hydrometeorological variables can be estimated from climate model outputs, including wind speed precipitation and soil moisture. Some outputs of climate reanalyses can be used directly to study natural hazards (Martius *et al.*, 2016; Sutanto *et al.*, 2020), while others are inputs for other models (hydrological, hydrodynamic) that provide estimates of other variables such as river discharge (Alfieri *et al.*, 2020) or sea level (Petroliagis, 2018). In the present work, I reviewed 8 different model output datasets relevant to the Atlantic region. These datasets provide data for 11 out of the 16 hazards relevant to this study. Most of the hydrological and atmospheric hazards can be studied with model output datasets. The homogeneity of the data provided by climate and hydrological models made these increasingly popular to study multiple natural hazards (Martius *et al.*, 2016; Petroliagis, 2018; Sutanto *et al.*, 2020; Vogel *et al.*, 2020). The spatial and temporal resolution of model output data is still too coarse to analyse local events (e.g. convective storms). Still, the promising improvements made in recent years in this area suggest that this limitation could be overcome in the near future.

3.4.3.4 Summary of the three types of numerical data

The three types of numerical data relevant to natural hazards that are presented have strength and limitations, in particular regarding two aspects: spatial and temporal coverages and spatial and temporal resolution:

- In-situ observation datasets provide in general local data with broad temporal coverages (**Appendix D**). Their spatial coverage is inhomogeneous and sparse in many regions of the world (Hou *et al.*, 2014; Sheffield *et al.*, 2018).
- Remote sensing offers homogeneous data over large regions of the world with thin spatial and temporal resolutions, but with limited temporal coverage due to this technology's relative novelty.
- Model output datasets offer global data for relatively long periods (>40 years), but with possible biases and coarse spatial and temporal resolution compared to the two other dataset types.

The choice of a dataset then depends on the multi-hazard network to be studied. **Figure 3.13** represents the availability of the three types of data presented in this section for the five multi-hazard networks with a chord diagram. Only in-situ observational datasets have been reviewed for the study of ground motion events despite progress in remotely sensed observations of hazards that compose this multi-hazard network (e.g., landslides, Abdulwahid and Pradhan, 2017). Datasets from the three types of numerical data have been reviewed for ETC (extratropical cyclone), CS (convective storm), CD (compound dry) and CC (compound cold) events.

Besides the availability of data from a given type, other criteria can drive the selection of datasets to model multi-hazard networks. The spatial and temporal scales of each multi-hazard network guides the choice of a relevant dataset. On the one hand, compound dry (CD) events occur on large scales and during periods spanning from days to months (**Figure 3.12**). Such events require datasets with extensive spatial coverages but do not need thin spatial and temporal resolutions (Sutanto *et al.*, 2020), suggesting that model output datasets are a good option for compound dry hazard events. Convective storms, on the other hand, are very local events and require datasets with small spatial and temporal resolutions to be appropriately characterized.

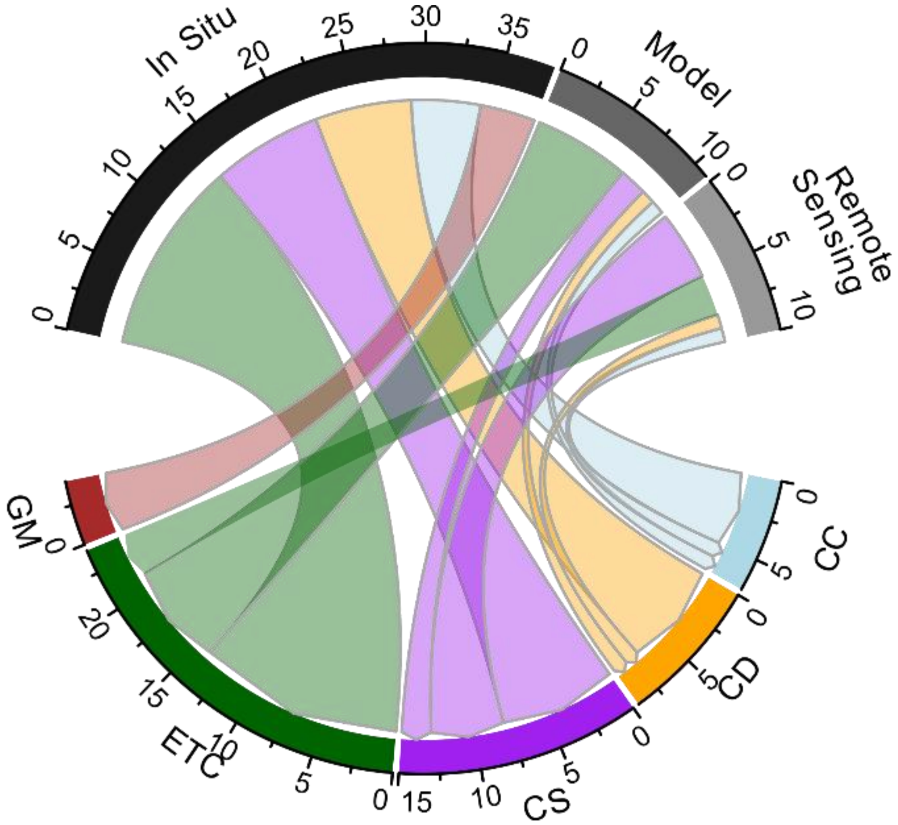

Figure 3.13 Availability of three types of data (in situ observations, model, remote sensing) for the five multi-hazard networks (Ground Motion (GM), Convective Storm (CS), Extratropical Cyclone (ETC), Compound Dry (CD) and Compound Cold (CC)) among the 34 datasets reviewed in Appendix 3.2.

The combination of different data types to create new datasets (Beck *et al.*, 2017) or improve the accuracy of models (Hersbach *et al.*, 2020) are initiatives that are gradually reducing the aforementioned data limitations. To study hazard interrelations, the combination of different data types is often a solution to overcome issues linked to spatial and temporal incompatibility between different in-situ observational datasets (Petroliagis, 2018; Couasnon *et al.*, 2019).

3.5 Discussion

Multi-hazard networks as developed in this chapter are generic multi-hazard events. In that regard, these represent a step forward compared to hazard interrelation matrices (**Section 2.3**) by associating more than two hazards. Multi-hazard networks could provide an initial framework to model interrelations between multiple hazards. Indeed, hazard interrelation matrices developed in **Chapter 2** allow the identification of one or more quantitative methods to model the hazard interrelations within a multi-hazard network. However, the transition from the semi-quantitative approach developed in **Section 3.4.2** requires overcoming several challenges mainly associated with (i) modelling capacities and (ii) data availability.

Modelling capacities: there are two main approaches to model multi-hazard networks and their multiple hazard interrelations. The first approach would be to use a single modelling framework for the whole network of interrelations. Methods such as Bayesian networks could be used to push forward the analysis carried over in **Section 3.4.2** and refine the assessment of dominant hazards and hazard interrelations. The second approach would combine several modelling methods reviewed in **Chapter 2** by attributing a method to each hazard interrelation. This model coupling approach has been undertaken to study compound flooding (Dietrich *et al.*, 2010; Bass and Bedient, 2018) by combining stochastic and mechanistic models. However, these studies remain site-specific and require important computational power (Bass and Bedient, 2018).

Data availability: the challenge of obtaining observational data for several hazards from different hazard categories (geophysical, meteorological) has been addressed in **Section 3.4.3**. Notwithstanding, every type of numerical data comes with its advantages and shortcomings and the combination of different datasets might be a necessity for some multi-hazard networks (e.g., convective storm). When combining different datasets, obtaining spatial and temporal consistency might come at the cost of a reduced resolution (Ridder *et al.*, 2020). The choice of appropriate spatial and temporal resolutions depend on the multi-hazard network studied (**Figure 3.12**). An extended multi-hazard catalogue (**Appendix C**) could be a relevant source of data for fitting a Bayesian network.

Besides these limitations, the concepts of dominant hazards and hazard interrelations developed in **Section 3.4.2** creates new modelling possibilities by focusing on one hazard or one hazard interrelation as the "central" parts of the multivariate analysis. One approach could be to focus on the value of one hazard and assess how other "satellite" hazards and hazard interrelations evolve regarding the "central" hazard.

3.6 Conclusion

This chapter focussed on the identification of natural hazard interrelations that are likely to develop over the EAR. The region and its climate have been presented in **Section 3.2**. The identification of relevant natural hazards for the EAR was performed for three main criteria: (i) frequency of occurrence, (ii) spatial relevance, (iii) potential to impact energy infrastructures. A total of 16 different natural hazards have been selected with this approach. These hazards were then grouped into multi-hazard networks. Multi-hazard networks are composed of a set of interrelated hazards and occur in a given space-time frame. These networks have been designed using knowledge relative to (a) physical processes and (b) interrelations between hazards. Five distinct multi-hazard networks that each include between 3 and 7 natural hazards have been designed and defined in **Section 3.3**: ground motion events, convective storms, extratropical cyclones, compound dry hazards, compound cold hazards.

To support this approach and characterize the different multi-hazard networks, a catalogue of 50 past multi-hazard events (10 per network) has been created using evidence from 32 natural hazard catalogues and 26 peer-reviewed articles (**Section 5.4.1**). Three attributes of multi-hazard networks were extracted from the catalogue: spatial and temporal scales, dominant natural hazards and hazard interrelations. These attributes are assessed semi-quantitatively, providing a prior assumption on the characteristics of multi-hazard networks. These assumptions can be useful when framing the quantitative analysis of multi-hazard networks. An overview of freely available numerical datasets to study quantitatively multi-hazard network has been provided in **Section 5.4.3**. A total of 34 datasets of three types (in-situ observations, model outputs, remote sensing) were reviewed, and their suitability for the five multi-networks was assessed.

In conclusion, this chapter proposes a framework to identify, group and quantify natural hazard interrelations in a given region. This approach synthesizes interdisciplinary knowledge on hazard interrelations, bringing together atmospheric, hydrological, geophysical and biophysical hazards and is supported by blended information sources. Multi-hazard networks developed here go beyond the matrices presented in **Chapter 2** in the visualization and grouping of natural hazards. The development of multi-hazard networks allows us to focus on a restricted number of hazard interrelations and links interrelations to physical processes and drivers. It also provides a clear view of the existing multi-hazard interrelations in the EAR. This work represents support for hazard interrelation modelling in **Chapter 4 and 5.**

Chapter 4: Evaluating the efficacy of bivariate extreme modelling approaches for multi-hazard scenarios

Summary:

Modelling multiple hazards interrelations remains a challenge for practitioners. This article primarily focuses on the interrelations between pairs of hazards. The efficacy of six distinct bivariate extreme models is evaluated through their fitting capabilities to 60 synthetic datasets. The properties of the synthetic datasets (marginal distributions, tail dependence structure) are chosen to match bivariate time series of environmental variables. The six models are copulas (one non-parametric, one semi-parametric, four parametric). We build 60 distinct synthetic datasets based on different parameters of log-normal margins and two different copulas. The systematic framework developed contrasts the model strengths (model flexibility) and weaknesses (poorer fits to the data). We find that no one model fits our synthetic data for all parameters, but rather a range of models depending on the characteristics of the data. To highlight the benefits of the systematic modelling framework developed, we consider the following environmental data: (i) daily precipitation and maximum wind gusts for 1971 to 2018 in London, UK; (ii) daily mean temperature and wildfire numbers for 1980 to 2005 in Porto district, Portugal. In both cases, there is good agreement in the estimation of bivariate return periods between models selected from the systematic framework developed in this study. Within this framework, we have explored a way to model multi-hazard events and identify the most efficient models for a given set of synthetic data and hazard sets.

***Published in *Natural Hazards and Earth System Sciences* in August 2020.** Minor edits have been made to ensure consistency in reference style and language with the rest of the thesis. The substance of the chapter remains unchanged.

Tilloy, A., Malamud, B. D., Winter, H. and Joly-Laugel, A.: Evaluating the efficacy of bivariate extreme modelling approaches for multi-hazard scenarios, *Nat. Hazards Earth Syst. Sci.*, 20(8), 2091–2117, 2020. doi: 10.5194/nhess-20-2091-2020.

4.1 Introduction

A multi-hazard approach considers more than one hazard in a given place and the interrelations between these hazards (Gill and Malamud, 2014). Multi-hazard events have the potential to cause damage to infrastructure and people that may differ greatly from the associated risks posed by a single hazard (Terzi *et al.*, 2019). Here, and as discussed in **Chapter** 1, natural hazards (which we will also refer to as 'hazards') will be defined as (UNDRR, 20217): a natural process or phenomenon that may have negative impacts on society. For modelling purposes, we consider two main mechanisms in natural hazards interrelations (Tilloy *et al.*, 2019): (i) *cascade interrelations* (i.e., when there are a temporal order and causality between natural hazards); (ii) *compound interrelations* (i.e., when several natural hazards are statistically dependent without causality).

Meteorological phenomena such as extratropical cyclones or convective storms often lead to the combination of multiple drivers and/or hazards and can therefore be related to compound events as defined by Zscheischler *et al.* (2018). This research concentrates on cascading and compound interrelations between natural hazards (e.g., a storm can include rain, lightning, hail, with rain and hail both potentially triggering landslides). Case examples of meteorological phenomena influencing natural hazard interrelations include the following:

(i) In 2010, storm Xynthia hit the west coast of France. The storm itself was not particularly extreme for the season but the compound effect of extreme wind, high tides, storm surge, extreme rainfall and the fact that the soils were already saturated, led to massive damage due to wind and flooding (CCR, 2019).

(ii) In summer 2010, Russia experienced a heatwave. Low precipitation in spring 2010 led to a summer drought that contributed to the heatwave having a large magnitude (Barriopedro *et al.*, 2011; Hauser *et al.*, 2015; Zscheischler *et al.*, 2018). The co-occurrence of extremely dry and hot conditions resulted in widespread wildfires, which damaged crops and caused human mortality (Barriopedro *et al.*, 2011).

(iii) Extreme thunderstorms occurred in the Paris region in 2001, involving lightning and extreme rainfall, with the rainfall triggering flooding, mudslides and ground collapse, with subsequent damage to railway networks (CCR, 2019).

In this context, the quantification of interrelations between natural hazards can play an important role in risk mitigation and disaster risk reduction. Some of the natural hazards presented in the above examples are extreme occurrences of environmental variables (e.g. extreme temperature) which have different characteristics and statistical distributions (e.g., wind and landslides). Natural hazards can be interrelated with different mechanisms (i.e. compound, cascade). For a given mechanism, interrelations also vary in strength and intensity. Additionally, as highlighted in Tilloy *et al.* (2019), different modelling approaches have been developed to quantify interrelations between variables. Here we focus on stochastic models that include copulas (Nelsen, 2006; Genest and Favre, 2007; Salvadori *et al.*, 2016), and multivariate extreme models (Heffernan and Tawn, 2004), limiting our analysis to the bivariate case. The potential for misinterpretation of the dependence structure of two variables presents a problem when end-users try to account for hazard interrelations.

We choose six distinct bivariate models able to handle different types of tail (extreme) dependence: one non-parametric (JT-KDE), one semi-parametric (Cond-Ex) and four different parametric copulas (Galambos, Gumbel, FGM, Normal) (see **Section 4.2**). The fitting capacities of each model are compared with the estimation of level curves. Level curves are extensively described in **Section 4.2.3**. However, these curves correspond to probabilities that can be related to compound and cascading hazard interrelations. Compound interrelations are represented with a joint probability while cascading (sequential) interrelations are represented with conditional probabilities.

Examples of joint and conditional probabilities are given in **Figure 4.1**. A joint probability is the probability of two events occurring together where both variables are extreme (also called AND probability) (**Figure 4.1a**) and a conditional probability is the probability of an event given that another has already occurred (**Figure 4.1b**). **Figure 4.1** illustrates the concepts of joint probability and conditional probability, with daily rainfall data from a high-resolution gridded data set of daily meteorological observations over Europe (termed 'E-OBS') (Cornes *et al.*, 2018) and daily maximum wind gust data at Heathrow airport provided by the Met Office (2019). A wind gust here is defined as the maximum value, over the observing cycle, of the 3-second running average wind speed (WMO,2019). These datasets and the interrelation between extreme rainfall and extreme wind are discussed in **Section 4.4.1**.

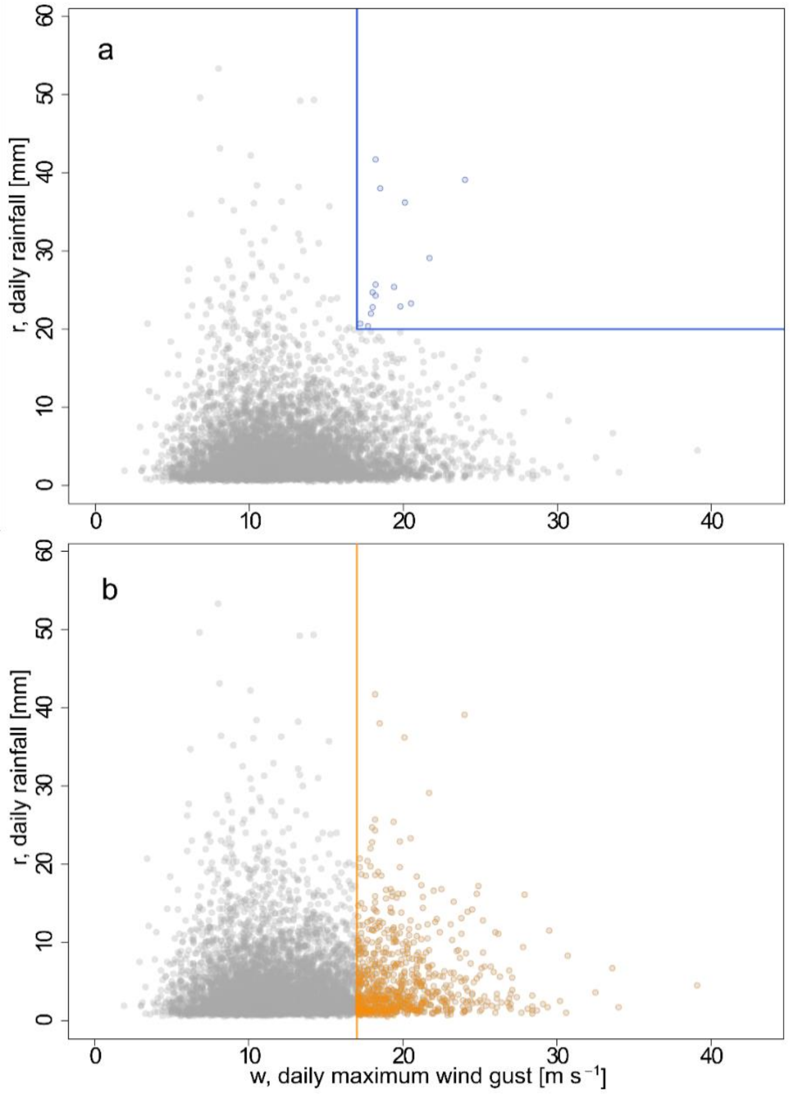

Figure 4.1: Illustration of joint and conditional extremes with daily rainfall *r* (mm day^{-1}) and daily maximum wind gust *w* (m s^{-1}) data at Heathrow airport for the period 1971–2018: (a) joint extremes (AND) of rainfall and wind gust (blue circles); (b) conditional extremes of rainfall given that wind gust is extreme (yellow circles). Daily rainfall data from E-OBS (Cornes *et al.*, 2018) and daily maximum wind gust (3 s period) data from the Met Office (2019).

Joint and conditional probabilities are relevant metrics for practitioners and have been studied and used in several studies in the environmental sciences (e.g., Hao *et al.*, 2017; Zscheischler and Seneviratne, 2017). However, as the most widely used level curve is the joint probability curve, we initially focus on it. To analyse our results and compare the performances of the models, we designed diagnostic tools that are presented in **Section 4.3.2**.

This chapter is organized as follows. We first (**Section 4.2**) provide a theoretical background on fundamental concepts used in this study and present the models and methodology used. We then (**Section 4.3**) discuss the characteristics of our synthetic dataset and present the results of the simulation study. The diagnostic tools used to compare models are also discussed (i.e., level curves and dependence measure). As a result, a heatmap exhibiting the strength and weaknesses of our six models is presented. It aims to provide objective criteria to justify the use of one model rather than another for a given set of hazards Two applications to pairs of natural hazards that can impact energy infrastructure are presented in **Section 4.4**.

The main purpose of these data applications is to illustrate our methodology, but the natural hazard interrelations studied have the potential to negatively impact energy infrastructure. The first application looks at compound daily extreme rainfall and wind in the United Kingdom. The combination of these two hazards can result in different and greater impacts than the addition of impacts due to extreme wind and extreme rainfall (e.g., strong wind destroying roof of a building can lead to greater damages from heavy rain) (Martius *et al.*, 2016). The second application studies extreme hot temperatures and wildfires in Portugal. Extreme temperatures can lead to damage on infrastructure (e.g., rail track deformation) and put pressure on the energy infrastructure by increasing the demand (Hatvani-Kovacs *et al.*, 2016; Vogel *et al.*, 2020), it also increases the probability of wildfires (Witte *et al.*, 2011; Perkins, 2015) which have the potential to cause fatalities and destroy infrastructures (Tedim *et al.*, 2018). We finish (**Section 4.5**) with discussion and conclusions.

4.2 Methods

We are interested in modelling interrelations between hazards (represented by environmental variables) in the extreme domain. This implies the use of methods and concepts coming from the broad area of Extreme Value Theory (EVT). Amongst the six models compared in this study, four are directly linked to EVT (JT-KDE, Cond-Ex, Galambos, Gumbel). Extreme Value Theory has its roots in univariate studies (Coles, 2001) and has been extended to the multivariate framework (Pickands, 1981; Davison and Huser, 2015). A theoretical background on extreme value theory is given in **Appendix F1**. In this study, we focus on modelling the dependence between two variables. Bivariate extreme value models developed within the statistical community (Resnick, 1987; Heffernan and Tawn, 2004; Cooley *et al.*, 2019) have been used for environmental application and therefore natural hazard interrelations (De Haan and De Ronde, 1998; Zheng *et al.*, 2014; Sadegh *et al.*, 2017). To reproduce the complexity and variety of natural hazard interrelations we use 60 synthetic datasets to compare the fitting performances of the models. In these synthetics datasets, we vary two main attributes of the bivariate datasets: the dependence structure and the marginal (individual) distributions. Of these 60 different synthetic datasets, 36 datasets have *asymptotically dependent variables* and 24 have *asymptotically independent variables* (see **Section 4.2.1** for a definition of these two concepts).

In this section, we first present the two types of asymptotic behaviour in bivariate extreme value statistics: asymptotic dependence and asymptotic independence and discuss different dependence measures for the estimation of the relationship between two variables (**Section 4.2.1**). The six bivariate models are then described (**Section 4.2.2**). Finally, we discuss the concept of the return level in the bivariate framework (**Section 4.2.3**).

4.2.1 **Bivariate extreme dependence**

4.2.1.1 Asymptotic dependence and asymptotic independence

Let $X_1, \ldots, X_n$ be n different variables, with each variable a vector that can take on multiple values. Assume that these vectors are random and independent and identically distributed (i.i.d). The asymptotic dependence implies that if one variable X_k for $k \in (1, n)$ has values X_k that are large, the other variable can take on values that are simultaneously extreme (Coles *et al.*, 1999). One way to characterize extremal dependence structures is to split them into those with asymptotic dependence and those with asymptotic independence. In the bivariate case, for (X_1, X_2) random pair with joint distribution G, the random variables X_1 and X_2 with common marginal distributions are asymptotically dependent if the following conditional probability (Heffernan, 2000)

$$P\ (X_1 > x \mid X_2 > x)\ \to c > 0\ as\ x \to x^* \tag{4.1}$$

Where $X_1 > x$ are those values of variable X_1 that are greater than a threshold x, the probability of both $X_1 > x$ and $X_2 > x$ is $c \in (0,1]$ and x^* is the upper-end point (maximum) of the common marginal distribution.

The variables X_1 and X_2 are asymptotically independent if (Heffernan, 2000)

$$P\ (X_1 > x \mid X_2 > x)\ \to 0\ as\ x \to x^* \tag{4.2}$$

where x is a high threshold. In practice (Davison and Huser, 2015), extremal dependence is often observed to weaken at high levels (i.e., as $x \to \infty$). Dependence between variables can be observed in the body of the joint distribution despite the multivariate distribution being in the max-domain of attraction of independence (Davison and Huser, 2015).

Using models that take the assumption of asymptotic dependence (independence) in the case of asymptotically independent (dependent) variables can lead to a large overestimation (underestimation) of the probability of joint extreme events (Ledford, 1996; Mazas and Hamm, 2017; Cooley *et al.*, 2019). Multivariate extreme value and regular variation theory presented in **Appendix F1** provides a rich theory for asymptotic dependence (De Haan and Resnick, 1977; Pickands, 1981) but are not able to distinguish between asymptotic independence and full independence.

4.2.1.2 Tail dependence measures

A popular method to analyse hazard interrelationships is to compute dependence measures (Zheng *et al.*, 2013; Petroliagkis, 2018). Dependence measures aim to describe how two (or more) variables are correlated.

When focusing on the dependence in the tails or extreme part of distributions, linear or rank dependence measures might not be accurate and other coefficients appear more relevant (Hao and Singh, 2016). Dependence between variables in the joint tail domain has been widely studied in the statistics community (Coles and Tawn, 1991; Ledford and Tawn, 1997; Coles *et al.*, 1999; Heffernan and Tawn, 2004; Zheng *et al.*, 2014). As explained in **Section 2.1.1**, in the tails, two variables can be either asymptotically independent or asymptotically dependent; different diagnostics and coefficients previously developed are summarized in Heffernan (2000).

In this study, we use the following tail dependence measures:

- the extremal dependence measures χ and $\bar{\chi}$ introduced by Coles *et al.* (1999);
- the coefficient of tail dependence η, introduced by Ledford and Tawn (1996).

These coefficients aim to measure the extremal dependence for bivariate random variables (X_1, X_2) and assume initially that (X_1, X_2) have a common marginal distribution. Coles *et al.* (1999) defined the extremal dependence measure:

$$\chi(x) = P(X_1 > x \mid X_2 > x) \text{ with } \lim_{x \to x^*} \chi(x) = \chi \tag{4.3}$$

with x* is the upper-end point (maximum) of the common marginal distribution and x a sufficiently high threshold. A sufficiently high threshold x is a value that can be considered as extreme within a given distribution (corresponding to a high quantile); the value of the threshold depends on the marginal distribution. The extremal dependence measure $\chi(x)$ is the probability of one variable (X_1 or X_2) being extreme given the other is extreme (X_2 or X_1). This measure χ varies in the range [0,1], where a value of $\chi = 0$ means that the two variables are asymptotically independent and $\chi = 1$ means that they are perfectly dependent. The extremal dependence measure χ is only suitable for asymptotic dependence. In the case of asymptotic independence ($\chi = 0$), Coles *et al.* (1999) introduced the measure $\bar{\chi}$ which falls between the range [-1,1], 1 being asymptotic independence. Ledford and Tawn (1996) defined their coefficient of tail dependence to be able to assess the strength of dependence between two asymptotically independent variables. They show that the joint survivor function for random variables (Z_1, Z_2) with common standard Fréchet margins can be expressed as (See **Appendix F**):

$$P(Z_1 > z, Z_2 > z) \sim \mathcal{L}(z)(P(Z_1 > z))^{1/\eta} \tag{4.4}$$

with z a sufficiently high threshold in the standard Fréchet space. $\mathcal{L}(z)$ a slowly varying function while $z \to \infty$ and η is the coefficient of tail dependence, lying in the range [0,1]. Different values of each coefficient and their implications are summarized in **Figure 4.2**. For large z, the three tail dependence measures presented above are related in the following way (Ledford and Tawn, 2003):

$$\bar{\chi} = \quad 2\eta - 1 \tag{4.5}$$

$$\chi = \begin{cases} 0 \; if \;\; \bar{\chi} \; = 1 \text{ and } \mathcal{L}(z) \rightarrow c > 0 \; as \; z \rightarrow z^{*} \\ 1 \; if \; \bar{\chi} \; < 1 \end{cases}$$

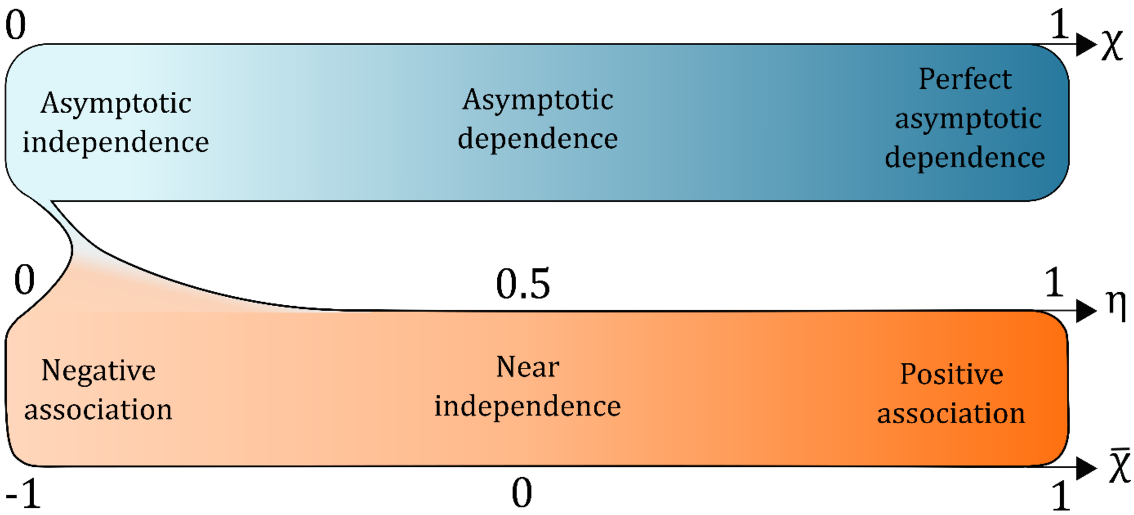

Figure 4.2: The three coefficients used in this study to assess the dependence between two variables at an extreme level. In the upper part of the plot (blue), the coefficient χ varies between perfect asymptotic dependence (light blue, χ = 0) and asymptotic independence (dark blue, χ = 1). In the lower part of the plot (orange), which is in the asymptotic independence domain (in other words, χ = 0) the coefficients $\bar{\chi}$ and η both vary between negative association (light orange, $\bar{\chi} = -1$; $\eta = 0$) and positive association (dark orange, $\bar{\chi} = \eta = 1$).

4.2.2 **Bivariate models**

Dependence measures are empirical measures which estimate the strength of the correlation, or dependence between two (or more) variables. Even though these measures provide crucial information, these do not allow to model joint (or conditional) exceedance probabilities. To model joint exceedance probabilities which represent the joint occurrence of hazards (here represented by extremes of environmental variables) in time and space, the use of stochastic models is required. In this section, we present the three stochastic approaches for multivariate modelling that are used in the simulation study: parametric copulas, the semi-parametric conditional extremes model and a non-parametric approach based on multivariate extreme value theory (see **Appendix F1**) and kernel density estimation.

4.2.2.1 Copulas

In the bivariate case, a copula is a joint distribution function which defines the dependence between two variables independently from the marginal distributions of these variables (Heffernan, 2000; Nelsen, 2006; Genest and Favre, 2007; Hao and Singh, 2016). Let the random variables (X_1, X_2) be vectors of i.i.d. values with marginal distributions $F_1(x_1)$ and $F_2(x_2)$ and a joint cumulative distribution function $F_{1,2}(x_1,x_2)$. Any bivariate distribution function with marginal distribution functions $F_{X1}(x_1)$ and $F_{X2}(x_2)$ can be expressed as a copula function as follows (Sklar, 1959; Nelsen, 2006):

$$F_1(x_1, x_2) = C\{F_1(x_1), F_2(x_2)\}, \tag{4.6}$$

where *C* is the copula function. Copulas are not limited to two variables and **Eq. 6** can be extended to higher dimensions. Several classes of copula with different properties are available, including Archimedean copulas, elliptical and extreme value copulas (e.g., Joe, 1997; Nelsen, 2006). Extreme value copulas have been used within various domains such as finance, insurance and hydrology because of their ability to model extremal dependence structures (Genest and Nešlehová, 2013).

However, extreme value copulas are by definition asymptotically dependent as they follow the rules of multivariate extreme value theory (see **Appendix F1**). The two types of extremal dependence were presented in **Section 4.2.1** and show that it is important to also consider asymptotic independence. Many copulas are asymptotically independent, including the normal copula and the Farlie-Gumbel-Morgenstern (FGM) copula (Heffernan, 2000). These two copulae will be used in the simulation analysis as asymptotically independent models (**Section 4.3**).

In the present study, the application of a copula model can be summarized in four main steps:

(i) Fitting marginal distributions to the two variables; empirical distribution below a threshold and General Pareto Distribution (GPD) above this threshold.

(ii) Transforming the variables to uniform margins. The transformed datasets no longer have information on the marginal distributions but keep the information about the dependence structure (Nelsen, 2006).

(iii) Fitting the copula function to the pseudo-observations by estimating the copula parameter(s) with an estimator (Genest and Favre, 2007).

(iv) Estimating the probability of joint events with the copula function previously fitted.

4.2.2.2 Conditional extreme model

The conditional extremes model (Heffernan and Tawn, 2004; Keef *et al.*, 2013) is a semi-parametric model designed to overcome several limitations of copulas and other approaches such as the joint tail methods in which all variables must become large at the same rate. The aforementioned methods can typically handle only one form of extremal dependence, either asymptotic dependence or asymptotic independence. The conditional extremes model can be more flexible with asymptotic dependence classes; it can account for asymptotic independence and asymptotic dependence (Heffernan and Tawn, 2004; Keef *et al.*, 2013). It can also be used to analyse more than two i.i.d variables more easily than copula-based methods (Winter and Tawn, 2016); we restrict the theory provided here to the bivariate case. The conditional model has been used for different purposes: spatial or temporal dependence between extremes (Winter and Tawn, 2016; Winter *et al.*, 2016), dependence between extreme hazards (Zheng *et al.*, 2014) and even financial purposes (Hilal *et al.*, 2011).

The conditional extremes model assesses the dependence structure between several variables conditioning on one being extreme and aims to model the conditional distribution. As in joint-tail models, the first step is to transform the marginal distributions; here the preferred marginal choice is the following: Laplace (or Gumbel) margins (Heffernan and Tawn, 2004; Keef *et al.*, 2013). Let the random variables (Y_1,Y_2) be vectors of i.i.d. values with Laplace distributions. The conditional extremes model aims to identify two normalizing functions $a(y_i)$ and $b(y_i)$ such that a satisfies $\mathbb{R}_+ \rightarrow \mathbb{R}$ and b satisfies $\mathbb{R}_+ \rightarrow \mathbb{R}_+$, Both are defined such that for $y > 0$ (Winter, 2016):

$$P\left(\frac{Y_2 - a[Y_1]}{b[Y_1]} \leq z, Y_1 - u > y | Y_1 > u\right) \longrightarrow exp(-y)\, G(z) \tag{4.7}$$

as u $\rightarrow \infty$, where G(z) is a non-degenerate distribution function. In the case of Laplace margins the normalising functions a and b are given by (Winter, 2016):

$$a[y] = \alpha y \quad and \quad b[y] = y^{\beta} \tag{4.8}$$

where $\alpha \in [-1, 1]$ and $\beta \in (-\infty, 1)$. The different values of α and β characterize different forms of tail dependence. In the case where $\alpha = 1$ and $\beta = 0$, variables (Y_1, Y_2) exhibit asymptotic positive dependence and the case of asymptotic negative dependence is given when $\alpha = -1$ and $\beta = 0$ (Winter, 2016). **Eq.4.7** and **Eq.4.8** aim to present the defining properties and mechanisms of the conditional extremes model , not an explicit expression of a distribution. For more information about the model, the reader can refer to Heffernan and Tawn (2004).

Formally, the application of the conditional extreme model can be summarized in four main steps:

(i) Fitting marginal distributions to the two variables; an empirical cumulative distribution function below a threshold and generalised Pareto distribution (GPD) above this threshold.

(ii) Transforming those distributions onto Laplace (or Gumbel) margins.

(iii) Estimating the dependence parameters using non-linear regression.

(iv) Estimating the probability of joint events by simulating new extreme data through the conditional model

4.2.2.3 Joint tail KDE (kernel density estimation) approach

The non-parametric approach used in this chapter is an adaptation of the non-parametric approach presented by Cooley *et al.* (2019). Moreover, the dependence measures η is estimated to determine whether data are asymptotically dependent or asymptotically independent. This approach is based on the 2D kernel density estimator and the multivariate extreme value framework (see **Appendix F1**).

The kernel density estimation (KDE) method has the advantage of being a non-parametric way to estimate the joint distribution of *n* variables. With KDE, we do not assume the underlying distribution of the margins or the dependence structure. The KDE centres a smooth kernel at each observation. The choice of the bandwidth is crucial when using this method (Duong, 2007; Hao and Singh, 2016). This selection was done automatically in our case within the kernel survival function estimation function from the R package ks (Duong, 2007, 2016).

The kernel density estimator is used here to estimate an empirical density distribution $\hat{f}(X)$ and a joint survival distribution $\hat{F}(X)$ of the bivariate dataset where $X=(X_1, X_2)$. The joint survival distribution corresponds to the joint exceedance probability of the two variables (See **Section 4.2.3**). From the joint survival distribution, it is possible to estimate level curves which are isolines corresponding to given joint probabilities of exceedance (see **Section 4.2.3**).

After estimating the joint survival distribution of the two variables with a kernel density estimator, the cumulative distributions $\widehat{F}_i(x)$ of the two random variables X_i ($i = 1, 2,\ldots$) are estimated empirically below a threshold and from a Generalized Pareto distribution above the threshold. The two marginal cumulative distribution functions are then transformed to Fréchet margins to allow the use of multivariate extreme value theory(Cooley *et al.*, 2019):

$$\widehat{T}_i(x) = \frac{-1}{ln(\widehat{F}_i(x))}. \tag{4.9}$$

Therefore, $Z = T(X) = \big(T_1(X_1), T_2(X_2)\big)$ can be assumed to be regularly varying with an index of regular variation 1 (see **Appendix F1**). An extrapolation from a base probability p_{base} (blue area in **Figure 4.3**) estimated with a kernel density to an objective probability p_{obj} (purple area in **Fig. 4.3**) is then done on the transformed space. Thus, on the transformed scale, it is possible to construct $\hat{l}_{\mathrm{Z(obj)}} = t\hat{l}_{\mathrm{Z(base)}}$ (Cooley *et al.*, 2019). To produce level curves on the original scale, the transformation in **Eq. 4.9** is reversed: $\hat{l}_{\text{obj}} = T^{-1}\hat{l}_{\mathrm{Z(obj)}}$. **Figure 4.3** gives a graphical representation of the extrapolation done within the joint tail KDE approach.

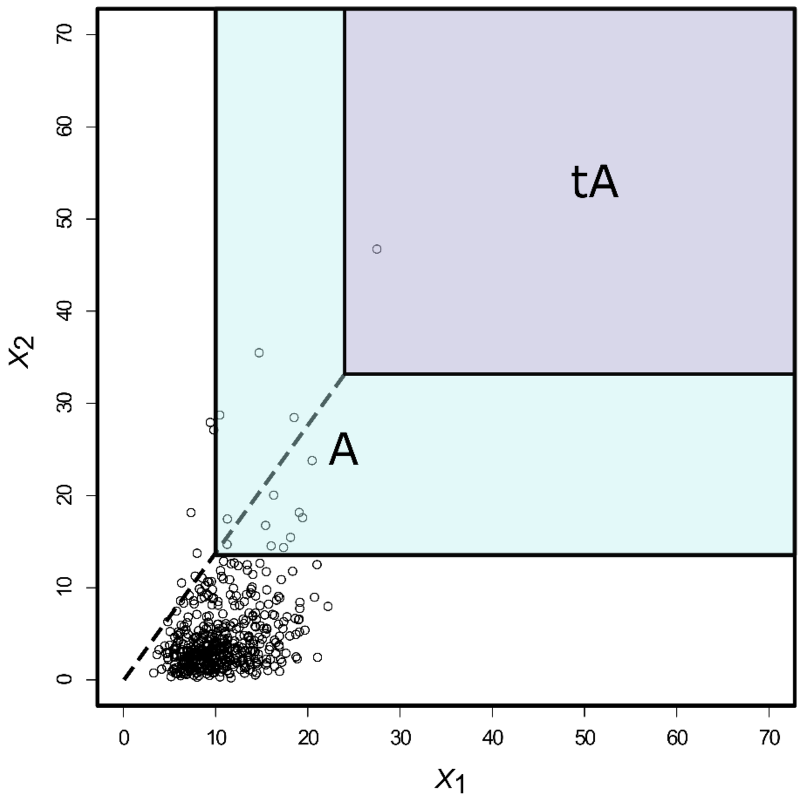

Figure 4.3: Extrapolation in a regularly varying tail for a distribution in the max-domain of attraction of some multivariate extreme value distribution. Black circles represent an asymptotically dependent bivariate dataset. To estimate the extreme joint probability $P(tA)$ (where tA is an extreme set represented by the purple area), one can compute $P(A) = P\{Z \in A\}$, (where A is a less extreme set than tA represented by the light blue area) with $t < 1$. More data points are available in A than tA, Then, from the regular variation framework $t\,P(tA) \approx tP(A)$. Adapted from Huser (2013)

The methodology presented above is only valid when the two variables X_1, X_2 are asymptotically dependent. In the asymptotic independence case, one needs to adjust the methodology. Two asymptotically independent variables follow the properties of hidden regular variation (Resnick, 2002; Maulik and Resnick, 2005) (see **Appendix F1.2.3**). Formally, the coefficient of tail dependence η is introduced such as (Cooley *et al.*, 2019):

$$\hat{l}_{Z(obj)} = t^{\frac{1}{\eta}} \hat{l}_{Z(base)} \tag{4.10}$$

The specificity of this approach (presented below) is that it combines a non-parametric estimation of the joint density and the framework of multivariate extreme value presented in **Appendix F1.2**. It can deal with both asymptotic dependence and independence. The coefficient of tail dependence estimation has an influence on the extrapolation process in the asymptotic independence case. Here we used the estimator presented in Winter (2016) which is derived from the joint-tail model of Ledford and Tawn (1997).

Formally, the application of the joint tail KDE model can be summarized in five main steps:

(i) Estimating the joint cumulative distribution of the variables with a kernel density estimator.

(ii) Fitting marginal distributions to the two variables; empirical distribution below a threshold and General Pareto Distribution (GPD) above this threshold.

(iii) Transforming those distributions into Fréchet margins.

(iv) Determining whether variables are asymptotically dependent or asymptotically independent by estimating the coefficients of tail dependence χ and η.

(v) Estimating the probability of joint events and extrapolate the base isoline to an objective isoline.

4.2.2.4 Return levels in the bivariate framework

Studying natural hazards as multivariate — and particularly bivariate — events is a growing practice in multiple disciplines, including the following: coastal engineering (Hawkes *et al.*, 2002; Mazas and Hamm, 2017); climatology Hao *et al.*, 2017, 2018; Zscheischler and Seneviratne, 2017); and hydrology (Zheng *et al.*, 2014; Hao and Singh, 2016). There has been debate among scientists trying to define a "multivariate return period" (Serinaldi, 2015; Gouldby *et al.*, 2017). Serinaldi (2015) defined seven different types of probabilities that can be considered as bivariate probabilities of exceedance. These can be expressed through copula notation.

Let the random variables (X_1, X_2) be vectors of i.i.d. values with marginal distributions $F_i(x_i)$ with i=1,2, C their copula function (**Section 4.2.3.1**) and $F_{1,2}\ (x_1, x_2) = C\{F_1(x_1), F_2(x_2)\} = C(u, v)$ where $F_{1,2}$ is the bivariate distribution function of X_1 and X_2, $U = F_1(X_1)$ and $V = F_2(X_2)$ are standard uniform random variables. The seven types of probability and their equations are given in **Table 4.1**.

Table 4.1: Types of probabilities for bivariate (*X,Y*) return period estimation. *u* and *v* are extreme thresholds. From (Serinaldi, 2015).

Type of probability	*Equation*	*Eq. #*
$\boldsymbol{P_{AND}}$	$P(U > u \cap V > v) = 1 - u - v + C(u,v)$	(4.11)
$\boldsymbol{P_{OR}}$	$P(U > u \cup V > v) = 1 - C(u,v)$	(4.12)
$\boldsymbol{P_{COND1}}$	$P(U > u \mid V > v) = (1 - u - v + C(u,v))/(1-u)$	(4.13)
$\boldsymbol{P_{COND2}}$	$P(U > u \mid V \leq v) = 1 - \frac{C(u,v)}{u}$	(4.14)
$\boldsymbol{P_{COND3}}$	$P(U > u \mid V = v) = 1 - \frac{\partial C(u,v)}{\partial u}$	(4.15)
$\boldsymbol{P_{K}}$	$P(C(u,v) > t) = 1 - K_C(t)$	(4.16)
$\boldsymbol{P_{S}}$	$P(g(U,V)) = 1 - F_Z(z)$	(4.17)

The function *Kc* in **Eq. 4.16** is the Kendall function and represents the distribution function of the copula (Salvadori and De Michele, 2010; Serinaldi, 2015). **Equation 4.17** refers to the "structure-based" return period introduced by Volpi and Fiori (2014). Among these seven types of probabilities, we selected the "AND" and the "COND1" probabilities (see **Figure 4.4**) as these are commonly used in the literature (Chebana and Ouarda, 2011; Tencer *et al.*, 2014; Sadegh *et al.*, 2018) and correspond to the two types of interrelations we are interested in (i.e., compound and cascade).

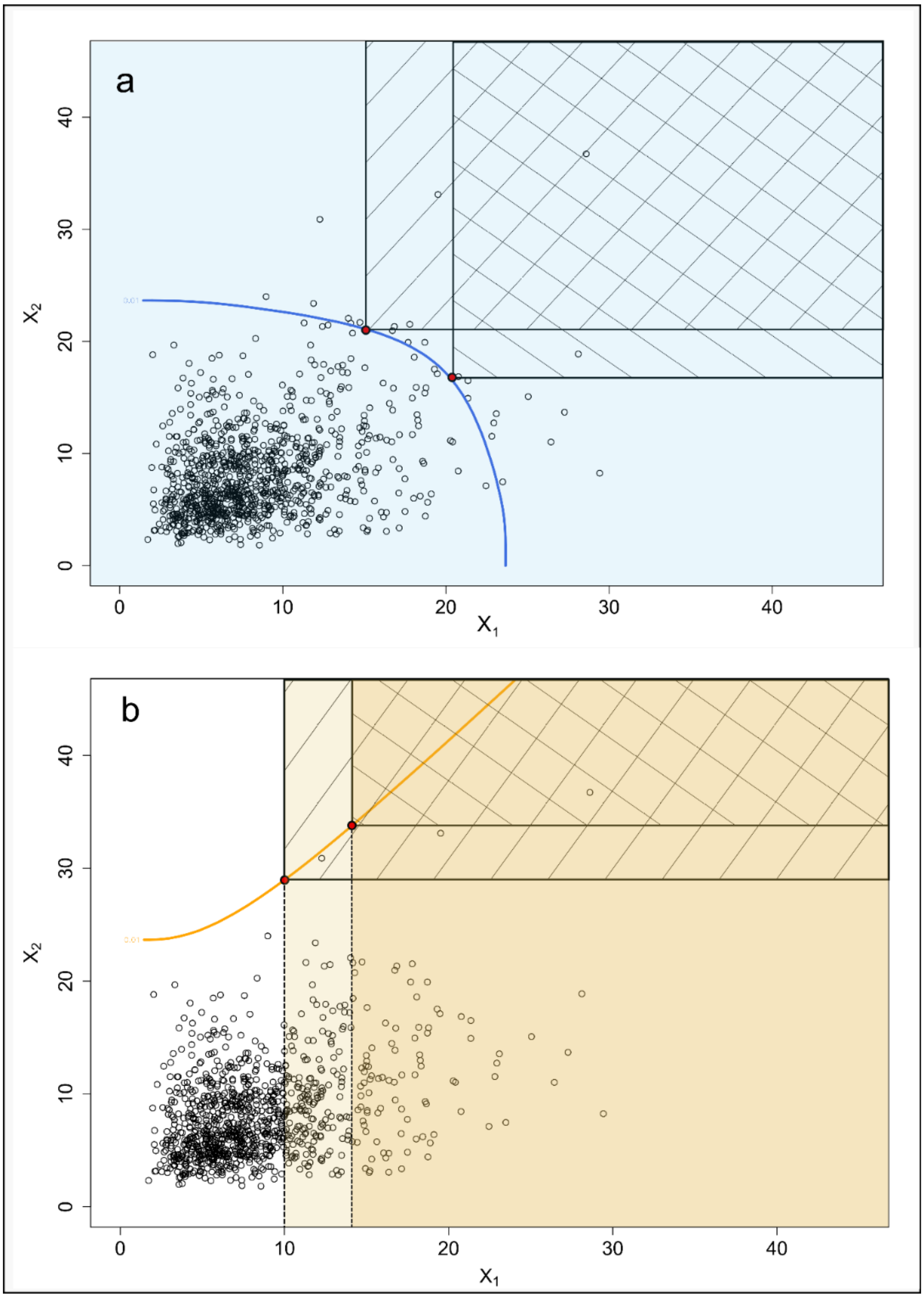

Figure 4.4: Graphical representation of two bivariate (X_1, X_2) probabilities of exceedance: (a) P_{AND} probability and (b) P_{COND} probability with level curves (blue in 'a' and orange in 'b') representing p = 0.01 (1000 data points on a Gumbel copula with log-normal marginal distributions). Colours represent the domain on which the probabilities are computed while the areas with diagonal hatching represent the critical regions which are the regions corresponding to the given probabilities.

In the 2D space, probabilities of exceedance (or quantiles) are not represented by a single value but by a curve with an infinite number of points with the same probability of exceedance.

However, as shown in **Figure 4.4**, these probabilities are defined by: (i) the domain where these are computed and (ii) the critical region corresponding to the probability type. For the AND probability, the computation domain remains similar when moving along the curve while the critical region evolves constantly. For the COND1 probability, both the computation domain and critical region evolve when moving along the curve (see **Figure 4.4**). Bivariate probabilities of exceedance are curves. These curves have been given various names in different research papers including the following:

- *isolines* (Salvadori, 2004; De Michele *et al.*, 2007; Salvadori *et al.*, 2016; Sadegh *et al.*, 2017, 2018)
- *level curves* (Coles, 2001; Salvadori, 2004; De Michele *et al.*, 2007; Volpi and Fiori, 2012; Serinaldi, 2015, 2016; Bevacqua *et al.*, 2017).

For the specific case of the AND probability, the following names have been used:

- *joint exceedance curves* (Hawkes *et al.*, 2002; Hawkes, 2008; Mazas and Hamm, 2017).
- *quantile curves* (De Haan and De Ronde, 1998; Chebana and Ouarda, 2011).

4.3 Simulation study

Here we are interested in comparing the abilities of six different models presented in **Section 4.2.3** to reproduce a given dependence structure. We create 60 different synthetic dataset types with varying marginal distributions and dependence structures. By doing this, we aim to produce bivariate synthetic datasets comparable to the ones studied in bivariate hazard analysis (Zheng *et al.*, 2014; Hendry *et al.*, 2019). This will allow us to confront the six models against the synthetic datasets, as a reference for bivariate hazard interrelation analysis (**See Section 4.4**). The six models compared in this simulation study are:

(i) the conditional extremes model (Cond-Ex) (**Section 4.2.3.2**);
(ii) the non-parametric joint-tail model (JT-KDE) (**Section 4.2.3.3**);
(iii) the Gumbel copula (Gumcop) (**Section 4.2.3.1**);
(iv) the normal copula (Normalcop) (**Section 4.2.3.1**);
(v) the Farlie-Gumbel-Morgenstern (FGMcop) copula (**Section 4.2.3.1**);
(vi) the Galambos copula (Galamboscop) (**Section 4.2.3.1**).

Among the four copulas used here, two are asymptotically dependent (Gumbel and Galambos) and two are asymptotically independent (normal and FGM). A description of the six models is given in **Table 4.2**. **Table 4.2** synthesizes a range of information about all the six models used in this simulation study including their type (nonparametric, semiparametric, parametric), equation, parameter range (if there is a parameter) and asymptotic modelling domain. This latter information is important to interpret the result of the simulation study in **Section 4.3.3**.

Table 4.2: Description of the six statistical models compared in this article. The description includes the model name and acronym (used throughout the article), type of model (parametric, semi-parametric, non-parametric), the mathematical description, the parameter range (where relevant) and the asymptotic modelling domain (AI for asymptotic independence and AD for asymptotic dependence)

Model name (Model acronym)	Model type	Mathematical description	Parameter range	Asymptotic modelling domain
Joint tail KDE (JT-KDE)	Non-Parametric	$P(Z \in sA^*) \approx s^{-1}P(Z \in A^*)$		AD
	Semi-parametric	$P(Z \in sA^*) \approx s^{-1/\eta}P(Z \in A^*)$	$\eta \in [0,1]$	AI
Conditional Extremes Model (Cond-Ex)	Semi-Parametric	$P\left(\frac{Y_2 - a[Y_1]}{b[Y_1]} \leq z\,,\ Y_1 - u > y \mid Y_1 > u\right) \rightarrow \exp(-y)\,G(z)$ for y> 0, as u → ∞ where G(z) is a non-degenerate distribution function.		AI and AD
Gumbel copula (Gumcop)	Parametric	$C(u,v) = \exp\left\{-\left[(-\ln(u))^{\theta} + (-\ln(v))^{\theta}\right]^{1/\theta}\right\}$	$\theta \in [1,\infty)$	AD
Normal copula (Normalcop)	Parametric	$C(u,v) = \int_{-\infty}^{\Phi^{-1}(u)} \int_{-\infty}^{\Phi^{-1}(v)} \frac{1}{2\pi\sqrt{1-\theta^2}} \exp\left(\frac{2\theta xy - x^2 - y^2}{2(1-\theta^2)}\right) dxdy$ With Φ(.) the standard Gaussian distribution function	$\theta \in [-1,1]$	AI
FGM copula (FGMcop)	Parametric	$C(u,v) = uv[1 + \theta(1-u)(1-v)]$	$\theta \in [-1,1]$	AI
Galambos copula (Galamboscop)	Parametric	$C(u,v) = uv\exp\left\{-\left[(-\ln(u))^{-\theta} + -(\ln(v))^{-\theta}\right]^{-1/\theta}\right\}$	$\theta \in [0,\infty)$	AD

In this section, we first describe and display the synthetic data that have been generated to conduct this study. We shall then present the measures used in this study to compare the level curves and the dependence measures estimated from the six models presented in **Table 4.2**. Finally, the results of the simulation will be displayed and analysed.

4.3.1 Synthetic data

Synthetic datasets are often used to compare different statistical models (Chebana and Ouarda, 2011; Zheng *et al.*, 2014; Cooley *et al.*, 2019). Here we generated 60 bivariate synthetic datasets representative of environmental data such as daily rainfall, daily wind gust and daily wildfire occurrences (see **Section 4.4**). The number of synthetic data points we use here have been fixed to 5000 for each dataset. For the asymptotic dependence case, 36 distinct datasets are generated from a Gumbel copula (see **Appendix F1.3.1**); for the asymptotic independence case, 24 datasets are generated from a normal copula (see **Appendix F1.3.2**). Each synthetic dataset set of parameters has been used to generate 100 realizations to produce confidence intervals.

The synthetic datasets are generated from two marginal distributions and a dependence model (i.e., copula). Both marginal distributions are log-normal; the log-normal distribution has been used (among others) for the modelling of a wide range of natural hazards, including wind, flood and rainfall (Malamud and Turcotte, 2006; Clare *et al.*, 2016; Loukatou *et al.*, 2018; Nguyen Sinh *et al.*, 2019).

Random variables X with a log-normal distribution are governed by two parameters: the location parameter μ and the shape parameter σ which correspond respectively to the mean and the standard deviation of Y, the variable's natural logarithm, i.e., $Y = \ln(X)$ (Aitchison, 1957). The parameter σ influences the shape of the distribution and the heaviness of the tail; the dispersion of a log-normal distribution mostly depends on the shape parameter (Koopmans *et al.*, 1964)

We can characterize log-normal distributions with the coefficient of variation c_v which is the ratio of the standard deviation s of the log-normally distributed variable x to its nonzero mean $\bar{x}$ (Malamud and Turcotte, 1999):

$$c_v = \frac{s}{\bar{x}} \tag{4.18}$$

The standard deviation s and the nonzero mean $\bar{x}$ are both related to the two parameters μ and σ of the log-normal distribution (see **Table 4.3**). The use of the coefficient of variation characterizes the log-normal distribution with one single parameter instead of two. The distribution used in the simulation study, the parameters and the relationship between these parameters and the different tail dependence measures are summarised in **Table 4.3**.

Table 4.3: Marginal distributions and copula used for the synthetic datasets

Distribution	Cumulative density function	Parameters	Parameters values
Log-normal distribution	$F(x) = \Phi\left(\frac{\ln(x) - \mu}{\sigma}\right)$	μ, σ of y, where $y = \ln(x)$ $\bar{x} = exp(\mu + \sigma^2/2)$ $s = \sqrt{(exp(\sigma^2 - 1)exp(2\mu + \sigma^2)}$ $c_v = s/\bar{x}$	**A**: c_v =0.25 **B**: c_v =0.53 **C**: c_v =2.91
Gumbel copula	$C(u,v) = exp\left\{-\left[(-\ln(u))^\theta + (-\ln(v))^\theta\right]^{1/\theta}\right\}$	$\theta = log_2(2 - \chi)$	χ = 0.05, 0.10, 0.30, 0.50, 0.70, 0.90
Normal copula	$C(u,v) = \int_{-\infty}^{\Phi^{-1}(u)} \int_{-\infty}^{\Phi^{-1}(v)} \frac{1}{2\pi\sqrt{1-\theta^2}} \exp\left(\frac{2\theta xy - x^2 - y^2}{2(1-\theta^2)}\right) dxdy$	$\theta = 2\eta - 1$	η = 0.25, 0.50, 0.75, 0.90

where Φ is the cumulative distribution function of the standard normal distribution

We use three different coefficients of variation: c_v = 0.25 (labelled as **A** for the rest of this chapter), 0.53 (labelled **B**) and 2.91 (labelled **C**) (See **Table 4.3**). The log-normal distribution **A** (c_v = 0.25) produces a distribution close to the normal distribution. The distribution **C** (c_v = 2.91) is a highly right-skewed distribution. The distribution **B** (c_v = 0.53) is intermediate skewness between **A** and **B**. In the bivariate context, there are six possible combinations of these distributions: **AA**, **AB**, **AC**, **BB**, **BC**, and **CC**.

The dependence structure is represented by a Gumbel copula in the case of asymptotic dependence (AD) and a normal copula in the case of asymptotic independence (AI) as no copula can be both asymptotically independent and asymptotically dependent (Heffernan, 2000; Coles, 2001). The Gumbel copula is an extreme value copula, asymptotically dependent**,** with one parameter θ which can be related to the extremal dependence measure χ. Here, we vary χ between 0.05 (very weak asymptotic dependence) and 0.9 (strong asymptotic dependence) (see **Figure 4.5**). The Normal (or Gaussian) copula is asymptotically independent. Its unique parameter is related to the coefficient of tail dependence η (Heffernan, 2000). We vary η from $\eta = 0.25$ (negative sub-asymptotic dependence) to $\eta = 0.9$ (positive sub-asymptotic dependence) (see **Figure 4.5**). In total, ten different dependence structures were simulated for each of the six combinations of marginal distributions. The 60 bivariate synthetic datasets used in this study are displayed in **Figure 4.5**.

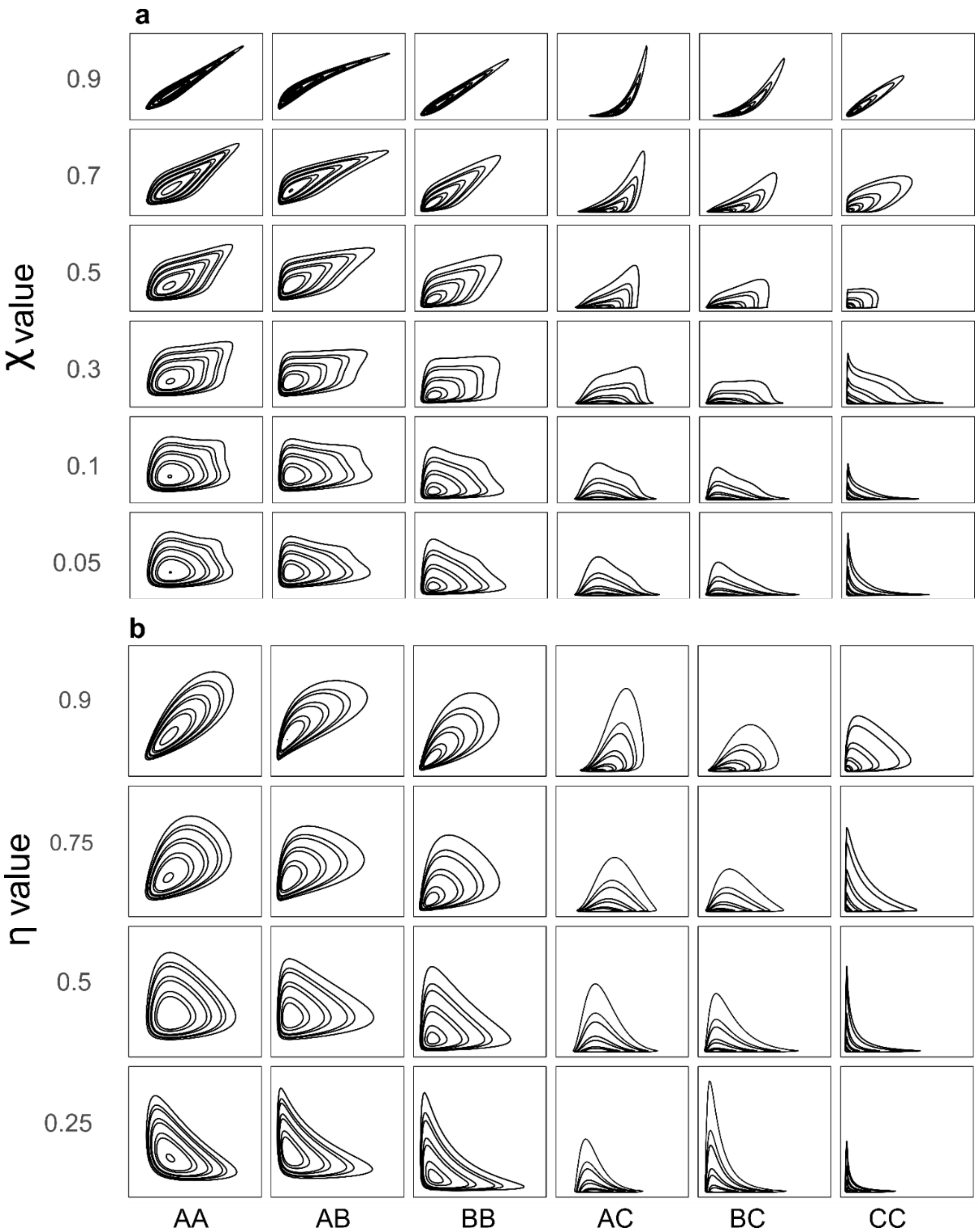

Figure 4.5: The 60 different synthetic bivariate datasets used in our simulation study. On the *y*-axis: the dependence strength (a) χ (for asymptotic dependence) and (b) η (for asymptotic independence), vary from slightly negative association to heavily dependent (see also Fig. 4.2). On the *x*-axis AA to CC represent the marginal distributions that are part of the bivariate distributions (see Table 4.3) with A, B, C representing log-normal distributions with different coefficient of variations c_v (A: c_v = 0.25; B: c_v = 0.47; C: c_v = 0.95).

To compare the fitting capabilities of the different models presented in **Section 4.2.3**, we vary several characteristics of the synthetic dataset:

(i) *The shape of the marginal distributions*. Natural hazards can exhibit very diverse statistical properties depending not only on their type but also on the location where they occur (Sachs *et al.*, 2012).

(ii) *The strength of the dependence represented by the parameter of the copula function*. The type and strength of the relationship between natural hazards can vary within a broad range depending on the natural hazard studied or the location (Gill and Malamud, 2014;

Martius *et al.*, 2016). To consider both the AD and AI cases, the two parameters χ and η (**Section 2.2**) are used.

4.3.2 Diagnostic tools

There are many diagnostic tools to assess the goodness-of-fit of parametric bivariate models (Arnold and Emerson, 2011; Couasnon *et al.*, 2018; Genest *et al.*, 2009, 2011; Genest and Nešlehová, 2013; Sadegh *et al.*, 2017). Amongst these, some of the most popular are the following:

- Cramer–von Mises statistic (Arnold, Taylor and Emerson, John, 2011)
- Kolmogorov-Smirnov test (Arnold, Taylor and Emerson, John, 2011)
- Akaike information criterion (AIC) (Akaike, 1974)
- Bayesian information criterion (BIC) (Schwarz, 1978)

These measures have been developed in a univariate framework and then extended to the bivariate framework. Genest (2009) proposed several approaches for Cramer–von Mises and Kolmogorov–Smirnov goodness-of-fit tests for copulas. There are two issues we faced using these measures for our study:

(i) These criteria are designed to measure the fit on the dependence structure of the whole dataset and not on the extreme dependence'.
(ii) In our study, we aim to compare parametric and non-parametric models.

To address the first issue, goodness-of-fit tests have been developed for extreme value copulas (Genest *et al.*, 2011). The latter issue is more complicated; each modelling approach has its own fitting methodologies, and although it is now possible to compare copulas against each other (Sadegh *et al.*, 2017; Couasnon *et al.*, 2018), it is more difficult to compare copulas against semi-parametric or non-parametric models. The measures mentioned above are not suitable for the present study as they require models to be parametric to be compared against observations (Stephens, 1970; Arnold, Taylor and Emerson, John, 2011). It is then not possible to compare the goodness-of-fit of the six models used in this study altogether.

However, we are interested in fitting capabilities in the extremes. The models will then be compared on the estimation of two attributes of the synthetic data detailed below:

(i) The P_{AND} probability of exceedance (**Section 4.2.3**) represented by the level curve at p = 0.001.
(ii) The tail dependence measures χ and η (**Section 4.2.2.2**).

We present here the diagnostic tools related to the level curve. The tools used to compare tails dependence measures can be found in **Appendix E**. Here we chose to compare our six models with respect to their ability to reproduce a reference level curve from the underlying bivariate (X_1, X_2) distribution of the data l_{obj} ('obj' is again used to indicate objective) which corresponds to an extreme joint probability $p = 0.001$. For each model i a level curve $l_{\text{obj},i}$ is computed. Several methods and criteria have been used in the literature to compare level curves to a reference including comparing the curves with vertical point-wise distances between the underlying curves (Chebana and Ouarda, 2011). This approach finds its limitation when level curves do not share the same *x*-axis coordinate (X_1 axis).

In **Figure 4.6** is presented our procedure for computation of the goodness-of-fit indicators (described in further detail below). In **Figure 4.6** the example modelled and reference curves do not reach the same coordinate on the X_1 axis, making it impossible to compare these two level curves between X_2=0.0 and X_2=0.3. Cooley *et al.* (2019) divided level curves into two parts, comparing six *x*-axis coordinates on one part and six *y*-axis coordinates on the other part, to overcome the aforementioned limitation. Here we chose to use a consistent criterion all along the curves to evaluate the distance between each modelled curve and the reference curve. The four steps we use are the following:

(i) Each modelled and reference level curve is normalized by dividing its coordinates by their maximum values. With that process, the curves are bounded in the [0,1] by [0,1] space. The different indicators are then computed in this normalized space.

(ii) Cartesian coordinates (x,y) of the modelled and reference level curves are transformed into polar coordinates (θ, r).

(iii) Each modelled and reference level curve is discretized via linear interpolation into points. Each point corresponds to an angle value (triangles and dots on the curves in **Figure 4.6**).

(iv) Points from both the modelled and reference level curves with the same angle are coupled. Indicators are computed at each of the 80 couples of points (see **Figure 4.6**).

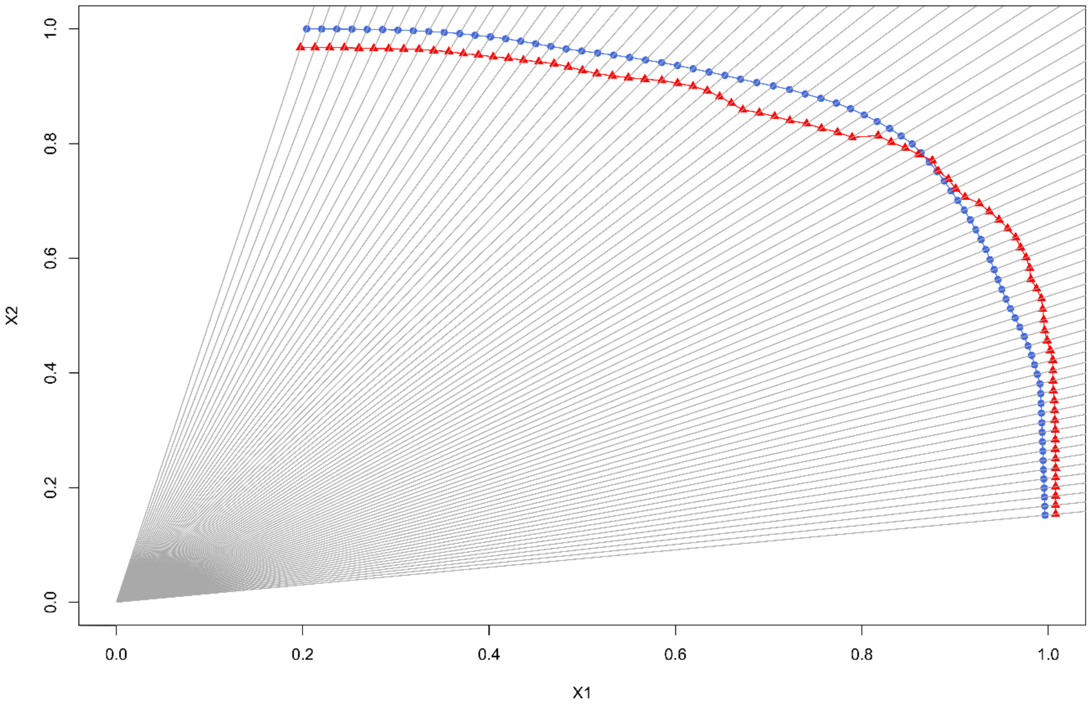

Figure 4.6: Procedure for computation of the goodness-of-fit indicators. Two variables are given, X_2 as a function of X_1. The red triangles and red curve represent the modelled level curve from a given model. The blue circles and blue curve are the reference level curve from the underlying bivariate (X_1, X_2) distribution of the data. Distance between the curves is calculated along the radius at 80 (X_1, X_2) coordinates (e.g., between the blue circles and the red triangles).

We used a weighted Euclidean distance (*wd*) as comparison criteria. The density of level curves (described in **Appendix F2**) allows one to weight the Euclidean distance of each of the 80 points by the local density of the curve. By weighting the Euclidean distance according to the reference bivariate distribution probability density function, we give more importance to the proper part of the curve where a bivariate event is more likely to occur, rather than the naïve part (here the naïve part is defined as where the bivariate event is less likely to occur) (Chebana and Ouarda, 2011; Volpi and Fiori, 2012).

$$wd = \sum_{i=1}^{N} w_i\left(\sqrt{(x_{mod,i} - x_{ref,i})^2 + (y_{mod,i} - y_{ref,i})^2}\right) \tag{4.19}$$

Where the number of points *N*=80, *i*=1,…,*N*, *w* is the weight, (x_{mod}, y_{mod}) are the coordinates of the modelled level curve and $(x_{\text{ref}}, y_{\text{ref}})$ the coordinated of reference the level curve

4.3.3 **Results**

Two analyses are conducted in parallel, one for asymptotic dependence (**AD**) and one for asymptotic independence (**AI**). In the case of asymptotic dependence, the Gumbel copula is used with 5000 data points. The χ value is the measure of interest under **AD**; values taken by χ have been presented in **Section 3.1**. For each χ value, we generated 100 realizations of the dataset from the same underlying bivariate distribution. The 100 realizations generated have two purposes: (i) increase the robustness of the results and (ii) create a confidence interval around the median which was set at the 95% confidence level by taking the quantiles Q2.5 and Q97.5 of the 100 realizations. To confront this approach, we generated two sets of 100 realizations which showed very small variations in the values of Q2.5, Q50 and Q97.5 without impacting our interpretation of the results. In the case of asymptotic independence, the normal copula is used.

The marginal distributions do not have any impact on the dependence structure (Nelsen, 2006; Genest and Favre, 2007). We show in **Appendix E** that marginal distributions also have a very small impact on the estimation of dependence measures. All the methods used in this study include a transformation of marginal distributions and the fitting of a GPD above an extreme threshold (**Section 4.2.3**). By varying the marginal distribution of the variables of our synthetic dataset we aim to capture uncertainties and errors arising from both the fitting of the marginal distributions and the dependence structure.

For both asymptotic dependence **AD** and asymptotic independence **AI**, the objective level curve l_{obj} to be compared has been fixed at the probability p_{obj} = 0.001. For each of the 60 bivariate datasets, the six models presented are fitted to the 100 realizations. The dependence measures $\hat{\chi}_i, \hat{\eta}_i$ as well as the level curve $\hat{l}_{obj,i}$ are estimated for every six models, with i∈ (1:6) correspond to each model. We then use the diagnostic tool and criteria presented in **Section 4.3.2** to compare the performance of the models. From the 100 realizations, 100 level curves $\hat{l}_{obj,i}$ are generated for each model. Three curves are designed: (i) the 2.5% quantile level curve, (ii) The median level curve, (iii) the 97.5 % quantile level curve.

Analogously, for each of the diagnostic tools presented in **Section 4.3.2**, three values are computed: (i) the 2.5% quantile, (ii) the median, (iii) the 97.5% quantile. To assess more accurately whether the models manage to represent the synthetic data in the large value extremes, we compared their fitting capabilities to a naïve approach. Here, the naïve approach is an empirical level curve. For each of the 60 synthetic datasets, we compute the *wd* of the empirical level curves to the reference curves following the same steps as for the six models. The empirical *wd* ($wd_{naïve}$) is therefore compared to the *wd* of each model (wd_m). Models that represent the data with more accuracy than a naïve approach ($wd_m < wd_{naïve}$) are considered to be representative of the data. **Figure 4.7** displays the values of the *wd* for each model applied to each bivariate dataset and highlights the cases where models outperform a naïve approach (blue bold). Squares are coloured according to the median of the *wd* and thickness of the edges is proportional to the size the confidence interval (i.e., the distance between the quantiles Q2.5 and Q97.5).

Figure 4.7: Weighted Normalized Euclidean Distance (*wd*) to the reference curve for all 60 different synthetic datasets. Fitting capacities of each model are represented. Values in cells and colours represent the median *wd* from low (dark green) to high (red). Bold blue values highlight cases where models are representative of the data. The thickness of borders represents the 95% uncertainty around the median value on a logarithmic scale.

It is important here to note that we tested more **AD** (36-60%) cases than **AI** (24-40%) cases. To assess the flexibility of models, in addition to comparison to the naïve approach, we also consider the proportion of cases where models have a $wd < 0.1$. From **Figure 4.7**, we observe the following:

- The Gumbel and normal copulas, which have been used to generate the synthetic datasets with **AD** and **AI**, generally outperform all the other models in **AD** and **AI** cases, respectively.
- The conditional extremes model and the joint-tail KDE model are the most flexible models tested here as they can handle (Cond-Ex) 98% [72–100%] and (JT KDE) 97% [65–100%] of the situation with a $wd < 0.1$; these values reach 100% for the **AI** cases.

However, the Cond-Ex model is slightly more flexible, having a representative fit to more datasets (95%) than the JT-KDE model (68%).

- The normal copula, even if asymptotically independent, is the most flexible copula model with $wd < wd_{naïve}$ in 47% of the cases, more than the number of **AD** datasets. The normal copula has a low *wd* (<0.1) in 76% [60–90%] of the cases and has a representative fit to the data for every **AI** case and in some **AD** cases.
- Gumbel and Galambos copulas have representative fits to only 57% of the **AD** datasets. Among the 36 AD cases, they fail to represent only two with χ=0.9. It is important to note that both aforementioned copulas cannot handle complete independence (η=0.5) or negative dependence (η = 0.25).
- The FGM copula can only handle one type of extremal dependence, which is asymptotic independence (**AI**) with η = 0.5. Consequently, it is the least flexible model in our results with a $wd < wd_{naïve}$.in only 10% of the cases.
- Higher shape parameters of the margins are associated with poorer goodness-of-fit for all models. It is particularly striking with the conditional extremes approach which exhibits high uncertainty and high *wd* when both margins have a standard deviation σ=1.5.

The Cond-Ex and JT-KDE provide close results according to **Figure 4.7,** despite adopting very different approaches. Thus, their flexibility arises from their semiparametric nature. **Figure 4.7** also displays the uncertainty of the estimate of *wd*. For all models, a more accurate fit is accompanied by a reduction in uncertainties. However, both Cond-Ex and JT-KDE have on average more uncertainty around its *wd* despite their good fitting capabilities. On average, copulas tend to have less uncertainty due to their parametric nature.

However, the copulas are penalized by the weighting function as they usually reproduce quite well the naïve part of the curve. By considering again the percentage of situations with a criterion below 0.1, the normal copula has its performances reduced by the weighting function (–6% compared to *d*). The JT-KDE model has its performance boosted by the weighting function (+7% compared to *d*).

4.4 Application to natural hazards

Results from the simulation study presented in the previous section (**Section 4.3**) can provide useful insights when modelling the interrelations between two natural hazards. In this section, we will show how results previously presented can be useful to identify the most relevant models for a given dataset according to its visual characteristics. The concordance (or discordance) of the relevant models can also increase (decrease) confidence around the results.

The methodology for model selection presented here is composed of five steps to select the most relevant models to estimate joint exceedance probability level curves:

(i) The two-tail dependence measures are estimated empirically with a 95% confidence interval. Datasets with a tail dependence measure falling in that confidence interval are suggested as analogues to the studied bivariate dataset. To select relevant combinations of marginal distribution, a scatterplot is compared visually to density plots for the 60 different datasets simulated in **Section 4.3** and displayed in **Figure 4.5**.

(ii) From the aforementioned 60 datasets, a set of one to six analogous datasets (i.e. with similar bivariate distribution) is taken.

(iii) A confidence score is used to compare the abilities of each model for the datasets selected in step (ii). For each model, the confidence score is $\overline{wd}$ the average of the computed weighted Euclidian distance *wd* for all datasets selected in step (ii). By taking the average of *wd*, a poor fit on one analogous dataset will have a high influence on the confidence score.

(iv) Models are fit to the bivariate hazard dataset and level curves from the most relevant models are kept.

(v) Tail dependence measures are estimated using the most relevant model with a possible new iteration of the four previous steps according to the value of the dependence measures.

To produce a confidence interval as was done in the simulation study (**Section 4.3**) and to visually measure the uncertainty associated with each level curve as in **Section 4.3**, we use a nonparametric bootstrap procedure. The function *tsboot* from the R package *boot* (Davison and Hinkley, 1997; Canty and Ripley, 2019) is used to generate 100 bootstrapped replicate datasets with the same number of observations as the original (but some are repeated). Our six models are then fitted to the original dataset and on the 100 bootstrapped replicates.

4.4.1 **Rain and wind gusts at Heathrow Airport (Asymptotic independence)**

Here, we study the interrelation between daily extreme wind gusts (*w*) and extreme rainfall (*r*) at London Heathrow airport, UK for the period 1 January 1971 to 31 May 2018, both introduced in **Figure 4.1**. The relationship between wind and rainfall has been studied both globally (Martius *et al.*, 2016) and locally (Johansson and Chen, 2003; Ming *et al.*, 2015). These two hazards are often associated with different types of storms (Dowdy and Catto, 2017) and in particular cyclones (Ming *et al.*, 2015; Raveh-Rubin and Wernli, 2016). In South England, these two hazards are mostly associated with extratropical cyclones in the winter season and thunderstorms in summer season (Hawkes, 2008; Anderson and Klugmann, 2014; Webb and Elsom, 2016; Hendry *et al.*, 2019).

The bivariate dataset used to study the interrelation between wing gusts and rainfall at Heathrow airport is composed of the following data:

i) *Daily Wind Gust (w):* daily maximum wind gust at London Heathrow airport (UK) weather station where a gust is the maximum value, over the observing cycle, of the 3-second running average wind speed (WMO, 2019). Wind gusts are short-lived wind peaks in speed that can inflict great damage during a storm. However, it might not capture the overall wind intensity (Met Office, 2019). The time range of the observations is 38 years, from 1 January 1971 to 31 May 2018 of which 74 days (0.4% of the data) had no values recorded and all other values in the dataset had $w > 0$ m s^{-1}. This observation data has been provided by the Met Office (2019).

ii) *Daily Rainfall (r):* daily total precipitation in a grid cell containing London Heathrow airport (UK). The data have been extracted from the E-OBS gridded database (Cornes *et al.*, 2018) which is formed from the interpolation of observations from 18,595 meteorological stations through Europe and the Mediterranean (including Heathrow airport station). It has been shown that E-OBS has excellent correlation with other high-resolution gridded datasets even if this correlation tends to decrease for extremes (Hofstra *et al.*, 2009). However, by selecting a grid containing a weather station we limit uncertainties arising from interpolation. The spatial resolution in the E-OBS dataset is 0.1° × 0.1° and the period covered is 1950 to 2019. Data from 1 January 1971 to 31 May 2018 (38 years) in the cell containing Heathrow airport is used, with a total of 6074 days (35.1% of the dataset) having nonzero rainfall $r > 0$ mm d^{-1}.

From 1 January 1971 to 31 May 2018, there are a total of 17,318 days (including leap years). Our bivariate wind gust-rainfall dataset is composed of those values where there is both non-zero rainfall $r > 0$ mm d^{-1} and wind gusts $w > 0$ m s^{-1} recorded, resulting in a total of 6044 bivariate observations (34.9% of the days in our record). An overview of both daily rainfall and daily wind gust is displayed in **Figure 4.8** in the form of monthly violin plots, where the probability density of w and r at different values are given, smoothed by a kernel density estimator.

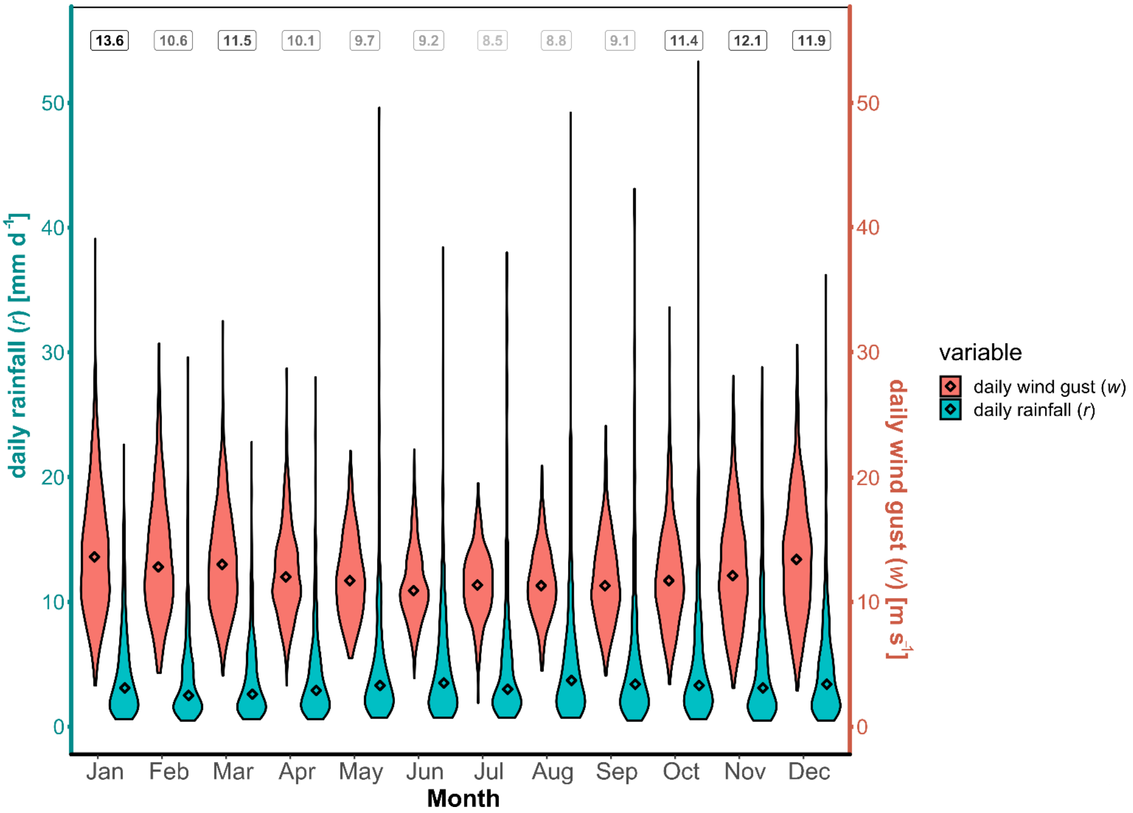

Figure 4.8: Violin plots of daily wind gust *w* (red) and daily non-zero rainfall *r* (blue) by month for the period 1 January 1971 to 31 May 2018 at Heathrow airport weather station, UK. Diamonds represent the median of all values for that month from 1971–2018. Numbers at the top of the graph represent the average number of days per month where there is recorded both non-zero rainfall $r > 0$ mm d^{-1} and wind gusts $w > 0$ m s^{-1}. Daily rainfall data from E-OBS (Cornes *et al.*, 2018) and wind gust data (maximum 3 s wind velocity in a day) from the Met Office (2019).

From **Figure 4.8** we observe a seasonality in daily wind gust speed. January is the month with the highest median (diamond symbol) and range of most values in the violin plot while July is the month with the lowest median and range of most values in the violin plot. The daily non-zero rainfall median per month varies between 2.5 mm in February and 3.5 mm in June, with the highest individual daily values occurring in October (53.3 mm d^{-1}), May (49.6 mm d^{-1}) and June (49.2 mm d^{-1}). The dataset is also represented as a scatterplot in **Figure 4.9**. The scatterplot will be used for the model selection methodology presented at the beginning of **Section 4.4.**

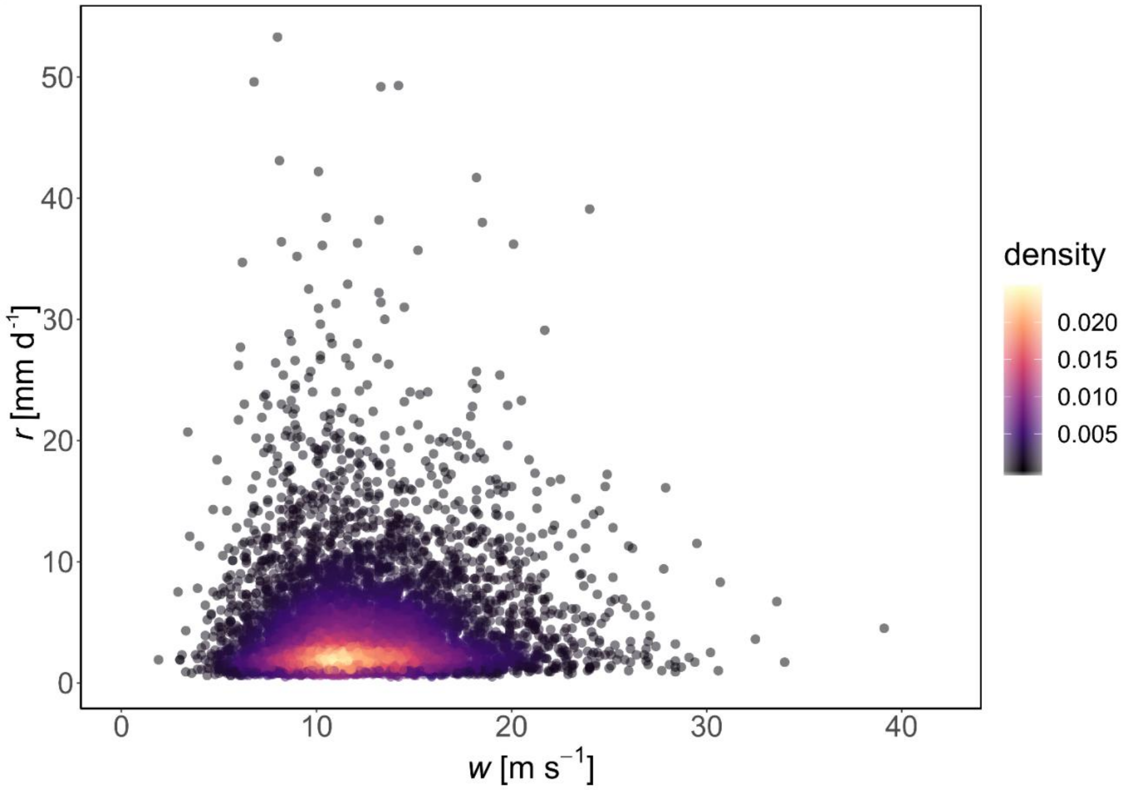

Figure 4.9: Days where there are recorded both daily wind gust (m s-1) w and nonzero daily rainfall (mm d-1) r > 0 mm d–1 at Heathrow airport (London, UK) for the period 1971–2018. Daily rainfall data from E-OBS (Cornes *et al.*, 2018) and wind gust data (the maximum 3 s wind velocity in a day) from the Met Office (2019). Colours (legend) represent the bivariate density estimated from a kernel density estimator with higher values and lighter colours representing a higher density of points at that bivariate value (r, w).

Extreme rainfall and extreme wind have a compound interrelation according to Tilloy *et al.* (2019). We then estimate the joint exceedance probability curve, corresponding to a P_{AND} probability (**Section 2.3**).

We now go through the four steps presented for rainfall and wind gusts in Heathrow.

(i) From **Figure 4.5** and **Figure 4.9**, along with empirical estimates of χ and η, we hypothesize that over our time range 1971–2018, daily rainfall and daily maximum wind gusts in London Heathrow Airport are asymptotically independent or weakly dependent ($\eta = 0.5$ / $\chi = 0.05$ / $\chi = 0.1$) and that both marginal distributions have a small shape parameter (**AB**, **BB**).

(ii) This then gives us four analogous datasets and it is then possible to visually infer from **Figure 4.6** which models are the most suitable for these conditions. The four analogous datasets are the following:

1. $\chi = 0.05$ and **AB**
2. $\chi = 0.05$ and **BB**
3. $\eta = 0.5$ and **AB**
4. $\eta = 0.5$ and **BB**
5. $\chi = 0.1$ and **AB**
6. $\chi = 0.1$ and **BB**

(iii) The *confidence score* for each model is $\overline{wd}$ the average of the weighted Euclidean distance *wd* from the four situations above. For the Gumbel and Galambos copulas, the cases of independence or negative dependence between variables are outside the modelling range (**Section 2.3.1**), and thus the confidence score for these models has been penalized by putting wd =1.0 for η = 0.5 and η = 0.25. The conditional extremes model has the smallest confidence score $\overline{wd}$=0.02 and is representative for all six analogous datasets. The JT-KDE model has a $\overline{wd}$ = 0.03 and is representative for 4 out of 6 analogous. The FGM and Normal copula have a confidence score of $\overline{wd}$ = 0.04 and are the only representative in AI cases. Gumbel and Galambos copulas have a confidence score of variable = 0.35 due to their penalty (**Table 4.4**).

According to these three first steps, the conditional extremes model appears to be the most suitable. However, we selected the four most relevant models for the bivariate dataset of daily rainfall and daily wind gust at London Heathrow Airport. The conditional extreme model, the JT-KDE model, the normal copula and the FGM copula all have low $\overline{wd}$ as can be seen in **Table 4.4**.

Table 4.4: Euclidian weighted distance (*wd*) for datasets 1 to 6 based on wind-rainfall and six models, along with confidence scores (average of the *wd* for datasets 1 to 6). In blue bold are highlighted the values below the naïve approach *wd* and the average values, four models with confidence scores < 0.1 are highlighted in bold.

Dataset	**Cond-Ex**	**JT-KDE**	**Gumcop**	**Normalcop**	**FGMcop**	**Galamboscop**
1	**0.03**	**0.03**	**0.02**	0.04	0.04	**0.02**
2	**0.02**	**0.02**	**0.01**	0.03	0.04	**0.02**
3	**0.02**	**0.02**	1.00	**0.01**	**0.01**	1.00
4	**0.01**	**0.01**	1.00	**0.01**	**0.01**	1.00
5	**0.02**	0.04	**0.02**	0.06	0.07	**0.02**
6	**0.03**	0.04	**0.02**	0.06	0.08	**0.02**
Average	**0.02**	**0.03**	0.35	**0.04**	**0.04**	0.35

(iv) For illustration and/or confronting our models with the data, the models are fit to the dataset and joint exceedance level cure are produced with a joint exceedance probability set at *p* = 0.001, corresponding to a bivariate return period of 8 years. However, another joint exceedance probability could have been chosen.

In **Figure 4.10** are displayed the level curves produced from the four models that were selected after steps (i) to (iii) above (Cond-Ex, JT-KDE, NormalCop and FGMCop) and presented in bold numbers in **Table 4.4**.

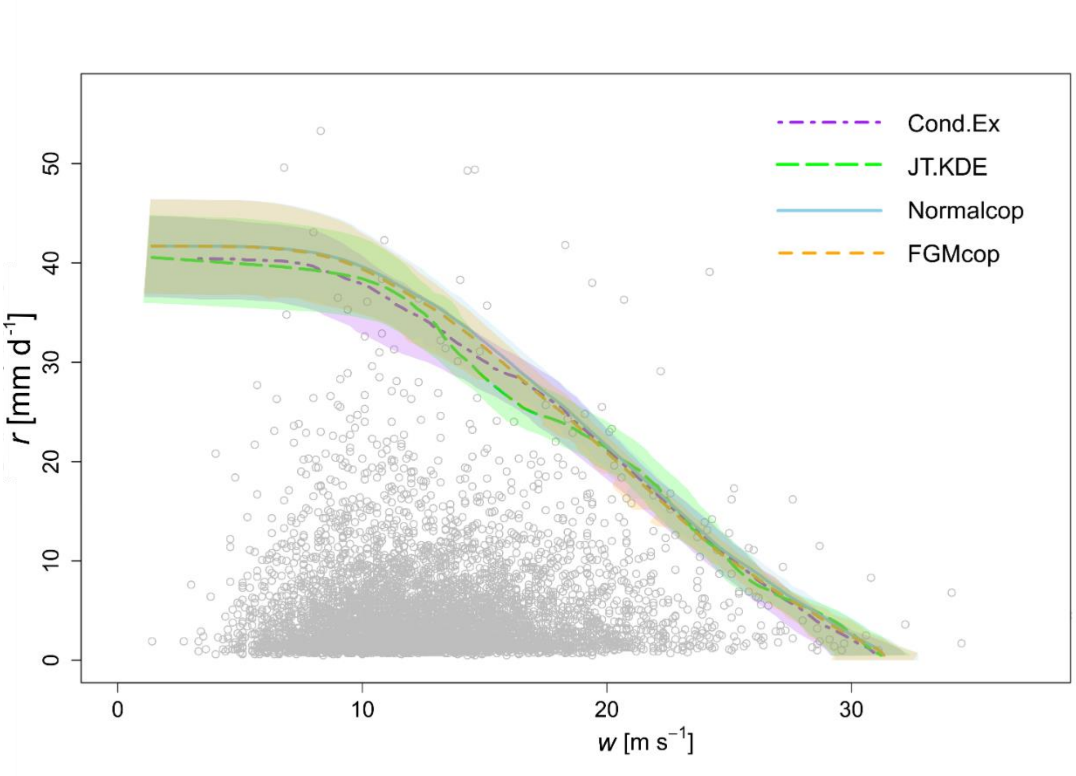

Figure 4.10: Level curves for a P_{and} joint probability p = 0.001 of daily wind gust and daily rainfall at Heathrow airport (London, UK). Level curves from the four models selected through the model selection methodology are displayed.

From **Figure 4.10,** we can observe that the conditional extremes model, the FGM and the normal copula all produce very similar joint exceedance curves and that their confidence intervals overlap. **Table 4.5** displays the estimates (with bounds of the 95% confidence interval) of the two dependence parameters χ and η from the six models. These estimates converge toward a very weak asymptotic dependence. However, the estimation of dependence parameters in near independence is highly uncertain (**Section 3.3.2**).

Table 4.5: Estimates of dependence parameters χ and η for extreme rainfall and wind gust at Heathrow airport for the time range 1971–2018

Models	**Cond-Ex**	**JT-KDE**	**Gumcop**	**Normalcop**	**FGMcop**	**Galamboscop**
χ	0.01	0.06	0.04	0.00	0.00	0.04
	[0.00,0.02]	[0.05,0.09]	[0.01,0.06]	[0.00,0.00]	[0.00,0.00]	[0.02,0.06]
η	0.49	0.54	1.00	0.52	0.50	1.00
	[0.45,0.54]	[0.49,0.59]	[1.00,1.00]	[0.51,0.54]	[0.50,0.50]	[1.00,1.00]

4.4.2 Daily wildfire number and temperature extremes in Portugal (Asymptotic dependence)

Here we present a second example of applying our models to natural hazards data, using as a case study daily temperature and daily number of wildfires in Portugal. Wildfire variables such as daily number and burned area depend on many influences such as wind speed/direction/gustiness, topography, type of fuel and soil moisture (Hinks *et al.*, 2013). The aim of our study is not to decipher the processes leading to a wildfire but rather to provide an exemplar study examining the relationship between the two variables, daily temperature and daily number of wildfires, in a given case study area. It has been shown that dry and warm conditions increase the risk of wildfire (Littell *et al.*, 2009; AghaKouchak *et al.*, 2018). Witte *et al.* (2011) established a direct link between a persistent heatwave and wildfire outbreaks in Russia and Eastern Europe in 2010. The Northern Mediterranean countries (Portugal, Spain, France, Italy and Greece) are particularly affected by summer fires (Vitolo *et al.*, 2019). Among these, Portugal holds the highest number of wildfires per land area (Pereira *et al.*, 2011). There are many environmental and anthropogenic factors influencing the rural fire regime in Portugal and making its territory a fire-prone area. However, the majority of rural fires are recorded during hot and dry conditions in the summer (Pereira *et al.*, 2011).

Here, we used the mainland continental Portuguese Rural Fire Database, that includes 450,000 fires and covers the period 1980–2005 (Pereira *et al.*, 2011), and includes data for all 18 districts in Portugal. This database is the largest such database in Europe in terms of the total number of recorded fires in the 1980–2005 period (Pereira *et al.*, 2011) and includes fires recorded down to a size of 0.001 ha. From the Portuguese Rural Fire database, we chose to focus on the Porto district, which was the worst affected in the period (out of the 18 Portugal districts) in terms of the number of wildfires, with 21.6% of the total fire recorded in the dataset between 1980 and 2005. The Porto district is situated in the northern part of Portugal (see **Figure 4.11**), has an area of 2,395 km^2 and is one of the most populated districts of Portugal with an estimated population of 1,778,146 in 2018 (Instituto Nacional de Estatística Portugal, 2019).

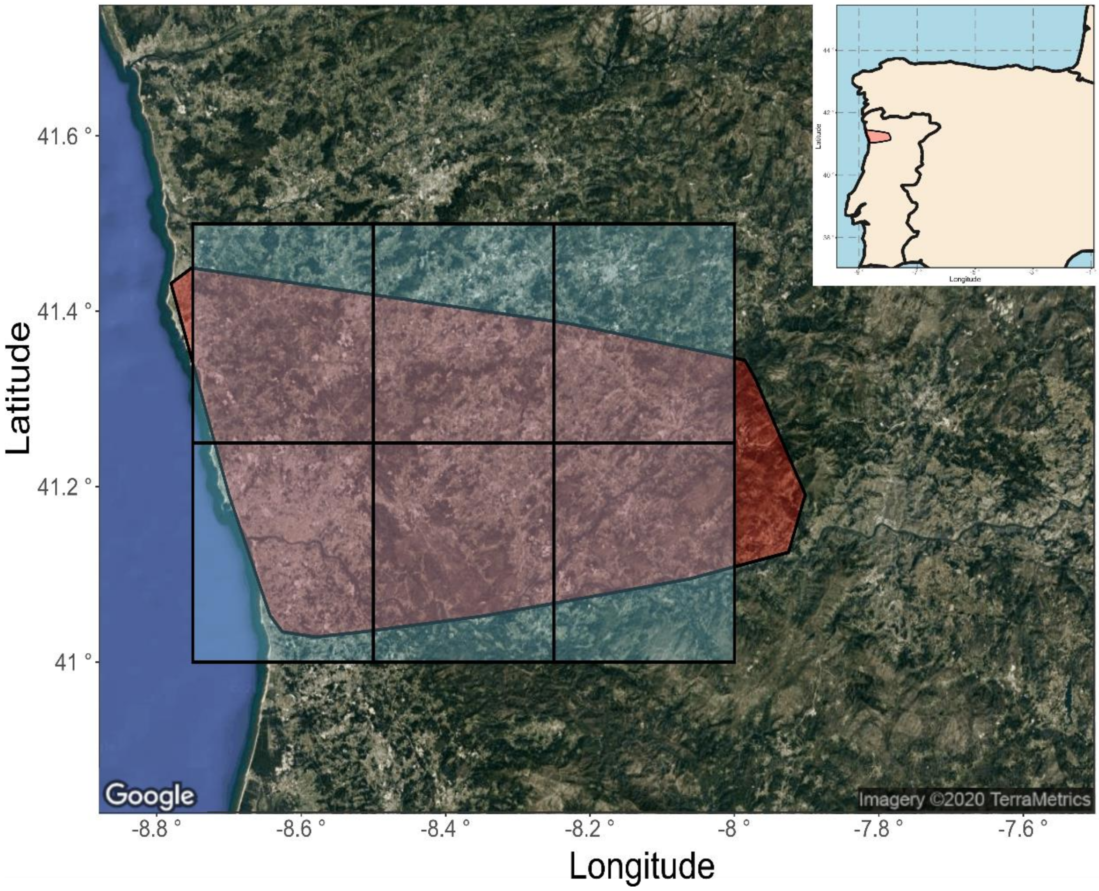

Figure 4.11: Portugal study area for the interrelation between extreme hot temperature and wildfire burned areas. The red area represents the Porto district in Portugal containing studied wildfire burned areas. The blue tiles represent cells from the high-resolution gridded data set of daily climates over Europe (E-OBS) (Cornes *et al.*, 2018) containing mean daily temperature data. Satellite image retrieved with ggmap (Kahle and Wickham, 2013). © Google Maps (2020).

The bivariate dataset used to study the interrelation between extreme temperature and wildfire burned areas in the Porto district is composed of the following data:

a) *Daily number of wildfires (f).* Daily number of wildfires for the 26-year period 1980–2005 for the Porto district were extracted from the Portuguese Rural Fire Database dataset from Pereira *et al.* (2011). To account for under-sampling of smaller wildfires in earlier years, and as suggested by Pereira *et al.* (2011), we used only those fires with a burned area $A_F \geq 0.1$ ha, resulting in 59,522 fires, an average of 6.3 fires per day (for those days with at least one fire occurrence) over the Porto district in Portugal (2395 km^2).

iii) *Daily temperature data (t).* Daily mean temperature was extracted from the E-OBS gridded dataset (Cornes *et al.*, 2018). We approximate the area in red in **Figure 4.11** (Porto district) for each day with one temperature value by taking the average of daily temperatures in each of the six 0.25° × 0.25° cells represented by blue rectangles in **Figure 4.11**. This assumption reduces the confidence in return level values and adds up with other interpolation uncertainties arising from the data (Hofstra *et al.*, 2009). Moreover, the temperature in the six cells are strongly correlated (Pearson correlation coefficient $\rho > 0.98$) and temperature variations are mostly due to the distance to the sea and altitude (Miranda *et al.*, 2002).

The 26 years from 1980–2005 have a total of 9496 days. Of these, a total of 3442 days (36% of the days) have both non-zero days for the number of wildfires and a mean temperature value, which are used in our final bivariate dataset. An overview of both daily mean temperature and daily number of wildfires is displayed in **Figure 4.12** in the form of monthly violin plots.

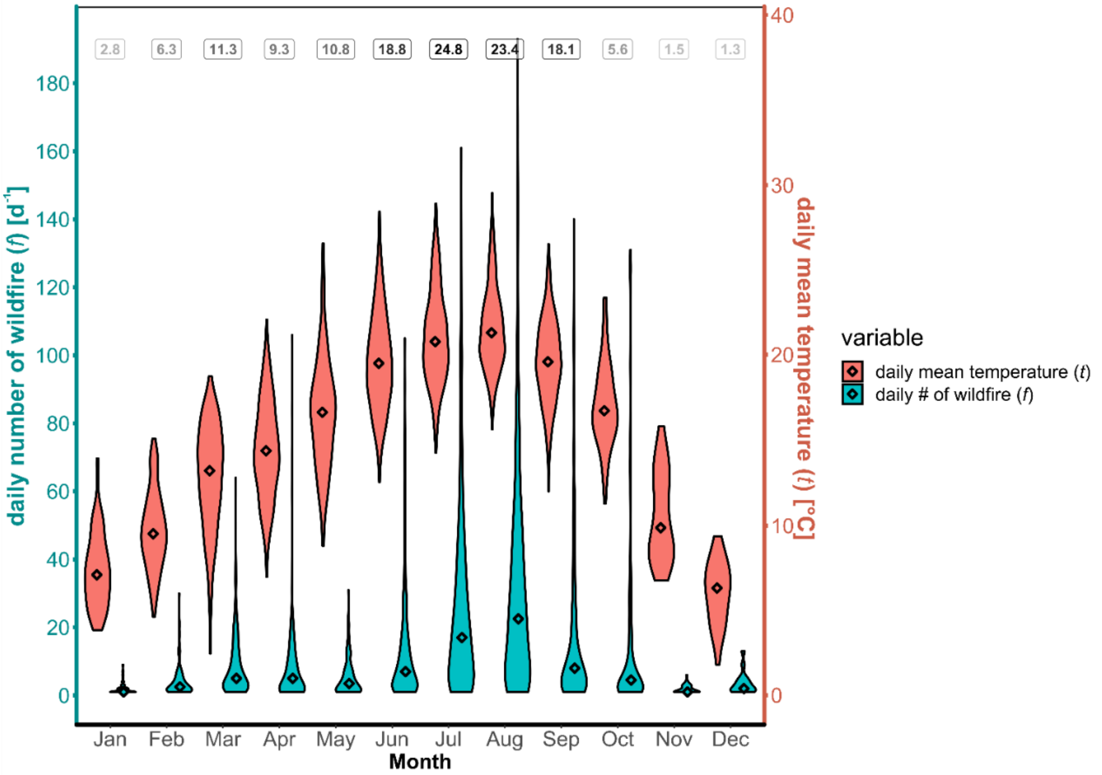

Figure 4.12: Violin plot of those days with both daily mean temperature (red, upper violin plots) *t* and daily number of wildfires (blue, lower violin plots) $f \geq 1$ fire d^{-1}, by month for the period 1980–2005 in Porto district (Portugal). Only those wildfires with burned area $A_F \geq 0.1$ ha are included. Diamonds for both temperature and wildfires represent the median of all values in that month throughout the record. Numbers at the top of the graph represent the average number of days per month where there are recorded both a temperature value *t* and at least one wildfire ($f \geq 1$ fire d^{-1}).). Daily mean temperature data from E-OBS (Cornes *et al.*, 2018) and wildfire data from Pereira *et al.* (2011).

From **Figure 4.12** we observe the seasonality in daily mean temperature with January the coldest month (median = 8.3°C) and August the warmest (median = 21.0°C). Daily number of wildfires (with burned area $A_F \geq 0.1$ ha) per month varies between the median of 1.0–2.5 fire d^{-1} in winter months (November to February) and 7.0–22.5 fire d^{-1} in summer months (from June to September). The dataset is also represented as a scatterplot in **Figure 4.13**. The scatterplot will be used for the model selection methodology presented at the beginning of **Section 4.4.**

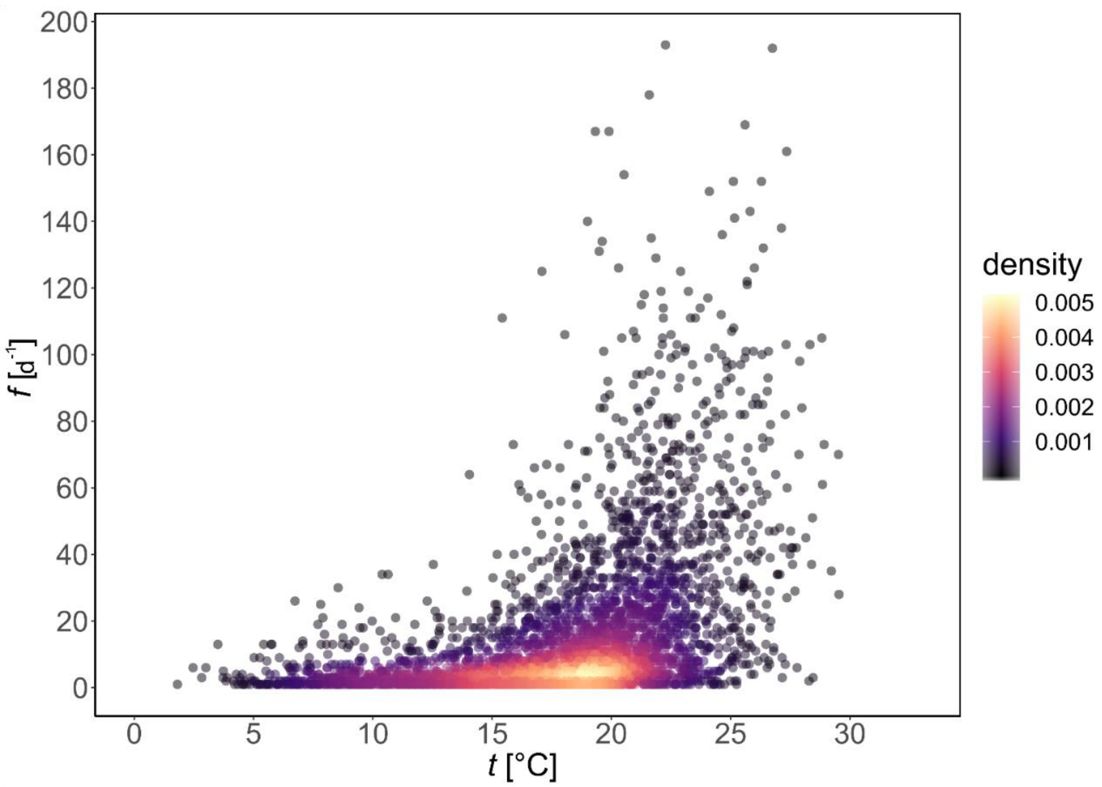

Figure 4.13: Scatter plot of temperature as a dependence of wildfire occurrence in Porto district, Portugal for the period 1980–2005, for those days where there are recorded both mean daily temperature (t) and at least one fire, with f the number of wildfires in one day. Only those wildfires with burned area AF ≥ 0.1 ha are included. Daily mean temperature data from E-OBS (Cornes *et al.*, 2018) and wildfire data from Pereira *et al.* (2011). Colours represent the bivariate density estimated from a kernel density estimator.

As discussed at the beginning of this section, extreme (hot) temperature and wildfire are interrelated. Indeed, extreme (hot) temperature may promote the development of wildfires (Witte *et al.*, 2011; Sutanto *et al.*, 2020). According to Tilloy *et al.* (2019), this is a change condition interrelation (i.e., one hazard changes environmental parameter that moves toward a change in the likelihood of another hazard). We then estimate the conditional exceedance probability curve (**Section 4.2.3**).

We now go through the four steps introduced at the beginning of **Section 4.4**.

(i) From **Figure 4.5** and **Figure 4.13,** along with empirical estimates of χ and η, we hypothesize that over our time range, there is asymptotic dependence for the mean daily temperature and the number of wildfire per day are asymptotically dependent (χ = 0.5 - χ = 0.3) and that one marginal distribution has a slightly small shape parameter and the other one is heavily right-skewed (**AC**, **BC**).

(ii) This then gives us four analogous datasets and it is then possible to know from **Figure 4.8** which models are the most adapted to these conditions. The four datasets are the following:

1. χ = 0.5 and **AC**
2. χ = 0.5 and **BC**
3. χ = 0.3 and **AC**

4. χ = 0.3 and **BC**

(iii) The confidence score for each model is the average of the wd from the four aforementioned datasets. Based on **Table 4.6**, the normal copula and FGM copula do not seem suitable to model the joint occurrence of wildfire and extreme temperature as these poorly fit the four datasets. The Gumbel and Galambos copula ($\overline{wd}$ = 0.02) and the conditional extremes model ($\overline{wd}$ = 0.04) are representative for the four analogous datasets. The joint tail-KDE model has a confidence score $\overline{wd}$ = 0.05 and is representative for two analogous datasets.

According to these three first steps, we can identify the most relevant model for the bivariate dataset of daily maximum temperature and daily wildfire occurrence in Porto district: the Gumbel copula, Galambos copula, the JT-KDE model and the conditional extremes model are the most relevant models for our dataset.

Table 4.6: Weighted Euclidean distance (*wd*) for datasets 1 to 4 based on extreme temperature-wildfire and six models, along with confidence scores (average of the *wd* for datasets 1 to 4).). In blue bold are highlighted the values below the naïve approach *wd* and the average values of the four models with confidence scores < 0.1 are highlighted in bold.

Dataset	**Cond-Ex**	**JT-KDE**	**Gumcop**	**Normalcop**	**FGMcop**	**Galamboscop**
1	**0.03**	**0.04**	**0.02**	0.12	0.29	**0.02**
2	**0.05**	**0.06**	**0.04**	0.18	0.42	**0.04**
3	**0.03**	0.05	**0.02**	0.13	0.2	**0.02**
4	**0.06**	0.07	**0.04**	0.19	0.28	**0.04**
Average	**0.04**	**0.05**	**0.03**	0.15	0.30	**0.03**

(iv) For illustration and/or confronting of the models with the data, the models are fit to the dataset and the joint exceedance level curves are produced with a joint exceedance probability set at p = 0.001, corresponding to a bivariate return period of approximately 8 years.

In **Figure 4.14** are displayed the conditional level curves produced from the four models that were selected after steps (i) to (iii) and shown in bold values in **Table 4.6** (Cond-Ex, JT-KDE, Gumbelcop and GalambosCop).

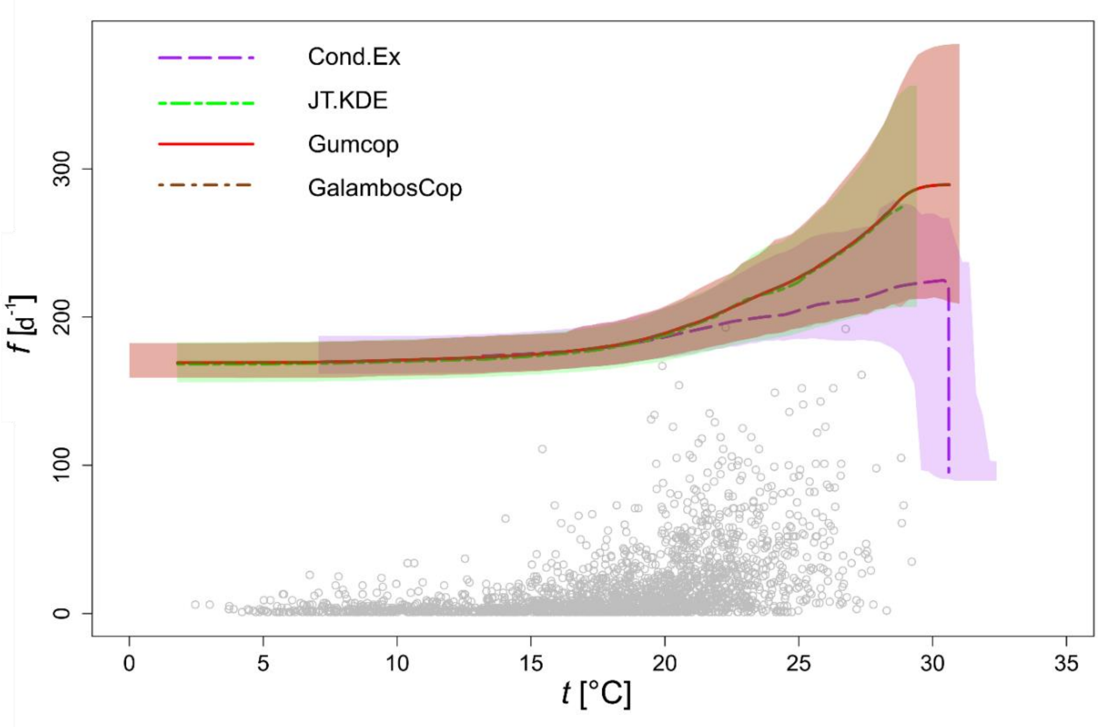

Figure 4.14: Level curves for a P_{and} joint probability p=0.001 of daily mean temperature and daily number wildfire occurrences in Porto district, Portugal, for the period 1980–2005. Level curves from the four models selected through the model selection methodology are displayed.

From **Figure 4.14,** we can observe that the JT-KDE and the Gumbel copula produce very similar conditional exceedance curves and that their confidence intervals strongly overlap. However, the conditional extreme model provides a lower estimate than the other approaches the number of wildfire conditioning on the temperature being above a given threshold.

In **Table 4.7**, we present the estimates (with bounds of the 95% confidence interval) of the two dependence parameters χ and η from the six models provide a bit more insight about the dependence structure. These estimates converge toward a moderate asymptotic dependence varying from $\chi = 0.15$ (Cond-Ex) to $\chi = 0.47$ (GumCop). Even if all models tend to show asymptotic dependence between the two variables, estimates of η are less than 1.0 for the normal copula, the JT-KDE model and the Cond-Ex with values varying between 0.67 and 0.79. This still implies a positive association between the two variables.

Table 4.7: Estimates of dependence parameters χ and η for mean daily temperature and daily occurrences of wildfire in Porto district for the period 1980–2005

Models	**Cond-Ex**	**JT-KDE**	**Gumcop**	**Normalcop**	**FGMcop**	**GalambosCop**
χ	0.15	0.26	0.47	0.00	0.00	0.46
	[0.06, 0.20]	[0.21, 0.30]	[0.45, 0.49]	[0.00, 0.00]	[0.00,0.00]	[0.44, 0.49]
η	0.67	0.67	1.00	0.79	0.50	1.00
	[0.59, 0.72]	[0.62, 0.71]	[1.00, 1.00]	[0.78,0.80]	[0.50, 0.50]	[1.00, 1.00]

4.5 Discussion and Conclusions

Quantifying and measuring the interrelations between different natural hazards is a crucial element when adopting a multi-hazard approach (Gill and Malamud, 2014; Leonard *et al.*, 2014). In this study, we focused on statistical approaches that are often used to characterize and model interrelations between hazards. Another focus has been on modelling relationships between hazards at an extreme level. In total, six statistical models with different characteristics (nature of asymptotic dependence, parametric/semi-parametric) were compared. Some of these models have already been used to study compound extremes in hydrology and climatology (Hao *et al.*, 2018; Liu *et al.*, 2018; Sadegh *et al.*, 2018; Cooley *et al.*, 2019). However, these have not been compared over a broad range of bivariate datasets and applied to the same natural hazards in the same location.

This section will discuss the following three themes before a short conclusion: (a) choices influencing the results of the simulation study; (b) uncertainties at the interface between asymptotic dependence and asymptotic independence; (c) possible extensions of this approach to more than two hazards.

Choices influencing the results of the simulation study. This study aimed to assess the fitting ability of several bivariate models to a broad range of datasets. To do so, models were compared in their ability to reproduce an extreme level curve (see **Section 4.3.2.1**). The level curve corresponding to the P_{AND} probability has been selected as a comparison point because it is commonly used in the literature and is relevant for practitioners. The choice of this level curve and its shape could influence our results. The extreme level curve probability was set at $p = 0.001$. The multivariate regular variation framework (Resnick, 1987) provides evidence supporting the fact that the dependence structure remains identical in the whole extreme domain. However, some results shown in **Section 4.3.3** might have been influenced by the value of the joint exceedance probability. In particular, it is likely that when decreasing the level curve probability (i.e., to more extreme values), the flexibility and abilities of the asymptotically independent normal copula will decrease. There are many copulas other than the four selected in this study (Nelsen, 2006; Sadegh *et al.*, 2017) that have been developed. Nevertheless, we believe the four copulas used in this study are suitable for bivariate extreme value analysis and are amongst the most widely used in the literature (Genest and Favre, 2007; Genest and Nešlehová, 2013). Another influential choice in this study has been the number of synthetic data points generated in each realization of the dataset. The number of data points and data set size is an important influence on uncertainty in natural hazard modelling and probabilistic approaches (Frau *et al.*, 2017; Liu *et al.*, 2018). For each simulation, we simulated $n = 5000$ data points. Some other simulation studies took a higher number of data points (Zheng *et al.*, 2014; Cooley *et al.*, 2019); however, we replicated 100 times and produced confidence intervals, thus ensuring consistency of our results. We also found that threshold selections, to fit the generalized Pareto distributions of the marginal distributions and to estimate the extremal dependence measures, also have an influence on our results.

Uncertainties at the interface between asymptotic dependence and asymptotic independence. From the results of the simulation study (**Section 4.3.3**) and the two case study applications (**Section 4.4**), one can observe that the interface between asymptotic dependence and asymptotic independence can be unclear. In **Section 4.3.3**, we discussed the decrease in model performance and the increase in uncertainty for low values of χ and high values of η. Taking the assumption of asymptotic independence or asymptotic dependence can have a significant impact on the estimation of joint return levels. We find that extra care is required when dealing with bivariate datasets which are near independence as in **Section 4.4.1**.

Possible extension of the approaches to more than two hazards. As presented through this chapter, the study of interrelations between natural hazards has primarily been done by hazard pairs (e.g., Gill and Malamud, 2014). Dependence measures and a variety of different models or level curves, all presented in this article, are powerful tools to assess, quantify and model interrelations between two hazards. However, in many cases, multi-hazard events include more than two hazards interacting in various ways (e.g., Gill and Malamud, 2014; Leonard *et al.*, 2014). The use of models presented in this article can be extended to more than two variables, sometimes with disadvantages. One of these disadvantages is that the parametric nature of copulas leads to a lack of flexibility when going to higher dimensionality (Bevacqua *et al.*, 2017; Hao *et al.*, 2018). The JT-KDE and Cond-Ex models are suitable for higher dimensions (Davison and Huser, 2015; Cooley *et al.*, 2019), although these have not been tested for high dimensional multi-hazard modelling yet (Tilloy *et al.*, 2019). Recent research conducted suggests pair-copula construction (Bedford and Cooke, 2002; Hashemi *et al.*, 2016; Bevacqua *et al.*, 2017, Lui *et al.*, 2018) and non-parametric Bayesian networks (NPBN) (Hanea *et al.*, 2015; Couasnon *et al.*, 2018) can be used to model multi-hazard events with more than two hazards. The vine copula framework allows one to select different bivariate copulas for each pair of variables, providing great flexibility in dependence modelling (Brechmann and Schepsmeier, 2013; Hao and Singh, 2016). Non-parametric Bayesian networks, which are associated with the structure of Bayesian network and copulas (Hanea, 2010; Hanea *et al.*, 2010, 2015), have been used to study multiple dependencies between river discharge and storm surges in the USA during a hurricane (Couasnon *et al.*, 2018).

In conclusion, we have compared and examined the strength and weaknesses of six distinct bivariate extreme models in the context of hazard interrelations. These six models are grounded in multivariate extreme value theory and represent the diversity of approaches (e.g., non-parametric vs parametric) currently applied to hazard interrelation analysis. With this study, we aimed to contribute to a better understanding of the applicability of bivariate extreme models to a wide range of natural hazard interrelations. The methodology developed in this article is aimed to be widely applicable to a variety of different hazards and different interrelations, here represented by the 60 synthetic datasets created. Abilities of each model have been assessed with two metrics: (i) dependence measure; (ii) bivariate return level (level curves). These two metrics and the different diagnostic tools developed in this study offer new intuitive ways to decipher the dependence between two variables. We recommend selecting a range of models rather than one when studying interrelations between two hazards. To highlight the benefits of the systematic framework developed, we studied the dependence between extremes (natural hazards) of the following environmental data: (i) daily precipitation accumulation and daily maximum wind gust (maximum over a period of 3 s) at Heathrow airport (UK) over the period 1971–2018; (ii) daily mean temperature and daily number of wildfires in Porto district, Portugal over the period 1980–2005. The two datasets represent different hazard interrelations: (i) compound interrelation between extreme wind and extreme rainfall and (ii) change condition interrelation where higher air temperature change condition for wildfire occurrence. In both cases, a sample of the most relevant models among the six used in this study has been selected and fitted to the bivariate datasets. The good agreement in the estimation of bivariate return period between models corroborates the relevance of the comparison metrics we developed.

Chapter 5: Spatiotemporal features of compound wind and precipitation extremes in Great Britain

Summary:

Interrelations between natural hazards operate on different spatial and temporal scales than single natural hazards. In this chapter, a methodolgy to identify spatiotemporal clusters of climate extremes and their interrelations is presented, the Compound Hazard Cluster Identification (CHCI) method. The approach is applied to the analysis of compound precipitation and wind extremes. This is done by extracting hourly values of precipitation and wind gust for the period 1979–2019 from climate reanalysis (ERA 5) within a region including Great Britain and the British channel. Extreme values (above the 99% quantile) of precipitation and wind gust are clustered with the Density-Based Spatial Clustering of Applications with Noise (DBSCAN) algorithm. Compound hazard clusters that correspond to the spatial overlap of hazard clusters during the aggregated duration of the two hazards are then identified. The method's ability to identify extreme precipitation and wind events is assessed with a catalogue of 157 significant events (96 extreme precipitation and 61 extreme wind events) that occurred over the period 1979–2019. Spatial and temporal co-occurrences between historic events and spatiotemporal clusters are computed. We find a good agreement between CHCI outputs and the catalogue with an overall hit rate (ratio between the number of joint events and the total number of events) of 93.7%. A total of 4555 compound hazard clusters are detected with this method over the period 1979–2019. By analysing these clusters, the study finds that the occurrences of wind and rain events are dependent, with significant spatial and seasonal variabilities. The main hotspots for compound hazards events are found to be on the South coast of England and mountainous areas. The months April to September were found to have a much lower occurrence of compound hazards events compared to October to March, indicating a link with the extratropical cyclone season.

5.1 Introduction

Spatial and temporal scales are significant contributors to the natural processes that result in extremes or natural hazards (e.g., geomorphic: Schumm and Lichty, 1965; Phillips, 1988; atmospheric: Orlanski, 1975; hydrologic: Blöschl and Sivapalan, 1995; ecologic: Schneider, 1994). Here, the spatial scale (the 'footprint') refers to the area over which the hazard occurs. The temporal scale is the duration over which the hazard acts on the natural environment. The extent of the temporal and spatial scales of these natural hazards includes many orders of magnitude, which can influence the relationship between natural hazards (Gill and Malamud, 2014; Leonard *et al.*, 2014).

Spatiotemporal clustering methods applied to environmental data can be powerful tools to understand the scales of different natural hazards by identifying natural hazard clusters (Barton *et al.*, 2016). Such methods allow the extraction of spatiotemporal and intensity characteristics of natural hazard clusters. The estimation of such characteristics is relevant when defining and understanding the potential impacts of natural hazards and their interrelations on society. Examples include the following:

- The duration of precipitation events (Yue, 2000; Vorogushyn *et al.*, 2010) has a significant role in dike failure, landslide triggering and flood losses.
- The relationship between the intensity, duration and area of heatwaves (Winter and Tawn, 2016; Vogel *et al.*, 2020) and drought (Corzo Perez *et al.*, 2011; Zhang *et al.*, 2015; Tosunoglu and Can, 2016) directly influences the severity of such events.

This chapter proposes a methodology for Compound Hazard Clusters Identification (CHCI), which we use to analyses the spatiotemporal features of wind and precipitation extremes in Great Britain, 1979–2019. This CHCI methodology is based on spatiotemporal clustering of extreme values, which are extracted from a gridded atmospheric dataset, the ERA5 climate reanalysis (Hersbach *et al.*, 2019). Compound hazard events in space and time are defined and identified from independent clusters of extreme wind and extreme precipitation (**Figure 5.1**). The identification of compound hazards is performed using hazard clusters rather than grid cells (Martius *et al.*, 2016; Ridder *et al.*, 2020). With this approach, we propose a robust method to capture the spatiotemporal features of compound hazards at various scales (from hours to days and from local to regional scale) with an application on compound wind and precipitation extremes in Great Britain.

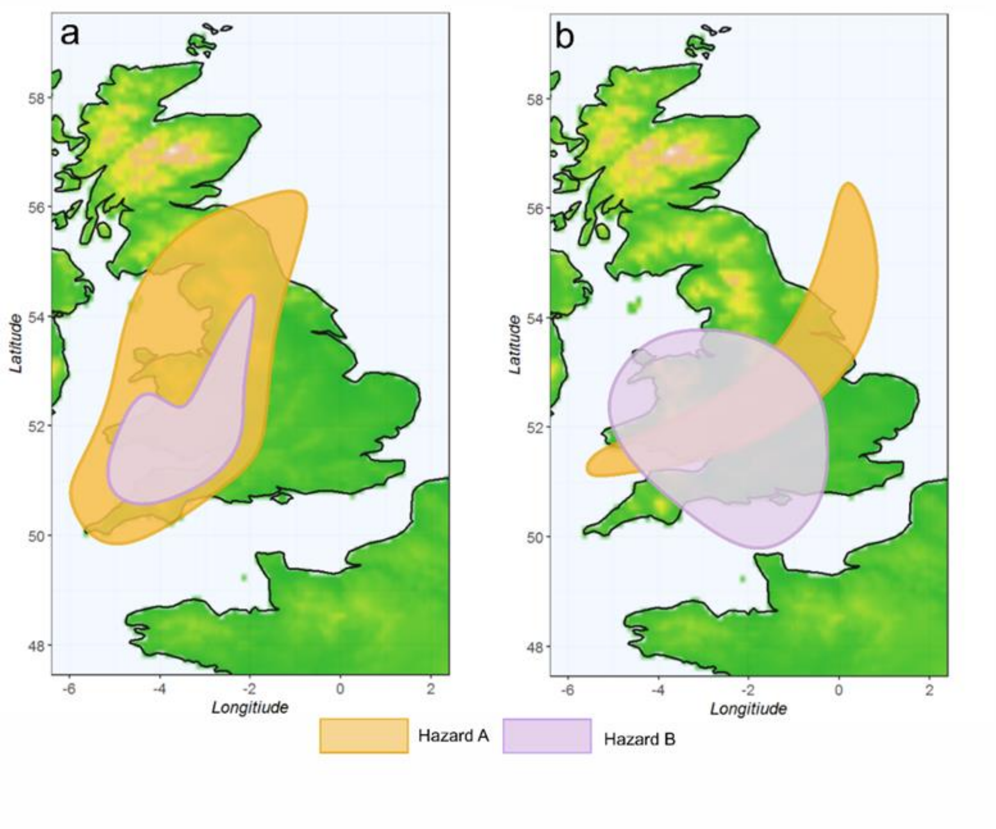

Figure 5.1: Cartoon illustration of a spatiotemporal compound hazard over Great Britain. Hazard A (orange) is a cluster of extreme occurrences of variable *x* and Hazard B (violet) is a cluster of extreme occurrences of variable *y*. In (a) and (b) are shown two hypothetical examples of their overlap, each a compound hazards event (CHE).

To illustrate our methodology, we will use two variables, extreme wind and extreme precipitation, both significant hazards in Great Britain (Pinto *et al.*, 2012; Huntingford *et al.*, 2014). These two hazards are usually associated with extratropical cyclones and severe storms (Zscheischler *et al.*, 2020). Extreme wind and extreme precipitation have been defined as compound hazards (i.e., statistically dependent without causality) (Tilloy *et al.*, 2019). Events, including precipitation and wind extremes, have been identified as multivariate compound events (co-occurrence of multiple hazards in the same geographical region, causing an impact) (Zscheischler *et al.*, 2020). The combination of wet and windy extremes can result in different and more significant impacts than the sum of the individual impacts due to extreme wind and extreme rainfall (e.g., the access to a flooded power plant due to heavy rain hindered by strong winds or road blocked by fallen trees) (Martius *et al.*, 2016). Previous studies have quantified the co-occurrences of extreme wind and extreme rainfall at large scales (Raveh-Rubin and Wernli, 2015; Martius *et al.*, 2016) by using climate reanalysis data, thus providing a common spatiotemporal frame to study multiple variables. To detect the occurrence of extreme wind and extreme precipitation events, Raveh-Rubin and Wernli (2015) averaged wind and precipitation anomalies spatially and temporally while Martius *et al.* (2016) used a threshold approach (set up a threshold above which wind and precipitation are considered as hazards).

This article is organized as follows. In **Section 5.2**, the spatiotemporal clustering algorithm used in the study and the gridded data retained for the analysis is introduced. Then in **Section 5.3**, the CHCI method to construct compound hazard clusters from extreme values of environmental variables is presented, along with the fundamental concepts associated with return periods in a bivariate framework. **Section 5.4** assesses the ability of the CHCI method to identify hazard events, where natural hazard clusters are confronted with a set of 157 major hazard events that impacted Great Britain, 1979–2019. Spatiotemporal and intensity properties of detected single and compound hazard clusters are then analysed and discussed. Finally, in **Section 5.5**, the limitations of the CHCI method and opportunities for its generalisation to other hazard interrelations are discussed.

5.2 Spatiotemporal clustering

Clustering is broadly defined as any process of grouping data by their similarities (Ansari *et al.*, 2020). It is a fundamental of data analysis in a wide variety of disciplines (e.g., biology, epidemiology, communication, criminology) (Xu and Tian, 2015). The large increase in spatiotemporal data available has created increased opportunities for spatiotemporal clustering approaches (Shi and Pun-Cheng, 2019; Ansari *et al.*, 2020). Many methods have been developed to cluster and classify data (e.g., partition, hierarchical, density-based, model-based clustering; see for a review Milligan and Cooper, 1987; Xu and Tian, 2015). Some clustering methods have been adapted to spatiotemporal clustering (e.g., Birant and Kut, 2007; Agrawal *et al.*, 2016; Yuan *et al.*, 2017; Huang *et al.*, 2019; Ansari *et al.*, 2020). Spatiotemporal clustering is usually done on three different values characterising the data: two spatial coordinates and time (Ansari *et al.*, 2020).

Three main approaches to spatiotemporal clustering exist (each with their own methods), including:

a) Point events spatiotemporal clustering: This approach aims to discover groups of events that are close to each other in space and time. It is used, for example, to cluster seismic events in time and space (Georgoulas *et al.*, 2013).

iv) Moving clusters: This approach aims to detect behaviours of moving objects. While the identity of a moving cluster does not change over time, other attributes might change. An example is the spatiotemporal clustering of lightning strikes resulting from moving convective storms (Strauss *et al.*, 2013).

v) Trajectory clustering: This approach aims to capture groups of objects with similar movement behaviours. In contrast to the moving cluster approach, where the moving object of interest, the variable of interest in trajectory clustering is the movement itself and not the object (Yuan *et al.*, 2017). Examples include cyclone track clustering in different world regions (Ramsay *et al.*, 2012; Rahman *et al.*, 2018).

The characteristics of the data used influences the choice of the spatiotemporal clustering methodology type. Climate reanalysis gridded data for wind and precipitation is used here, with a temporal resolution of one hour and a spatial resolution of 0.25° × 0.25°. Each grid cell containing a hazard occurrence (extreme wind, extreme precipitation, or both) is treated as a point by the clustering algorithm. Therefore, the point events spatiotemporal clustering approach is used here.

5.2.1 **Spatiotemporal data and study area**

Spatiotemporal data includes information about the location (here longitude and latitude) and time of the variable of interest. Here, the variables of interest are two atmospheric natural hazards: extreme precipitation and extreme wind. Spatiotemporal datasets of hydrometeorological data can be derived from interpolated observations (e.g. E-OBS), climate model outputs (e.g., ERA 5) or remote sensing (e.g., CMORPH) To ensure spatial and temporal consistency between the two hazards, we use a single gridded dataset based on climate reanalysis data. Climate reanalysis offers homogeneous datasets for numerous environmental variables, including precipitation and wind gust, with different spatial and temporal resolutions. Those data are outputs of climate models calibrated on observed data across the world (Brönnimann *et al.*, 2018). Two major climate reanalysis datasets are the following:

i) the Climate Forecast System Reanalysis (Saha *et al.*, 2010) developed by the USA *National Centre for Atmospheric Research* (NCAR, 2020);
ii) ERA5 (Hersbach *et al.*, 2020) developed by the *European Centre for Medium-Range Weather Forecasts* (ECMWF, 2020).

ERA5 (ECMWF Reanalysis 5th Generation) is used in the present study.

ERA5 was released in 2019 by ECMWF and benefits from the latest improvements in the field (Hersbach *et al.*, 2020). ERA5 data (ECMWF, 2020) is available for 1979 to present (up to September 2019 is used here), with a spatial resolution of 0.25° × 0.25° and an hourly temporal resolution. The data resolves the atmosphere using 137 levels from the surface up to a height of 80 km (ECMWF, 2020). ERA5 data are generated with a short forecast of 18 h twice a day (06:00 and 18:00 UTC) and assimilated with observed data (ECMWF, 2020).

Reanalysis data are not observed data and are obtained from short-term model forecasts and can be affected by forecast errors (Pfahl and Wernli, 2012). Furthermore, reanalysis data offers a large amount of usable data for spatiotemporal clustering methods, meaning that the method used in this study could be easily extended to other atmospheric or hydrological hazards (e.g., extreme temperature) (Sutanto *et al.*, 2020). The two following variables are extracted from the product:

- *Extreme rainfall (r):* accumulated liquid and frozen water, comprising rain and snow, that falls to the Earth's in one hour (mm). This value is averaged over a grid cell.
- *Extreme wind (w):* hourly maximum wind gust at a height of 10 m above the surface of the Earth (m s^{-1}). The WMO defines a wind gust as the maximum of the wind averaged over 3 s intervals. As this duration is shorter than a model time step, this value is deduced from other parameters such as surface stress, surface friction, wind shear and stability. This value is averaged over a grid cell.

Limitations of ERA5

The use of a climate reanalysis product to study extreme events induces several limitations compared to observational data (Donat *et al.*, 2014; Angélil *et al.*, 2016). In climate reanalysis, variables are computed over a grid cell, and the resulting value is, therefore, an average. This often leads to a smoothing of local extreme values (Donat *et al.*, 2014). The accuracy of reanalysis data also depends on various observation types (Hersbach *et al.*, 2019). ERA5 benefits from the latest methodological improvements in data assimilation and modelling (Hersbach *et al.*, 2018; ECMWF, 2020). Compared to its predecessor ERA-Interim, it offers finer spatial and temporal resolution, but most importantly produces more accurate weather and climate data in most world regions. Despite these improvements, the spatial resolution is still relatively coarse and small scale convective events are still poorly captured as it is the case for most reanalysis products (Holley *et al.*, 2014; Kendon *et al.*, 2017; Beck *et al.*, 2018a). Furthermore, precipitation is not assimilated (calibrated on observations) in ERA5 outside the USA. Nevertheless, ERA5 seems to outperform other global reanalysis products for extreme precipitation (Mahto and Mishra, 2019) and captures a majority of observed daily precipitation extremes over Germany and Europe (Hu and Franzke, 2020; Rivoire *et al.*, 2021). It also allows us to conduct the analysis at an hourly time scale rather than daily.

Discussion of the Study area and its Coherence Around Figure 5.2

The rectangular study area selected for the spatiotemporal clustering contains Great Britain and North-West France (**Figure 5.2**). It has an area of 647,900 km^2 which represents approximately 500 km (33 cells) by 1200 km (45 cells), or a total of 1485 cells, each cell 0.25° × 0.25° (cells range from 18.6 km × 27.8 km in the south of the study region, to 14.3 km × 27.8 km in the north). The temporal resolution used is one hour over the period from January 1979 to September 2019. When considering the study area boundaries, two factors are important to consider: (i) the variability of climate, geology or topography within the study area. (ii) the possibility of not capturing an event in its totality because of edge effects (Cressie, 1993).

Both Great Britain and northern France share the same temperate oceanic climate (Koppen climate classification Cfb) (Beck *et al.*, 2018b). However, within this broad region, there are variations in precipitation and wind exposure, particularly with coastal areas being more exposed to high wind and mountainous areas being wetter (Hulme and Barrow, 1997). This variability is taken into account into our methodology when sampling extreme events (this is discussed below in **Section 5.3.1**).

Edge effects have the potential to bias the clustering analysis as points on the edge have fewer neighbouring cells than other cells within the domain (Cressie, 1993). To mitigate this issue, a buffer area is set around the domain (**Figure 5.2**). Clusters need to include extreme values (points) that are some distance away (here 2 cells) from the edge of the study area. A cluster of extreme values (points) exclusively within the buffer area will not be retained, but values in the buffer area can be part of other clusters.

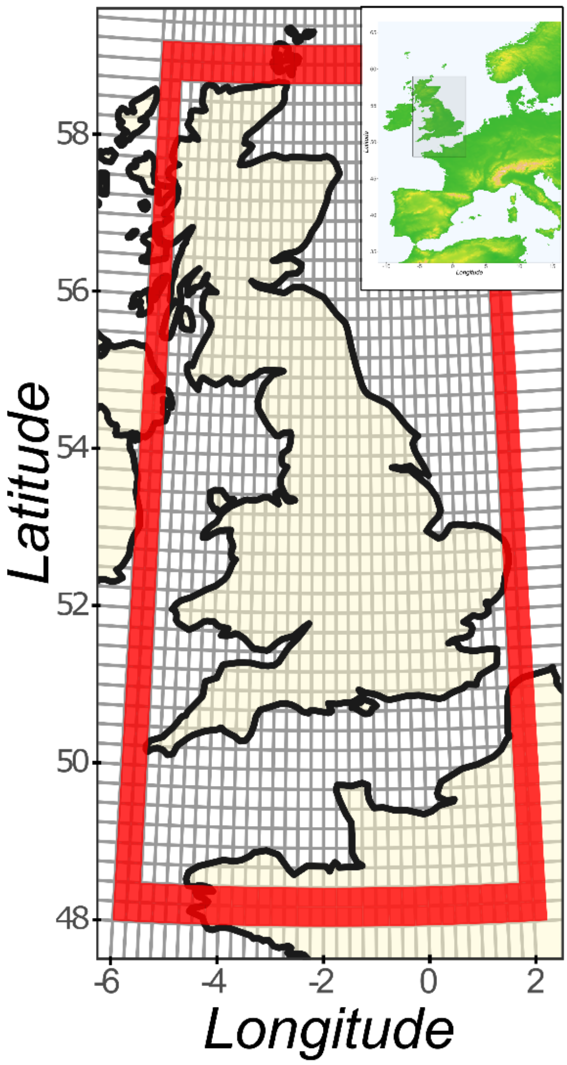

Figure 5.2: Study area with the grid representing the 1485 cells used for spatiotemporal clustering of extreme rain and extreme wind. The area includes Great Britain and the British channel. The red frame is the buffer area.

5.2.2 Clustering algorithm: DBSCAN

The specific clustering method used here for identifying spatiotemporal clustering of extreme wind and precipitation point events needs to comply with different characteristics of our spatiotemporal data:

(i) *The large size of the dataset:* ERA5 data is available for 40 years with an hourly timestep; this implies a significant amount of data over our study area of 1485 cells (>5×10^8 values).

(ii) *Noise level:* The method used to sample extreme occurrences of wind gust and precipitation (see **Section 5.3.1**) can produce objects scattered in space and time, which cannot be associated with a hazard cluster.

To ensure flexibility in the specific point events clustering methodology developed, it was decided not to assume a given shape for the natural hazard clusters. The characteristics of climate reanalysis data and the absence of assumptions about the shape of our hazard clusters guided the choice of a clustering algorithm toward the Density-Based Spatial Clustering of Applications with Noise (DBSCAN) algorithm (Ester *et al.*, 1996). There are five main types of clustering methods that can be used for a point event spatiotemporal clustering: Density-based, Partitional, Hierarchical, Grid-based and Model-based methods (Birant and Kut, 2007; Xu and Tian, 2015). Density-based clustering methods aim to define a structure that accurately represents the underlying density of the data (Hahsler *et al.*, 2017). Density-based clustering methods are non-parametric methods able to find clusters with arbitrary shapes and do not require the predetermination of the number of clusters to be detected (Birant and Kut, 2007).

DBSCAN is a clustering algorithm for identifying clusters with arbitrary shapes (Shi and Pun-Cheng, 2019). The primary idea behind DBSCAN is that for each point of a cluster, the neighbourhood of a given radius (ε) has to contain at least a minimum number of points (μ), i.e. the density in the neighbourhood needs to be above a threshold (Ester *et al.*, 1996). The shape of a neighbourhood is conditioned by choice of the distance function used (e.g., Manhattan, Euclidean, Minkowski) (Ester *et al.*, 1996). DBSCAN estimates the density around each data point by counting the number of points in the radius ε. DBSCAN identifies three types of objects: (i) core points; (ii) border points; (iii) noise points (Hahsler *et al.*, 2017). A point c is a core point if at least μ other points are within the distance ε of it. Points that are not core points but in the neighbourhood of core points are called border points. All points not reachable from any other point are outliers (Ester *et al.*, 1996) (see **Figure 5.3**). To create clusters, a key concept of the method is the density-reachability. Density-reachability is obtained when there is a chain of core points where one falls in the neighbourhood (distance<ε) of the next (see **Figure 5.3**). All the points from the chain are said to be “density-connected” and form clusters (see **Figure 5.3**). Each cluster contains at least one core point (Yuan *et al.*, 2017). **Figure 5.3** illustrates the basic concepts and terms of DBSCAN in two dimensions with Euclidean distance as a distance metric. For more details on the DBSCAN algorithm, the reader can refer to Ester *et al.* (1996) and Hahsler *et al.* (2017) for details about implementing the algorithm in R.

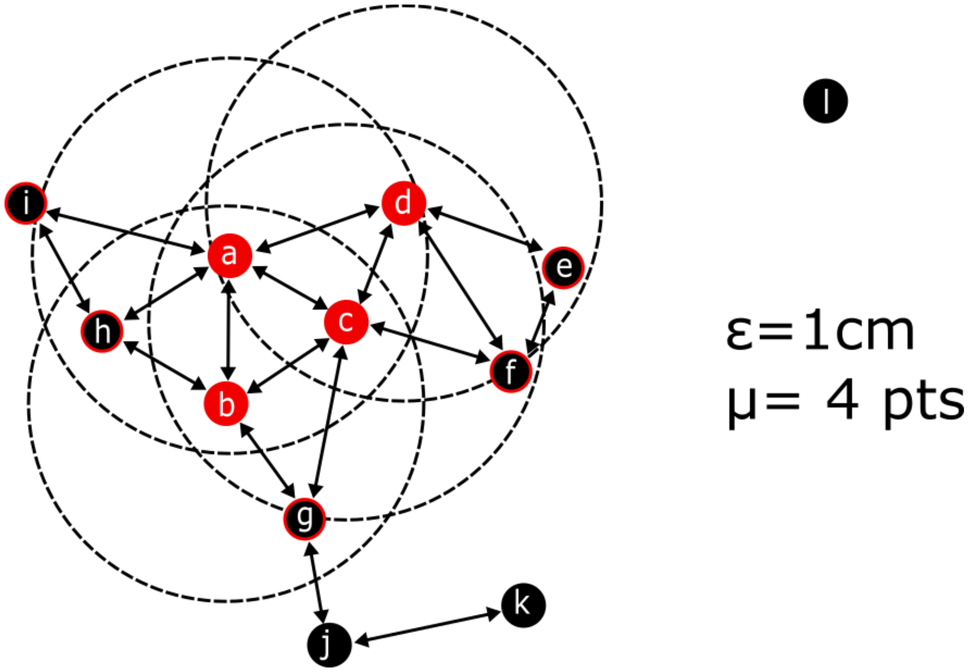

Figure 5.3: illustration of DBSCAN. Basic concepts and terms: dashed large circles represent the distance with a radius ε. Small red filled circles (a, b, c, d) are core points. Small black circles (red outline) (e, f, g, h, i) are border points. Black circles (no red outline) (j, k, l) are noise points. Points i and d are density-reachable from a; i and e are density-connected via object a. Black arrows represent the connection between two density-reachable points. The cluster detected by DBSCAN contains points a, b, c, d, e, f, g, h, i and j, k, l that are noise points.

The two input parameters of the DBSCAN algorithm are the density threshold μ and neighbour parameter ε and are set by the user. The usual rule to follow when defining μ is to use at least the number of dimensions of the dataset plus one (i.e., three for two-dimensional data as in **Figure 5.3**). Regarding the ε parameter, the selection is usually made by plotting the points' kNN distances (i.e., the distance to the kth nearest neighbour) in decreasing order and identifying the knee in the plot (Hahsler *et al.*, 2017) (see **Section 5.3.2**). In this study, the rules mentioned above are associated with considerations arising from the definition of hazard objects (**Section 5.3.2**).

DBSCAN relies heavily on forming neighbourhoods. A simple approach is to compute the distances to all other points to find the closest points. This requires O(n) operations for each time a neighbourhood is needed, with n being the number of data points. Since the operation is repeated for each data point once, this results in an O(n^2) runtime complexity. As a result, the size of the full distance matrix becomes very large and is slow to compute for medium to large data sets. To reduce computation time, spatial indexing methods provide a mechanism to quickly locate single or multiple objects and extract desired information from a database. A spatial index is a data structure that optimizes data processing in large datasets (Azri *et al.*, 2013). DBSCAN relies on space partitioning data structure called k-d trees (Bentley, 1975). The k-d trees divide the space into non-overlapping regions and allow DBSCAN to run more efficiently in sub-linear time using on average only $O(\log(n))$ operations per query. The result is a reduced runtime complexity of $O(n \log(n))$ (Hahsler *et al.*, 2017).

5.3 Methodology for compound hazard clusters identification (CHCI)

Samples of extreme events are extracted from the ERA5 data. The DBSCAN algorithm is used to create spatiotemporal clusters of (i) extreme rainfall events; (ii) extreme wind event. Wind and rain clusters are then paired according to their spatial and temporal overlap to create compound hazards clusters. The methodology to create spatiotemporal clusters is described in **Figure 5.4,** a flowchart of the method steps.

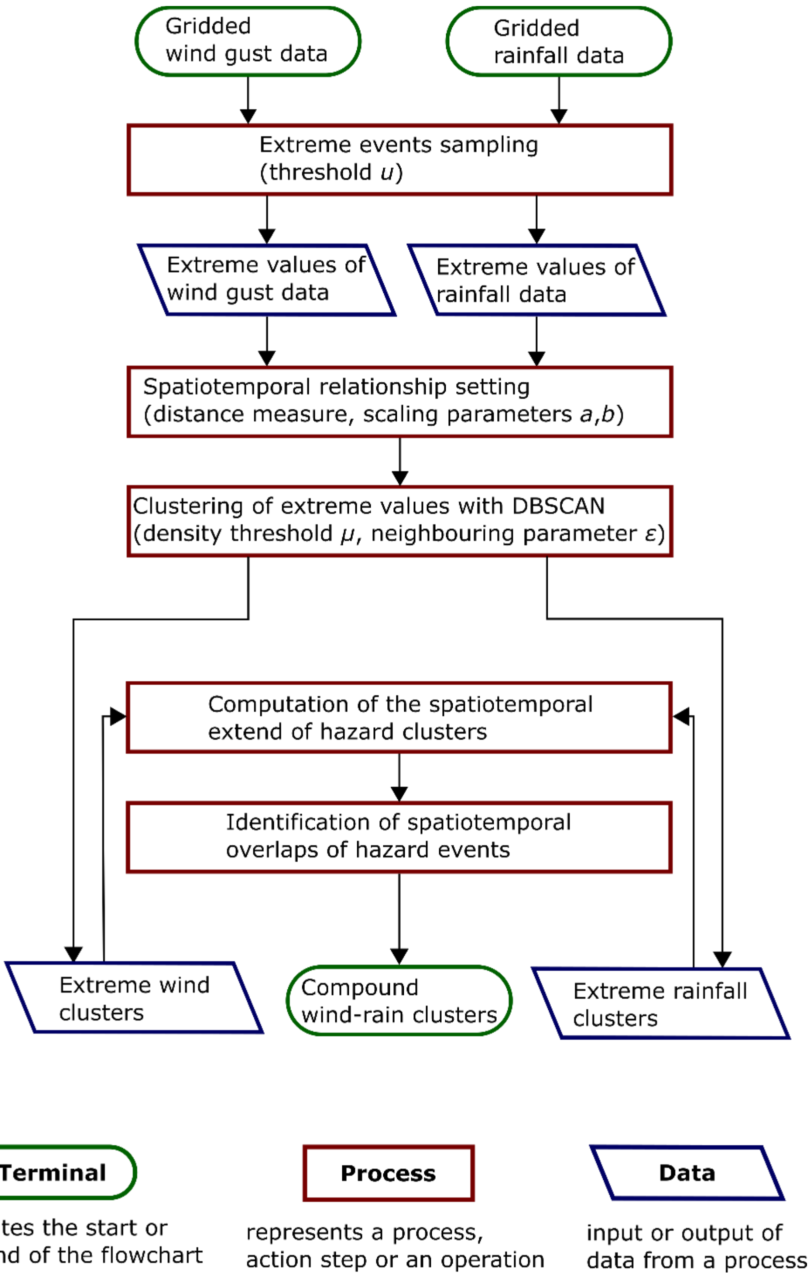

Figure 5.4: Flowchart of the methodology developed, Compound Hazard Cluster Identification (CHCI), for wind and rainfall data in Great Britain.

Figure 5.4 represents the main steps and data used to create compound wind-rain clusters in **Chapter 5**. Three main steps which are discussed in this section are highlighted in **Figure 5.4**:

(i) *The definition of a threshold u* selected to sample extreme events (Section 5.3.1)

(ii) *The setting of the ratio* r of the spatiotemporal scaling parameters and the clustering procedure (Section 5.3.2)

(iii) *The identification of spatiotemporal overlap* between hazard cluster to create compound hazard events (Section 5.3.3)

The sensitivity of the procedure displayed in **Figure 5.4** to the different input parameters is discussed and quantified in **Appendix G**.

5.3.1 Defining a hazard threshold

The spatiotemporal methodology developed here uses extreme occurrences of climate variables proxies for the occurrence of natural hazards, in this case, extreme wind and extreme rainfall. The use of a threshold to analyse the spatiotemporal occurrence of different extremes and their potential combinations have been done on daily data by Martius *et al.* (2016), Sedlmeier *et al.* (2018) and Sutanto *et al.* (2020). In the latter two studies, two approaches are used to define the value of a threshold: (i) an impact-based approach where the threshold is related to a tipping point where impacts (e.g., to society) start occurring (Sedlmeier *et al.*, 2018); (ii) a percentile-based approach where the threshold is related to an empirical extreme quantile of the studied variable (Tencer *et al.*, 2014; Visser-Quinn *et al.*, 2019; Sutanto *et al.*, 2020). In the second approach, hazards are extreme events relative to the distribution of the studied variable.

The percentile-based approach was chosen here as it provides a large sample size for robust statistical analysis. The percentile-based approach, while not being linked to a specific impact, can also be impact-relevant (Zhang *et al.*, 2011), with extreme occurrences of hourly maximum wind gusts and hourly accumulated precipitation potentially leading to a negative impact on society. The connection between maximum wind speed and impact has been broadly acknowledged (Pinto *et al.*, 2012). It has been shown that a local 98th percentile is an impact-relevant wind threshold (Ulbrich *et al.*, 2009). However, as our data are not local, a 99th percentile was used here to increase the probability of detecting potentially damage-relevant events.

The choice of an impact-relevant threshold for rainfall is more complex, as the impact of extreme precipitation depends on the duration and the intensity of an event. Martius *et al.* (2016) selected the 98th percentile of daily precipitation to define their extreme precipitation events. Pfahl *et al.* (2014) used the 99th percentile as a threshold for extreme precipitation. For the sake of consistency, the same percentile is used for the definition of extreme events of both hazards. Our data's hourly temporal resolution also allows us to use the 99th percentile while keeping a large sample size. The threshold is computed for each of the 1485 cells of the domain studied. The threshold value varies between u = 16.6 m s^{-1} and u = 26.8 m s^{-1} for hourly maximum wind gust and between u = 1.46 mm h^{-1} and u = 2.74 mm h^{-1} for precipitation. The value of this the selected percentile (here 99th) and the corresponding threshold value has a significant influence on the clustering procedure (**Appendix G**)

The threshold values u for wind gust and precipitation over the study area are displayed in **Figure 5.5.** In this figure, the wind gust threshold is higher in coastal regions and the North of England, Scotland and Wales, whilst South England and North-West France have significantly lower threshold values. For precipitation, one can observe a clear division between the Eastern and Western part of Great Britain, with the western part having significantly higher threshold values. The sample of extreme events is composed of two distinct sets: (i) occurrences of extreme wind gust and (ii) occurrences of extreme precipitation. These extreme events are then represented as point objects with coordinates in space (latitude and longitude) and time (date). Here, both hazards are studied separately before being paired into compound hazard events. The clustering algorithm is then applied to the points representing extreme wind and precipitation values.

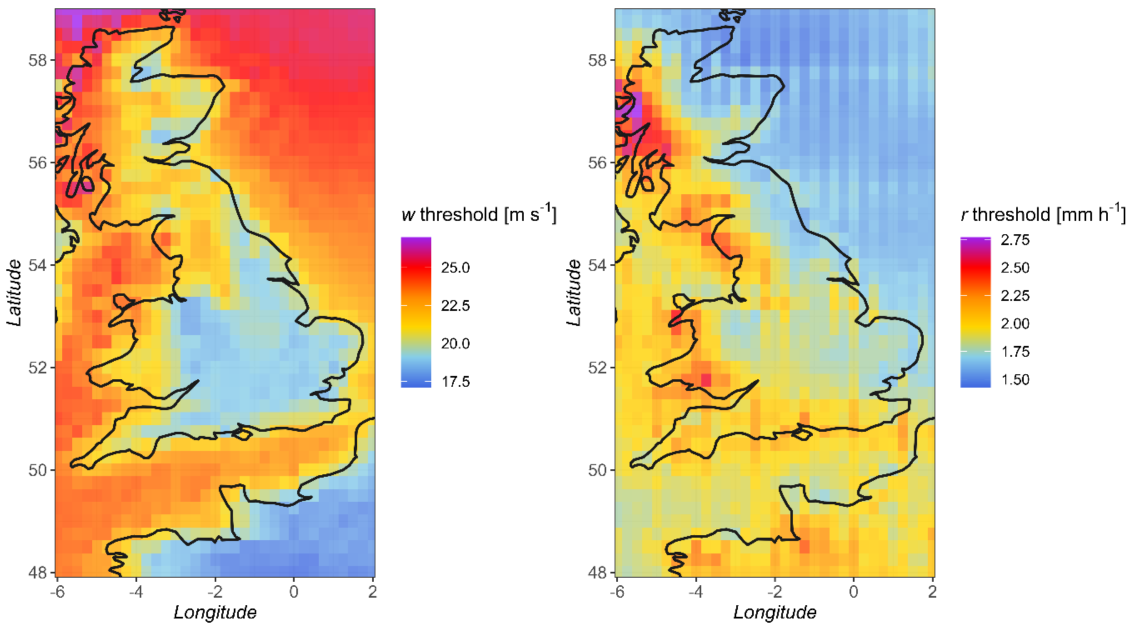

Figure 5.5: Threshold values used to extract extreme values for the clustering process. The values correspond to the 99th percentile on each grid cell during the period 1979–2019 for (a) hourly maximum wind gust (w) and (b) hourly rainfall accumulation (r). Data from ERA5 (Hersbach *et al.*, 2020).

5.3.2 Hazard events and cluster construction

A method for defining thresholds and sampling extreme values has been presented in **Section 5.3.1.** These extreme values are the input data for the cluster construction. Hazard events are defined here as clusters of these values in space and time representing a singular phenomenon's footprint.

To perform spatiotemporal clustering with DBSCAN, Birant and Kurt (2007) used two neighbour parameters ε, one for spatial values and one for non-spatial (i.e., temporal) values in their ST-DBSCAN algorithm. The distance measure they used for both spatial and non-spatial values is the Euclidean distance. The Euclidean distance is preferred to other distance measures in this study for simplicity. Here, one distance measure is used for both space and time as it is implemented in the original DBSCAN algorithm. The spatiotemporal domain is then assumed to be a space-time cube as is done in various studies (Bach *et al.*, 2014). One of the advantages of this approach is that it is possible to take advantage of the spatial index structure (see **Section 2.2**) to significantly speed up the runtime complexity (Hahsler *et al.*, 2017). Three parameters are ruling the clustering procedure: (i) the relationship between spatial distance and temporal lag; (ii) the density threshold (μ) for our cluster; (iii) the neighbour parameter ε. These three parameters are now discussed:

(i) *First parameter: the relationship between spatial distance and temporal lag*. The first step of our cluster event construction is to define the importance of spatial distance relative to temporal distance when computing the Euclidean distance between objects. This is done according to physical considerations. Each object in our input data represents one occurrence of an extreme event in one grid cell. Each grid cell is 0.25° latitude (≃27.8 km) by 0.25° longitude (ranging from 14.3 km in the southern part of our study area to 18.6 km in the northern part), with areas of grid cells ranging from 397 km^2 (in the south of our study area) to 517 km^2 (in the north). The distance between each extreme value is at least one hour. Scaling factors are then introduced to give more importance to space or time distance in a three-dimensional space-time cube (Ansari *et al.*, 2020). The spatiotemporal Euclidean distance d_{p-q} between two points p and q is expressed as:

$$d_{p-q} = \sqrt{a(x_p - x_q)^2 + a(y_p - y_q)^2 + b(t_p - t_q)^2} \quad (5.1)$$

for $i = (p,q)$, x_i the latitude of the extreme value, y_i its longitude, t_i its temporal coordinate, and a and b two scaling parameters. The ratio $r = a/b$ is the parameter controlling the relationship between spatial distance and temporal lag. The following parameter values are chosen: a = 4.0 deg^{-1} and b = 1.0 h^{-1}, and therefore r = 4.0 h deg^{-1}, meaning that a distance of 0.25° in space is weighted similarly to a distance of 1.0 h in time (**Figure 5.6**). This allows a normalized three-dimensional space-time cube-data structure as displayed in **Figure 5.6**. Each point is spaced out by a distance of 1.0 [various units] in each dimension (longitude, latitude, time). Nevertheless, even if each point is equally spaced in term of longitude and latitude, this is not the case in term of geographical distance.

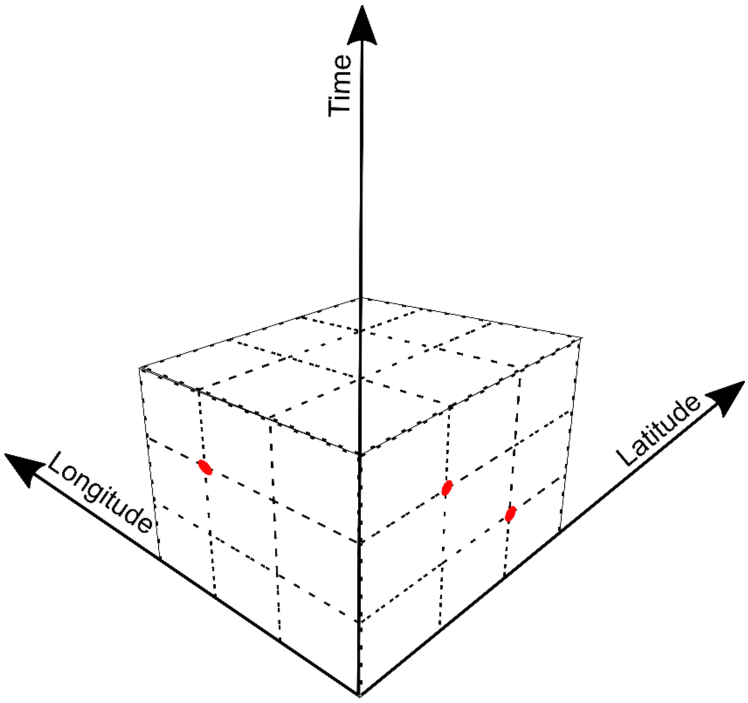

Figure 5.6: Space-time cube as used in the CHCI methodology. The three small red dots represent extreme values. Each cube is latitude 0.25° × longitude 0.25° × time period 1.0 h.

(ii) *Second parameter: the density threshold μ.* This parameter represents the number of neighbours a point needs to have to be considered a core point, and therefore generates a new cluster. This value needs $\mu > 4$ points in our dataset (number of dimensions plus one). However, the detection of intense small scale events (e.g., Bracknell storm, 2000) is not intended here because of the relatively coarse resolution of ERA5 and its tendency to smooth local extremes. The aim remains to detect different meteorological events of varying size. Small scale and short duration extreme precipitation and/or wind events in Great Britain are often associated with convective events (See **Chapter 3**). The size of such events varies from hundreds of km^2 to tens of thousands of km^2 (Chazette *et al.*, 2016; Rigo *et al.*, 2019), while their duration goes from hours to days (**Chapter 3**). Knowing that the area of the cells in the study area ranges between 400 and 520 km^2, it was decided to take a density threshold μ = 10 points, meaning that the smallest events captured should last from 1 to 10 hours, cover an area between 5200 and 400 km^2 while being composed of at least 10 extreme values.

(iii) *Third parameter: neighbour parameter ε.* This is the radius ε in which μ points should be included to create a cluster. We would like the radius to include at least two neighbours in time and two neighbours in space, as shown in **Figure 5.6,** meaning $\varepsilon > 2$ (unitless). To select a relevant radius for the data, the points' k–NN distances are plotted (i.e., the distance to the k^{th} nearest neighbour) in increasing order, to look for a knee in the plot (Hahsler *et al.*, 2017). The idea behind this practice is to differentiate neighbours from noise within the whole dataset. **Figure 5.7** displays the 10^{th} nearest neighbour distance increasing order. The knee in the plot is identified around ε = 2.24 for extreme wind gust and ε = 2.45 for extreme precipitation values.

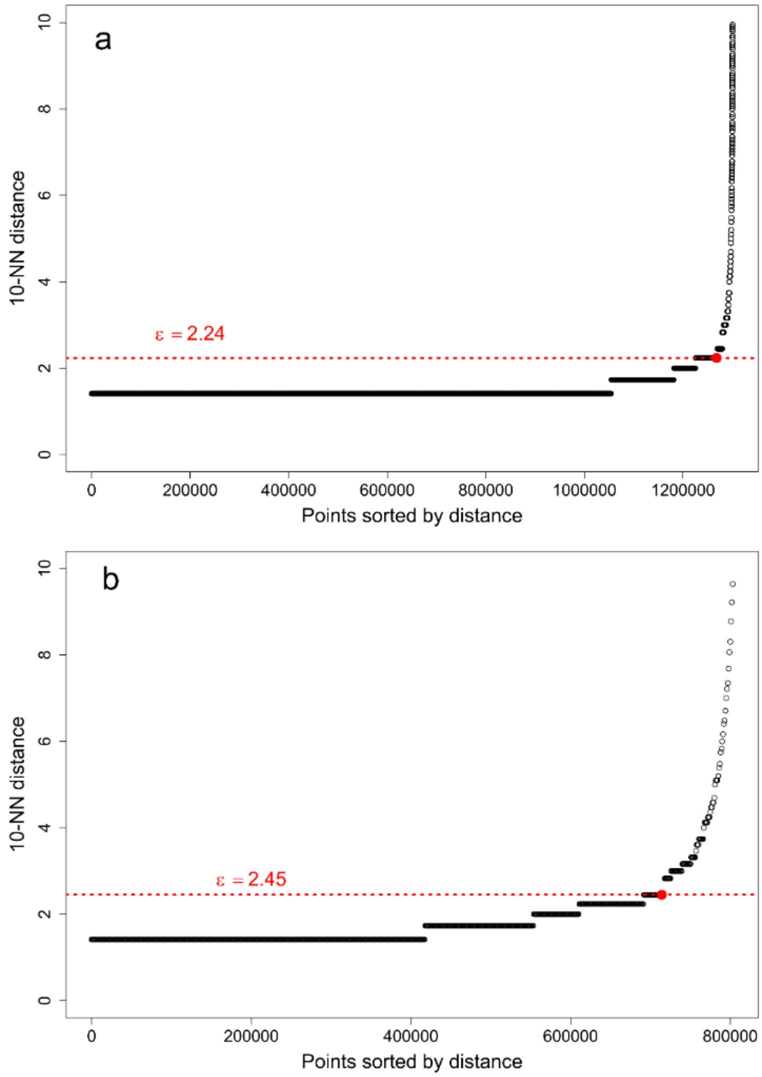

Figure 5.7: Sorted Euclidean distance to the 10th nearest neighbour (10-NN) for sampled hourly wind and rainfall extreme values over Great Britain for the period 1979–2019. (a) Extreme wind events and (b) extreme rainfall events. The dotted lines represent the knee of the distribution (ε). This value is the neighbouring parameter of the DBSCAN algorithm.

The spatiotemporal space is discretized in a space-time cube (**Figure 5.6**). Each grid point (representing one grid cell of input data) is spaced by a unit distance in each direction (longitude, latitude, time), with a unit distance representing 0.25° in both spatial dimension and one hour in time. The density threshold (μ) is fixed at μ = 10 points. With these two parameters, a k Nearest Neighbour (k–NN) search is performed, with k = μ =10 points. As a result, a distance matrix containing the distance of each point to its 10–NN is created. From the matrix, neighbour parameters are fixed at ε = 2.24 for extreme wind and ε = 2.45 for extreme precipitation values. Neighbour parameters allow to estimate the spatiotemporal neighbourhood in which the 10–NN needs to be for a point to become a core point. This neighbourhood is highlighted in **Figure 5.8**, showing that the 10–NN neighbourhood includes 44 points with a maximum temporal distance of two hours and a maximum spatial distance of 0.5° in latitude or longitude. The sensitivity of the clustering procedure to the threshold selected to sample extreme events u, the ratio r of the spatiotemporal scaling parameter a and to the density threshold μ is assessed in **Appendix G**.

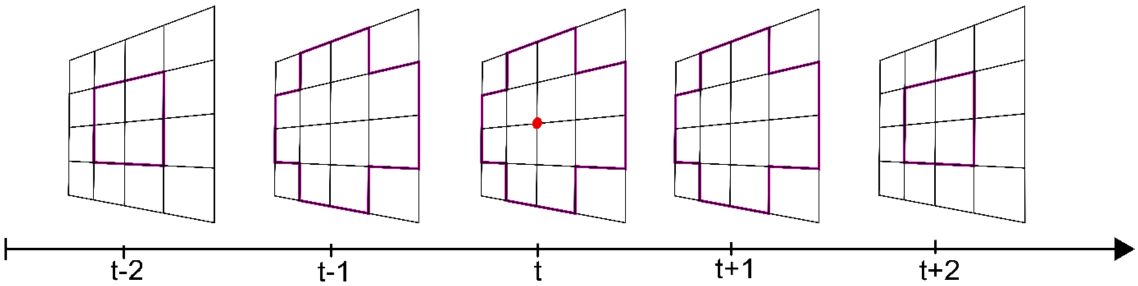

Figure 5.8: reachable distance in the spatiotemporal space used in this study. The arrow represents time steps and each node is a potential spot for an extreme value. The red point represents extreme value. To be neighbours, other extreme values need to be within the space delimited by the purple line. For a new cluster to be created, an extreme value needs to have at least 10 (out of 44 possibilities) extreme value neighbours.

5.3.3 Compound hazard events

One commonly used option to study compound extremes is to sample only the joint extreme events (i.e., extreme wind and extreme rain at a given location and time) (Martius *et al.*, 2016; Tencer *et al.*, 2016; Sutanto *et al.*, 2020). When it comes to the spatial and temporal characteristics of compound extremes, this option has weaknesses that the present approach aims to overcome. The weaknesses include: (i) It highly relies on the spatial and temporal resolution of the input data in the definition of “compound”; (ii) It cannot consider the lag time between different extremes. (iii) It fails to decipher the spatial structure of extreme events.

Here, hazards events are created for both extreme precipitations and extreme wind gusts; compound hazard events are detected by matching extreme precipitation and extreme wind gust events in time and space. The hazard event’s footprint is the total area where the hazard occurred during the whole duration of the event. To define the spatial and temporal scales of compound hazard events, one can look at the overlap in time (t) and space (S) of hazard events. This overlap can be the intersection AND ($t_{w\cap r}, S_{w\cap r}$) or the union OR ($t_{w\cup r}, S_{w\cup r}$) of two hazard events in space and time. There are, therefore, four different possible definitions of a compound hazard event in space and time depending on the definition chosen for the overlap in space and time, as displayed in **Figure 5.9**. The extent of the compound hazard event footprint widely varies depending on which combination of spatial and temporal overlap is retained. One can consider the following:

a) The duration of a compound hazard event can either be defined as the time during which both hazards occur (AND) or as the aggregated duration of both hazards (OR). As the potential impact caused by a hazard can remain after the occurrence of this hazard (e.g., fallen trees blocking a road), the temporal scale of a compound hazard is then defined as the aggregated duration ($t_{\mathrm{w\cup r}}$) of both hazard.

iii) Footprints from different hazards need to overlap at least at one point to create a compound hazard event. The spatial scale of compound hazards is defined here as the intersection ($S_{w \cap r}$) of the spatial footprint of the two hazards.

An overlap of the two hazards' footprint does not mean that the two hazards occur in the overlapping area at the same time (here same hour), but that the two hazards occurred, during at least 1.0 h each, in that area during the same compound hazard event. This approach overcomes the weaknesses mentioned above of a joint occurrence sampling method without introducing a lag time (Klerk *et al.*, 2015; Iordanidou *et al.*, 2016). The time window in which a compound event can occur is flexible and fixed by the duration of both hazard events.

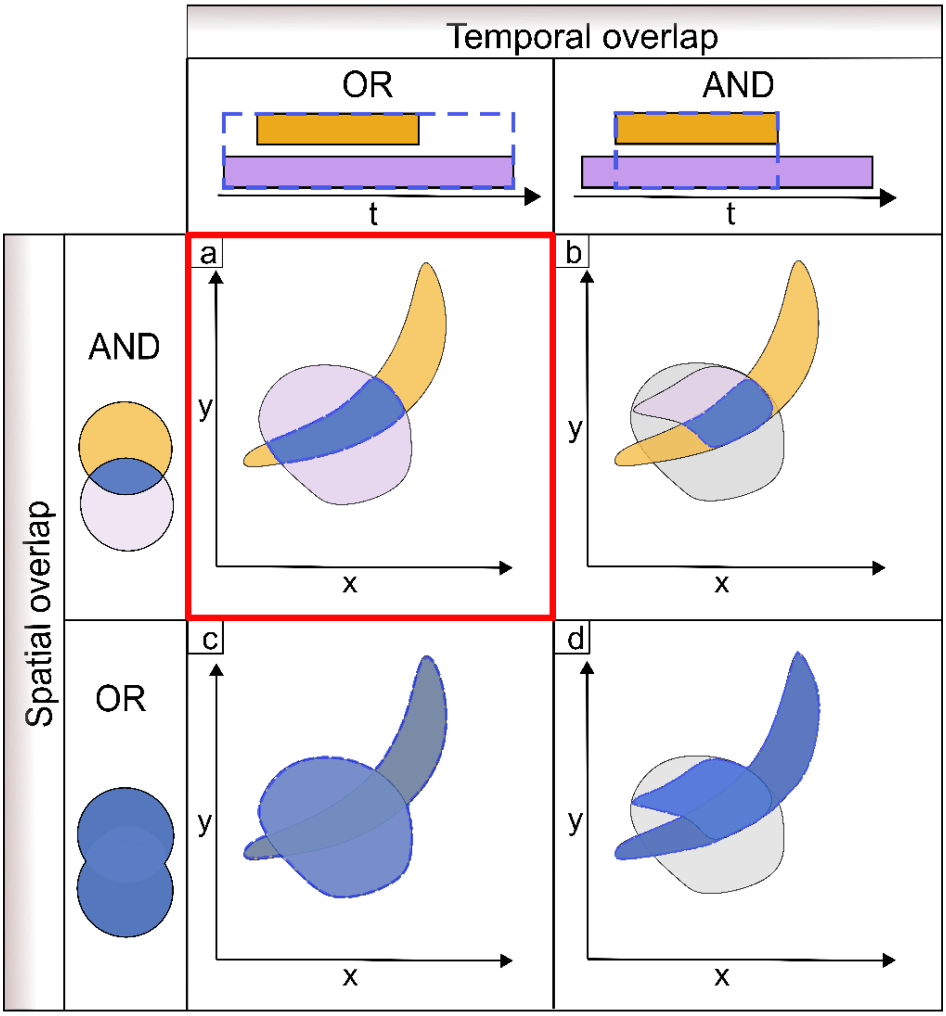

Figure 5.9: Different spatial and temporal scales considered in this study to define compound hazard events, with each case representing a combination of spatial and temporal overlap. (a) spatial AND with temporal OR, (b) spatial AND with temporal AND, (c) spatial OR with temporal OR, and (d) spatial OR with temporal AND. Hazard A is in orange, hazard B in purple, compound hazard in blue and parts of footprints outside the temporal boundaries are in grey. The definition retained for the rest of the study is highlighted with a red frame (a).

I define here a compound hazard event footprint (**Figure 5.9a**) as the intersecting area (AND) on which two (or more) hazards develop during the aggregated union of the time periods (OR) of the two hazard events. From this definition and illustration in **Figure 5.9a**, the spatial (S) and temporal (t) scales of a compound ("Comp") hazard event that includes wind (w) and rain (r) events are defined as follow:

$$
\begin{aligned}
t_{Comp} &= t_{w\cup r} = t_{w} + t_r - t_{w\cap r} \\
S_{Comp} &= S_{w\cap r} = S_{w} + S_r - S_{w\cup r}
\end{aligned} \tag{5.2}
$$

With t_{comp}, t_w, t_r the duration of the compound hazard event, wind event and rain event respectively and S_{comp}, S_w, S_r the area of the compound hazard event, wind event and rain event respectively. The duration of a compound hazard event corresponds to the union of the durations of both hazard events involved meaning that $t_{Comp} \geq max(t_{w}, t_r)$. This piece of work examine compound wind-rain events; however, this definition aims to be applicable for other compound hazards (e.g., extreme hot temperature and drought).

5.4 Results

Each hazard cluster created is characterized by a set of attributes. Similarly to Visser-Quinn *et al.* (2019), three attributes (or metrics) were developed : (i) intensity attributes, (ii) spatiotemporal attributes (iii) historical attributes as follows:

(iv) *Intensity attributes*. To represent the intensity/magnitude of a rain event, the maximum rain accumulation in mm (r_a) in a grid cell over the duration of an event was used. Here, the rain accumulation represents the total amount of rain, including also timesteps when the rain value is inferior to the 99th percentile threshold. The intensity of a wind event is expressed by the maximum wind gust during the event in m s^{-1}. In this research, this is called the value wind accumulation (w_a).

(v) *Spatiotemporal attributes*. The spatial extent is measured in the number of spatial cells (0.25 × 0.25) with at least one extreme value during the event. The temporal extended (or duration) is measured in hours. The spatiotemporal scale represents the number of extreme spatiotemporal values (points) in the hazard event.

(vi) *Historical attributes.* These attributes include the start and end date of an event, its season (i.e., December/January/February [DJF], March/April/May [MAM], June/July/August [JJA], September/October/November [SON]) and its year of occurrence from 1979 to 2019.

Table 5.1 displays the intensity and spatiotemporal attributes and their availability for rain, wind and compound clusters.

Table 5.1: Intensity and spatiotemporal attributes of hazard events and their availability for wind, rain and compound hazard events in the present study

	Attribute	*Wind events*	*Rain events*	*Compound wind-rain events*
Intensity	*r_a (mm)*		✔	✔
	w_a (m s^{-1})	✔		✔
Scales	*Spatial footprint (%)*	✔	✔	✔
	Duration (h)	✔	✔	✔
Historical	*Start time (h)*	✔	✔	✔
	End time (h)	✔	✔	✔

From these attributes (**Table 5.1**), the hazard clusters created are confronted with a catalogue of 157 observed significant events that occurred in the study area. This confrontation highlights the capabilities of the method but also of the ERA5 reanalysis to catch different types of extreme events in Great Britain (**Section 5.4.1**).

5.4.1 Event identification: Confrontation with major events

To assess the capacity of our method to identify hazard events, natural hazard clusters are confronted to a set of past extreme wind and extreme precipitation events that impacted Great Britain. To do so, a catalogue of 157 major hazard events that occurred between January 1989 and September 2019 is created (See **Appendix I**). The 157 major events selected aim to be representative of the broad range of events, including extreme rainfall and/or extreme wind occurring in Great Britain. The construction of the catalogue is done using four primary sources:

i. Philip Eden: British Weather disasters (1901-2008). A book containing a chronology of severe weather events in the UK.
ii. Dartmouth Flood Observatory: Global Active Archive of Large Flood Events (1985-Present). An archive of flood events derived from news, governmental, instrumental, and remote sensing sources.
iii. CRED: EM-DAT (1984-2020). A record of disasters maintained by the Centre for Research on the Epidemiology of Disasters (CRED, 2018).
iv. Met Office: Past weather events website (1990-2020). Archive of reports on past weather events from the UK Met Office.

As these sources do not focus exclusively on extreme precipitation and extreme wind events, the catalogue's creation involves a pre-selection based on the relevance of the event to the study. For example, extreme rainfall events associated with flooding with a duration larger than 10 days are not retained as these events cannot be associated with one specific extreme rainfall cluster. The four sources are used to identify events timing, their location and their duration. Duration is expressed in days, while the location of the events corresponds to the 11 NUTS 1 regions of Great

Britain as follows: North East (England), North West (England), Yorkshire and The Humber, East Midlands (England), West Midlands (England), East of England, London, South East (England), South West (England), Wales and Scotland. An event can occur over 1 or more regions (see **Figure 5.10**). Events in the catalogue (**Appendix I**) are also characterized by their dominant hazards (the primary hazard reported in the sources). Events are therefore divided into two categories: rain events (*R*) and wind events (*W*), depending on their dominant hazard. Some significant events also include associated hazards (e.g., landslides) when reported in the sources. The catalogue contains 96 extreme precipitation events and 61 extreme wind events. **Figure 5.10** shows the date and locations of occurrences of the 157 major events in the catalogue. Rain and wind events are displayed with blue circles and orange crosses. Moreover, the 83 events identified as compound hazard events by the CHCI method are highlighted with green crosses in circles.

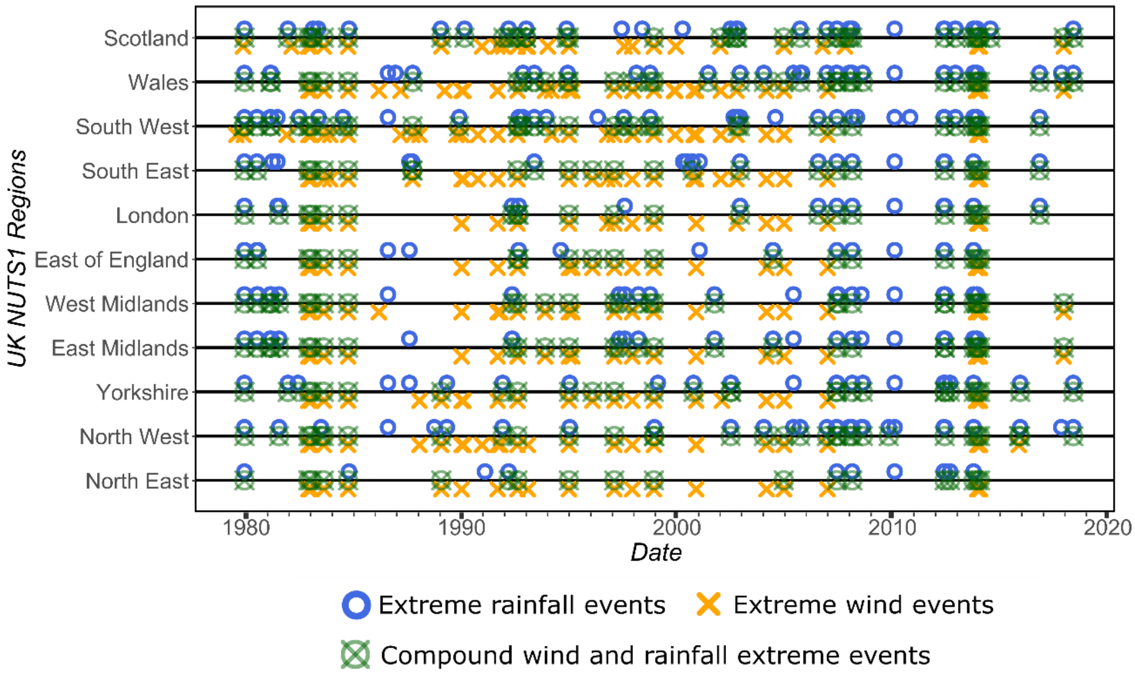

Figure 5.10: Timeline of the 157 major events in the catalogue used to assess the detection abilities of the CHCI method of the 11 NUTS1 regions of Great Britain. Major events are considered as "rain" (blue circles) or "wind" (orange crosses) events. Events that are identified as compound hazard events by the CHCI method are highlighted with green rectangles.

In **Figure 5.10**, the interconnections between areas impacted by the same events can be observed (e.g., January 2010 rain event) and the clustering of events in time. Some regions are also more represented than others in the catalogue. The number of events per regions is displayed in **Figure 5.11a**, with South-West England and Wales being the regions with the most events and North-East and East England being the regions with the fewer events. The date and locations of the 157 events are used to assess the CHCI clustering method's ability to capture extreme wind or extreme rainfall events. For each past major event, a temporal and spatial match is performed to identify the corresponding cluster(s). The hit rate (ratio between the number of events with corresponding clusters and the total number of events) is used to assess the capacity of the CHCI method. Over Great Britain, 147 out of 157 (hit rate = 93.4%) significant events have one or more corresponding hazard cluster(s). Among these 147 events, 64 (43.5%) have one corresponding cluster. The percentage of detected events for each NUTS1 region varies between 91.7% (South-East England) and 100% (North-West England, North-East England) and is displayed in **Figure 5.11b**.

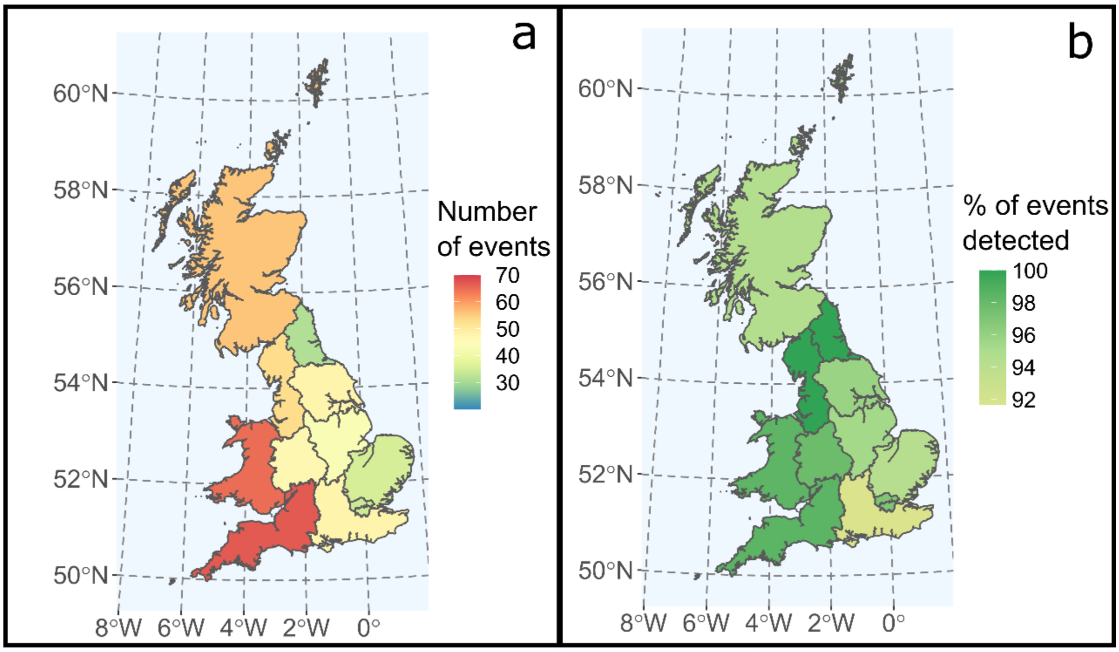

Figure 5.11: Maps of Great Britain divided into 11 NUTS1 regions showing: (a) the number of events per region from the catalogue and (b) the hit rate (ratio between the number of joint events and the total number of events) for each region

The relatively high hit rate provides confidence in the ability of the method to identify extreme events. However, for more than 50% of the historical events, there is more than one associated cluster, meaning that the method detected several hazard clusters associated with an event. The average number of clusters detected per event (for events with corresponding clusters) is 2.5. Here detected clusters are confronted to observed events. As the method presented in **Section 5.3** highly relies on the quality and accuracy of input data, it was decided not to compare intensity attributes with observations. Nevertheless, the hit rate for extreme precipitation events of the CHCI method with ERA5 hourly data (92.7%) is higher than the one observed in other studies over parts of Europe which is around 50% for ERA5 daily extremes (Hu and Franzke, 2020; Rivoire *et al.*, 2021) without clustering. This suggests that the use of this approach with hourly data might more accurately detect observed extreme events, although more studies are required to confirm this result.

5.4.2 **Spatial and temporal properties compound wind-rain events in Great Britain**

Over the period 1979–2019, a total of 18,086 rainfall clusters and 6190 wind clusters are detected. Despite suggesting that rainfall events are on average smaller and shorter than wind events, this also highlights the capacities of our approach to adapt to different input data. A total of 4555 compound hazard clusters as defined in **Section 3** are detected over the period. These 4555 compound hazard clusters are composed of 3565 rainfall clusters (20% of total) and 2913 wind clusters (47% of total). Some extreme rainfall or extreme wind clusters are parts of more than one compound cluster. For example, an extra-tropical cyclone bringing extreme rainfall scattered in space and time can be represented by several clusters and/or one single extreme wind cluster.

In this section, different characteristics of the 4555 compound hazard clusters are extracted and analysed. The fraction of compound clusters among wind and rain clusters is investigated in space (**Figure 5.12)** and time **(Figure 5.15)**. The strength of the spatiotemporal dependence between rain clusters and wind clusters is assessed through the Likelihood Multiplication Factor (LMF) (**Figure 5.13b)**. The occurrence frequency of compound wind-rain over Great Britain is estimated, allowing the identification of compound wind-rain hotspots (**Figure 5.13a**). The seasonality of wind, rain and compound hazard clusters is analysed in **Figure 5.14** and **Figure 5.15.**

Over the study area, the proportion of compound wind-rain clusters among the rainfall clusters detected is 20%, while 47% of the wind clusters are compound hazards clusters. However, this proportion is variable across Great Britain. **Figure 5.12** displays the fraction of compound hazard clusters among (a) wind clusters and (b) rain clusters. It highlights the spatial variability of compound event prevalence. Among the geographical features that may influence the frequency of compound hazards clusters among rain and wind clusters, orography probably plays an important role. The frequency of compound wind-rain clusters is the highest in mountainous areas, while lowlands of the west coast have a much lower frequency of compound wind-rain clusters among both rain and wind clusters. Duration of compound wind-rain clusters varies from 3 hours to 4 days and spatial footprints range from one grid cell, which represents less than 0.1% of the study area to 89% of the study area. However, compound wind-rain clusters are more prevalent among the most intense hazard clusters. The latter represents 58 of the 100 most intense rain clusters and 95 of the 100 most intense wind clusters. The intensity of rain and wind clusters is assessed with the intensity attributes presented in **Table 5.1**. The proportion of compound wind-rain clusters also increase with duration and footprint for both rain and wind clusters (**Appendix H**).

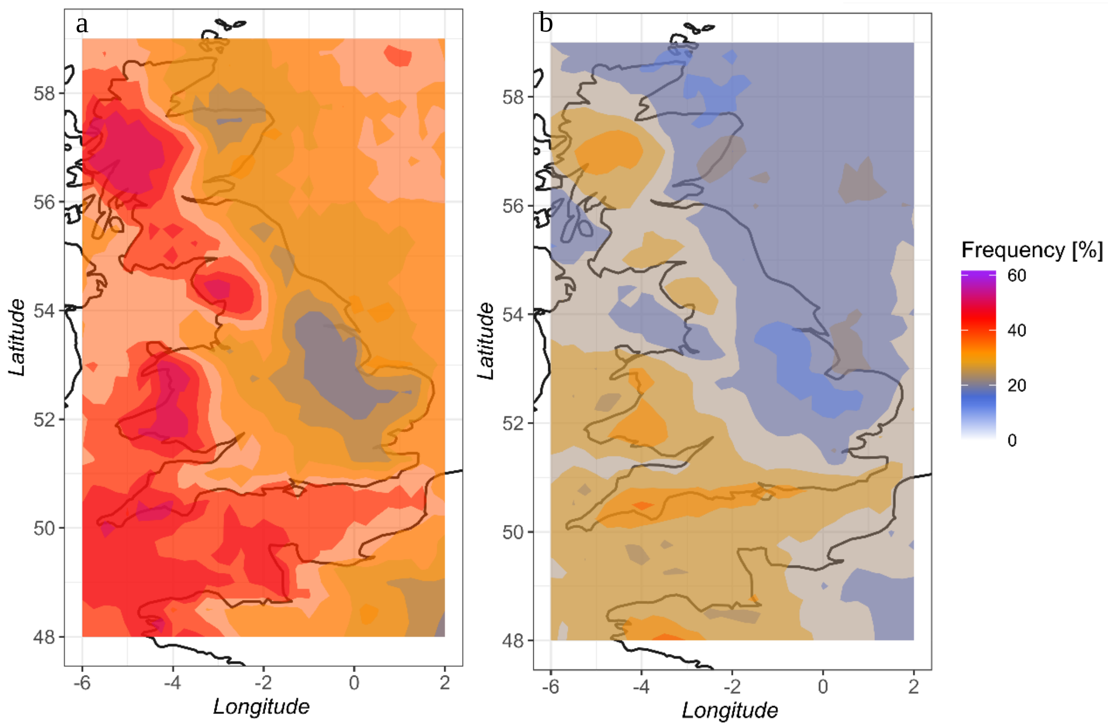

Figure 5.12: Compound hazard (wind-rain) clusters fractions among (a) wind clusters and (b) precipitation clusters during the period 1979–2019 in Great Britain. Data from ERA5 (Hersbach *et al.*, 2020).

As the duration of compound wind-rain clusters highly varies, their frequency of occurrence in the study area is assessed by counting the number of hours in a compound event (as defined in Section **5.3.3**) at each grid cell. The average number of hours per year in a compound event over the period 1979–2019 is displayed in **Figure 5.13a**. This value varies between 20 and 95 hours in the study area. **Figure 5.13a** highlights areas that are more likely to be affected by compound wind-rain clusters with hotspots in mountainous area (as for **Figure 5.12**). Nevertheless, the south-east coast of Great Britain is the primary hotspot for compound wind-rain clusters. The frequency of compound clusters gradually decreases eastward from Cornwall and Wales toward Anglia and East Midlands, showing a west-east decreasing gradient across all of Great Britain. A similar pattern has been found for extreme precipitation (Blenkinsop *et al.*, 2017) and compound flooding (Hendry *et al.*, 2019). The prevailing direction of cyclonic weather systems and orography partly explains this pattern for compound wind-rain clusters (Hulme and Barrow, 1997).

The dependence between extreme wind and extreme rainfall (w,r) can influence the estimation of the joint return period. The influence of the dependence between extreme wind and extreme rainfall cluster occurrence is quantified using the likelihood multiplication factor (LMF) (Zscheischler and Seneviratne 2017). The LMF is the ratio between the joint return period considering the two variables dependent (T_{dep}) and independent (T_{ind}) of each other (Manning *et al.*, 2019):

$$LMF = \frac{T_{ind}}{T_{dep}} \tag{5.3}$$

The likelihood multiplication factor (LMF) quantifies here the influence of the dependence between wind clusters and rain clusters on the estimation of the frequency of compound wind-rain clusters (**Figure 5.13a**). The LMF (**Figure 5.13b**) shows the strength of the dependence between wind and rain clusters. The LMF > 1.0 in all parts of the study area, suggesting that rain and wind clusters do not occur independently. The LMF is particularly high along the south coast of Great Britain, in the British Channel and North West France. While occurrences of compound wind-rain clusters exhibit an East–West pattern, the strength of the dependence between wind and rain hazard clusters has a South–North pattern.

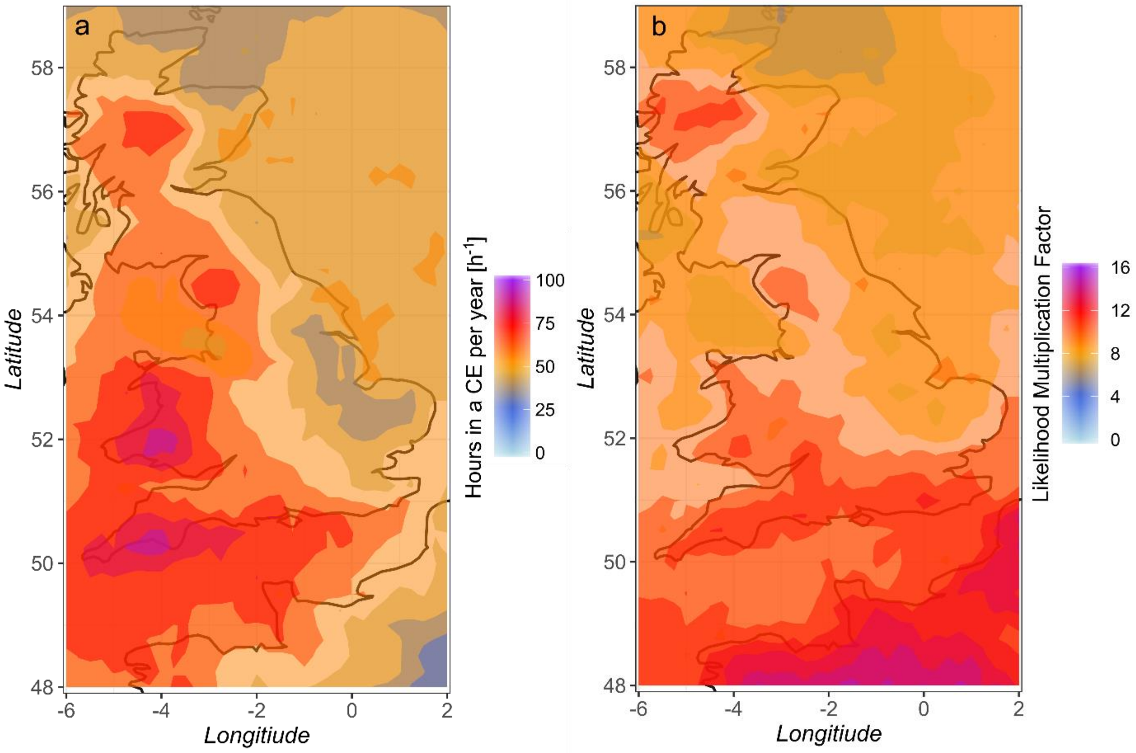

Figure 5.13: Hotspots for compound wind-rain clusters in Great Britain. Showing (a) the average number of hours in a compound hazards event in a year during the period 1979–2019 and (b) the likelihood multiplication factor (LMF) that quantifies the influence of the dependence between wind and rain event on the estimation of the probability of occurrence of compound hazards clusters. Data from ERA5 (Hersbach *et al.*, 2020).

The spatial features of compound wind-rain clusters have been identified in **Figure 5.12** and **Figure 5.13**. Spatial disparities in their frequency and in the dependence between wind and rain clusters have been highlighted. These features also vary in time and with seasons. To look at the seasonality of single (wind only, rain only) and compound hazard clusters, all hazard clusters have been taken into account and divided into three categories: wind, rain and compound. Wind clusters that are part of a compound cluster (*N*=2913) are removed from the category "wind", while rain clusters that are part of a compound cluster are removed from the category "rain" (*N*=3565). Monthly occurrences of these three categories of clusters are displayed in **Figure 5.14**.

While occurrences of wind and compound clusters are correlated, with a high season in extended winter (October to March) and a low season in the extended summer (April to September), rain clusters occurrence is following an opposite pattern with a high season in AMJJAS and a low season in ONDJFM. Around 82% of all recorded compound hazard clusters occur during the extended winter.

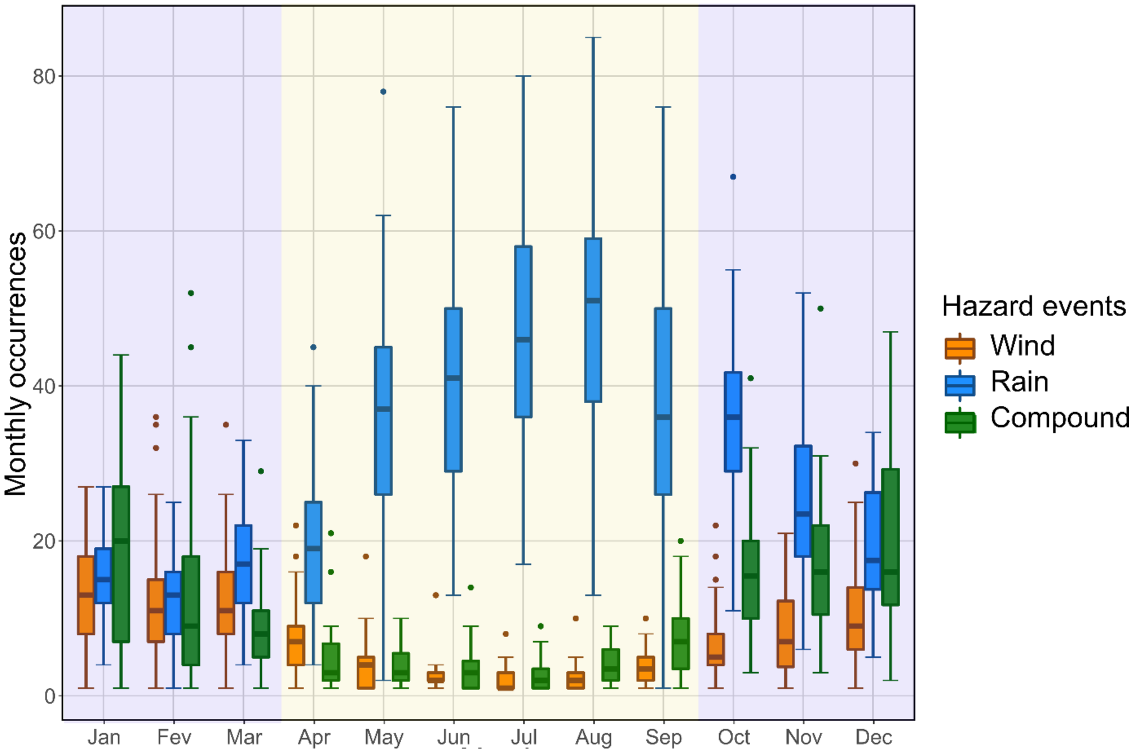

Figure 5.14: Boxplots of the monthly number of wind (dark orange), rain (blue), and compound (green) hazard clusters in Great Britain over the period 1979–2019. Background colours represent the two seasons. Data from ERA5 (Hersbach *et al.*, 2020).

Figure 5.15 provides a slightly different perspective on the seasonality of compound wind-rain clusters. It displays the proportion of compound wind-rain clusters among all clusters. This proportion shows a seasonal pattern similar to the one observed in **Figure 5.15**. This suggests that extreme rainfall and extreme wind clusters are more likely to co-occur during the extended winter. One possible explanation is that conditions leading to compound wind-rain clusters are occurring during the extended winter (Hillier *et al.*, 2020). This season coincides with the extratropical cyclones season in western Europe (Mailier *et al.*, 2006; Ulbrich *et al.*, 2009; Deroche *et al.*, 2014). Extra-tropical cyclone can bring several hazards, including strong wind, storm surge, heavy rainfall and high waves (**Chapter 3**). The influence of cyclonic weather systems coming from the Atlantic on compound wind-rain clusters was already suggested by **Figure 5.13a** and highlighted in previous research (Hawcroft *et al.*, 2012; Dowdy and Catto, 2017). However, this does not mean that every compound hazard event occurring during the extended winter is an extratropical cyclone but suggests that such weather systems are drivers of compound wind-rain events**.**

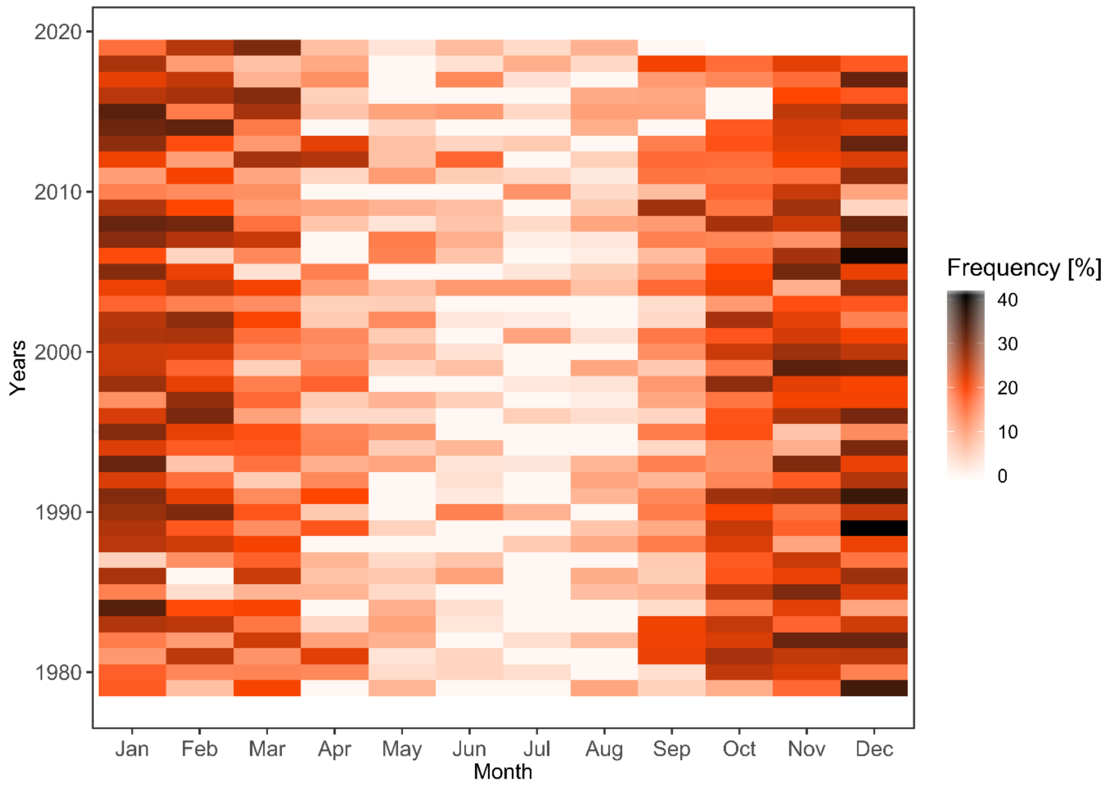

Figure 5.15: Monthly fraction of compound hazards clusters among the total number of clusters (wind+rain+compound) for 1979–2019 over the study area (Figure 5.2). Each tile represents a month-year, darker tiles meaning that the fraction of compound hazards clusters is greater.

Different spatial and temporal features of single and compound hazards clusters detected through the spatiotemporal clustering method presented in **Section 5.3** have been studied. The proportion of compound hazards clusters among rain and wind clusters shows regional disparities in Great Britain, with orography playing an important role. Western parts of Great Britain are more prone to experience compound wind-rain clusters, while the areas where the association between rain and wind event is the strongest are located on the South coast. Similarly to wind clusters, compound wind-rain clusters mainly occur during an extended winter season. The compound hazard high season coincides with the extratropical cyclone season, suggesting that the latter is a driver for compound wind-rain hazards in Great Britain. The subsample of clusters occurring in the extended summer season display a different pattern compared to the whole population of clusters (**Appendix H**), highlighting that compound wind-rain clusters have multiple drivers. The strength of association between wind clusters and rain clusters have been demonstrated in space and time; however, the intensities of the hazards also play a role when it comes to impact (Merz *et al.*, 2020). From the 4555 compound hazards that occurred 1979–2019, only a few led to considerable damages (e.g., Great Storm of 1987, Storm Desmond). The intensity of compound wind-rain clusters and their relationships with duration and spatial footprint are discussed in the next section.

5.5 Discussion

Assessing the characteristics of compound hazards events in space and time brings valuable insight into the nature of the relationship between the hazards involved in the event. It overcomes the main limitations of compound hazards studies which focus on interrelations at specific sites (Sadegh *et al.*, 2018). However, spatiotemporal analysis of compound hazards brings its own set of uncertainties and limitations. This section will discuss the following four main limitations arising from the presented study:

– parameters influencing the clustering procedure,
– the subjective definition of compound hazards events in space and time,
– uncertainties around the estimation of attributes and input data

Parameters influencing the clustering procedure. Three main parameters are influencing the clustering process and consequent results; their influence is discussed further and quantified in **Appendix G**.

(vii) The threshold (u) selected to sample extreme values. This study is based on the assumption that an extreme enough occurrence of an environmental variable can be used as a proxy for natural hazard identification. A threshold is then set to sample the extreme occurrence of environmental variables. Even if this threshold has been selected in light of previous works on wind and rain extremes (Ulbrich *et al.*, 2009; Martius *et al.*, 2016), its value remains subjective. A seasonal threshold could also have been used to detect more clusters during the extended summer. The value of the threshold directly influences the number of extreme clusters sampled and, therefore, on the selection of the other clustering parameters (**Appendix G**).

(viii) The ratio r of the spatiotemporal scaling parameters a and b. A three-dimensional Euclidean distance is used as a distance measure for the clustering procedure. The value of the distance between each extreme event is controlled by the importance given to spatial (longitude and latitude) and temporal (time) component in the input data. Here, each component was set to have the same importance in the distance computation, but more importance could be given to the time (or space) component depending on a prior assumption (Zscheischler *et al.*, 2013; Vogel *et al.*, 2020).

(ix) The density threshold μ. While the neighbouring parameter ε is set in a systematic manner (**Section 5.3.2**), its value depends on the density threshold, which gives the minimum number of detected values per cluster. The selection of μ is based on a prior assumption about the minimum size a compound hazard event can have in the study context.

The subjective definition of compound hazards events in space and time. **Section 5.3.3** presented four different possible definitions for a compound hazards event in time and space. It was chosen to define the duration as the aggregated duration of all hazard events; however, one could be more interested in extracting the simultaneous duration of both hazards.

Biases and uncertainties around the estimation of attributes. There are biases and uncertainties around the values of intensity attributes of the clusters. These biases are partly due to the nature of the data used in this study: climate reanalysis data (**Section 2**). Higher uncertainty arises from the estimation of rain accumulation as precipitation observations are not assimilated in ERA5 over the study area. For a better estimate of precipitation extremes, gridded observation-based data sets (e.g., E-OBS) are generally closer to observed daily precipitation extremes than reanalysis data sets (Hu and Franzke, 2020). Biases might also be more pronounced over mountainous areas for both wind and precipitation extremes (Skok *et al.*, 2016; Sharifi *et al.*, 2019; Zscheischler *et al.*, 2021) which are more exposed to compound wind and precipitation clusters (**Figure 5.13**). The size of the study area also leads to some events being detected only partially which could bias our estimates of size and duration of events.

5.6 Conclusion

This study aims to characterize more accurately the spatiotemporal aspects of the interrelationship between extreme rainfall and extreme wind events in Great Britain. By clustering extreme occurrences of maximum hourly wind gust and hourly precipitation from ERA5, 4555 compound wind-rain clusters over Great Britain were identified for 1979–2019. To assess the approach's ability to identify the occurrence of extreme events in time and space, a catalogue of 157 extreme precipitation and/or extreme wind events that occurred in Great Britain over the period 1979-2019 was created. The confrontation was done at a regional (11 NUTS1 regions) and daily scale. The average hit rate (the ratio between the number of identified events and the total number of events) over the whole area is 93.7%, meaning that our approach successfully identifies most extreme rainfall and wind events. According to our methodology, 53% of the hazard events among the 157 of the catalogue were compound events (wind-rain). Occurrences of wind and rain events are found to be dependent, with significant spatial and seasonal variabilities. The main hotspots for compound hazards clusters are the South coast of England and mountainous areas. A low (AMJJAS) and a high (ONDJFM) season were identified for compound hazard clusters and outline a link with extratropical cyclone season.

One important limitation of this approach is its reliance on the input data. To estimate with more accuracy intensity attributes (particularly for precipitation), one would require to use a statistical correction of the simulated precipitation (Widmann and Bretherton, 2000) or other gridded datasets based on observations (e.g., E-OBS). However, reanalysis data have potential to study compound hazard events on a global scale as they offer homogenised values for a significant number of variables. This approach can be transposed to the analysis of other compound events such as compound hot and dry events (Sutanto *et al.*, 2020), compound cold and snow events (Hillier *et al.*, 2020). The definition of compound hazard in time and space as proposed in this piece of work also stands for more than two hazards, allowing potential extension to more complex compound events (e.g., compound hot-dry event with extreme wind, extreme heat, drought and wildfires).

Nevertheless, many spatiotemporal aspects of compound hazards events have not been analysed in the present work. For example, the temporal sequencing of hazards within compound hazard events has not been explored. It has been shown that extratropical cyclones can occur in sequences (Mailier *et al.*, 2006). A way forward could be to use clusters created in this study to identify sequences of single and compound hazard events. To go further, the influence of climate change on the frequency, duration and magnitude of compound hazards could be assessed using climate projection

Chapter 6: Summary, conclusions and future research directions

6.1 Introduction

As introduced in **Chapter 1** and revisited throughout the thesis, hazard interrelations can play a decisive role in hazard probability, which is a component of risk. The interest around hazard interrelations has been growing over the past twenty years in different scientific disciplines (e.g., Kameshwar and Padgett, 2014; Xu *et al.*, 2014; Sadegh *et al.*, 2018) and industrial sectors (Matos *et al.*, 2015; Ciurean *et al.*, 2018; Narsis, 2020). Different intergovernmental organisations and frameworks have emphasised the need for multi-hazard approaches (UNDRR, IPCC). This work sits at the intersection between environmental sciences, engineering and disaster risk reduction.

However, adopting a multi-hazard approach implies rethinking several components of risk and hazards analysis. A quantitative multi-hazard approach requires developing new measures (e.g., multivariate return period) and modelling methods. It also opens new challenges linked to physical drivers leading to such events, interaction mechanisms, spatial dependencies, cascading effects. This doctoral research tackled some of these challenges. It aimed to develop a framework for a quantitative multi-hazard approach building on the latest developments in geomorphology, hydrology, climate science, engineering and statistics. In this final chapter, I consider the results and conclusions of **Chapters 2–5** in the context of the original research questions (**Section 6.2**) and discuss future research directions in the extension of this latter (**Section 6.3**). This chapter ends with concluding remarks (**Section 6.4**).

The rest of this **Section 6.1** provides an abbreviated summary of **Chapters 2** to **5**:

Chapter 2: This chapter develops a framework for quantifying natural hazard interrelations by reviewing current research available. Interrelations between 14 natural hazards are classified into 5 interrelation types. A total of 19 modelling methods to quantify natural hazard interrelationships were reviewed, providing a clear view of the state-of-the-art in hazard interrelation modelling. Modelling methods were clustered into three broad modelling approaches: stochastic, empirical, and mechanistic. The application of each modelling approach to different hazard interrelations was discussed with case study examples.

Chapter 3: This chapter builds on the findings of **Chapter 2** to assess the regional multi-hazard landscape of the European Atlantic Region. A set of 16 natural hazards (12 in common with Chapter 2) relevant to the European Atlantic Region (EAR) were selected. To narrow down the number of possible multi-hazard scenarios, physical processes (e.g., meteorological features) leading to hazard interrelations were identified to differentiate five groups of interrelated hazards named multi-hazard networks. The five multi-hazard networks (Ground movements, Convective storms, Extratropical cyclones, Compound dry hazards, Compound cold hazards) were discussed and illustrated with a catalogue of 50 events that occurred in the EAR, highlighting dominant hazard interrelations and cascades in Western Europe. The 34 freely available numerical datasets for hazard interrelation modelling of three types (in-situ observations, remote sensing and model output) were reviewed. The availability of the three types of data for the five interrelation networks was also assessed.

Chapter 4: This chapter focused on hazard interrelations modelling and aimed to evaluate the efficacy of six distinct bivariate extreme models through their fitting capabilities to 60 synthetic datasets. The systematic framework developed contrasts model strengths (model flexibility) and weaknesses (poorer fits to the data). The benefits of the systematic modelling framework developed have been highlighted in the context of the regional multi-hazard landscape of the EAR. Two pairs of hazards have been considered with the following environmental data: (i) daily precipitation and maximum wind gusts for 1971–2018 in London, UK; (ii) daily mean temperature and wildfire numbers for 1980–2005 in Porto district, Portugal.

Chapter 5: This chapter focused on increasing the understanding of spatial and temporal components of hazard interrelations in the context of the regional multi-hazard landscape of the EAR. The study analysed the spatiotemporal features of compound extreme wind and precipitation in Great Britain. Climate reanalysis data (ERA5) during the period 1979–2019 have been used. A clustering algorithm has been applied to create clusters of extreme precipitation and wind gust. Clusters of extreme precipitation and extreme wind gust were coupled to create 4555 compound hazard clusters. Spatial distribution of compound wind-rain events was assessed as well as their seasonality. Bivariate extreme modelling was used to quantify the interrelation between the two hazards and discuss the relationship between spatiotemporal overlap and the strength of the interrelation between hazards.

6.2 Relationship of the thesis to Original Research Objectives and Questions

In **Chapter 1**, I set out the aim of this thesis' research: "to develop a quantitative multi-hazard approach by (i) increase the understanding of hazard interrelations (ii) provide tools to quantify model natural hazard interrelations that can be useful for energy infrastructures". **Figure 6.1** synthesizes the main contributions of **Chapters 2 to 5** and their interconnections. These contributions correspond to each chapter's aims displayed in **Figure 1.5** and are linked by their colour to the five key aspects of the quantitative multi-hazard approach displayed in **Figure 1.4** in **Chapter 1**. **Figure 6.1** highlights each chapter's contributions to research objectives and the linkages between concepts, classifications and measures developed in each chapter. I will now synthesise the results and conclusions of **Chapters 2** to **5** to address the four objectives and 15 related research questions set to meet our research aims.

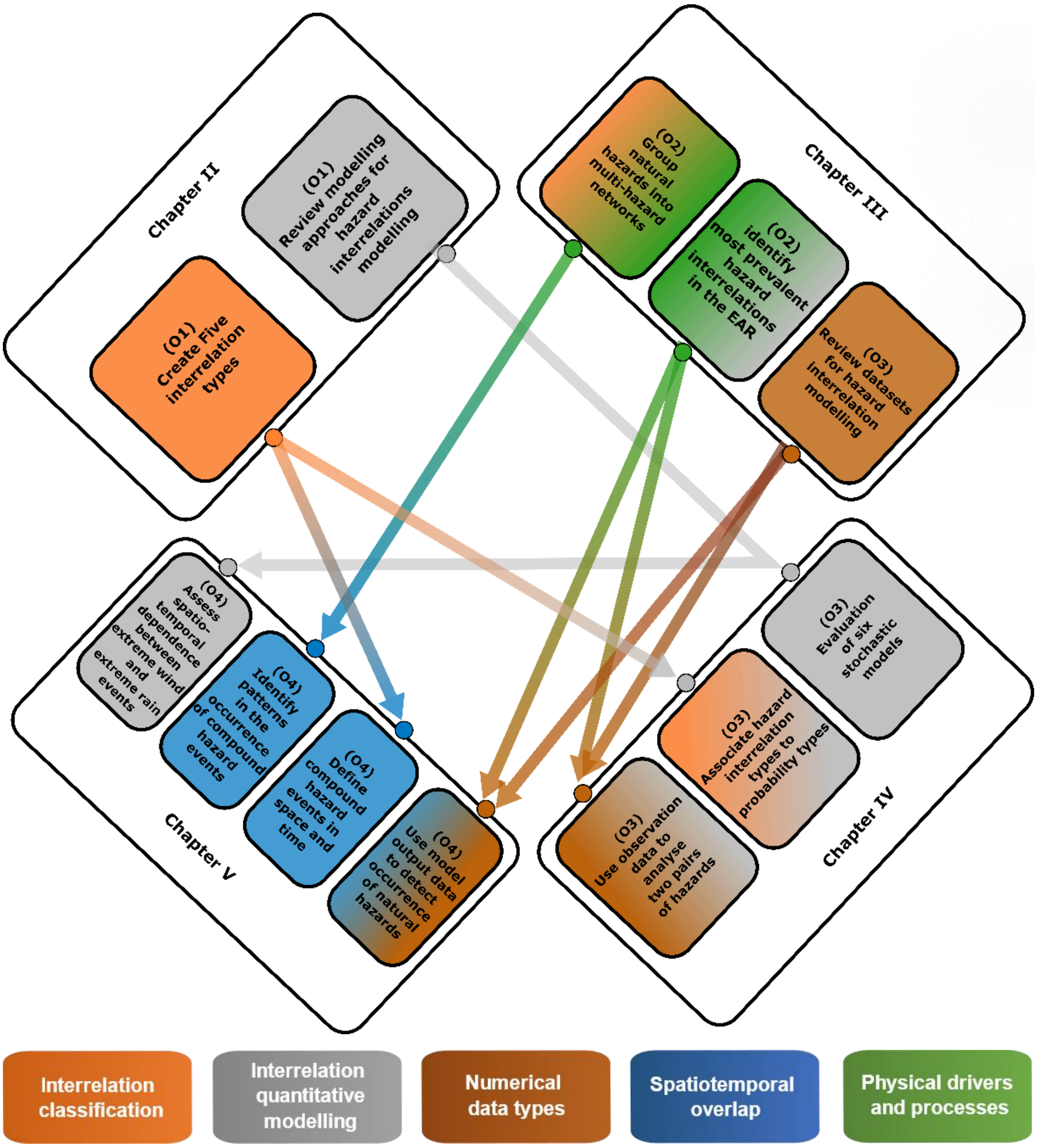

Figure 6.1: Main contributions of each of the four research chapters of the thesis and their associated objectives. Contributions are linked by their colour to the five key aspects of the quantitative multi-hazard approach displayed in Figure 1.4. Arrows highlight linkages between contributions from different chapters.

O1: Identify and classify approaches to quantify specific hazard interrelations (Ch. 2)

This first objective has mainly been addressed in **Chapter 2,** which is a critical literature review. The identification and classification of approaches to quantify hazard interrelations was the basis for the design of **Chapter 4**, which focuses on assessing the suitability of different models to different natural hazard interrelations. This objective has been broken down into four different research questions, which are now discussed.

Q1.1: What methods have been used in the literature for quantitative multi-hazard assessment?
One of the main challenges when adopting a multi-hazard approach is the diversity of natural hazards and processes leading to hazard interrelations. A total of 14 different natural hazards were considered in **Chapter 2** to review methods for quantitative multi-hazard assessments. These 14 natural hazards were divided into three categories that acknowledge their diversity. The extensive literature review performed in **Chapter 2** highlighted three different approaches (stochastic, empirical, mechanistic) to model interrelations between hazards.

Q1.2: How does one create a classification for natural hazard interrelation models?
To create a classification for natural hazards interrelations, a critical literature review was performed to understand and group the different terminologies gravitating around the concept of "multi-hazard" currently used in the literature. This allowed us to identify and relate different terms used to designate hazard interrelations in various scientific communities. The different terms reviewed often referred to as hazard interrelation mechanisms. Based on this terminology and previous research on multi-hazard (e.g., Gill and Malamud, 2014; Decker and Brinkman, 2015), a new classification of natural hazard interrelation types has been designed. To create a classification for natural hazard interrelation models, two databases have been created (**Appendicies A** and **B**) offering evidence for (i) hazard interrelation occurrence, (ii) hazard interrelation classification and (iii) use of models to quantify hazard interrelations.

Q1.3: How to model quantitively the relationship within different natural hazards pairs?
As discussed under Q1.1 above, approaches to model hazard interrelations have been reviewed in **Chapter 2**. Two hazard interrelation matrices were designed, one for cascading hazards and one for compound hazards. Interrelations between the 14 natural hazards considered in **Chapter 2** have been mapped on these two matrices along with relevant modelling approaches (when possible). A total of 19 modelling methods distributed into the three modelling approaches were reviewed, their popularity analysed, and examples provided. Using the Hazards Interrelations Database (**Appendix B**), the relevance of the three modelling approaches depending on the interrelation type (triggering, change condition, compound) were discussed. As a result, it was found that stochastic approaches have mostly been used to model compound interrelations,

mechanistic models are more popular to model triggering interrelations and empirical models were mainly used for triggering and compound interrelations.

Q1.4: What model is the most suitable for a given natural hazard interrelation?

Based on the finding of **Chapter 2**, **Chapter 4** focused on one modelling approach: stochastic models, as these models have the potential to produce robust extrapolation in the extreme domain. In this chapter, 60 different synthetic datasets were generated to assess the relevance of different stochastic models for various hazard pairs. The properties of the synthetic datasets (marginal distributions, tail dependence structure) were chosen to match bivariate time series of environmental variables. A methodological framework was produced to determine the most suitable model to quantify the interrelation of a given natural hazards pair. The methodology is based on the estimation of tail dependence measures and level curves which represents bivariate return periods (**Chapter 4**). From the results of this chapter, I recommended selecting a range of models rather than one, although non-parametric and semi-parametric models (conditional extremes and joint-tail KDE models) were identified as the most flexible (compared to parametric copulas).

O2: Design multi-hazard scenarios for Western Europe (Ch. 3)

This Objective 2 was the main driver for **Chapter 3,** which adapts some of the findings of **Chapter 2** for use in regional settings (European Atlantic Region). While **Chapter 2** focused on interrelations between two hazards, **Chapter 3** examines events including more than two interrelated hazards. This research objective was broken down into three research questions which are now discussed.

Q2.1: How to select relevant natural hazards and hazards interrelations for a given region?

In **Chapters 2** and **3**, relevant natural hazards for a given region were selected based on past disaster occurrences. The disaster database EM-DAT as well as publications and reports about single hazards in Europe were used to retrieve past occurrences of natural hazards and disasters. There are several criteria for a disaster to be included in the dataset, including ≥ 10 people who died or ≥100 people affected or declaration of a state of emergency or a call for international assistance (CRED, 2018). Depending on the region of interest (whole Europe in **Chapter 2** and western Europe in **Chapter 3**), natural hazards selected with this approach slightly differ. The methodology used in **Chapter 3** to identify relevant hazard interrelations is also based on previous occurrences of natural hazards. It provides tools for the industry to prioritize which hazard interrelations to analyse and can be adapted depending on the assets.

Q2.2: Which hazards are more likely to occur within the same multi-hazard event?

Chapter 2, similarly to previous reviews on multi-hazards (Gill and Malamud, 2014), mainly focused on interrelations between pairs of hazards. One limitation of such an approach is that multi-hazard often encompasses more than two hazards. For the set of 14 hazards considered in **Chapter 2**, there are 196 possible pairs of natural hazards, 2,744 triples of natural hazards, 38,416 quadruplets and so on. To reduce the complexity arising from the multiplication of potential interrelations, the 16 natural hazards considered in **Chapter 3** were assorted in five multi-hazard networks (ground movements, convective storms, extratropical cyclones, compound dry hazards and compound cold hazards). These networks were designed based on (i) interrelation matrices developed in **Chapter 2**; (ii) hydrometeorological drivers, (iii) geophysical drivers. The development of multi-hazard networks allows focusing on a restricted number of hazard interrelations.

Q2.3: Which natural hazards interrelations should be studied in priority?

This is a question that is frequently asked by engineers when discussing hazard interrelations, and a very complex one to answer. The answer also varies depending on the location and on the vulnerability of the concerned infrastructure, city or settlement. Nevertheless, the design of multi-hazard networks in **Chapter 3** already provides evidence to focus on a particular set of hazard interrelations. A multi-hazard events catalogue containing 10 major multi-hazard events per network was produced and is available in **Appendix C.** Besides offering empirical justifications to the concept of a multi-hazard network, the catalogue was used to assess the importance of natural hazard within the five multi-hazard events. Dominant natural hazard(s) and natural hazard interrelation(s) for each multi-hazard events were identified. This work provides indicators to prioritize the study of hazard interrelations. For example, the interrelation between extreme precipitation and extreme wind occurs in two networks (convective storm and extratropical cyclone) and is dominant within extratropical cyclones. It was therefore analysed in **Chapter 4** and **5**.

O3: Apply quantitative models to diverse hazard interrelations (Ch. 4)

After reviewing modelling methods to quantify hazard interrelations and analysing mechanisms behind these hazard interrelations, another main objective of this doctoral research was to apply some of the reviewed methods to different types of hazard interrelations. It was decided to focus on stochastic models and in particular bivariate extreme value models as there was a demand from engineers to develop a systematic methodology to use such models. **Chapter 4** addressed this objective by comparing six bivariate extreme models and applying these to two hazard interrelations. This research objective was broken up into three research questions which are now discussed.

Q3.1: How to systematically select the most suitable model for a given hazard interrelation?

In **Chapter 2**, 19 modelling methods and their previous applications to 24 hazard interrelations were reviewed. From the reviewed literature, stochastic models appear more suitable for compound interrelations, while mechanistic models have mostly been applied to triggering interrelations. A common practice to quantify hazard interrelations is to estimate the dependence between the two hazards. In that setting, natural hazards are usually represented by environmental variables. The use of dependence measures to quantify hazard interrelations is discussed in **Chapter 2** with an application example. As natural hazard are rare phenomena, tail dependence measures are used in **Chapter 4** to assess the strength of dependence between two natural hazards. Assessing the tail dependence of hazards is a crucial step toward using models to extrapolate beyond observed data and therefore estimate attributes of an extreme multi-hazard event. Using a model that does not represent the dependence structure of the data can result in over (under) estimating the risk associated with hazard interrelations. In **Chapter 4**, 60 bivariate synthetic datasets with properties matching bivariate time series of environmental variables were generated. Comparing models on synthetic data enabled the development of a systematic framework to choose the most appropriate model for a given hazard interrelation depending on the estimation of the tail dependence of the two variables representing the hazards.

Q3.2: How to translate hazard interrelation types into probability types?

One challenge around using statistical modelling and bivariate extreme models to quantify hazard interrelation is to associate different interrelation types to probability types and therefore estimate the return level of a combination of hazards. In **Chapter 4**, different probability types used in the literature to estimate the bivariate return period have been reviewed. Two probability types among the most popular were selected: (i) the joint exceedance probability which is the probability of the two variables being extreme (above a threshold) simultaneously; (ii) the conditional probability which is the probability of one variable being extreme knowing the other variable is extreme. These two probability types correspond to two interrelation mechanism (compound and cascading) associated with the two interrelation matrices presented in **Chapter 2**. Bivariate probability of exceedance are curves, and the shape of these curves drastically changes depending on the type of probability selected. It is therefore important to be consistent when associating hazard interrelation types with probability types. In **Chapter 5**, the bivariate return period of compound wind-rain events in Great Britain was estimated with a joint exceedance probability type, providing a single value to estimate the intensity of a bivariate event. It is also possible to extend this approach to other hazard interrelations and interrelations networks using the concepts of dominant hazards and dominant hazard interrelations introduced in **Chapter 3**.

***Q3.3**: What are the different types of numerical data available to study hazard interrelations in the EAR?*

In **Chapter 3**, freely available datasets to quantitatively study the five multi-hazard event groups have been reviewed. The 35 datasets reviewed were classified into three main types: (i) in-situ observations; (ii) remote sensing; (iii) model outputs. Each type of data presented in **Chapter 3** has its strength and weaknesses. The choice of a dataset is ultimately driven by the availability and compatibility of different data types for hazards within a multi-hazard network. Indeed, one of the main challenges in multi-hazard studies is to identify data with compatible spatial and temporal coverage for different natural hazards. In **Chapter 4**, the interrelation between extreme precipitation and extreme wind gust at Heathrow Airport (UK) was studied. Data for both natural hazards were daily in-situ observations, with precipitation data gridded based on in-situ observations. The second example assessed the interrelation between extreme air temperature and wildfire activity. While both datasets were also in-situ observations, the spatial scale of the two datasets was different. The temperature was therefore average over the Porto district, potentially leading to biases in the results. In **Chapter 5**, the interrelation between extreme precipitation and extreme wind gust was also studied with gridded model output data, which offered less accuracy in term of the local intensity of the hazards but offered the opportunity to analyze the spatiotemporal features of the hazard interrelation.

O4: Analyse spatiotemporal features of hazard interrelations with gridded data (Ch. 5)

When defining hazard interrelations, the idea of two (or more) hazards occurring at the same time and place is broadly accepted (IPCC, UNDRR). However, the notions of the same time and place are often unclear. This last objective investigates the spatial and temporal aspects of hazards interrelation, starting from identifying single hazard events to the definition of hazard interrelations in space and time. Spatiotemporal features are key aspects of hazards interrelations. This research objective has been divided into four research questions.

***Q4.1:** How to identify occurrences of natural hazards with climate reanalysis data?*

The spatiotemporal features of the interrelation between extreme precipitation and extreme wind gust in Great Britain were analysed in **Chapter 5**. Based on the review of freely available numerical data conducted in **Chapter 3**, model output data (ERA5) was selected as it provides data for both hazards at an hourly timestep with global coverage. A percentile-based approach was chosen to identify occurrences of extreme precipitation and extreme wind gust. This approach is characterized by an extreme threshold above which precipitation and wind gust are considered extreme enough to be hazards. The selected percentile of precipitation and wind gust over the period 1979–2019 was computed for each grid cell. By producing a threshold on each grid cell, regional and local variations were taken into account in the hazard detection. Nevertheless, extreme occurrences of wind and precipitation often occur in areas larger than the size of a grid cell (here 0.25° × 0.25°) and can last more than one hour. Extreme occurrences of each variable (above the extreme threshold) were then clustered in space and time to identify hazard footprints. Extreme occurrences of wind and rainfall were clustered separately. As a result of the clustering procedure, hazard events with variable intensity, duration (from 1 hour to four days), and spatial footprint (from thousand to hundreds of thousand square kilometres).

Q4.2: How to define hazard interrelations in space and time?

As discussed in **Chapter 5**, there is no unified definition of temporal and spatial components of hazard interrelations, and this latter mostly depends on the needs behind the studies. In **Chapter 5**, four different spatiotemporal scales of hazard interrelations were proposed based on spatial and temporal overlap (**Figure 5.9**). One of these four definitions was retained to define compound hazard events in space and time in **Chapter 5**. Therefore, a compound hazard event was defined as the area where two (or more) hazard occur during the aggregated duration of an event. A compound hazard event in space and time is consequently the occurrence of two hazards (in **Ch. 5** extreme precipitation and extreme wind) at the same location(s) (e.g., a set of grid cells) during a period lasting between the beginning of the first hazard event and the end of the second hazard event.

Q4.3: What is the influence of the intensity of natural hazards on the spatiotemporal features of compound hazards?

An essential feature of natural hazards and extremes is the relationship between duration, spatial extent and intensity (Lavell *et al.*, 2012). The influence of the joint intensity of natural hazards on the spatiotemporal features of hazard interrelation is therefore also important to assess. In **Chapter 5**, the joint return period of the identified compound hazard events was computed using the joint tail KDE model assessed in **Chapter 4**. Maximum precipitation and wind gust were used in **Chapter 5** as intensity attributes for each compound hazard event. The joint return periods was used as a proxy for the intensity of the compound hazard events. **Chapter 5** discussed the relationship between the joint return period, finding that most extreme compound hazard events (with a return period above 1 year) are on average larger and last longer than less intense compound wind-rain events. This suggests that the most intense compound wind and precipitation events in Great Britain are large scale events that can occur over whole regions. However, spatial and temporal resolutions of the data used (ERA5) are not able to be analysed for very localized and short-duration events. Spatial footprint and duration of major compound hazard events studied in **Chapter 5** also correspond to the footprint and duration of extratropical cyclones discussed in **Chapter 3**.

6.3 Contribution to a quantitative multi-hazard framework: characterisation and modelling of a hazard interrelation

As discussed in **Section 6.1** and **6.2**, this thesis addresses different aspects that the author believes essential to move toward a quantitative multi-hazard framework. In this section, the contribution to a quantitative multi-hazard framework is highlighted, with a practical guide provided on how to use the findings, tools and supplementary materials of the thesis. The contributions of each chapter are highlighted in the context of one examples which addresses the assessment and quantification of one particular hazard interrelation using tools and recommendations developed through the thesis.

This section answers a simple question related to hazard interrelations: What are the interrelationships between "*hazard A*" and "*hazard B*"? As this thesis has extensively analyzed the interrelation between *extreme wind* and *extreme precipitation*, these two hazards will be used in this example. The characterization of the interrelation between extreme precipitation and extreme wind is done using tools, recommendations and resources from this thesis and divided into 5 steps:

- **Step 1:Are two hazards interrelated and how are they interrelated?**
- **Step 2:What are the possible drivers of interrelation(s) identified?**
- **Step 3: What datasets are available for this hazard pair?**
- **Step 4: How can one model the interrelation(s) between the two hazards?**
- **Step 5:What is the scale of the interrelation(s)?**

Step 1:Are two hazards interrelated and how are they interrelated?

After reading this thesis, the reader might already have some clues to this question "are the two hazards interrelated and how are they interrelated?". To know if two hazards are interrelated, the first step would be to determine if these two hazards are part of the hazard interrelation matrices developed in **Chapter 2** (**Table 2.3**). If the hazards of interest are in **Table 2.3**, one can then identify whether the two hazards are interrelated (**Figure 2.5**, **Figure 2.6**), with which mechanism (compound vs cascade) and with which interrelation types (**Figure 2.5**, **Figure 2.6**). In the case of one or both hazards not being part of **Table 2.3**, the reader can refer to other studies mentioned in **Chapter 2** (e.g., Gill and Malamud, 2014).

Step 2:What are the possible drivers of interrelation(s) identified?

In **Chapter 3**, 16 natural hazards are grouped into five multi-hazard networks. These multi-hazard networks are based on geophysical drivers. If the two hazards of interest are part of a multi-hazard network, it means that their hazard interrelation could be associated with other natural hazards of the network. Multi-hazard networks and their associated hazards are presented in **Figure 3.5,** while each network is displayed and discussed in **Section 3.3**. The interrelations between extreme precipitation and extreme wind is part of two multi-hazard networks and is the dominant interrelation for extratropical cyclone (meaning it is the most likely interrelation).

Step 3: What datasets are available for this hazard pair?

Chapter 3 presents three main types of environmental data (in-situ observations, model outputs and remote sensing datasets) and comes with a database of free numerical data for quantitative multi-hazard approach (**Appendix D**). This database is composed of 34 freely available datasets to study and model the five multi-hazard networks presented in **Section 3.3**. According to this database, the interrelation between extreme precipitation and extreme wind can be modelled with in-situ observations (e.g., Hadley Centre observations datasets) or model output (e.g., ERA5) datasets. Depending on the requirements of the analysis (local vs. global), the user can favor one type of data over others and mix different types of data (e.g., remote sensing for precipitation and reanalysis for wind gust). **Chapters 4** and **5** offer some insights on problems around data when analyzing hazard interrelations. Nonetheless, this thesis does not pretend to fully answer this question, but rather highlights the main strength and weaknesses of different types of environmental data.

Step 4: How can one model the interrelation(s) between the two hazards?

This question is central to this thesis and is particularly addressed in **Chapters 2** and **4.** The classification displayed in **Figure 2.7** provides an overview of possible modelling approaches available to model hazard interrelations. If the two hazards of interest are part of **Table 2.3**, one can refer to **Figures 2.5** and **2.6** to know which modelling approach has been used and which interrelation mechanism (compound, cascade) correspond to the interrelation of interest. More insights on which model to use are available in **Appendix B**. **Chapter 4** focuses on stochastic models suitable for bivariate extreme value analysis. It also presents two types of probabilities corresponding to two interrelation mechanisms. **Figure 4.8** is a heatmap of model abilities for different scenarios (bivariate datasets). **Section 4.4** develops a tutorial on using the results of **Chapter 4** with two applications to natural hazards. From **Figure 2.6**, the interrelations between extreme precipitation and extreme wind have been modelled with stochastic and empirical models. Three studies in **Appendix B** analyze this interrelation with a regression, a multivariate model and a copula. **Chapter 4** and **Figure 4.8** allow one to select the most appropriate bivariate model to estimate the extremal dependence structure and model extreme bivariate return periods of joint wind and precipitation extremes.

Step 5:What is the scale of the interrelation(s)?

This question is addressed with different approaches in **Chapters 3** and **5**. In **Chapter 3**, the spatial and temporal scales of 50 historic multi-hazard events are recorded. The catalogue is available in **Appendix C**. Spatial and temporal scales of each event are displayed in **Figure 3.12** and grouped by network, allowing one to visualize the range of spatial and temporal scale of each of the five multi-hazard networks presented in **Section 3.3**. In **Chapter 5**, compound wind and precipitation extremes are identified by clustering extreme values of wind and precipitation over Great Britain using climate reanalysis data. **Chapter 5** provides a robust definition of compound hazard in space and time. The method developed in **Chapter 5** estimates the spatial footprint and duration of compound wind and precipitation events and offers a tool to analyze the attributes of compound hazard events (**Section 5.4.2**, **Appendix H**). The method used in **Chapter 5** can be applied to other hazard interrelations and other gridded datasets. It can also be extended to more than two hazards.

A summary of **Steps 1 to 5** given above, their interrelation characteristics, and where in this thesis these approaches are described can be found in **Table 6.1**. The characteristics of the interrelation between extreme precipitation and extreme wind are highlighted in **blue**.

Table 6.1: Summary of the contribution to a quantitative multi-hazard network. Characteristics of the interrelation between extreme wind and extreme precipitation are displayed in blue to illustrate the approach.

Steps		Interrelation characteristics	Resources
Step 1	Interrelation	**Yes**/No	**Table 2.3; Figures 2.5 and 2.6**
	Interrelation mechanism	**Compound**/Cascade	**Section 2.3; Figures 2.5 and 2.6**
	Interrelation type	**Compound**/Triggering/Change condition	**Section 2.2; Table 2.1**
	Additional information available	**Yes**/No	**Appendix A**
Step 2	Part of the same MH network	**Yes**/No	**Table 3.1; Figure 3.4**
	MH networks	GM/**CS**/**ETC**/CD/CC	**Section 3.3; Table 3.2**
	Dominant interrelation	**Yes**/No (**ETC**)	**Figure 3.11; Table 3.3**
	Examples of past multi-hazard events	**Yes**/No	**Appendix C**
Step 3	Type of environmental data available	**In-situ observation**/Remote sensing/ **Model output**	**Figure 3.13; Appendix D**
Step 4	Suitable models	**Stochastic/Empirical**/Mechanistic	**Figures 2.5, 2.6, 2. 7**
	Previous studies of this interrelation	**Yes**/No; 3	**Appendix B**
	Probability type for modelling	**P_{AND}**/P_{COND}	**Figure 4.4, Table 4.1**

Steps		Interrelation characteristics	Resources
	Most appropriate model for bivariate extreme modelling	Depends on the scatterplot	**Figures 4.5 and 4.8**
Step 5	Qualitative estimate of the spatial and temporal scales	**Yes**/No	**Figure 3.12; Appendix C**
	Spatiotemporal clustering applicable	Requires geospatial data	**Section 5.3; Appendix D**
	Quantitative estimate of the spatial and temporal scales	**Yes**/No	**Section 5.4.2; Appendix H**

6.4 Future research directions

In **Chapters 3**, **4** and **5** new gaps and ways of going further in the understanding and quantification of hazard interrelations were identified. Three future research areas are discussed and illustrated in detail here:

- Expand methodologies developed in Chapters 4 and 5 to interrelations between more than two hazards
- Systematically attribute occurrences of specific natural hazards to a multi-hazard network
- Adopt event-based storyline approaches

6.4.1 Expand methodologies developed in Chapters 4 and 5 to interrelations between more than two hazards

In this thesis, methods to quantify hazard interrelations were reviewed in **Chapter 2**. This review was mainly done in the context of interrelations between two hazards. In **Chapter 4**, the abilities of six bivariate extreme models to model different hazard interrelations were assessed. Bivariate models can only model interrelations between two natural hazards. Case studies for two pairs of natural hazards were conducted in **Chapter 4**. The first one was the compound interrelation between extreme wind and extreme precipitation in Heathrow Airport (UK) and the second one was the change condition interrelation between extreme hot temperature and wildfire activity in Porto district (Portugal). In **Chapter 5**, the spatiotemporal footprint of compound extreme wind and precipitation events over Great Britain were analysed. The study area selected was South-East England. Research directions for the future could be to include other natural hazards in the analysis of interrelations.

In **Chapter 3**, networks were used to visualize the multiple hazard interrelations within multi-hazard events. The use of such a network is a promising direction to go from hazard pairs to multiple hazards. To use multi-hazard networks as a basis for hazard interrelation modelling, methods that can handle multiple interdependencies between variables are required. Copulas presented in **Chapter 4** suffer from a lack of flexibility in higher dimensions as these require all pairs of variables to have the same type of dependence (Brechmann and Schepsmeier, 2013). Two methods with the ability to overcome this limitation have increasingly been used in previous years to model networks of interrelated hazards or drivers (Weber *et al.*, 2012; Bauer, 2013; Liu *et al.*, 2015; Bevacqua *et al.*, 2017; Liu *et al.*, 2017): Bayesian network and pair-copula constructions These two methods are also topical in current conferences and workshops. Both are now presented and discussed.

6.4.1.1 Multivariate modelling method: Bayesian network

When dealing with networks of dependence and risk analysis, over the last decade Bayesian networks (BNs) have appeared more frequently in the literature, and there is an increasing trend towards the use of this type of method (Gutierrez *et al.*, 2011; Duval *et al.*, 2012; Nadim *et al.*, 2013; Wang *et al.*, 2013; Poelhekke *et al.*, 2016; Sperotto *et al.*, 2017; Tierz *et al.*, 2017). This trend is due to the benefits offered by BNs in contrast with other methods of dependability analysis (Weber *et al.*, 2012). Recent multi-hazard risk analysis studies focused on BNs (Nadim *et al.*, 2013b; Liu *et al.*, 2015; van Verseveld *et al.*, 2015; Hashemi *et al.*, 2016; Kwag and Gupta, 2017) to model interactions and dependence between natural hazards and their potential impacts.

The concept of a BN was developed to manage various statistical dependencies directly. Bayesian networks are probabilistic networks that rely on Bayes Theorem to draw an inference based on prior evidence. A BN is a *Direct Acyclic Graph* which is composed of nodes and arcs, which can either represent dependencies or cause-effect relationships between variables **(Figure 6.2)**. Each node defines either a discrete or continuous random variable, even if there are still substantial limitations when dealing with continuous variables. Each node of a BN has a parent and a child node (if not, it is a root node). Each node has a conditional probability table that describes the quantitative relationship with its connected nodes.

To overcome the limitations when dealing with continuous variables, there are several options including: Gaussian Bayesian networks (Scutari, 2009), hybrid Bayesian networks than can associate discrete and continuous variables (Langseth *et al.*, 2009), and non-parametric Bayesian networks (NPBN) which associates the structure of Bayesian network and copulas (Hanea, 2009; Hanea *et al.*, 2010, 2015). This last method has been used to study multiple dependence between river discharge and storm surge in the USA during a hurricane (Couasnon *et al.*, 2018). The association of copulas and BN is a dynamic area of study, and different approaches have already been developed with very few applications to natural hazards (Hanea, 2009; Elidan, 2010; Bauer and Czado, 2016; Pircalabelu *et al.*, 2017). However, one current limitation of NPBN is that they have been developed with the normal copula (Couasnon *et al.*, 2018; Paprotny *et al.*, 2020), which is asymptotically independent (See **Chapter 4).**

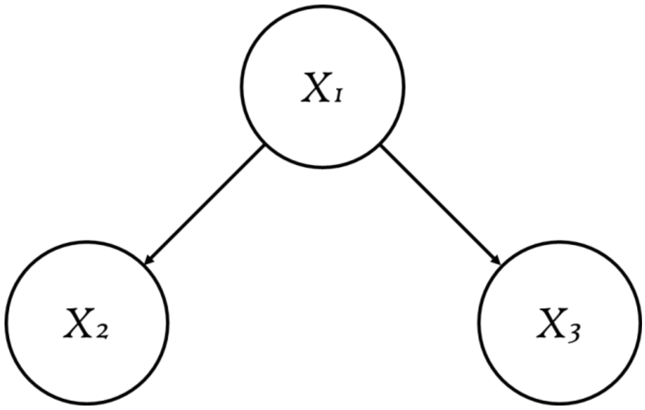

Figure 6.2: Graphical representation of a simple Bayesian Network with three nodes (X_1, X_2, X_3) and two arcs (X_1 to X_2 and X_1 to X_3).

6.4.1.2 Multivariate modelling method: Pair copula constructions

Copulas have already been extensively discussed in **Chapter 2** and **Chapter 4**. Copulas' main limitations arise when increasing the number of variables to be studied. Multivariate parametric copulas lack flexibility when modelling systems with high dimensionality and heterogeneous dependencies among the different pairs (Bevacqua *et al.*, 2017). A way to overcome limitations of copulae is the pair-copula construction (PCC) also called vine copula (Bedford and Cooke, 2002; Aas *et al.*, 2009; Vaz de Melo Mendes *et al.*, 2010; Hashemi *et al.*, 2016; Bevacqua *et al.*, 2017a). PCCs decomposes a *n*-dimension copula into the product of $n(n–1)/2$ bivariate copulas, providing higher flexibility. Different types of structures exist for vines, such as the C-vine and D-vine. The decomposition which is operated in vine copulas allows selecting different bivariate copulas for each pair of variables, providing enormous flexibility in dependence modelling (Brechmann and Schepsmeier, 2013; Hao and Singh, 2016).

Bevacqua *et al.* (2017) used vine copulas to model compound flooding in Italy. In this study, two rivers are included. Two other variables called predictors are also added to the model. These predictors are based on other environmental variables such as rainfall, sea level pressure, and wind speed. Predictors allow an insight into physical processes. Five dependent variables are part of this model, and pair copula construction avoids the necessity of homogeneity of the pair-dependencies. Finally, there are many assumptions made with these methods (e.g. threshold choice, copula selection) which can lead to additional uncertainty.

NPBN and PCC are both able to model complex dependency patterns between numerous continuous variables. These methods have already been applied to model compound flooding

(Bevacqua *et al.*, 2017; Couasnon *et al.*, 2018) and compound dry hazards (Manning *et al.*, 2018). Strengths and weaknesses of these two methods for applications to hazard interrelations are summarized in **Table 6.2.**

Table 6.2: Strengths and weaknesses of pair copula constructions (PCC) and non-parametric Bayesian network (NPBN) for hazard interrelations modelling.

Modelling methods	Strengths	Weaknesses	Applications to multi-hazard
Non-parametric Bayesian Network	Low computational requirements, flexibility of the Normal copula, intuitive graphical representations	Currently only implemented with the Normal copula, no package in R	Couasnon *et al.*, 2018
Pair copula constructions	Flexibility due to a large number of possible copulas to be implemented, packages available in R (e.g., CDVine)	A lot of possible constructions and decompositions, important computational requirements, graphical representation less intuitive	Bevacqua *et al.* (2017), Manning *et al.* (2018)

6.4.1.3 Metrics and measures for multiple hazard interrelations

The return period concept was initially defined in a univariate framework and extended into the multivariate framework (Singh *et al.*, 2007). Defining a return period for a combination of two hazards requires carefully selecting the type of probability to be computed as discussed in **Chapter 4**. Moreover, while a return period is represented by a single value in a univariate context, it is represented by a curve containing an infinite amount of couples of values in a bivariate context. With three variables, the return period becomes a surface, and it becomes hard to visually represent with more than three variable and ultimately loses its sense in a multivariate framework (Serinaldi, 2015). Other metrics and ways to estimate extreme multivariate events are necessary to expand the framework developed in this thesis beyond hazard pairs modelling. The concepts of dominant hazards and dominant hazard interrelations introduced in **Chapter 3** could help to simplify the concept of return period in a multivariate context. Multi-hazard Networks and dominant hazards also offer opportunities to analyse multi-hazard events from multiple perspectives.

6.4.2 Systematically attribute occurrences of specific natural hazards to a multi-hazard events

There is one well-known limitation to the application of extreme value statistic to natural hazards. The observations (or data) studied needs to be a sequence of independent and identically distributed (i.i.d) random variables. However, for many types of data, this assumption is not realistic. For example, if extreme precipitation has occurred at a given hour, the conditions on the following hour will likely be closely related to the conditions on the current hour. To address this issue, two main modelling approaches have been developed in a univariate context (i) the block maxima approach and (ii) the peak over threshold approach (Coles, 2001; Davison and Huser, 2015). In recent years the peaks over threshold approach has become increasingly popular as it allows to incorporate more data into the statistical model than a block maxima approach (Dutfoy *et al.*, 2014). For the peaks over threshold approach, methods to optimize the threshold selection and to decluster extreme observation have been developed since the mid-1990s (Bernardara *et al.*, 2014). Declustering ensures that observations used as input for a statistical model are independent, but not that they belong to the same underlying distribution. For example, two observations of extreme precipitation at a given location can belong to two different underlying distributions. The assumption here is that observation natural hazards can be split into more homogeneous sub-samples in term of physical processes and genesis.

Natural hazard observations have been attributed to atmospheric conditions or weather pattern to create meaningful sub-samples. Such an approach has been performed for extreme precipitation (Hand *et al.*, 2004; Garavaglia *et al.*, 2010), wildfire (Amraoui *et al.*, 2015), rainfall-triggered landslides (Wood *et al.*, 2016), extreme waves and storm surge (Rueda *et al.*, 2016) and compound flooding (Hendry *et al.*, 2019). Weather patterns or weather types are atmospheric circulation types over a defined region (Neal *et al.*, 2016). One well-known classification for British weather in the Lamb weather type (LWT) classification (Hulme and Barrow, 1997). This classification is based on daily sea-level pressure and has been performed on different periods and with different input data (Jones *et al.*, 2013). In this classification, seven main weather types are recognised: the anticyclonic (A), easterly (E), southerly (S), westerly (W), northwesterly (NW), northerly (N) and cyclonic (C) types. The remaining days are classified into 19 hybrid combinations of the main types (Wilby and Quinn, 2013). Other classifications have been developed for Great Britain (Neal *et al.*, 2016) or Europe (Philipp *et al.*, 2010).

In **Figure 6.3** are displayed the LWT that are the most frequently associated with compound wind and precipitation events as defined in **Chapter 5.** Four LWT are represented: the cyclonic (C), which encompasses the vast majority of the area, the southwesterly (SW) on North East England and most of Scotland, the westerly (W) on north Scotland and the southerly (S) weather type of the eastern edge of the study area. **Figure 6.3** provides a supplementary layer of information about compound rain and wind events in Great Britain. However, weather classifications have limitations and cannot be the unique tool to attribute the occurrence of a hazard to a multi-hazard network. For example, the Lamb classification represents the circulation over a very wide area, and this means that it can be challenging to relate the information in the catalogue to local conditions (Hulme and Barrow, 1997). Such classifications are in general most relevant for use in forecasting and to examine broad characteristics of the climate of a region.

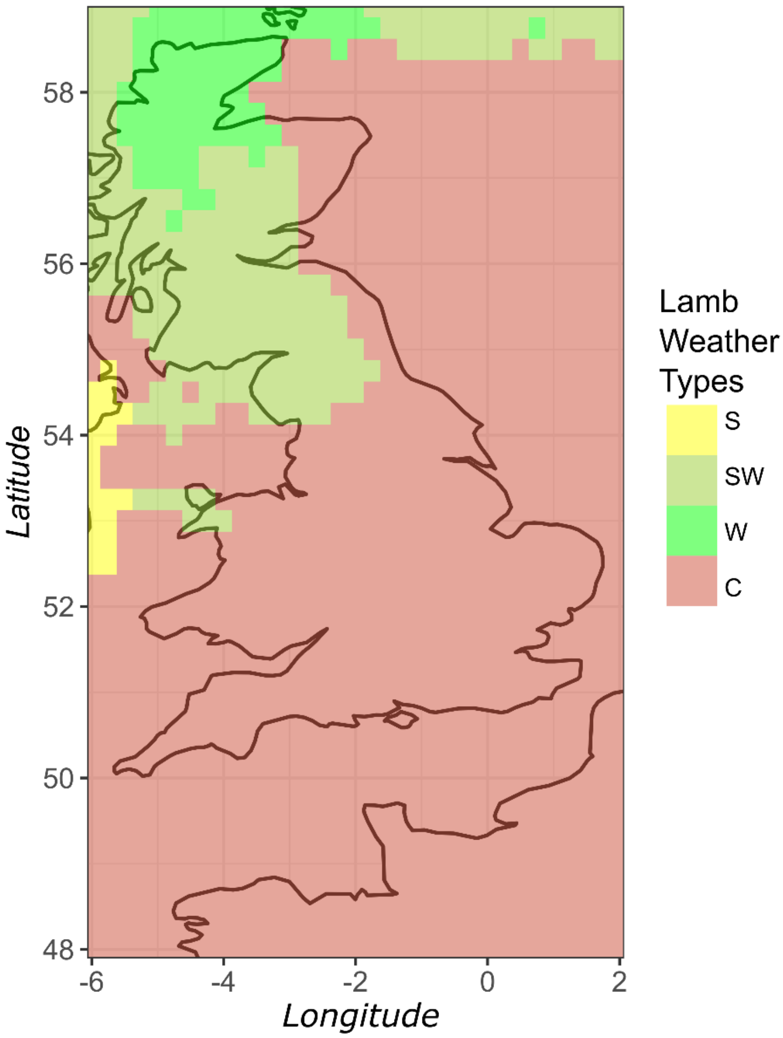

Figure 6.3: Lamb Weather Types associated with compound wind and precipitation extremes during the period 1979–2019. The map shows the Lamb Weather Type that is most frequently associated with compound extreme precipitation and wind event in each grid cell.

Classifying natural hazards according to atmospheric circulation patterns, seasonality or other potential drivers aims to create more homogenous data samples and facilitate the application of extreme value statistics. In **Chapter 3** natural hazards are grouped, and hazard interrelations are contextualized into multi-hazard networks (e.g., extratropical cyclones, convective storms). Seasonal patterns in the occurrence of compound wind and precipitation events over Great Britain are highlighted in **Appendix H**. However, further research is needed to refine the link between seasonality, atmospheric conditions and multi-hazard networks defined in **Chapter 3**. Dowdy and Catto (2017) analysed extreme weather caused by front, cyclone and thunderstorm occurrence at a global level. They identified types of storm combinations that are most frequently associated with extreme precipitation and extreme wind events. The identification of "storm types" associated with natural hazards has already been performed in hydrology (Hand *et al.*, 2004) to categorize extreme precipitation events. This approach is particularly valuable when some natural hazards can be part of several multi-hazard networks. This is the case for extreme rainfall (extratropical cyclone, convective storm), extreme wind (extratropical cyclone, convective storm, compound dry, compound cold) or landslides (extratropical cyclone, convective storm, ground movements).

6.4.3 **Adopt event-based storyline approaches**

Another challenge associated with multi-hazard and extreme events, in general, is the lack of observations. Indeed, extreme events are by nature rare and multiple or compound extremes tend to be even rarer. Here is sketched an event-based stroyline approach, which should be seen as complementary to the two other research directions described in **Sections 6.4.1** and **6.4.2**. Adopting event-based storyline approaches is particularly relevant to analyze extreme low probability-high impact events, the so-called "black swan" or "perfect storm" (Paté-Cornell, 2012).

Event-based storylines emphasize the plausibility of events rather than their probability (Sillmann *et al.*, 2021). They acknowledge the complexity of the interrelations between natural hazards, their drivers and the difficulty to analyze multi-hazard events in a probabilistic manner. Schauwecker *et al.* (2019) analyzed cascading effects leading to three multi-hazard events. They show that an event-based pathway scheme allows visualizing complex effects within a multi-hazard event. Understanding drivers and attributes of a multi-hazard event also allows estimating attributes of unseen events by tweaking some characteristics of the event or its drivers. Thompson *et al.* (2017) used a large ensemble of climate simulations to assess the chances of unprecedented extreme precipitation events in the current climate. This study was the base for an event-based storyline approach where a counterfactual "black swan" version of Storm Desmond (**Appendix C**) was created by artificially increasing its precipitation (HM Government, 2016; Sillmann *et al.*, 2021). Such an approach could also be taken in a multi-hazard context by building on multi-hazard networks designed in **Chapter 3**.

Besides offering tools to visualize and understand interrelations between hazards and drivers within a multi-hazard event, detailed analysis of major multi-hazard events could be used (i) to anticipate plausible unseen multi-hazard events and (ii) as training tools for complex multi-hazard models discussed in **Section 6.4.1**.

6.5 Concluding remarks

This thesis focused on the concept of multi-hazard and the quantification of hazard interrelations. The need for a framework that includes multiple hazards and possible interrelations at a given location has been advocated for almost 50 years (Hewitt and Burton, 1971). As discussed in

Chapter 2, significant progress has been achieved in the past 20 years at different levels (research, industry, policy) to identify, classify and assess hazard interrelations (Kappes *et al.*, 2010; Gill and Malamud, 2014; Leonard *et al.*, 2014; Decker and Brinkman, 2015; Ciurean *et al.*, 2018; Zscheischler *et al.*, 2020). **Chapter 2** contributes to harmonising the terminology around the concepts of multi-hazard and compound events and proposes new classifications of hazard interrelations and associated modelling approaches. This thesis contributes to creating a multi-hazard framework that benefits from interconnections between different disciplines working on hazard interrelations.

Adopting a multi-hazard approach means moving from a list of single hazard relevant to a place and time period to a holistic multi-hazard framework that includes all potential hazard interrelationships. **Chapter 3** contextualized this work in a geographical context by assessing the multi-hazard landscape of the European Atlantic Region. The concept of multi-hazard networks is defined to create generic sets of interrelated hazards and highlighting the most likely natural hazard interrelations, providing evidence for practitioners when selecting which hazards to be considered.

The definition of spatial and temporal scales of hazard interrelation poses several problems (compatibility of different data sources, potential time lags). **Chapter 3** highlights the problem of compatibility of different data sources by reviewing 35 databases of environmental data and qualitatively assessing the spatial and temporal attributes of different multi-hazard networks. In **Chapter 5**, a clear definition of the boundaries of compound hazards in space and time is provided and stresses the need to consider hazard interrelations on flexible spatial and temporal scales rather than within blocks (e.g., hours, days, grid cell, observation station).

The funding for this PhD thesis and its conception was with respect to the assessment of multi-hazard risk relevant to energy infrastructures. **Chapter 4** is particularly aimed at engineers and practitioners of the energy, transport and geotechnical sectors. Different methods to model hazard interrelations have been assessed systematically, offering an accessible framework for considering the strength and weaknesses of the models and guidance for further applications. Metrics and measures used to assess the interrelation between hazards, and their probability (e.g., return period) are therefore tailored for engineering purposes. **Chapter 4** is done within the British and European context. Features of the interrelations between extreme precipitation and extreme wind have been extensively analysed and discussed in **Chapters 3**, **4** and **5**. While these two hazards are of global relevance (Martius *et al.*, 2016; Dowdy and Catto, 2017), they play a major role in the British (hazard) landscape. Methodologies developed to classify quantification methodologies (**Chapter 2**), design multi-hazard networks (**Chapter 3**), quantify the dependence between hazards (**Chapter 4**) and assess spatiotemporal features of hazard interrelations (**Chapter 5**) are aimed to be widely applicable in term of geographical location.

To conclude, this thesis proposed a quantitative framework for multi-hazard analysis based on five key aspects which have been addressed through the thesis:

(i) classify hazard interrelations

(ii) assess modelling methods for hazard interrelations,

(iii) catalogue datasets suitable multi-hazard assessment,

(iv) consider spatiotemporal scales of hazard interrelations

(v) identify the physical processes behind multi-hazard.

This thesis adds to existing literature and understanding, helping to advance our current multi-hazard frameworks. There are many remaining opportunities to develop and improve current knowledge, in particular, to assess methodologies to model hazard interrelations and as discussed in **Section 6.3** to identify physical processes behind multi-hazard**.**

References

Aas, K., Czado, C., Frigessi, A. and Bakken, H.: Pair-copula constructions of multiple dependence, Insur. Math. Econ., 44(2), 182–198, 2009.

Acreman, M. .: Extreme Historical UK Floods and Maximum Flood Estimation, Water Environ. J., 3(4), 404–412, 1989.

Ager, D. V.: The geological evolution of Europe, Proc. Geol. Assoc., 86(2), 127–154, 1975.

AghaKouchak, A., Cheng, L., Mazdiyasni, O. and Farahmand, A.: Global warming and changes in risk of concurrent climate extremes: Insights from the 2014 California drought, Geophys. Res. Lett., 41(24), 8847–8852, 2014.

AghaKouchak, A., Huning, L. S., Chiang, F., Sadegh, M., Vahedi- fard, F., Mazdiyasni, O., Moftakhari, H., and Mallakpour, I.: How do natural hazards cascade to cause disasters?, Nature, 561, 458– 460, 2018.

Agrawal, K. P., Garg, S., Sharma, S. and Patel, P.: Development and validation of OPTICS based spatio-temporal clustering technique, Inf. Sci. 369, 388–401, 2016.

Aitchison, J.: Lognormal Distribution, Cambridge University Press., Cambridge, UK, 1957.

Akaike, H.: A new look at the statistical model identification, IEEE Trans. Automat. Contr., 19, 716–723, 1974

Alexander, D. E.: Natural Disasters, UCL Press, London., 1993.

Alexander, L.: Climate science: Extreme heat rooted in dry soils, Nat. Geosci., 4(1), 12–13, 2011.

Alfieri, L., Lorini, V., Hirpa, F. A., Harrigan, S., Zsoter, E., Prudhomme, C. and Salamon, P.: A global streamflow reanalysis for 1980–2018, J. Hydrol. X, 6, 100049, 2020.

Alfieri, L., Pappenberger, F., Wetterhall, F., Haiden, T., Richardson, D. and Salamon, P.: Evaluation of ensemble streamflow predictions in Europe, J. Hydrol., 517, 913–922, 2014.

Amraoui, M., Pereira, M. G., DaCamara, C. C. and Calado, T. J.: Atmospheric conditions associated with extreme fire activity in the Western Mediterranean region, Sci. Total Environ., 524–525, 32–39, 2015.

Anderson, G. and Klugmann, D.: A European lightning density analysis using 5 years of ATDnet data, Nat. Hazards Earth Syst. Sci., 14(4), 815–829, 2014.

Añel, J. A., Fernández-González, M., Labandeira, X., López-Otero, X. and de la Torre, L.: Impact of cold waves and heat waves on the energy production sector, Atmosphere (Basel)., 8(11), 1–13, 2017.

Angélil, O., Perkins-Kirkpatrick, S., Alexander, L. V., Stone, D., Donat, M. G., Wehner, M., Shiogama, H., Ciavarella, A. and Christidis, N.: Comparing regional precipitation and temperature extremes in climate model and reanalysis products, Weather Clim. Extrem., 13, 35–43, 2016.

Ansari, M. Y., Ahmad, A., Khan, S. S., Bhushan, G. and Mainuddin: Spatiotemporal clustering: a review, Artif. Intell. Rev., 53(15), 2381-2423, 2020.

Arnold, T. B. and Emerson, J. W.: Nonparametric goodness-of-fit tests for discrete null distributions, R J., 3, 34–39, 2011. Barriopedro, D., Fischer, E. M., Luterbacher, J., Trigo, R. M., and García-Herrera, R.: The hot summer of 2010: Redrawing the temperature map of Europe, Science, 332, 220–224, 2011.

Aspinall, W., Bengoubou-Valerius, M., Desramaut, N., Di Ruocco, A., Fleming, K., Garcia-Aristizabal, A., Gasparini, P., Gehl, P., Khazai, B., Komendantova, N., Laskowski, S., Liu, Z., Marti, J., Marzocchi, W., Mignan, A., Monfort-Climent, D., Mrzyglocki, R., Nadim, F., Parolai, S., Patt, A., Réveillère, A., Scolobig, A., Tyagunov, S., van Gelder, P., Vidar Vangelsten, B., Vinchon, C., Vorogushyn, S., Wang, J., Wenzel, F., Woo, G., Zschau, J.MATRIX. Reference Reports, (Scientific Technical Report; 14/13). Potsdam, Deutsches GeoForschungsZentrum GFZ. https://doi.org/10.2312/GFZ. b103-14137, 2014.

Azri, S., Ujang, U., Anton, F., Mioc, D. and Rahman, A. A.: Review of Spatial Indexing Techniques for Large Urban Data Management, Int. Symp. Exhib. Geoinf., (January), 1–23, 2013.

Bach, B., Dragicevic, P., Archambault, D., Hurter, C. and Carpendale, S.: A Review of Temporal Data Visualizations Based on Space-Time Cube Operations, Eurographics Conf. Vis., 00(00), 23–41, 2014.

Baldwin, J. W., Dessy, J. B., Vecchi, G. A. and Oppenheimer, M.: Temporally Compound Heat Wave Events and Global Warming: An Emerging Hazard, Earth's Futur., 7(4), 411–427, 2019.

Barriopedro, D., Fischer, E. M., Luterbacher, J., Trigo, R. M. and Garcia-Herrera, R.: The Hot Summer of 2010: Redrawing the Temperature Record Map of Europe, Science, 220–224, 2011.

Barton, Y., Giannakaki, P., von Waldow, H., Chevalier, C., Pfahl, S. and Martius, O.: Clustering of regional-scale extreme precipitation events in southern Switzerland, Mon. Weather Rev., 144(1), 347–369, 2016.

Bass, B. and Bedient, P.: Surrogate modeling of joint flood risk across coastal watersheds, J. Hydrol., 558, 159–173, 2018.

Bauer, A. X.: Pair-copula constructions for non-Gaussian Bayesian networks, PhD thesis. Technische Universität München., 2013.

Bauer, A., Czado, C.:, Pair-copula bayesian networks. J. Comput. Graph. Stat. 25, 1248–1271. https://doi.org/10.1080/10618600.2015.1086355, 2016.

Beck, H. E., Van Dijk, A. I. J. M., Levizzani, V., Schellekens, J., Miralles, D. G., Martens, B. and De Roo, A.: MSWEP: 3-hourly 0.25° global gridded precipitation (1979-2015) by merging gauge, satellite, and reanalysis data, Hydrol. Earth Syst. Sci., 21(1), 589–615, 2017.

Beck, H. E., Pan, M., Roy, T., Weedon, G. P., Pappenberger, F., van Dijk, A. I. J. M., Huffman, G. J., Adler, R. F. and Wood, E. F.: Daily evaluation of 26 precipitation datasets using Stage-IV gauge-radar data for the CONUS, Hydrol. Earth Syst. Sci. Discuss., 1–23, 2018.

Beck, H. E., Zimmermann, N. E., McVicar, T. R., Vergopolan, N., Berg, A. and Wood, E. F.: Present and future köppen-geiger climate classification maps at 1-km resolution, Sci. Data, 5, 1–12, 2018.

Bedford, T. and Cooke, R. M.: Vines : A New Graphical Model for Dependent Random Variables, Ann. Stat., 30(4), 1031–1068, 2002.

Bentley, J. L.: Multidimensional Binary Search Trees Used for Associative Searching, Commun. ACM, 18(9), 509–517, 1975.

Berghuijs, W. R., Harrigan, S., Molnar, P., Slater, L. J. and Kirchner, J. W.: The Relative Importance of Different Flood-Generating Mechanisms Across Europe, Water Resour. Res., 55(6), 4582–4593, 2019.

Bernardara, P., Mazas, F., Kergadallan, X. and Hamm, L.: A two-step framework for over-threshold modelling of environmental extremes, Nat. Hazards Earth Syst. Sci., 14(3), 635–647, 2014.

Bevacqua, E., Maraun, D., Hobæk Haff, I., Widmann, M., Vrac, M.: Multivariate statistical modelling of compound events via pair-copula constructions: analysis of floods in Ravenna (Italy). Hydrol. Earth Syst. Sci. 21, 2701–2723. https://doi.org/10. 5194/hess-21-2701-2017, 2017.

BGS (British Geological Survey): A catalogue of tsunamis reported in the UK , available at: http://nora.nerc.ac.uk/id/eprint/513298/ (Accessed 12 February 2020), 2018.

Bingham, N. H., Goldie, C. M. and Teugels, J. L.: Regular variation, Cambridge University Press, Cambridge., 1987.

Bingham, N. H.: Regular variation and probability: The early years, J. Comput. Appl. Math., 200(1), 357–363, 2007.

Birant, D. and Kut, A.: ST-DBSCAN: An algorithm for clustering spatial-temporal data, Data Knowl. Eng., 60(1), 208–221, 2007.

Blanchet, G.: Régimes météorologiques et diversité climatique dans l'espace rhonalpin / Meteorological regimes and climatic diversity in the Rhône-Alpes area, Rev. géographie Lyon, 65(2), 106–117, 1990.

Blenkinsop, S., Lewis, E., Chan, S. C. and Fowler, H. J.: Quality-control of an hourly rainfall dataset and climatology of extremes for the UK, Int. J. Climatol., 37(2), 722–740, 2017.

Blöschl, G. and Sivapalan, M.: Scale issues in hydrological modelling: A review, Hydrol. Process., 9(3–4), 251–290, 1995.

Bogaard, T., Maharjan, L. D., Maquaire, O., Lissak, C. and Malet, J.-P.: Identification of Hydro-Meteorological Triggers for Villerville Coastal Landslide, in Landslide Science and Practice, pp. 141–145, Springer Berlin Heidelberg, Berlin, Heidelberg., 2013.

Bolado-Lavin, R. and Badea, A.: Review of Sensitivity Analysis Methods and Experience for Geological Disposal of Radioactive waste and Spent Nuclear Fuel. JRC Scientific and Technical Reports, Luxembourg, 2008.

Booij, N., Holthuijsen, L.H., Ris, R.C. The “Swan” wave model for shallow water. Coast. Eng. 668–676. https://doi.org/10.9753/icce.v25.%p., 1996.

Booth, G.: Winter 1947 in the British isles, Weather, 62(3), 61–68, 2007.

Borgonovo, E., Castaings, W., Tarantola, S. Model emulation and moment-in- dependent sensitivity analysis: an application to environmental modelling. Environ. Model. Softw. 34, 105–115. https://doi.org/10.1016/j.envsoft.2011.06.006., 2012.

Bout, B., Lombardo, L., van Westen, C.J., Jetten, V.G., 2018. Integration of two-phase solid fluid equations in a catchment model for flashfloods, debris flows and shallow slope failures. Environ. Model. Softw. 105, 1–16. https://doi.org/10.1016/j.envsoft. 2018.03.017.

Brechmann, E. C. and Schepsmeier, U.: Modeling Dependence with C- and D-Vine Copulas: The RPackage CDVine, J. Stat. Softw., 52, 1–27, 2013. https://doi.org/10.18637/jss.v052.i03, 2013.

Brönnimann, S. and Martius, O. (eds.): Weather extremes during the past 140 years, Geographica Bernensia G89., University of Bern, 2013.

Brönnimann, S., Allan, R., Atkinson, C., Buizza, R., Bulygina, O., Dahlgren, P., Dee, D., Dunn, R., Gomes, P., John, V. O., Jourdain, S., Haimberger, L., Hersbsbach, H., Kennedy, J., Poli, P., Pulliainen, J., Rayner, N., Saunders, R., Schulz, J., Sterin, A., Stickler, A., Titchner, H., Valente, M. A., Ventura, C. and Wilkinson, C.: Observations for reanalyses, Bull. Am. Meteorol. Soc., 99(9), 1851–1866, 2018.

Brugnara, Y., Good, E., Squintu, A. A., van der Schrier, G. and Brönnimann, S.: The EUSTACE global land station daily air temperature dataset, Geosci. Data J., 6(2), 189–204, 2019.

Caine, N., The rainfall intensity - duration control of shallow landslides and debris flows. Geogr. Ann. Ser. A Phys. Geogr. 62, 23–27. https://doi.org/10.1080/ 04353676.1980.11879996, 1980.

Calow, P.: The Encyclopedia of Ecology & Environmental Management, Blackwell Publishing Ltd., Oxford, UK., 1999.

Cannon, S.H., Gartner, J.E., Wilson, R.C., Bowers, J.C., Laber, J.L. Storm rainfall conditions for floods and debris flows from recently burned areas in southwestern Colorado and southern California. Geomorphology 96 (3–4), 250–269. https://doi. org/10.1016/j.geomorph.2007.03.019, 2008.

Canty, A. and Ripley, B. D.: boot: Bootstrap R (S-Plus) Functions, available at: https://cran.r-project.org/web/packages/boot/ citation.html (Accessed 22 June 2020), 2019.

Cao, H., Zhang, H., Wang, C. and Zhang, B.: Operational flood detection using Sentinel-1 SAR data over large areas, Water (Switzerland), 11(4), 2019.

Capéraà, P., Fougères, A. L. and Genest, C.: A nonparametric estimation procedure for bivariate extreme value copulas, Biometrika, 84(3), 567–577, 1997.

Carey, L.D., Rutledge, S.A., Petersen, W.A.: The relationship between severe storm reports and cloud-to-ground lightning polarity in the contiguous United States from 1989 to 1998.

Mon. Weather Rev. 131, 1211–1228. https://doi.org/10.1175/1520-0493(2003)131<1211:TRBSSR>2.0.CO;2, 2003.

Catane, S.G., Abon, C.C., Saturay, R.M., Mendoza, E.P.P., Futalan, K.M. Landslide- amplified flash floods—the June 2008 Panay Island flooding, Philippines. Geomorphology 169–170, 55–63. https://doi.org/10.1016/j.geomorph.2012.04.008, 2012.

Catto, J. L.: Extratropical cyclone classification and its use, Rev. Geophys., 54, 486–520, 2016.

CCR (Caisse Centrale de Réassurance): E-risk database, Paris, France, available at: https://catastrophes-naturelles.ccr.fr (Accessed 1 December 2019), 2019.

Chazette, P., Flamant, C., Raut, J., Totems, J. and Shang, X.: Tropical moisture enriched storm tracks over the Mediterranean and their link with intense rainfall in the Cevennes-Vivarais area during HyMeX, Q. J. R. Meteorol. Soc., 142(August), 320–334, 2016.

Chebana, F. and Ouarda, T. B. M. J.: Multivariate quantiles in hydrological frequency analysis, Environmetrics, 22, 63–78, 2011.

Chen, T., Tang, W., Lu, Y., Tu, X. Rank regression: an alternative regression approach for data with outliers. Shanghai Arch. Psychiatry 26, 310–316. https://doi. org/10.11919/j.issn.1002-0829.214148, 2014.

Chester, D. K.: The 1755 Lisbon earthquake, Prog. Phys. Geogr., 25(3), 363–383, 2001.

Ciurean, R., Gill, J., Reeves, H., O’Grady, S. and Aldridge, T.: Review of environmental multi-hazards research and risk assessments. British Geological Survey Open Report, 2018.

Clague, J. and Stead, D.: Landslides: Types, Mechanisms and Modelling, Cambridge University Press., 2012.

Clare, M. A., Talling, P. J., Challenor, P. G., and Hunt, J. E.: Tempo and Triggering of Large Submarine Landslides: Statistical Anal- ysis for Hazard Assessment, in: Advances in Natural and Tech- nological Hazards Research, Vol. 41, edited by: Lamarche, G., Mountjoy, J., Bull, S., Hubble, T., Krastel, S., Lane, E., Mi- callef, A., Moscardelli, L., Mueller, C., Pecher, I., and Woelz, S., Springer International Publishing, Cham, Switzerland, 509–517, 2016.

Clayton, K.: Quantification of the Impact of Glacial Erosion on the British Isles, Trans. Inst. Br. Geogr., 21(1), 124, 1996.

Coles, S.: An Introduction to Statistical Modeling of Extreme Values, Springer Series in Statistics. Springer-Verlag, London, 2001.

Coles, S., Heffernan, J., Tawn, J., 1999. Dependence measures for extreme value analyses. Extremes 2, 339–365. https://doi.org/10.1023/A:1009963131610.

Coles, S. and Tawn, J. A.: Modelling Extreme Multivariate Events, J. R. Stat. Soc. Ser. B, 53(2), 285–339, 1991.

Coles, S.G., Tawn, J.A., 1994. Statistical methods for multivariate extremes: an applica- tion to structural design. J. R. Stat. Soc.: Ser. C: Appl. Stat. 43, 1–31. https://doi.org/ 10.2307/2986112.

Cooley, D., Thibaud, E., Castillo, F., and Wehner, M. F.: A non- parametric method for producing isolines of bivariate exceedance probabilities, Extremes, 22, 373–390, 2019.

Cornes, R. C., van der Schrier, G., van den Besselaar, E. J. M., and Jones, P. D.: An ensemble version of the E-OBS temperature and precipitation data sets, J. Geophys. Res.-Atmos., 123, 9391–9409, 2018.

Coron, L., Thirel, G., Delaigue, O., Perrin, C., Andréassian, V.: The suite of lumped GR hydrological models in an R package. Environ. Model. Softw. 94, 166–171. https://doi.org/10.1016/j.envsoft.2017.05.002, 2017.

Corzo Perez, G. A., Van Huijgevoort, M. H. J., Voß, F. and Van Lanen, H. A. J.: On the spatio-temporal analysis of hydrological droughts from global hydrological models, Hydrol. Earth Syst. Sci., 15(9), 2963–2978, 2011.

Costa, J.E., Schuster, R.L.: The formation and failure of natural dams. Geol. Soc. Am. Bull. 100, 1054–1068. https://doi.org/10.1130/0016-7606(1988), 1988.

Couasnon, A., Sebastian, A., and Morales-Nápoles, O.: A copula- based Bayesian network for modeling compound flood hazard from riverine and coastal interactions at the catchment scale: an application to the Houston ship channel, Texas, Water, 10, 1190, https://doi.org/10.3390/w10091190, 2018.

Couasnon, A., Eilander, D., Muis, S., Veldkamp, T. I. E., Haigh, I. D., Wahl, T., Winsemius, H. C. and Ward, P. J.: Measuring compound flood potential from river discharge and storm surge extremes at the global scale and its implications for flood hazard, Nat. Hazards Earth Syst. Sci. Discuss., (July), 1–24, 2019.

Cox, D.R., Miller, H.D.: The Theory of Stochastic Processes. CRC Press, Boca Raton, 1965.

CRED: EM-DAT: The Emergency Events Database. Université Catholique de Louvain (UCL), available at: www.emdat.be (Accessed 12 November 2018), 2018.

Cressie, N. A. C.: Statistics for spatial data, Wiley series in probability and mathematical statistics. Applied probability and statistics section, John Wiley & Sons, Inc., New York, 1993.

Dan, G., Sultan, N. and Savoye, B.: The 1979 Nice harbour catastrophe revisited: Trigger mechanism inferred from geotechnical measurements and numerical modelling, Mar. Geol., 245(1–4), 40–64, 2007.

Das, B.: Conditional extreme value model and related topics, PhD thesis, Cornell University., 2009.

Davis, I. (Ed.).: Disaster Risk Management in Asia and the Pacific. Routledge, New York, 2015.

Davison, A. C. and Huser, R.: Statistics of Extremes, Annu. Rev. Stat. Its Appl., 2(1), 203–235, 2015.

Davison, A. C. and Hinkley, D. V.: Bootstrap Methods and Their Applications, Cambridge University Press, Cambridge, UK, 1997.

Davison, A. C. and Smith, R. L.: Models for Exceedances over High Thresholds, J. R. Stat. Soc. Ser. B, 52(3), 393–442, 1990.

de Haan, L.: On Regular Variation and Its Application to the Weak Convergence of Sample Extremes., 1970.

de Haan, L. and De Ronde, J.: Sea and wind: multivariate extremes at work, Extremes, 1, 7–45, 1998.

de Haan, L. and Resnick, S. I.: Limit theory for multivariate sample extremes, Zeitschrift für Wahrscheinlichkeitstheorie und Verwandte Gebiete, 40(4), 317–337, 1977.

de Haan, L. and Resnick, S. I.: Second-order regular variation and rates of convergence in extreme-value theory, Ann. Probab., 24(1), 97–124, 1996.

De Michele, C., Salvadori, G., Passoni, G., and Vezzoli, R.: A multi- variate model of sea storms using copulas, Coast. Eng., 54, 734– 751, 2007.

De Pippo, T., Donadio, C., Pennetta, M., Petrosino, C., Terlizzi, F., Valente, A.: Coastal hazard assessment and mapping in Northern Campania, Italy. Geomorphology 97, 451–466. https://doi.org/10.1016/j.geomorph.2007.08.015, 2008.

de Ruiter, M. C., Couasnon, A., van den Homberg, M. J. C., Daniell, J. E., Gill, J. C. and Ward, P. J.: Why We Can No Longer Ignore Consecutive Disasters, Earth's Futur., 8(3), 2020.

Decker, K., Brinkman, H.: List of external hazards to be considered in ASAMPSA _ E. Advanced Safety Assessment Methodologies: extended PSA. In: Technical Report ASAMPSA_E / WP21 / D21.2 / 2015-10, Reference IRSN PSN-RES/SAG/2015-00085, available at: https://inis.iaea.org/search/search.aspx?orig_q=RN:48055409 (Accessed 7 February 2018), 2015.

Defra (Department for Environment Food and Rural Affairs): The threat posed by tsunami to the UK, Edinburgh, available at. http://geodesy.unr.edu/hanspeterplag/library/projects/eseas_white/UK_report_4404.0.rep_5apr05.pdf (Accessed 17 September 2019), 2005.

Della-Marta, P. M., Mathis, H., Frei, C., Liniger, M. A., Kleinn, J. and Appenzeller, C.: The return period of wind storms over Europe, Int. J. Climatol., 29(3), 437–459, 2009.

Deroche, M. S., Choux, M., Codron, F. and Yiou, P.: Three variables are better than one: Detection of european winter windstorms causing important damages, Nat. Hazards Earth Syst. Sci., 14(4), 981–993, 2014.

Devia, G.K., Ganasri, B.P., Dwarakish, G.S.: A review on hydrological models. Aquat. Proc. 4, 1001–1007. https://doi.org/10.1016/j.aqpro.2015.02.126, 2015.

Diederen, D. and Liu, Y.: Dynamic spatio-temporal generation of large-scale synthetic gridded precipitation: with improved spatial coherence of extremes, Stoch. Environ. Res. Risk Assess., 9(2005), 2019.

Dietrich, J.C., Bunya, S., Westerink, J.J., Ebersole, B.A., Smith, J.M., Atkinson, J.H., Jensen, R., Resio, D.T., Luettich, R.A., Dawson, C., Cardone, V.J., Cox, A.T., Powell, M.D., Westerink, H.J., Roberts, H.J.: A high-resolution coupled riverine flow, tide, wind, wind wave, and storm surge model for southern Louisiana and Mississippi. Part II: synoptic description and analysis of hurricanes Katrina and Rita. Mon. Weather Rev. 138, 378–404. https://doi.org/10.1175/2009MWR2907.1, 2010.

Disse, M. and Engel, H.: Flood events in the Rhine basin: Genesis, influences and mitigation, Nat. Hazards, 23(2–3), 271–290, 2001.

Dizerens, C., Lenggenhager, S., Schwander, M., Buck, A. and Foffa, S.: The 1956 Cold Wave in Western Europe, In: Brönnimann, S. (Ed.) Historical Weather Extremes in Reanalyses. Geographica Bernensia G92, pp. 101-111, 2017.

Donat, M. G., Sillmann, J., Wild, S., Alexander, L. V., Lippmann, T. and Zwiers, F. W.: Consistency of temperature and precipitation extremes across various global gridded in-situ and reanalysis datasets, J. Clim., 27(13), 5019–5035, 2014.

Dong, S., Gao, J., Li, X., Wei, Y., Wang, L.: A storm surge intensity classification based on extreme water level and concomitant wave height. J. Ocean Univ. China 14, 237–244. https://doi.org/10.1007/s11802-015-2342-5, 2015.

Dorigo, W., Wagner, W., Albergel, C., Albrecht, F., Balsamo, G., Brocca, L., Chung, D., Ertl, M., Forkel, M., Gruber, A., Haas, E., Hamer, P. D., Hirschi, M., Ikonen, J., de Jeu, R., Kidd, R., Lahoz, W., Liu, Y. Y., Miralles, D., Mistelbauer, T., Nicolai-Shaw, N., Parinussa, R., Pratola, C., Reimer, C., van der Schalie, R., Seneviratne, S. I., Smolander, T. and Lecomte, P.: ESA CCI Soil Moisture for improved Earth system understanding: State-of-the art and future directions, Remote Sens. Environ., 203, 185–215, 2017.

Dotzek, N. and Friedrich, K.: Downburst-producing thunderstorms in southern Germany: Radar analysis and predictability, Atmos. Res., 93(1–3), 457–473, 2009.

Dotzek, N., Groenemeijer, P., Feuerstein, B. and Holzer, A. M.: Overview of ESSL's severe convective storms research using the European Severe Weather Database ESWD, Atmos. Res., 93(1–3), 575–586, 2009.

Dowdy, A.J., Catto, J.L.: Extreme weather caused by concurrent cyclone, front and thunderstorm occurrences. Sci. Rep. 7, 1–8. https://doi.org/10.1038/srep40359, 2017.

Drobinski, P., Ducrocq, V., Alpert, P., Anagnostou, E., Béranger, K., Borga, M., Braud, I., Chanzy, A., Davolio, S., Delrieu, G., Estournel, C., Filali Boubrahmi, N., Font, J., Grubišić, V., Gualdi, S., Homar, V., Ivančan-Picek, B., Kottmeier, C., Kotroni, V., Lagouvardos, K., Lionello, P., Llasat, M. C., Ludwig, W., Lutoff, C., Mariotti, A., Richard, E., Romero, R., Rotunno, R., Roussot, O., Ruin, I., Somot, S., Taupier-Letage, I., Tintor, J., Uijlenhoet, R. and Wernli, H.: HYMEX: A 10-year multidisciplinary program on the mediterranean water cycle, Bull. Am. Meteorol. Soc., 95(7), 1063–1082, 2014.

Dung, N. V., Merz, B., Bárdossy, A. and Apel, H.: Handling uncertainty in bivariate quantile estimation - An application to flood hazard analysis in the Mekong Delta, J. Hydrol., 527, 704–717, 2015.

Duong, T.: ks: Kernel density estimation and kernel discrimi- nant analysis for multivariate data, R, J. Stat. Softw., 21, 1–16, https://doi.org/10.18637/jss.v021.i07, 2007.

Duong, T.: Non-parametric smoothed estimation of multivariate cu- mulative distribution and survival functions, and receiver operat- ing characteristic curves, J. Korean Stat. Soc., 45, 33–50, 2015.

Dutfoy, A., Parey, S., Roche, N.: Multivariate extreme value theory - a tutorial with applications to hydrology and meteorology. Depend. Model. 2, 30–48. https://doi. org/10.2478/demo-2014-0003, 2014.

Dutykh, D., Poncet, R., Dias, F.: The VOLNA code for the numerical modeling of tsunami waves: Generation, propagation and inundation. Eur. J. Mech. B/Fluids 30, 598–615. https://doi.org/10.1016/j.euromechflu.2011.05.005, 2011.

Duval, C., Fallet-Fidry, G., Iung, B., Weber, P., Levrat, E.: A Bayesian network-based integrated risk analysis approach for industrial systems: application to heat sink system and prospects development. Proc. Inst. Mech. Eng. Part O J. Risk Reliab. 226, 488–507. https://doi.org/10.1177/1748006X12451091, 2012.

Eden, P.: Great British Weather Disasters, Continuum. London, 2008.

Ehhalt, D. H.: In-situ observations, Philos. Trans. R. Soc. London. Ser. A, Math. Phys. Sci., 296(1418), 175–189, 1980.

Elidan, G.: Copula bayesian networks. In: Lafferty, J.D., Williams, C.K.I., Shawe- Taylor, J., Zemel, R.S., Culotta, A. (Eds.), Advances in Neural Information Processing Systems 23. Curran Associates, pp. 559–567, 2010.

Eschenburg, P.: Properties of extreme-value copulas, PhD thesis, Technische Universitat Munchen, 2013.

Eshrati, L., Mahmoudzadeh, A., Taghvaei, M., 2015.: Multi hazards risk assessment, a new methodology. Int. J. Health Syst. Disaster Manag. 3 (2), 79–88. https://doi.org/10. 4103/2347-9019.151315.

Ester, M., Kriegel, H.-P., Sander, J. and Xu, X.: A Density-Based Algorithm for Discovering Clusters in Large Spatial Databases with Noise, in KDD, vol. 2, pp. 635–654., 1996.

ETI (Energy Technologies Institute): Enabling Resilient UK Energy Infrastructure: Natural Hazard Characterisation Technical Volumes and Case Studies, Volume 7 : Seismic , Volcanic and Geological Hazards., 2018.

EEA (European Environment Agency): Biogeographical regions in Europe. The Atlantic region – mild and green, fragmented and close to the rising sea., Copenhagen, 2003.

EEA (European Environment Agency): EEA Glossary, available at: https://www.eea.europa.eu/help/glossary (Accessed 21 September 2020), 2020.

EEA (European Environment Agency): Europe's biodiversity – biogeographical regions and seas, Copenhagen, 2002.

ESPON (European Spatial Planning Observation Network): Objectives of ESPON 2006, available at: https://www.espon.eu/programme/espon/objectives-espon-2006 (Accessed 21 September 2020), 2006.

Fan, X., Scaringi, G., Korup, O., West, A. J., van Westen, C. J., Tanyas, H., Hovius, N., Hales, T. C., Jibson, R. W., Allstadt, K. E., Zhang, L., Evans, S. G., Xu, C., Li, G., Pei, X., Xu, Q. and Huang, R.: Earthquake-Induced Chains of Geologic Hazards: Patterns, Mechanisms, and Impacts, Rev. Geophys., 57(2), 421–503, 2019.

Favre, A.-C., El Adlouni, S., Perreault, L., Thiémonge, N., Bobée, B.: Multivariate hydrological frequency analysis using copulas. Water Resour. Res. 40, 1–12. https:// doi.org/10.1029/2003WR002456, 2004.

FEMA (Federal Emergency Management Agency): Flood after Fire Fact Sheet. National Flood Insurance Program, available at. https://www.fema.gov/ media-library/assets/documents/93830 (Accessed 17 April 2018), 2012.

Fink, A. H., Brücher, T., Krüger, A., Leckebusch, G. C., Pinto, J. G. and Ulbrich, U.: The 2003 European summer heatwaves and drought -synoptic diagnosis and impacts, Weather, 59(8), 209–216, 2004.

Fisher, R. A. and Tippett, L. H. C.: Limiting forms of the frequency distribution of the largest or smallest member of a sample, Math. Proc. Cambridge Philos. Soc., 24(2), 180–190, 1928.

Frame, T., Harrisonm, G., Hewson, T. and Roberts, N.: Meteorological Risk: extra-tropical cyclones, tropical cyclones and convective storms, in Science for Disaster Risk Management 2017: Knowing Better and Losing Less, pp. 246–256, Publications Office of the European Union, Luxembourg., 2017.

Frau, R., Andreewsky, M., and Bernardara, P.: The use of his- torical information for regional frequency analysis of extreme skew surge, Nat. Hazards Earth Syst. Sci., 18, 949–962, https: //doi.org/10.5194/nhess-18-949-2018, 2018.

Frey, C., Mokhtari, A. and Danish, T.: Evaluation of Selected Sensitivity Analysis Methods Based Upon Applications to Two Food Safety Process Risk Models, Washington D.C., 2003.

Frigg, R., Hartmann, S.: Models in Science. In: Zalta, E.N. (Ed.), The Stanford Encyclopaedia of Philosophy, (Summer 2018 Ed.), available at: https://plato. standford.edu/archives/sum2018/entries/models-science (Accessed 1 October 2018), 2012.

Fritsche, S. and Fäh, D.: The 1946 magnitude 6.1 earthquake in the Valais: Site-effects as contributor to the damage, Swiss J. Geosci., 102(3), 423–439, 2009.

Fujita, T. : Manual of downburst identification for project NIMROD, Chicago., 1978.

Fujita, T. : Downbursts : Meteorological Features and Wind Field Characteristics, J. Wind Eng. Ind. Aerodyn., 36, 75–86, 1990.

Gall, M., Borden, K.A., Cutter, S.L:. When do losses count? Bull. Am. Meteorol. Soc. 90, 799–810. https://doi.org/10.1175/2008BAMS2721.1, 2009.

Gallina, V., Torresan, S., Critto, A., Sperotto, A., Glade, T., Marcomini, A:. A review of multi-risk methodologies for natural hazards: Consequences and challenges for a climate change impact assessment. J. Environ. Manag. 168, 123–132. https://doi. org/10.1016/j.jenvman.2015.11.011, 2016.

Ganteaume, A., Camia, A., Jappiot, M., San-Miguel-Ayanz, J., Long-Fournel, M. and Lampin, C.: A review of the main driving factors of forest fire ignition over Europe, Environ. Manage., 51(3), 651–662, 2013.

Garavaglia, F., Gailhard, J., Paquet, E., Lang, M., Garçon, R. and Bernardara, P.: Introducing a rainfall compound distribution model based on weather patterns sub-sampling, Hydrol. Earth Syst. Sci., 14(6), 951–964, 2010.

García-Ortega, E., Trobajo, M. T., López, L. and Sánchez, J. L.: Synoptic patterns associated with wildfires caused by lightning in Castile and Leon, Spain, Nat. Hazards Earth Syst. Sci., 11(3), 851–863, 2011.

Gatlin, P. N. and Goodman, S. J.: A total lightning trending algorithm to identify severe thunderstorms, J. Atmos. Ocean. Technol., 27(1), 3–22, 2010.

Geist, E.L., Lynett, P.J., Chaytor, J.D.: Hydrodynamic modeling of tsunamis from the Currituck landslide. Mar. Geol. 264, 41–52. https://doi.org/10.1016/j.margeo. 2008.09.005, 2009.

Geist, E. L. and Parsons, T.: Probabilistic analysis of tsunami hazards, Nat. Hazards, 37(3), 277–314, 2006.

Genest, C., Favre, A.C:. Everything you always wanted to know about copula modeling but were afraid to ask. J. Hydrol. Eng. 12, 347–368. https://doi.org/10. 1061/(ASCE)1084-0699(2007)12:4(347), 2007.

Genest, C., Kojadinovic, I., Nešlehová, J., and Yan, J.: A goodness- of-fit test for bivariate extreme-value copulas, Bernoulli, 17, 253–275, 2011.

Genest, C. and Nešlehová, J.: Copula Modeling for Extremes, in: Encyclopedia of Environmetrics, John Wiley & Sons Ltd, Chich- ester, UK, 1–6, 2013.

Genest, C., Rémillard, B., and Beaudoin, D.: Goodness-of-fit tests for copulas: A review and a power study, Insur. Math. Econ., 44, 199–213, 2009.

Georgoulas, G., Konstantaras, A., Katsifarakis, E., Stylios, C. D., Maravelakis, E. and Vachtsevanos, G. J.: “Seismic-mass” density-based algorithm for spatio-temporal clustering, Expert Syst. Appl., 40(10), 4183–4189, 2013.

Giardini, D., Wössner, J. and Danciu, L.: Mapping Europe’s Seismic Hazard, Eos, Trans. Am. Geophys. Union, 95(29), 261–262, 2014.

Gill, J. C.: Increasing the Understanding and Characterisation of Natural Hazard Interactions, PhD thesis, King’s College London., 2016.

Gill, J.C., Malamud, B.D:. Reviewing and visualizing the interactions of natural hazards. Rev. Geophys. 52, 680–722. https://doi.org/10.1002/2013RG000445, 2014.

Gill, J.C., Malamud, B.D.: Hazard interactions and interaction networks (cascades) within multi-hazard methodologies. Earth Syst. Dyn. 7, 659–679. https://doi.org/10. 5194/esd-7-659-2016, 2016.

Gill, J. C., Malamud, B. D., Barillas, E. M. and Noriega, A. G.: Construction of regional multi-hazard interaction frameworks, with an application to Guatemala, Nat. Hazards Earth Syst. Sci., 20(1), 149–180, 2020.

Glade, T:. Applying probability determination to refine landslide-triggering rainfall thresholds using an empirical antecedent daily rainfall model. Pure Appl. Geophys. 157, 1059–1079. https://doi.org/10.1007/s000240050017, 2000.

Gleixner, S., Demissie, T. and Diro, G. T.: Did ERA5 improve temperature and precipitation reanalysis over East Africa?, Atmosphere (Basel)., 11(9), 1–19, 2020.

Gouldby, B., Wyncoll, D., Panzeri, M., Franklin, M., Hunt, T., Hames, D., Tozer, N., Hawkes, P., Dornbusch, U., and Pullen, T.: Multivariate extreme value modelling of sea conditions around the coast of England, Proc. Inst. Civ. Eng. Marit. Eng., 170, 3– 20, 2017.

Gr̈aler, B., Van Den Berg, M. J., Vandenberghe, S., Petroselli, A., Grimaldi, S., De Baets, B. and Verhoest, N. E. C.: Multivariate return periods in hydrology: A critical and practical review focusing on synthetic design hydrograph estimation, Hydrol. Earth Syst. Sci., 17(4), 1281–1296, 2013.

Greiving, S., Fleischhauer, M., Lückenkötter, J.: A methodology for an integrated risk assessment of spatially relevant hazards. J. Environ. Plan. Manag. 49, 1–19. https://doi.org/10.1080/09640560500372800, 2006.

Grünthal, G., Thieken, A.H., Schwarz, J., Radtke, K.S., Smolka, A., Merz, B.: Comparative risk assessments for the city of Cologne – storms, floods, earthquakes. Nat. Hazards 38, 21–44. https://doi.org/10.1007/s11069-005-8598-0, 2006.

Gudendorf, G., Segers, J.: Extreme-value copulas. In: Copula Theory and Its Applications. Springer, Berlin, pp. 127–145. https://doi.org/10.1007/978-3-642- 12465-5_6, 2010.

Gümbel, E.J.: Statistics of Extremes. Columbia U. Press, New York (396 pp.), 1958.

Gumbel, E.J.: Bivariate logistic distributions. J. Am. Stat. Assoc. 56, 335–349. https://doi.org/10.1080/01621459.1961.10482117, 1961.

Gutierrez, B.T., Plant, N.G., Thieler, E.R.: A Bayesian network to predict coastal vulnerability to sea level rise. J. Geophys. Res. Earth Surf. 116, 1–15. https://doi.org/ 10.1029/2010JF001891, 2011.

Guzzetti, F., Peruccacci, S., Rossi, M., Stark, C.P. Rainfall thresholds for the initiation of landslides in central and southern Europe. Meteorog. Atmos. Phys. 98, 239–267. https://doi.org/10.1007/s00703-007-0262-7, 2007.

Hahsler, M., Piekenbrock, M. and Doran, D.: dbscan : Fast Density-based Clustering with R, , (1990), 2017.

Haigh, I. D., Wadey, M. P., Gallop, S. L., Loehr, H., Nicholls, R. J., Horsburgh, K., Brown, J. M. and Bradshaw, E.: A user-friendly database of coastal flooding in the United Kingdom from 1915-2014, Sci. Data, 2, 1–13, 2015.

Haigh, I. D., Wadey, M. P., Wahl, T., Ozsoy, O., Nicholls, R. J., Brown, J. M., Horsburgh, K. and Gouldby, B. P.: Analysis : Spatial and temporal analysis of extreme sea level and storm surge events around the coastline of the UK, , 1–14, 2016.

Hall, J. and Blöschl, G.: Spatial patterns and characteristics of flood seasonality in Europe, Hydrol. Earth Syst. Sci., 22(7), 3883–3901, 2018.

Hamby, D. M.: a Review of Techniques for Parameter Sensitivity, Environ. Monit. Assess. , 32(c), 135–154, 1994.

Hand, W. H., Fox, N. I. and Collier, C. G.: A study of twentieth - Century extreme rainfall events in the United Kingdom with implications for forecasting, Meteorol. Appl., 11(1), 15–31, 2004.

Hanea, A.: Non-parametric Bayesian belief nets versus vines. In: Joe, H., Kurowicka, D. (Eds.), Dependence Modeling: Vine Copula Handbook. World Scientific, Singapore, pp. 281–303. https://doi.org/10.1142/9789814299886_0014, 2010.

Hanea, A.M., Kurowicka, D., Cooke, R.M., Ababei, D.A. Mining and visualising ordinal data with non-parametric continuous BBNs. Comput. Stat. Data Anal. 54, 668–687. https://doi.org/10.1016/j.csda.2008.09.032, 2010.

Hanea, A., Morales Napoles, O., Ababei, D.: Non-parametric Bayesian networks: improving theory and reviewing applications. Reliab. Eng. Syst. Saf. 144, 265–284. https://doi.org/10.1016/j.ress.2015.07.027, 2015.

Hao, Z., Hao, F., Singh, V.P., Ouyang, W. Quantitative risk assessment of the effects of drought on extreme temperature in eastern China. J. Geophys. Res. Atmos. 122, 9050–9059. https://doi.org/10.1002/2017JD027030, 2017.

Hao, Z., Singh, V. P. and Asce, F.: Compound Events under Global Warming : A Dependence Perspective, , 25(9), 1–12, 2020.

Hao, Z., Singh, V., and Hao, F.: Compound extremes in hydroclimatology: A review, Water, 10, 718, https://doi.org/10.3390/w10060718, 2018.

Hao, Z., Singh, V.P.: Review of dependence modeling in hydrology and water re- sources. Prog. Phys. Geogr. 40, 549–578. https://doi.org/10.1177/ 0309133316632460, 2016.

Hashemi, S.J., Ahmed, S., Khan, F.I.: Correlation and dependency in multivariate process risk assessment. IFAC-PapersOnLine, 48, 1339–1344. https://doi.org/10. 1016/j.ifacol.2015.09.711, 2015.

Hashemi, S.J., Khan, F., Ahmed, S.: Multivariate probabilistic safety analysis of process facilities using the Copula Bayesian Network model. Comput. Chem. Eng. 93, 128–142. https://doi.org/10.1016/j.compchemeng.2016.06.011, , 2016.

Hatvani-Kovacs, G., Belusko, M., Pockett, J., and Boland, J.: As- sessment of heatwave impacts, Procedia. Engineer., 169, 316– 323, 2016.

Hauser, M., Orth, R., and Seneviratne, S. I.: Role of soil moisture vs. recent climate change for heat waves in western Russia, Geo- phys. Res. Lett., 43, 2819–2826, 2015.

Hawcroft, M. K., Shaffrey, L. C., Hodges, K. I. and Dacre, H. F.: How much Northern Hemisphere precipitation is associated with extratropical cyclones?, Geophys. Res. Lett., 39(24), 1–7, 2012.

Hawkes, P.J.: Joint probability analysis for estimation of extremes. J. Hydraul. Res. 46, 246–256. https://doi.org/10.1080/00221686.2008.9521958, 2008.

Hawkes, P.J., Gouldby, B.P., Tawn, J.A., Owen, M.W.: The joint probability of waves and water levels in coastal engineering design. J. Hydraul. Res. 40, 241–251. https://doi.org/10.1080/00221680209499940, 2002.

Heffernan, J.: A directory of coefficients of tail dependence. Extremes 279–290. https://doi.org/10.1023/A:1011459127975, 2001.

Heffernan, J., Tawn, J.:. A conditional approach for multivariate extreme values (with discussion). J. R. Stat. Soc. Ser. B (Stat. Methodol.) 66, 497–546. https://doi.org/10.1111/j.1467-9868.2004.02050.x, 2004.

Hendry, A., Haigh, I. D., Nicholls, R. J., Winter, H., Neal, R., Wahl, T., Joly-Laugel, A., and Darby, S. E.: Assessing the characteristics and drivers of compound flooding events around the UK coast, Hydrol. Earth Syst. Sci., 23, 3117–3139, https://doi.org/10.5194/hess-23-3117-2019, 2019.

Hersbach, H., Bell, B., Berrisford, P., Horányi, A., Sabater, J. M., Nicolas, J., Radu, R., Schepers, D., Simmons, A., Soci, C. and Dee, D.: Global reanalysis: goodbye ERA-Interim, hello ERA5, ECMWF Newsl., (159), 17–24, 2019.

Hersbach, H., Bell, B., Berrisford, P., Hirahara, S., Horányi, A., Muñoz-Sabater, J., Nicolas, J., Peubey, C., Radu, R., Schepers, D., Simmons, A., Soci, C., Abdalla, S., Abellan, X., Balsamo, G., Bechtold, P., Biavati, G., Bidlot, J., Bonavita, M., De Chiara, G., Dahlgren, P., Dee, D., Diamantakis, M., Dragani, R., Flemming, J., Forbes, R., Fuentes, M., Geer, A., Haimberger, L., Healy, S., Hogan, R. J., Hólm, E., Janisková, M., Keeley, S., Laloyaux, P., Lopez, P., Lupu, C., Radnoti, G., de Rosnay, P., Rozum, I., Vamborg, F., Villaume, S. and Thépaut, J. N.: The ERA5 global reanalysis, Q. J. R. Meteorol. Soc., (March), 1–51, 2020.

Hersbach, H., De Rosnay, P., Bell, B., Schepers, D., Simmons, A., Soci, C., Abdalla, S., Balmaseda, A., Balsamo, G., Bechtold, P., Berrisford, P., Bidlot, J., De Boisséson, E., Bonavita, M., Browne, P., Buizza, R., Dahlgren, P., Dee, D., Dragani, R., Diamantakis, M., Flemming, J., Forbes, R., Geer, A., Haiden, T., Hólm, E., Haimberger, L., Hogan, R., Horányi, A., Janisková, M., Laloyaux, P., Lopez, P., Muñoz-Sabater, J., Peubey, C., Radu R., Richardson, D., Thépaut, J.-N., Vitart, F., Yang, X., Zsótér, E. and Zuo, H.: Operational global reanalysis: progress, future directions and synergies with NWP including updates on the ERA5 production status, ERA Rep. Ser., 27(8th October), 1–63, 2018.

Hewitt, K., Burton, I.: The Hazardousness of a Place: A Regional Ecology of Damaging Events. U. of Toronto Press, Toronto (154 pp.), 1971.

Hilal, S., Poon, S. H., and Tawn, J.: Hedging the black swan: Conditional heteroskedasticity and tail dependence in S&P500 and VIX, J. Bank. Financ., 35, 2374–2387, 2011.

Hillier, J. K., Matthews, T., Wilby, R. L. and Murphy, C.: Multi-hazard dependencies can increase or decrease risk, Nat. Clim. Chang., 10(7), 595–598, 2020.

Hincks, T. K., Malamud, B. D., Sparks, R. S. J., Wooster, M. J., and Lynham, T. J.: Risk assessment and management of wildfires, in: Risk and uncertainty assessment for natural hazards, edited by: Rougier, J., Sparks, S., and Hill, L., Cambridge University Press, Cambridge, 398–444, 2013.

HM Government: National Flood Resilience Review, available at: https://www.gov.uk/government/publications/national-flood-resilience-review (Accessed 20 October 2020). 2016

Hofstra, N., Haylock, M., New, M., and Jones, P. D.: Testing E-OBS European high-resolution gridded data set of daily precipitation and surface temperature, J. Geophys. Res.-Atmos., 114, D21101, https://doi.org/10.1029/2009JD011799, 2009.

Holley, D. M., Dorling, S. R., Steele, C. J. and Earl, N.: A climatology of convective available potential energy in Great Britain, Int. J. Climatol., 34(14), 3811–3824, 2014.

Hou, A. Y., Kakar, R. K., Neeck, S., Azarbarzin, A. A., Kummerow, C. D., Kojima, M., Oki, R., Nakamura, K. and Iguchi, T.: The global precipitation measurement mission, Bull. Am. Meteorol. Soc., 95(5), 701–722, 2014.

Houze, R. A. and Hobbs, P. V.: Organization and structure of precipitating cloud systems., Adv. Geophys. 24, 225–315, 1982.

Hu, G. and Franzke, C. L. E.: Evaluation of Daily Precipitation Extremes in Reanalysis and Gridded Observation-Based Data Sets Over Germany, Geophys. Res. Lett., 47(18), 2020.

Huang, W., Xu, S., Yan, Y. and Zipf, A.: An exploration of the interaction between urban human activities and daily traffic conditions: A case study of Toronto, Canada, Cities, 2019.

Hulme, M. and Barrow, E.: Climates of the British Isles, Routledge, London, 1997.

Huser, R.: Statistical Modeling and Inference for Spatio-Temporal Extremes, PhD thesis, EPFL, available at: https://infoscience. epfl.ch/record/188557?ln=en (Accessed 28 January 2020), 2013.

Infoclimat: HistorIC, available at: https://www.infoclimat.fr/historic/ (Accessed 20 October 2020), 2020.

Instituto National de Estatistica Portugal, available at: https://www.ine. pt/xportal/xmain?xpid=INE&xpgid=ine_indicadores& indOcorrCod=0004168&contexto=bd&selTab=tab2, (Accessed 1 December 2019), 2019.

International Energy Agency (IEA): World Energy Outlook 2018., 2018.

Iordanidou, V., Koutroulis, A.G., Tsanis, I.K., 2016. Investigating the relationship of lightning activity and rainfall: a case study for Crete Island. Atmos. Res. 172–173, 16–27. https://doi.org/10.1016/j.atmosres.2015.12.021.

IPCC: Managing the Risks of Extreme Events and Disasters to Advance Climate Change Adaptation - SREX, edited by C. B. Field, V. Barros, T. F. Stocker, and Q. Dahe, Cambridge University Press, Cambridge., 2012

IPCC: The Ocean and Cryosphere in a Changing Climate. A Special Report of the Intergovernmental Panel on Climate Change, Intergov. Panel Clim. Chang., 1–765, 2019

IRDR (Integrated Research on Disaster Risk): Perils Classification and Hazards Glossary (IRDR DATA Publication No.1), Beijing., 2014.

Jaroszweski, D., Hooper, E., Baker, C., Chapman, L. and Quinn, A.: The impacts of the 28 June 2012 storms on UK road and rail transport, Meteorol. Appl., 22(3), 470–476, 2015.

Jebson, S.: National Meteorological Library and Archives Fact sheet No 2 Thunderstorm. Met Office, (2), 1–27, 2007.

Joe, H.: Multivariate Models and Multivariate Dependence Concepts. Monographs on Statistics and Applied Probability 73. Chapman and Hall/CRC, London (420 pp.),1997.

Johansson, B. and Chen, D.: The influence of wind and topography on precipitation distribution in Sweden: Statistical analysis and modelling, Int. J. Climatol., 23, 1523–1535, 2003.

Jonkman, S.N., 2005. Global perspectives on loss of human life caused by floods. Nat. Hazards 34, 151–175. https://doi.org/10.1007/s11069-004-8891-3.

Kahle, D. and Wickham, H.: ggmap: Spatial Visualization with gg- plot2, R Journal., 5, 144–161, 2013.

Kameshwar, S. and Padgett, J. E.: Multi-hazard risk assessment of highway bridges subjected to earthquake and hurricane hazards, Eng. Struct., 78, 154–166, 2014.

Kappes, M.S., Gruber, K., Frigerio, S., Bell, R., Keiler, M., Glade, T.: The MultiRISK platform: the technical concept and application of a regional-scale multihazard ex- posure analysis tool. Geomorphology 151–152, 139–155. https://doi.org/10.1016/j. geomorph.2012.01.024, 2012a.

Kappes, M.S., Keiler, M., Glade, T.: From single- to multi-hazard risk analyses: a concept addressing emerging challenges. In: Malet, J.P., Glade, R.,. Casagli, N. (Eds.), Mountain Risks: Bringing Science to Society. CERG Editions, Strasbourg, France, pp. 351–356, 2010.

Kappes, M.S., Keiler, M., von Elverfeldt, K., Glade, T.: Challenges of analyzing multi-hazard risk: a review. Nat. Hazards 64, 1925–1958. https://doi.org/10.1007/ s11069-012-0294-2, 2012b.

Kašpar, M., Müller, M., Crhová, L., Holtanová, E., Polášek, J.F., Pop, L., Valeriánová, A.: Relationship between Czech windstorms and air temperature. Int. J. Climatol. 37, 11–24. https://doi.org/10.1002/joc.4682, 2017.

Keef, C., Papastathopoulos, I., Tawn, J.A.: Estimation of the conditional distribu- tion of a multivariate variable given that one of its components is large: additional constraints for the Heffernan and Tawn model. J. Multivar. Anal. 115, 396–404. https://doi.org/10.1016/j.jmva.2012.10.012, 2013.

Keefer, D.K.: The importance of earthquake-induced landslides to long-term slope erosion and slope-failure hazards in seismically active regions. In: Geomorphology and Natural Hazards. Elsevier, pp. 265–284. https://doi.org/10.1016/B978-0-444- 82012-9.50022-0, 1994.

Keefer, D.K.: Investigating landslides caused by earthquakes - a historical review. Surv. Geophys. 23, 473–510. https://doi.org/10.1023/A:1021274710840, 2002.

Kendon, E. J., Ban, N., Roberts, N. M., Fowler, H. J., Roberts, M. J., Chan, S. C., Evans, J. P., Fosser, G. and Wilkinson, J. M.: Do convection-permitting regional climate models improve projections of future precipitation change?, Bull. Am. Meteorol. Soc., 98(1), 79–93, 2017.

Klerk, W.J., Winsemius, H.C., van Verseveld, W.J., Bakker, A.M.R., Diermanse, F.L.M.: The co-incidence of storm surges and extreme discharges within the Rhine–Meuse Delta. Environ. Res. Lett. 10, 035005. https://doi.org/10.1088/1748- 9326/10/3/035005, 2015.

Koopmans, L. H., Owen, D. B., and Rosenblatt, J. I.: Confidence intervals for the coefficient of variation for the normal and log normal distributions, Biometrika, 51, 25–32, 1964.

Köppen, W.: Die Wärmezonen der Erde, nach der Dauer der heissen, gemässigten und kalten Zeit und nach der Wirkung der Wärme auf die organische Welt betrachtet. Meteorologische, Meteorol. Zeitschrift, 1(21), 5–226, 1884.

Koutroulis, A.G., Grillakis, M.G., Tsanis, I.K., Kotroni, V., Lagouvardos, K.: Lightning activity, rainfall and flash flooding – occasional or interrelated events? A case study in the island of Crete. Nat. Hazards Earth Syst. Sci. 12, 881–891. https:// doi.org/10.5194/nhess-12-881-2012, 2012.

Kumar, M., Klug, J., Alzbutas, R., Burgazzi, L., Farcasiu, M., Nitoi, M., Ivanov, I., Bogdanov, D., Hashimoto, K., Hirata, K., La Rovere, S., Sevbo, O., Vitazkova, J., Hustak, S., Wielenberg, A. and Raimond, E.: Lessons of the Fukushima Dai-ichi accident for PSA (IRSN-PSN-RES-SAG--2017-00021). IRSN, 2016.

Kumasaki, M., King, M., Arai, M., Yang, L.: Anatomy of cascading natural disasters in Japan: main modes and linkages. Nat. Hazards 80 (3), 1425–1441. https://doi. org/10.1007/s11069-015-2028-8, 2016.

Kumbier, K., Carvalho, R.C., Vafeidis, A.T., Woodroffe, C.D.: Investigating com- pound flooding in an estuary using hydrodynamic modelling: a case study from the Shoalhaven

River, Australia. Nat. Hazards Earth Syst. Sci. 18, 463–477. https://doi. org/10.5194/nhess-18-463-2018, 2018.

Kwag, S., Gupta, A.: Probabilistic risk assessment framework for structural systems under multiple hazards using Bayesian statistics. Nucl. Eng. Des. 315, 20–34. https://doi.org/10.1016/j.nucengdes.2017.02.009, 2017.

Lambert, J. and Pedreros, R.: BD Tsunamis. Inventaire historique des tsunamis en France. Bilan des travaux 2011. Rapport final. BRGM/RP-61152-FR. BRGM, 2012.

Lang, T.J., Rutledge, S.A.: Relationships between convective storm kinematics, precipitation, and lightning. Mon. Weather Rev. 130, 2492–2506. https://doi.org/10. 1175/1520-0493(2002)130<2492:RBCSKP>2.0.CO;2, 2002.

Langseth, H., Nielsen, T. D., Rumí, R. and Salmerón, A.: Inference in hybrid Bayesian networks, Reliab. Eng. Syst. Saf., 94(10), 1499–1509, 2009.

Lavell, A., Oppenheimer, M., Diop, C., Hess, J., Lempert, R., Li, J., Muir-Wood, R., Myeong, S., Moser, S., Takeuchi, K., Cardona, O.-D., Hallegatte, S., Lemos, M., Little, C., Lotsch, A., Weber, E.: Climate change: new dimensions in disaster risk, exposure, vulnerability, and resilience. In: Field, C.B., Barros, V., Stocker, T.F., Dahe, Q. (Eds.), Managing the Risks of Extreme Events and Disasters to Advance Climate Change Adaptation. Cambridge Univ. Press, Cambridge, pp. 25–64. https://doi.org/ 10.1017/CBO9781139177245.004, 2012.

Leckebusch, G. C., Renggli, D. and Ulbrich, U.: Development and application of an objective storm severity measure for the Northeast Atlantic region, Meteorol. Zeitschrift, 17(5), 575–587, 2008.

Ledesma, J. L. J. and Futter, M. N.: Gridded climate data products are an alternative to instrumental measurements as inputs to rainfall–runoff models, Hydrol. Process., 31(18), 3283–3293, 2017.

Ledford, A.: Statistics for near independence in multivariate extreme values. Biometrika 83, 169–187. https://doi.org/10.1093/biomet/83.1.169, 1996.

Ledford, A., Tawn, J.: Modelling dependence within joint tail regions. J. R. Stat. Soc. Ser. B (Stat. Methodol.) 59, 475–499. https://doi.org/10.1111/1467-9868. 00080, 1997.

Ledford, A. and Tawn, J.: Diagnostics for dependence within time series extremes, J. Roy. Stat. Soc. B, 65, 521–543, 2003.

Leonard, M., Westra, S., Phatak, A., Lambert, M., van den Hurk, B., McInnes, K., Risbey, J., Schuster, S., Jakob, D., Stafford-Smith, M.: A compound event framework for understanding extreme impacts. Wiley Interdiscip. Rev. Clim. Chang. 5, 113–128. https://doi.org/10.1002/wcc.252, 2014.

Lhotka, O. and Kyselý, J.: Characterizing joint effects of spatial extent, temperature magnitude and duration of heat waves and cold spells over Central Europe, Int. J. Climatol., 35(7), 1232–1244, 2015.

Lian, J.J., Xu, K., Ma, C.: Joint impact of rainfall and tidal level on flood risk in a coastal city with a complex river network: a case study of Fuzhou City, China. Hydrol. Earth Syst. Sci. 17, 679–689. https://doi.org/10.5194/hess-17-679-2013, 2013.

Liberato, M. L. R., Pinto, J. G., Trigo, R. M., Ludwig, P., Ordóñez, P., Yuen, D. and Trigo, I. F.: Explosive development of winter storm Xynthia over the subtropical North Atlantic Ocean, Nat. Hazards Earth Syst. Sci., 13(9), 2239–2251, 2013.

Littell, J. S., McKenzie, D., Peterson, D. L., and Westerling, A. L.: Climate and wildfire area burned in western US ecoprovinces, 1916–2003, Ecol. Appl., 19, 1003–1021, 2009.

Littell, J.S., Peterson, D.L., Riley, K.L., Liu, Y., Luce, C.H.: A review of the re- lationships between drought and forest fire in the United States. Glob. Chang. Biol. 22 (7), 2353–2369. https://doi.org/10.1111/gcb.13275, 2016.

Liu, B., Siu, Y.L., Mitchell, G.: Hazard interaction analysis for multi-hazard risk assessment: a systematic classification based on hazard-forming environment. Nat. Hazards Earth Syst. Sci. 16, 629–642. https://doi.org/10.5194/nhess-16-629-2016, 2016.

Liu, B., Siu, Y. L. and Mitchell, G.: A quantitative model for estimating risk from multiple interacting natural hazards: an application to northeast Zhejiang, China, Stoch. Environ. Res. Risk Assess., 31(6), 1319–1340, 2017.

Liu, Z., Nadim, F., Garcia-Aristizabal, A., Mignan, A., Fleming, K., Luna, B.Q.: A three-level framework for multi-risk assessment. Georisk: Assessment and Management of Risk for Engineered Systems and Geohazards 9 (2), 59–74. https:// doi.org/10.1080/17499518.2015.1041989, 2015.

Liu, Z., Cheng, L., Hao, Z., Li, J., Thorstensen, A., and Gao, H.: A framework for exploring joint effects of conditional factors on compound floods, Water Resour. Res., 54, 2681–2696, 2018.

Lizundia-Loiola, J., Otón, G., Ramo, R. and Chuvieco, E.: A spatio-temporal active-fire clustering approach for global burned area mapping at 250 m from MODIS data, Remote Sens. Environ., 236, 111493, 2020.

Loukatou, A., Howell, S., Johnson, P., and Duck, P.: Stochastic wind speed modelling for estimation of expected wind power output, Appl. Energ., 228, 1328–1340, 2018.

Luger, S.A., Harris, R.L.: Modelling tsunamis generated by earthquakes and sub- marine slumps using MIKE 21. In: International MIKE by DHI Conference 2010, 6–8 Sep. 2010, Copenhagen, Denmark, Conference Proceedings. vol. P017. pp. 1–13, available at. https://www.dhigroup.com/upload/publications/mike21/Luger_2010.pdf, 2010.

Lung, T., Lavalle, C., Hiederer, R., Dosio, A. and Bouwer, L. M.: A multi-hazard regional level impact assessment for Europe combining indicators of climatic and non-climatic change, Glob. Environ. Chang., 23(2), 522–536, 2013.

Mahlstein, I., Daniel, J. S. and Solomon, S.: Pace of shifts in climate regions increases with global temperature, Nat. Clim. Chang., 3(8), 739–743, 2013.

Mahto, S. S. and Mishra, V.: Does ERA-5 Outperform Other Reanalysis Products for Hydrologic Applications in India?, J. Geophys. Res. Atmos., 124(16), 9423–9441, 2019.

Mailier, P. J., Stephenson, D. B., Ferro, C. A. T. and Hodges, K. I.: Serial clustering of extratropical cyclones, Mon. Weather Rev., 134(8), 2224–2240, 2006.

Malamud, B. D. and Turcotte, D. L.: Self-affine time series: I. Generation and analyses, Adv. Geophys., 40, 1–90, 1999.

Malamud, B. D., Turcotte, D. L., Guzzetti, F. and Reichenbach, P.: Landslide inventories and their statistical properties, Earth Surf. Process. Landforms, 29(6), 687–711, 2004.

Malamud, B. D. and Turcotte, D. L.: The applicability of power-law frequency statistics to floods, J. Hydrol., 322, 168–180, 2006.

Malamud, B. D., Turcotte, D. L. and Brooks, H. E.: Spatial-temporal clustering of tornadoes, Nat. Hazards Earth Syst. Sci., 16(12), 2823–2834, 2016.

Manning, C., Widmann, M., Bevacqua, E., Van Loon, A. F., Maraun, D. and Vrac, M.: Soil moisture drought in Europe: A compound event of precipitation and potential evapotranspiration on multiple time scales, J. Hydrometeorol., 19(8), 1255–1271, 2018.

Manning, C., Widmann, M., Bevacqua, E., Van Loon, A. F., Maraun, D. and Vrac, M.: Increased probability of compound long-duration dry and hot events in Europe during summer (1950-2013), Environ. Res. Lett., 14(9), 2019.

Martius, O., Pfahl, S., and Chevalier, C.: A global quantification of compound precipitation and wind extremes, Geophys. Res. Lett., 43, 7709–7717, 2016.

Marzocchi, W., Garcia-Aristizabal, A., Gasparini, P., Mastellone, M.L., Di Ruocco, A.: Basic principles of multi-risk assessment: a case study in Italy. Nat. Hazards 62, 551–573. https://doi.org/10.1007/s11069-012-0092-x, 2012.

Masarotto, G. and Varin, C.: Gaussian copula regression in R, J. Stat. Softw., 77(1), 2017.

Masina, M., Lamberti, A., Archetti, R.: Coastal flooding: a copula based approach for estimating the joint probability of water levels and waves. Coast. Eng. 97, 37–52. https://doi.org/10.1016/j.coastaleng.2014.12.010, 2015.

Matos, J. P., Mignan, A. and Schleiss, A. J.: Vulnerability of large dams considering hazard interactions: conceptual application of the Generic Multi-Risk framework, in 13th ICOLD International Benchmark Workshop on Numerical Analysis of Dams, pp. 1–8., 2015.

Maulik, K. and Resnick, S.: Characterizations and examples of hid- den regular variation, Extremes, 7, 31–67, 2005.

Mazas, F., Hamm, L.: An event-based approach for extreme joint probabilities of waves and sea levels. Coast. Eng. 122, 44–59. https://doi.org/10.1016/j.coastaleng. 2017.02.003, 2017.

McGuire, R. K.: Probabilistic seismic hazard analysis: Early history, Earthq. Eng. Struct. Dyn., 37(3), 329–338, 2008.

Melet, A., Teatini, P., Le Cozannet, G., Jamet, C., Conversi, A., Benveniste, J. and Almar, R.: Earth Observations for Monitoring Marine Coastal Hazards and Their Drivers, Springer Netherlands, 2020.

Menberg, K., Heo, Y. and Choudhary, R.: Sensitivity analysis methods for building energy models: Comparing computational costs and extractable information, Energy Build., 133, 433–445, 2016.

Meng, L., Shen, Y.: On the relationship of soil moisture and extreme temperatures in East China. Earth Interact. 18, 1–20. https://doi.org/10.1175/2013EI000551.1, 2014.

Merz, B., Kuhlicke, C., Kunz, M., Pittore, M., Babeyko, A., Bresch, D. N., Domeisen, D. I. V., Feser, F., Koszalka, I., Kreibich, H., Pantillon, F., Parolai, S., Pinto, J. G., Punge, H. J., Rivalta, E., Schröter, K., Strehlow, K., Weisse, R. and Wurpts, A.: Impact Forecasting to Support Emergency Management of Natural Hazards, Rev. Geophys., 58(4), 1–52, 2020.

Met Office: Winter Storms, January to February 2014. available at: www. metoffice.gov.uk/climate/uk/interesting/2014-janwind (Accessed 17 September 2017),2015.

Met Office: How we measure wind, available at: https: //www.metoffice.gov.uk/weather/guides/observations/ how-we-measure-wind, (Accessed 12 November 2019), 2019.

Met Office: Past weather events, available at: https://www.metoffice.gov.uk/weather/learn-about/past-uk-weather-events (Accessed 28 October 2020), 2020.

Meunier, P., Hovius, N. and Haines, A. J.: Regional patterns of earthquake-triggered landslides and their relation to ground motion, Geophys. Res. Lett., 34(20), 1–5, 2007.

Mignan, A., Wiemer, S., Giardini, D.: The quantification of low-probability–high- consequences events: part I. a generic multi-risk approach. Nat. Hazards 73, 1999–2022. https://doi.org/10.1007/s11069-014-1178-4, 2014.

Mignan, A., Scolobig, A., Sauron, A.: Using reasoned imagination to learn about cascading hazards: a pilot study. Disaster Prev Manag 25, 329–344. https://doi.org/ 10.1108/DPM-06-2015-0137, 2016.

Milligan, G. W. and Cooper, M. C.: Methodology Review: Clustering Methods, Appl. Psychol. Meas., 11(4), 329–354, 1987.

Ming, X., Xu, W., Li, Y., Du, J., Liu, B., Shi, P.: Quantitative multi-hazard risk assessment with vulnerability surface and hazard joint return period. Stoch. Environ. Res. Risk Assess. 29, 35–44. https://doi.org/10.1007/s00477-014-0935-y, 2015.

Minola, L., Zhang, F., Azorin-Molina, C., Pirooz, A. A. S., Flay, R. G. J., Hersbach, H. and Chen, D.: Near-surface mean and gust wind speeds in ERA5 across Sweden: towards an improved gust parametrization, Clim. Dyn., 55(3–4), 887–907, 2020.

Miralles, D. G., Teuling, A. J., Van Heerwaarden, C. C. and De Arellano, J. V. G.: Mega-heatwave temperatures due to combined soil desiccation and atmospheric heat accumulation, Nat. Geosci., 7(5), 345–349, 2014.

Miranda, P. M. A., Coelho, F. E. S., Tomé, A. R., Valente, M. A., Carvalho, A., Pires, C., Pires, H. O., Pires, V. C., and Ramalho, C.: 20th Century Portuguese Climate and Climate Scenarios, in: Climate Change in Portugal. Scenarios, Impacts and Adaptation Measures – SIAM Project, edited by: Santos, F. D., Forbes, K., and Moita, R., Gradiva Publishers, Lisbon, 28–83, 2002.

Miyagi, T., Higaki, D., Yagi, H., Doshida, S., Chiba, N., Umemura, J. and Satoh, G.: Reconnaissance report on landslide disasters in northeast Japan following the M 9 Tōhoku earthquake, Landslides, 8(3), 339–342, 2011.

Moftakhari, H.R., Salvadori, G., AghaKouchak, A., Sanders, B.F., Matthew, R.A.: Compounding effects of sea level rise and fluvial flooding. Proc. Natl. Acad. Sci. 114, 9785–9790. https://doi.org/10.1073/pnas.1620325114, 2017.

Molinari, J., Moore, P., Idone, V.: Convective structure of hurricanes as revealed by lightning locations. Mon. Weather Rev. 127, 520–534. https://doi.org/10.1175/ 1520-0493(1999)127<0520:CSOHAR>2.0.CO;2, 1999.

Morel, C. and Senesi, S.: A climatology of mesoscale convective systems over Europe using satellite infrared imagery. I: Methodology, Q. J. R. Meteorol. Soc., 128(584 PART B), 1953–1971, 2002.

Myers, R.K., van Lear, D.H.: Hurricane-fire interactions in coastal forests of the south: a review and hypothesis. Forest Ecol. Manag. 103 (2–3), 265–276. https://doi. org/10.1016/S0378-1127(97)00223-5, 1998.

Nadim, F., Liu, Z., Woo, G., Zschau, J., Zhongqiang, L., Woo, G. and Zschau, J.: D5.2 Framework for multi-risk assessment. MATRIX, Potsdam, pp. 1–57, 2013.

Narsis: NARSIS project, available at: http://www.narsis.eu/, (Accessed 12 September 2020), 2020.

NASA: What is Remote Sensing?, available at: https://earthdata.nasa.gov/learn/remote-sensing, (Accessed 12 September 2020), 2020.

Nash, J.E., Sutcliffe, J.V.: River flow forecasting through conceptual models part I — a discussion of principles. J. Hydrol. 10, 282–290. https://doi.org/10.1016/0022- 1694(70)90255-6, 1970.

Neal, R., Fereday, D., Crocker, R. and Comer, R. E.: A flexible approach to defining weather patterns and their application in weather forecasting over Europe, Meteorol. Appl., 23(3), 389–400, 2016.

Nelder, J.A., Baker, R.J.: Generalized linear models. In: Kotz, S., Read, C.B., Balakrishnan, N., Vidakovic, B., Johnson, N.L. (Eds.), Encyclopedia of Statistical Sciences. John Wiley &

Sons, Inc., Hoboken, NJ, USA, pp. 370–384. https://doi.org/10.1002/0471667196.ess0866.pub2, 2006.

Nelsen, R.: An Introduction to Copulas, Springer Series in Statistics. Springer- Verlag, London. https://doi.org/10.1007/0-387-28678-0, 2006.

Nguyen Sinh, H., Lombardo, F. T., and Letchford, C.: Multivariate simulation for assessing the joint wind and ice hazard in the United States, J. Wind Eng. Ind. Aerodyn., 184, 436–444, 2019.

Nguyen, A. T. and Reiter, S.: A performance comparison of sensitivity analysis methods for building energy models, Build. Simul., 8(6), 651–664, 2015.

Norio, O., Ye, T., Kajitani, Y., Shi, P. and Tatano, H.: The 2011 eastern Japan great earthquake disaster: Overview and comments, Int. J. Disaster Risk Sci., 2(1), 34–42, 2011.

Orencio, P.M., Fujii, M.: A spatiotemporal approach for determining disaster-risk potential based on damage consequences of multiple hazard events. J. Risk Res. 17, 815–836. https://doi.org/10.1080/13669877.2013.816334, 2014.

Paprotny, D., Kreibich, H., Morales-Nápoles, O., Terefenko, P. and Schröter, K.: Estimating exposure of residential assets to natural hazards in Europe using open data, Nat. Hazards Earth Syst. Sci., 20(1), 323–343, 2020.

Pelinovsky, E., Poplavsky, A.: Simplified model of tsunami generation by sub- marine landslides. Phys. Chem. Earth 21, 13–17. https://doi.org/10.1016/S0079- 1946(97)00003-7, 1996.

Pereira, M. G., Malamud, B. D., Trigo, R. M., and Alves, P. I.: The history and characteristics of the 1980–2005 Portuguese rural fire database, Nat. Hazards Earth Syst. Sci., 11, 3343–3358, https://doi.org/10.5194/nhess-11-3343-2011, 2011.

Perkins, S. E.: A review on the scientific understanding of heatwaves-Their measurement, driving mechanisms, and changes at the global scale, Atmos. Res., 164–165, 242–267, 2015

Pescaroli, G., Alexander, D.: Understanding compound, interconnected, interacting, and cascading risks: a holistic framework. Risk Anal. 38, 2245–2257. https://doi.org/10.1111/risa.13128, 2018.

Petroliagkis, T.I.: Estimations of statistical dependence as joint return period modulator of compound events – part 1: storm surge and wave height. Nat. Hazards Earth Syst. Sci. 18, 1937–1955. https://doi.org/10.5194/nhess-18-1937-2018, 2018.

Pfahl, S., Madonna, E., Boettcher, M., Joos, H. and Wernli, H.: Warm conveyor belts in the ERA-Interim Dataset (1979-2010). Part II: Moisture origin and relevance for precipitation, J. Clim., 27(1), 27–40, 2014.

Pfahl, S. and Wernli, H.: Quantifying the relevance of cyclones for precipitation extremes, J. Clim., 25(19), 6770–6780, 2012.

Philipp, A., Bartholy, J., Beck, C., Erpicum, M., Esteban, P., Fettweis, X., Huth, R., James, P., Jourdain, S., Kreienkamp, F., Krennert, T., Lykoudis, S., Michalides, S. C., Pianko-Kluczynska, K., Post, P., Álvarez, D. R., Schiemann, R., Spekat, A. and Tymvios, F. S.:

Cost733cat - A database of weather and circulation type classifications, Phys. Chem. Earth, 35, 360–373, 2010.

Phillips, J. D.: The Role of Spatial Scale in Geomorphic Systems, Geogr. Anal., 20(4), 308–317, 1988.

Pickands, J.: Statistical Inference Using Extreme Order Statistics, Ann. Stat., 3(1), 119–131, 1975.

Pickands, J.: Multivariate extreme value distribution, in Proceedings of the 43th Session of International Statistical Institution, Buenos Aires., 1981.

Piepgrass, M. V, Krider, E. P. and Moore, C. B.: Lightning and surface rainfall during Florida thunderstorms, J. Geophys. Res. Ocean., 87(C13), 11193–11201, 1982.

Pinto, J. G., Karremann, M. K., Born, K., Della-Marta, P. M. and Klawa, M.: Loss potentials associated with European windstorms under future climate conditions, Clim. Res., 54(1), 1–20, 2012.

Pircalabelu, E., Claeskens, G., Gijbels, I.: Copula directed acyclic graphs. Stat. Comput. 27, 55–78. https://doi.org/10.1007/s11222-015-9599-9, 2017.

Poelhekke, L., Jäger, W.S., van Dongeren, A., Plomaritis, T.A., McCall, R., Ferreira, Ó.: Predicting coastal hazards for sandy coasts with a Bayesian Network. Coast. Eng. 118, 21–34. https://doi.org/10.1016/j.coastaleng.2016.08.011, 2016.

Poljansek, K., Marin Ferrer, M., De Groeve, T. and Clark, I.: Science for disaster risk management 2017. Knowing better and losing less, Publications Office of the European Union, Luxembourg., 2017.

Power, W., Clark, K., King, D.N., Borrero, J., Howarth, J., Lane, E.M., Goring, D., Goff, J., Chagué-Goff, C., Williams, J., Reid, C.: Tsunami runup and tide-gauge ob- servations from the 14 November 2016 M7. 8 Kaikōura earthquake, New Zealand. Pure Appl. Geophys. 174 (7), 2457–2473. https://doi.org/10.1007/s00024-017- 1566-2, 2017.

Prein, A. F. and Holland, G. J.: Global estimates of damaging hail hazard, Weather Clim. Extrem., 22, 10–23, 2018.

Price, C., Federmesser, B.: Lightning-rainfall relationships in Mediterranean winter thunderstorms. Geophys. Res. Lett. 33, L07813. https://doi.org/10.1029/ 2005GL024794, 2006.

Priestley, M. D. K., Dacre, H. F., Shaffrey, L. C., Hodges, K. I. and Pinto, J. G.: The role of serial European windstorm clustering for extreme seasonal losses as determined from multi-centennial simulations of high-resolution global climate model data, Nat. Hazards Earth Syst. Sci., 18(11), 2991–3006, 2018.

Punge, H. J. and Kunz, M.: Hail observations and hailstorm characteristics in Europe: A review, Atmos. Res., 176–177, 159–184, 2016.

Radovanovic, M., Vyklyuk, Y., Stevancevic, M., Milenkovic, M., Jakovljevic, D., Petrovic, M., Malinovic-Milicevic, S., Vukovic, N., Vujko, A., Yamashkin, A., Sydor, P., Vukovic, D.

and Skoda, M.: Forest fires in Portugal - case study, 18 june 2017, Therm. Sci., 23(1), 73–86, 2019.

Rahman, M. S., Yang, R. and Di, L.: Clustering Indian Ocean tropical cyclone tracks by the standard deviational ellipse, Climate, 6(2), 2018.

Ramsay, H. A., Camargo, S. J. and Kim, D.: Cluster analysis of tropical cyclone tracks in the Southern Hemisphere, Clim. Dyn., 39(3–4), 897–917, 2012.

Raveh-Rubin, S. and Wernli, H.: Large-scale wind and precipitation extremes in the Mediterranean: dynamical aspects of five se- lected cyclone events, Q. J. R. Meteorol. Soc., 142, 3097–3114, 2016.

Rebetez, M., Dupont, O. and Giroud, M.: An analysis of the July 2006 heatwave extent in Europe compared to the record year of 2003, Theor. Appl. Climatol., 95(1–2), 1–7, 2009.

Reichenbach, P., Rossi, M., Malamud, B., Mihir, M., Guzzetti, F.: A review of statistically-based landslide susceptibility models. Earth Sci. Rev. 180, 60–91. https://doi.org/10.1016/j.earscirev.2018.03.001, 2018.

Resnick, S. I.: Extreme Values, Regular Variation and Point Processes, Springer New York, New York, USA, 1987.

Resnick, S. I.: Hidden regular variation, second order regular variation and asymptotic independence, Extremes, 5, 303–336, 2002.

Ridder, N. N., Pitman, A. J., Westra, S., Ukkola, A., Hong, X. Do, Bador, M., Hirsch, A. L., Evans, J. P., Di Luca, A. and Zscheischler, J.: Global hotspots for the occurrence of compound events, Nat. Commun., 11(1). https://doi.org/10.1038/s41467-020-19639-3, 2020.

Rigo, T., Berenguer, M. and Llasat, M. del C.: An improved analysis of mesoscale convective systems in the western Mediterranean using weather radar, Atmos. Res., 227(November 2018), 147–156, 2019.

Rivoire, P., Martius, O. and Naveau, P.: A comparison of moderate and extreme ERA-5 daily precipitation with two observational data sets, Earth Sp. Sci., 1–23, 2021.

Roberts, J. F., Champion, A. J., Dawkins, L. C., Hodges, K. I., Shaffrey, L. C., Stephenson, D. B. and Stringer, M. A.: The XWS open access catalogue of extreme European windstorms from 1979 to 2012, , 2487–2501, 2014.

Rodríguez, C. E., Bommer, J. J. and Chandler, R. J.: Earthquake-induced landslides: 1980-1997, Soil Dyn. Earthq. Eng., 18(5), 325–346, 1999.

Rueda, A., Camus, P., Tomás, A., Vitousek, S., Méndez, F.J.: A multivariate extreme wave and storm surge climate emulator based on weather patterns. Ocean Model 104, 242–251. https://doi.org/10.1016/j.ocemod.2016.06.008, 2016.

Sachs, M. K., Yoder, M. R., Turcotte, D. L., Rundle, J. B., and Malamud, B. D.: Black swans, power laws, and dragon-kings: Earthquakes, volcanic eruptions, landslides, wildfires, floods, and SOC models, Eur. Phys. J. Spec. Top., 205, 167–182, 2012.

Sadegh, M., Ragno, E., AghaKouchak, A.: Multivariate copula analysis toolbox (MvCAT): describing dependence and underlying uncertainty using a Bayesian fra- mework. Water Resour. Res. 53, 5166–5183. https://doi.org/10.1002/ 2016WR020242, 2017.

Sadegh, M., Moftakhari, H., Gupta, H. V., Ragno, E., Mazdiyasni, O., Sanders, B., Matthew, R., and AghaKouchak, A.: Multihaz- ard scenarios for analysis ofcompound extreme events, Geophys. Res. Lett., 45, 5470–5480, 2018.

Saha, S., Moorthi, S., Pan, H. L., Wu, X., Wang, J., Nadiga, S., Tripp, P., Kistler, R., Woollen, J., Behringer, D., Liu, H., Stokes, D., Grumbine, R., Gayno, G., Wang, J., Hou, Y. T., Chuang, H. Y., Juang, H. M. H., Sela, J., Iredell, M., Treadon, R., Kleist, D., Van Delst, P., Keyser, D., Derber, J., Ek, M., Meng, J., Wei, H., Yang, R., Lord, S., Van Den Dool, H., Kumar, A., Wang, W., Long, C., Chelliah, M., Xue, Y., Huang, B., Schemm, J. K., Ebisuzaki, W., Lin, R., Xie, P., Chen, M., Zhou, S., Higgins, W., Zou, C. Z., Liu, Q., Chen, Y., Han, Y., Cucurull, L., Reynolds, R. W., Rutledge, G. and Goldberg, M.: The NCEP climate forecast system reanalysis, Bull. Am. Meteorol. Soc., 91(8), 1015–1057, 2010.

Saltelli, A., Tarantola, S., Campolongo, F. and Ratto, M.: Sensitivity Analysis in Practice: A Guide to Assessing Scientific Models. John Wiley & Sons, Ltd, Chichester, 2004.

Salvadori, G.: Bivariate return periods via 2-Copulas, Stat. Methodol., 1, 129–144, 2004.

Salvadori, G. and De Michele, C.: Multivariate multiparameter extreme value models and return periods: A cop- ula approach, Water Resour. Res., 46, 2009WR009040, https://doi.org/10.1029/2009WR009040, 2010.

Salvadori, G., Durante, F., De Michele, C., Bernardi, M., and Petrella, L.: A multivariate copula-based framework for dealing with hazard scenarios and failure probabilities, Water Resour. Res., 52, 3701–3721, 2016.

Salvadori, G., Tomasicchio, G. R. and D'Alessandro, F.: Practical guidelines for multivariate analysis and design in coastal and off-shore engineering, Coast. Eng., 88, 1–14, 2014.

San-Miguel-Ayanz, J., Moreno, J. M. and Camia, A.: Analysis of large fires in European Mediterranean landscapes: Lessons learned and perspectives, For. Ecol. Manage., 294, 11–22, 2013.

Schauwecker, S., Gascón, E., Park, S., Ruiz-Villanueva, V., Schwarb, M., Sempere-Torres, D., Stoffel, M., Vitolo, C. and Rohrer, M.: Anticipating cascading effects of extreme precipitation with pathway schemes - Three case studies from Europe, Environ. Int., 127, 291–304, 2019.

Schmidt, J., Matcham, I., Reese, S., King, A., Bell, R., Henderson, R., Smart, G., Cousins, J., Smith, W. and Heron, D.: Quantitative multi-risk analysis for natural hazards: A framework for multi-risk modelling, Nat. Hazards, 58(3), 1169–1192, 2011.

Schmidt-Thomé, P. and Kallio, H.: Natural and technological hazard maps of Europe, In: Schmidt-Thomé, P. (Ed.), Natural and Technological Hazards and Risks Affecting the

Spatial Development of European Regions. Geological Survey of Finland Special Paper, vol. 42. pp. 17–63, 2006.

Schoenenwald, N.: Les tempêtes en France et dans les îles Britanniques : des aléas aux événements. PhD thesis, Université Paris I Panthéon-Sorbonne, 2013.

Schultz, C.J., Petersen, W.A., Carey, L.D.: Lightning and severe weather: a com- parison between total and cloud-to-ground lightning trends. Weather Forecast. 26, 744–755. https://doi.org/10.1175/WAF-D-10-05026.1, 2011.

Schumm, S. A. and Lichty, R. W.: Time, space, and causality in geomorphology, Am. J. Sci., 263(2), 110–119, 1965.

Schwarz, G.: Estimating the dimension of a model, Ann. Stat., 6, 461–464, 1978.

Scutari, M.: Learning Bayesian Networks with the bnlearn R Package, , VV(Ii), 2009.

Sedlmeier, K., Feldmann, H. and Schädler, G.: Compound summer temperature and precipitation extremes over central Europe, Theor. Appl. Climatol., 131(3–4), 1493–1501, 2018.

Seneviratne, S.I., Nicholls, N., Easterling, D., Goodess, C.M., Kanae, S., Kossin, J., Luo, Y., Marengo, J., McInnes, K., Rahimi, M., Reichstein, M., Sorteberg, A., Vera, C., Zhang, X., Rusticucci, M., Semenov, V., Alexander, L.V., Allen, S., Benito, G., Cavazos, T., Clague, J., Conway, D., Della-Marta, P.M., Gerber, M., Gong, S., Goswami, B.N., Hemer, M., Huggel, C., van den Hurk, B., Kharin, V.V., Kitoh, A., Tank, A.M.G.K., Li, G., Mason, S., McGuire, W., van Oldenborgh, G.J., Orlowsky, B., Smith, S., Thiaw, W., Velegrakis, A., Yiou, P., Zhang, T., Zhou, T., Zwiers, F.W.: Changes in climate extremes and their impacts on the natural physical environment. In: Field, C.B., Barros, V., Stocker, T.F., Dahe, Q. (Eds.), Managing the Risks of Extreme Events and Disasters to Advance Climate Change Adaptation. Cambridge Univ. Press, Cambridge, pp. 109–230. https://doi.org/10.1017/CBO9781139177245.006, 2012.

Serinaldi, F.: Dismissing return periods!, Stoch. Environ. Res. Risk Assess., 29, 1179–1189, 2015.

Serinaldi, F.: Can we tell more than we can know? The limits of bivariate drought analyses in the United States, Stoch. Environ. Res. Risk Assess., 30, 1691–1704, https://doi.org/10.1007/s00477-015-1124-3, 2016.

Shakesby, R.A., Doerr, S.H., Wildfire as a hydrological and geomorphological agent. Earth Sci. Rev. 74 (3–4), 269–307. https://doi.org/10.1016/j.earscirev.2005. 10.006, 2006.

Sharifi, E., Eitzinger, J. and Dorigo, W.: Performance of the state-of-the-art gridded precipitation products over mountainous terrain: A regional study over Austria, Remote Sens., 11(17), 1–20, 2019.

Sharkey, P.: Statistical models for extreme weather events. PhD thesis, Lancaster University, 2018.

Sheffield, J., Wood, E. F., Pan, M., Beck, H., Coccia, G., Serrat-Capdevila, A. and Verbist, K.: Satellite Remote Sensing for Water Resources Management: Potential for Supporting

Sustainable Development in Data-Poor Regions, Water Resour. Res., 54(12), 9724–9758, 2018.

Shi, Z. and Pun-Cheng, L. S. C.: Spatiotemporal data clustering: A survey of methods, ISPRS Int. J. Geo-Information, 8(3), 2019.

Schneider, D.C.: Quantitative ecology: spatial and temporal scaling. Academic Press, San Diego, 1994.

Sillmann, J., Shepherd, T. G., van den Hurk, B., Hazeleger, W., Martius, O., Slingo, J. and Zscheischler, J.: Event‐Based Storylines to Address Climate Risk, Earth’s Futur., 9(2). http://dx.doi.org/10.1016/j.wace.2016.07.001, 2021.

Silva-Araya, W., Santiago-Collazo, F., Gonzalez-Lopez, J., Maldonado-Maldonado, J.: Dynamic modeling of surface runoff and storm surge during hurricane and tropical storm events. Hydrology 5, 13. https://doi.org/10.3390/hydrology5010013, 2018.

Silvestro, F., Rebora, N., Rossi, L., Dolia, D., Gabellani, S., Pignone, F., Trasforini, E., Rudari, R., De Angeli, S., Masciulli, C.: What if the 25 October 2011 event that struck Cinque Terre (Liguria) had happened in Genoa, Italy? Flooding scenarios, hazard mapping and damage estimation. Nat. Hazards Earth Syst. Sci. 16, 1737–1753. https://doi.org/10.5194/nhess-16-1737-2016, 2016.

Simon, T., Fabsic, P., Mayr, G. J., Umlauf, N. and Zeileis, A.: Probabilistic forecasting of thunderstorms in the Eastern Alps. Working Papers in Economics and Statistics, University of Innsbruck, 25, 2017.

Singh, V. P., Jain, S. K., Tyagi, A. and Drive, A. B.: Risk and Reliability Analysis, American Society of Civil Engineers. American Society of Civil Engineers, Reston, 2007.

Sklar, A.: Fonction de répartition dont les marges sont données, Publications de l’Institut Statistique de l’Université de Paris, 8, 229–231, 1959.

Stephens, M. A.: Use of the Kolmogorov-Smirnov, Cramer-Von Mises and related statistics without extensive tables, J. R. Stat. Soc. Ser. B, 32, 115–122, 1970.

Skok, G., Žagar, N., Honzak, L., Žabkar, R., Rakovec, J. and Ceglar, A.: Precipitation intercomparison of a set of satellite- and raingauge-derived datasets, ERA Interim reanalysis, and a single WRF regional climate simulation over Europe and the North Atlantic, Theor. Appl. Climatol., 123(1–2), 217–232, 2016.

Smith, L. C.: Satellite remote sensing of river inundation area, stage, and discharge: A review, Hydrol. Process., 11(10), 1427–1439, 1997.

Soubeyroux, J.-M., Dosnon, F., Richon, J., Schneider, M. and Lassegues, P.: Caractérisation à haute résolution spatiale des tempêtes historiques en métropole : application à la tempête Zeus du 6 mars 2017, Climatologie, 14, 96–106, 2017.

Sperotto, A., Molina, J.L., Torresan, S., Critto, A., Marcomini, A.: Reviewing Bayesian networks potentials for climate change impacts assessment and manage- ment: a multi-risk perspective. J. Environ. Manag. 202, 320–331. https://doi.org/10.1016/j.jenvman.2017.07.044, 2017.

Spinoni, J., Barbosa, P., De Jager, A., McCormick, N., Naumann, G., Vogt, J. V., Magni, D., Masante, D. and Mazzeschi, M.: A new global database of meteorological drought events from 1951 to 2016, J. Hydrol. Reg. Stud., 22, 100593, 2019.

Starkel, L.: Space and time scales in geomorphology, Zeitschrift fur Geomorphol. Suppl., 115, 19–33, 1999.

Stefanon, M., Dandrea, F. and Drobinski, P.: Heatwave classification over Europe and the Mediterranean region, Environ. Res. Lett., 7(1), 2012.

Steyn, D. G., Oke, T. R., Hay, J. E. and Knox, J. L.: On scales in meteorology and climatology, Climatol. Bull., 39, 1–8, 1981.

Strauss, C., Rosa, M. B. and Stephany, S.: Spatio-temporal clustering and density estimation of lightning data for the tracking of convective events, Atmos. Res., 134, 87–99, 2013.

Suppasri, A., Imamura, F., Koshimura, S., 2012. Tsunamigenic ratio of the Pacific Ocean earthquakes and a proposal for a tsunami index. Nat. Hazards Earth Syst. Sci. 12, 175–185. https://doi.org/10.5194/nhess-12-175-2012.

Sutanto, S. J., Vitolo, C., Di Napoli, C., D'Andrea, M., and Van Lanen, H. A. J.: Heatwaves, droughts, and fires: Exploring com- pound and cascading dry hazards at the pan-European scale, Environ. Int., 134, 105276, https://doi.org/10.1016/j.envint.2019. 105276, 2020.

Suursaar, Ü., Kullas, T., Otsmann, M., Saaremäe, I., Kuik, J. and Merilain, M.: Cyclone Gudrun in January 2005 and modelling its hydrodynamic consequences in the Estonian coastal waters, Boreal Environ. Res., 11(2), 143–159, 2006.

Svensson, C., Jones, D.A.: Dependence between sea surge, river flow and pre- cipitation in south and West Britain. Hydrol. Earth Syst. Sci. 8, 973–992. https://doi. org/10.5194/hess-8-973-2004, 2004.

Tarvainen, T., Jarva, J., Greiving, S.: Spatial pattern of hazards and hazard inter- actions in Europe. In: Schmidt-Thomé, P. (Ed.), Natural and Technological Hazards and Risks Affecting the Spatial Development of European Regions. Geological Survey of Finland Special Paper 6, vol. 42. pp. 83–91, 2006.

Tawn, J.: Bivariate extreme value theory: Models and estimation. Biometrika 75, 397–415. https://doi.org/10.1093/biomet/75.3.397, 1988.

Tawn, J.: Modelling multivariate extreme value distributions. Biometrika 77, 245–253. https://doi.org/10.1093/biomet/77.2.245, 1990.

Tedim, F., Leone, V., Amraoui, M., Bouillon, C., Coughlan, M., De- logu, G., Fernandes, P., Ferreira, C., McCaffrey, S., McGee, T., Parente, J., Paton, D., Pereira, M., Ribeiro, L., Viegas, D. and Xanthopoulos, G.: Defining Extreme Wildfire Events: Difficulties, Challenges, and Impacts, Fire, 1, 9, https://doi.org/10.3390/ fire1010009, 2018.

Tencer, B., Bettolli, M. L. and Rusticucci, M.: Compound temperature and precipitation extreme events in southern South America: Associated atmospheric circulation, and simulations by a multi-RCM ensemble, Clim. Res., 68(2–3), 183–199, 2016.

Tencer, B., Weaver, A., and Zwiers, F.: Joint occurrence of daily temperature and precipitation extreme events over Canada, J. Appl. Meteorol. Climatol., 53, 2148–2162, 2014.

Terzi, S., Torresan, S., Schneiderbauer, S., Critto, A., Zebisch, M., Marcomini, A.: Multi-risk assessment in mountain regions: a review of modelling approaches for climate change adaptation. J. Environ. Manag. 232, 759–771. https://doi.org/10.1016/j.jenvman.2018.11.100, 2019.

Thorne, C.: Geographies of UK flooding in 2013/4, Geogr. J., 180(4), 297–309, 2014.

Tiago de Oliveira, J.: Extreme values and meteorology, Theor. Appl. Climatol., 37(4), 184–193, 1986.

Tierz, P., Woodhouse, M. J., Phillips, J. C., Sandri, L., Selva, J., Marzocchi, W. and Odbert, H. M.: A Framework for Probabilistic Multi-Hazard Assessment of Rain-Triggered Lahars Using Bayesian Belief Networks, Front. Earth Sci., 5(September), 1–23, 2017.

Tilloy, A., Malamud, B. D., Winter, H., and Joly-Laugel, A.: A review of quantification methodologies for multi- hazard interrelationships, Earth-Sci. Rev., 196, 102881, https://doi.org/10.1016/j.earscirev.2019.102881, 2019.

Tilloy, A.: Bivariate_models, available at: https://gitlab.com/ doudeg/bivariate_models, (Accessed 11 January 2020), 2020a.

Tilloy, A.: Comparison of bivariate extreme modelling approaches for multi-hazard scenarios, Zenodo, https://doi.org/10.5281/zenodo.3686962, 2020b.

Tinti, S., Pagnoni, G., Piatanesi, A.: Simulation of tsunamis induced by volcanic activity in the Gulf of Naples (Italy). Nat. Hazards Earth Syst. Sci. 3, 311–320. https://doi.org/10.5194/nhess-3-311-2003, 2003.

Tosunoglu, F. and Can, I.: Application of copulas for regional bivariate frequency analysis of meteorological droughts in Turkey, Nat. Hazards, 82(3), 1457–1477, 2016.

Twardosz, R. and Kossowska-Cezak, U.: Exceptionally cold and mild winters in Europe (1951–2010), Theor. Appl. Climatol., 125(1–2), 399–411, 2016.

UERRA: UERRA Project, available at: http://www.uerra.eu/, (Accessed 12 February 2020), 2020.

Ulbrich, U., Leckebusch, G. C. and Pinto, J. G.: Extra-tropical cyclones in the present and future climate: A review, Theor. Appl. Climatol., 96(1–2), 117–131, 2009.

UNDRR (United Nations Office for Disaster Risk Reduction): Sendai Framework for Disaster Risk Reduction, United Nations, Geneva, 2015.

UNDRR (United Nations Office for Disaster Risk Reduction): DRR Terminology, available at: https://www.unisdr.org/we/inform/ terminology (Accessed 29 November 2019), 2017.

UNISDR (United Nations International Strategy for Disaster Reduction (UNISDR)): 2009 UNISDR Terminology on Disaster Risk Reduction, United Nations, Geneva, 2009.

Valenzuela, P., Zêzere, J. L., Domínguez-Cuesta, M. J. and Mora García, M. A.: Empirical rainfall thresholds for the triggering of landslides in Asturias (NW Spain), Landslides, 16(7), 1285–1300, 2019.

Van Den Eeckhaut, M., Hervás, J., Jaedicke, C., Malet, J.-P., Montanarella, L. and Nadim, F.: Statistical modelling of Europe-wide landslide susceptibility using limited landslide inventory data, Landslides, 9(3), 357–369, 2012.

van den Hurk, B., van Meijgaard, E., de Valk, P., van Heeringen, K.-J., Gooijer, J.: Analysis of a compounding surge and precipitation event in the Netherlands. Environ. Res. Lett. 10, 035001. https://doi.org/10.1088/1748-9326/10/3/035001, 2015.

van Verseveld, H. C. W., van Dongeren, A. R., Plant, N. G., Jäger, W. S. and den Heijer, C.: Modelling multi-hazard hurricane damages on an urbanized coast with a Bayesian Network approach, Coast. Eng., 103, 1–14, 2015.

van Westen, C.J., Greiving, S.: Multi-hazard risk assessment and decision making. In: Dalezios, N.R. (Ed.), Environmental Hazards Methodologies for Risk. Int. Water Assoc. (IWA) Publishing, London, pp. 31–94, 2017.

van Westen, C., Kappes, M. S., Luna, B. Q., Frigerio, S., Glade, T. and Malet, J.-P.: Medium-Scale Multi-hazard Risk Assessment of Gravitational Processes, in Mountain Risks: From Prediction to Management and Governance, edited by T. van Asch, J. Corominas, S. Greiving, J.-P. Malet, and S. Sterlacchini, pp. 201–231, Springer Netherlands., 2014.

van Westen, C.J., Montoya, L., Boerboom, L.: Multi-Hazard Risk Assessment using GIS in urban areas: A case study for the city of Turrialba, Costa-Rica. In: Proceedings Regional Workshop on Best Practises in Disaster Mitigation, 24–26 Sep 2002, Bali, Indonesia, pp. 53–72, 2002.

Vaz de Melo Mendes, B., Mendes Semeraro, M. and Câmara Leal, R. P.: Pair-copulas modeling in finance, Financ. Mark. Portf. Manag., 24(2), 193–213, 2010.

Visser-Quinn, A., Beevers, L., Collet, L., Formetta, G., Smith, K., Wanders, N., Thober, S., Pan, M. and Kumar, R.: Spatio-temporal analysis of compound hydro-hazard extremes across the UK, Adv. Water Resour., 130, 77–90, 2019.

Vitolo, C., Di Napoli, C., Di Giuseppe, F., Cloke, H. L., and Pappen- berger, F.: Mapping combined wildfire and heat stress hazards to improve evidence-based decision making, Environ. Int., 127, 21– 34, 2019.

Vogel, M. M., Zscheischler, J., Fischer, E. M. and Seneviratne, S. I.: Development of future heatwaves for different hazard thresholds, J. Geophys. Res. Atmos., 125, e2019JD032070. https://doi.org/ 10.1029/2019JD032070, 2020.

Volpi, E. and Fiori, A.: Design event selection in bivariate hydrolog- ical frequency analysis, Hydrol. Sci. J., 57, 1506–1515, 2012.

Vorogushyn, S., Merz, B., Lindenschmidt, K. E. and Apel, H.: A new methodology for flood hazard assessment considering dike breaches, Water Resour. Res., 46(8), http://dx.doi.org/10.1029/2009WR008475, 2010.

Wahl, T., Jain, S., Bender, J., Meyers, S.D., Luther, M.E.: Increasing risk of com- pound flooding from storm surge and rainfall for major US cities. Nat. Clim. Chang. 5, 1093–1097. https://doi.org/10.1038/nclimate2736, 2015.

Wang, J., Gao, W., Xu, S., Yu, L.: Evaluation of the combined risk of sea level rise, land subsidence, and storm surges on the coastal areas of Shanghai, China. Clim. Chang. 115, 537–558. https://doi.org/10.1007/s10584-012-0468-7, 2012.

Wang, J., Gu, X. and Huang, T.: Using Bayesian networks in analyzing powerful earthquake disaster chains, Nat. Hazards,68, 509–527, 2013.

Ward, P.J., Couasnon, A., Eilander, D., Haigh, I.D., Hendry, A., Muis, S., Veldkamp, T.I.E., Winsemius, H.C., Wahl, T.: Dependence between high sea-level and high river discharge increases flood hazard in global deltas and estuaries. Environ. Res. Lett. 13, 084012. https://doi.org/10.1088/1748-9326/aad400, 2018.

Webb, J. D. C. and Elsom, D. M.: Severe Hailstorms in the United Kingdom and Ireland: A Climatological Survey with Recent and Historical Case Studies, in: Extreme Weather: Forty Years of the Tornado and Storm Research Organisation (TORRO), edited by: Doe, R. K., John Wiley Sons, Chichester, UK, 155–194, 2016.

Weber, P., Medina-Oliva, G., Simon, C., Iung, B.: Overview on Bayesian networks applications for dependability, risk analysis and maintenance areas. Eng. Appl. Artif. Intell. 25, 671–682. https://doi.org/10.1016/j.engappai.2010.06.002, 2012.

Weiss, J.: Analyse régionale des aléas maritimes extrêmes, PhD Thesis, Université Paris-Est, 2014.

Widmann, M. and Bretherton, C. S.: Validation of mesoscale precipitation in the NCEP reanalysis using a new gridcell dataset for the Northwestern United States, J. Clim., 13(11), 1936–1950, 2000.

Wilby, R. L. and Quinn, N. W.: Reconstructing multi-decadal variations in fluvial flood risk using atmospheric circulation patterns, J. Hydrol., 487, 109–121, 2013.

Winter, H. C. and Tawn, J.: Modelling heatwaves in central France: A case-study in extremal dependence, J. R. Stat. Soc. Ser. C Appl. Stat., 65(3), 345–365, 2016.

Winter, H. C., Tawn, J., and Brown, S. J.: Modelling the effect of the El Niño-southern oscillation on extreme spatial temperature events over Australia, Ann. Appl. Stat., 10, 2075–2101, 2016.

Winter, H. C.: Extreme Value Modelling of Heatwaves, PhD thesis, Lancaster University, available at: https://eprints.lancs.ac.uk/id/ eprint/79961/ (Accessed 28 December 2019), 2016.

Witte, J. C., Douglass, A. R., da Silva, A., Torres, O., Levy, R., and Duncan, B. N.: NASA A-Train and Terra observations of the 2010 Russian wildfires, Atmos. Chem. Phys., 11, 9287–9301. https://doi.org/10.5194/acp-11-9287-2011, 2011.

WMO (World Meteorological Organization) OSCAR: Details for Variable: Wind gust, available at: https://www.wmo-sat.info/ oscar/variables/view/205 (Accessed 23 June 2019), 2019.

Wood, J. L., Harrison, S., Turkington, T. A. R. and Reinhardt, L.: Landslides and synoptic weather trends in the European Alps, Clim. Change, 136(2), 297–308, 2016.

Wu, W., McInnes, K., O'Grady, J., Hoeke, R., Leonard, M. and Westra, S.: Mapping Dependence Between Extreme Rainfall and Storm Surge, J. Geophys. Res. Ocean., 123(4), 2461–2474, 2018.

Xu, D. and Tian, Y.: A Comprehensive Survey of Clustering Algorithms, Ann. Data Sci., 2(2), 165–193, 2015.

Xu, K., Ma, C., Lian, J., Bin, L.: Joint probability analysis of extreme precipitation and storm tide in a coastal city under changing environment. PLoS One 9, e109341. https://doi.org/10.1371/journal.pone.0109341, 2014a

Xu, L., Meng, X., Xu, X.: Natural hazard chain research in China: a review. Nat. Hazards 70, 1631–1659. https://doi.org/10.1007/s11069-013-0881-x, 2014b.

Yang, X., Zhang, Q.: Joint probability distribution of winds and waves from wave simulation of 20 years (1989-2008) in Bohai Bay. Water Sci. Eng. 6, 296–307. https://doi.org/10.3882/j.issn.1674-2370.2013.03.006, 2013.

Yuan, G., Sun, P., Zhao, J., Li, D. and Wang, C.: A review of moving object trajectory clustering algorithms, Artif. Intell. Rev., 47(1), 123–144, 2017.

Yue, S.: The Gumbel logistic model for representing a multivariate storm event. Adv. Water Resour. 24, 179–185. https://doi.org/10.1016/S0309-1708(00)00039-7, 2000.

Zhang, X., Alexander, L., Hegerl, G. C., Jones, P. D., Tank, A. K., Peterson, T. C., Trewin, B. and Zwiers, F. W.: Indices for monitoring changes in extremes based on daily temperature and precipitation data, Wiley Interdiscip. Rev. Clim. Chang., 2(6), 851–870, 2011.

Zhang, L. M. and Singh, V. P.: Trivariate Flood Frequency Analysis Using the Gumbel–Hougaard Copula, J. Hydrol. Eng., 12(4), 431–439, 2007.

Zhang, Q., Xiao, M. and Singh, V. P.: Uncertainty evaluation of copula analysis of hydrological droughts in the East River basin, China, Glob. Planet. Change, 129, 1–9, 2015.

Zheng, F., Westra, S., Sisson, S.A.: Quantifying the dependence between extreme rainfall and storm surge in the coastal zone. J. Hydrol. 505, 172–187. https://doi. org/10.1016/j.jhydrol.2013.09.054, 2013.

Zheng, F., Westra, S., Leonard, M., Sisson, S.A.: Modeling dependence between extreme rainfall and storm surge to estimate coastal flooding risk. Water Resour. Res. 50, 2050–2071. https://doi.org/10.1002/2013WR014616, 2014.

Zou, K.H., Tuncali, K., Silverman, S.G.: Correlation and simple linear regression. Radiology 227, 617–628. https://doi.org/10.1148/radiol.2273011499, 2003.

Zscheischler, J., Mahecha, M. D., Harmeling, S. and Reichstein, M.: Detection and attribution of large spatiotemporal extreme events in Earth observation data, Ecol. Inform., 15, 66–73, 2013.

Zscheischler, J., Martius, O., Westra, S., Bevacqua, E., Raymond, C., Horton, R. M., van den Hurk, B., AghaKouchak, A., Jézéquel, A., Mahecha, M. D., Maraun, D., Ramos, A. M., Ridder, N. N., Thiery, W. and Vignotto, E.: A typology of compound weather and climate events, Nat. Rev. Earth Environ., 2020.

Zscheischler, J., Seneviratne, S.I.: Dependence of drivers affects risks associated with compound events. Sci. Adv. 3, e1700263. https://doi.org/10.1126/sciadv. 1700263, 2017.

Zscheischler, J., Westra, S., Van Den Hurk, B. J. J. M., Seneviratne, S. I., Ward, P. J., Pitman, A., Aghakouchak, A., Bresch, D. N., Leonard, M., Wahl, T., and Zhang, X.: Future climate risk from compound events, Nat. Clim. Change, 8, 469–477, 2018.

Appendices

Appendix A: Multi-hazard Database

This appendix is a database of 146 references related to **Chapter 2** and consists of the following:

- **Table A1**. Multi-hazard Database Structure. Detailed metadata information describing **Table A2**
- **Table A2**. Multi-hazard Database: 146 multi-hazard references (rows) with 14 attributes (columns) for each reference including citation information, keywords, hazards studied, and then information about the modelling method (if appropriate).

Table A1: Multi-hazard Database Structure. Detailed metadata information describing Table A2.

Attributes	Definition
Reference ID	
Subgroup	T for terminology; M for models and I for interrelations
TS (Terminology stream)	MH for "multi-hazard"; CH for "compound hazard"
Ref type	article; book; book chapter; conference proceeding; PhD thesis; MSc thesis; report
Citation	
Keywords	
Interrelation studied (Y/N)	Is the source focusing on natural hazard interrelations
Studied area	
Hazards	
Quantitative/Semi quantitative/Qualitative	Is the source using quantitative (Quant), semi-quantitative (S-Quant) or qualitative (Qual)method to study hazard interrelations.
Modelling method	Semi-quantitative or quantitative method used to model interrelations or connection between hazards/disasters/variables. Can be: Logistic regression; Fuzzy logic; Hydrodynamic model; Fault tree; Bayesian Network; Empirical counting; Markov chain; Extreme value copula; Vine copula; Linear regression; Rank correlation; Hydrological model; Archimedean copula; Event tree; Climate model; Atmospheric model; Tail dependence; Power regression; Polynomial regression; Joint tail model; Multivariate extreme model; Gaussian copula; Quantile regression; Conditional extreme model

Table A2: Multi-hazard Database. Given are 146 multi-hazard references (rows) with 14 attributes (columns) for each reference, including citation information, keywords, hazards studied, and then information about the modelling method (if appropriate). A detailed description of each column is given in Table A1.

ID	Sub-group	TS	Ref type	Citation	Keywords	Inter-relation	Studied Area	Hazards	Quant / Semi-quant/ Qual	Modelling method
1	T	MH	article	Abdulwahid, W.M. and Pradhan, B., 2017. Landslide vulnerability and risk assessment for multi-hazard scenarios using airborne laser scanning data (LiDAR). Landslides, 14(3), pp.1057-1076.	landslides; remote sensing; hazard assessment; vulnerability; risk; lidar; GIS	Yes	Malaysia	Landslide; Extreme Rainfall	S-Quant	Logistic Regression
2	T	MH	MSc Thesis	Ahuja, A., 2011. Review of assessment, design, and mitigation of multiple hazards.		No	USA	Multiple		
3	T	MH	article	Araya-Muñoz, D., Metzger, M.J., Stuart, N., Wilson, A.M.W. and Carvajal, D., 2017. A spatial fuzzy logic approach to urban multi-hazard impact assessment in Concepción, Chile. Science of The Total Environment, 576, pp.508-519.	developing countries; bottom-up evaluation; fuzzy modelling; geographical information system (GIS); vulnerability	Yes	Chili	Drought; River Flooding; Extreme hot temperature; Sea Level Rise; Wildfire	S-Quant	Fuzzy Logic
4	T	MH	article	Asare-Kyei, D., Renaud, F.G., Kloos, J., Walz, Y. and Rhyner, J., 2017. Development and validation of risk profiles of West African rural communities facing multiple natural hazards. PloS one, 12(3), p.e0171921.		No	West Africa	Drought; Flood		
5	T	MH	article	Bernal, G.A., Salgado-Gálvez, M.A., Zuloaga, D., Tristancho, J., González, D. and Cardona, O.D., 2017. Integration of probabilistic and multi-hazard risk assessment within urban development planning and emergency preparedness and response: Application to Manizales, Colombia. International Journal of Disaster Risk Science, 8(3), pp.270-283.	Manizales (Colombia); multi-hazard risk assessment; probabilistic hazard analysis; probabilistic risk assessment; urban planning; emergency response	No	Colombia	Earthquake; Landslide; Volcanic Eruption		

ID	Sub-group	TS	Ref type	Citation	Keywords	Inter-relation	Studied Area	Hazards	Quant / Semi-quant/ Qual	Modelling method
6	T	MH	article	Birkmann, J., Wenzel, F., Greiving, S., Garschagen, M., Vallée, D., Nowak, W., Welle, T., Fina, S., Goris, A., Rilling, B. and Fiedrich, F., 2016. Extreme Events, Critical Infrastructures, Human Vulnerability and Strategic Planning: Emerging Research Issues. Journal of Extreme Events, 3(04), p.1650017.	critical infrastructure; urban planning; spatial planning; risk management; climate change; extreme events; cascading effects	Yes	Germany		Qual	
7	T	MH	conference proceeding	Cardona, O.D., Ordaz, M., Reinoso, E., Yamín, L.E. and Barbat, A.H., 2012, September. CAPRA–comprehensive approach to probabilistic risk assessment: international initiative for risk management effectiveness. In Proceedings of the 15th World Conference on Earthquake Engineering. Lisbon, Portugal.	seismic risk; building damage; insurance; risk reduction; loss scenarios	No	multiple	Earthquake		
8	T	MH	article	Chen, L., van Westen, C.J., Hussin, H., Ciurean, R.L., Turkington, T., Chavarro-Rincon, D. and Shrestha, D.P., 2016. Integrating expert opinion with modelling for Quant multi-hazard risk assessment in the Eastern Italian Alps. Geomorphology, 273, pp.150-167.	hydro-meteorological hazards; Italy; multi-hazard; quant risk assessment; uncertainty; vulnerability; GIS	Yes	Italy	River Flooding; Landslide	Quant	Hydrodynamic model
9	T	MH&C	book	Davis, I. ed., 2014. Disaster risk management in Asia and the Pacific. Routledge.		No	Asia	Na		
10	T	MH	report	Delmonaco, G., Margottini, C. and Spizzichino, D., 2006. ARMONIA methodology for multi-risk assessment and the harmonisation of different natural risk maps. Deliverable 3.1. 1, ARMONIA.		No	NA	Earthquake; River Flooding; Landslide; Forest Fire; Avalanche; Volcanic Eruption		

ID	**Sub-group**	**TS**	**Ref type**	**Citation**	**Keywords**	**Inter-relation**	**Studied Area**	**Hazards**	**Quant / Semi-quant/ Qual**	**Modelling method**
11	T	MH&C	article	Eshrati, L., Mahmoudzadeh, A. and Taghvaei, M., 2015. Multi hazards risk assessment, a new methodology. International Journal of Health System and Disaster Management, 3(2), p.79.	indicator-based vulnerability; new methodology; risk assessment; domino effects; multi-hazard	No	NA	Na		
12	T	MH	article	Forzieri, G., Bianchi, A., e Silva, F.B., Herrera, M.A.M., Leblois, A., Lavalle, C., Aerts, J.C. and Feyen, L., 2018. Escalating impacts of climate extremes on critical infrastructures in Europe. Global Environmental Change, 48, pp.97-107.	climate change impact; critical infrastructures; loss and damage; multiple climate hazards	No	Europe	Extreme Hot temperature; Extreme Cold temperature; Drought; Wildfire; Floods; Windstorm		
13	T	MH	article	Forzieri, G., Feyen, L., Russo, S., Vousdoukas, M., Alfieri, L., Outten, S., Migliavacca, M., Bianchi, A., Rojas, R. and Cid, A., 2016. Multi-hazard assessment in Europe under climate change. Climatic Change, 137(1-2), pp.105-119.	climate change; Europe; resilience; scenarios; multi-hazards	No	Europe	Extreme Hot temperature; Extreme Cold temperature; Drought; Wildfire; Floods; Windstorm		
14	T	MH&C	article	Gallina, V., Torresan, S., Critto, A., Sperotto, A., Glade, T. and Marcomini, A., 2016. A review of multi-risk methodologies for natural hazards: Consequences and challenges for a climate change impact assessment. Journal of environmental management, 168, pp.123-132.	multi-hazard multi-hazard risk multi-risk climate change	No	NA	Multiple		

ID	Sub-group	TS	Ref type	Citation	Keywords	Inter-relation	Studied Area	Hazards	Quant / Semi-quant/ Qual	Modelling method
15	T	MH	article	Garcia-Aristizabal, A., Bucchignani, E., Palazzi, E., D'Onofrio, D., Gasparini, P. and Marzocchi, W., 2015. Analysis of non-stationary climate-related extreme events considering climate change scenarios: an application for multi-hazard assessment in the Dar es Salaam region, Tanzania. Natural Hazards, 75(1), pp.289-320.	non-stationary extreme events; climate change; multi-hazard; Bayesian inference; extreme precipitation; extreme temperature; Dar Es Salaam, Tanzania	No	Tanzania	Extreme Rainfall; Extreme Temperature		
16	T	MH	report	Garcia-Aristizabal, A., Marzocchi, W., Woo, G., Reveillere, A., Douglas, J., Le Cozannet, G., Rego, F., Colaco, C., Fleming, K., Pittore, M. and Tyagunov, S., 2012. Review of existing procedures for multi-hazard assessment.		No	NA	Multiple		
17	T	MH	conference proceeding	Gehl, P. and D'Ayala, D., 2015, July. Integrated multi-hazard framework for the fragility analysis of roadway bridges. In 12th international conference on applications of statistics and probability in civil engineering (ICASP12), Vancouver, BC, Canada (pp. 12-15).		No	NA	Earthquake; River Flooding; Ground Failure		
18	T+I	MH	article	Gill, J.C. and Malamud, B.D., 2014. Reviewing and visualizing the interactions of natural hazards. Reviews of Geophysics, 52(4), pp.680-722.	hazard combination; multi-hazard	No	Multiple	Multiple		
19	T	MH	article	Gill, J.C. and Malamud, B.D., 2016. Hazard interactions and interaction networks (cascades) within multi-hazard methodologies. Earth System Dynamics, 7(3), p.659.	hazard combination; multi-hazard	No	Italy	Multiple		

ID	**Sub-group**	**TS**	**Ref type**	**Citation**	**Keywords**	**Inter-relation**	**Studied Area**	**Hazards**	**Quant / Semi-quant/ Qual**	**Modelling method**
20	T	MH	article	Gill, J.C. and Malamud, B.D., 2017. Anthropogenic processes, natural hazards, and interactions in a multi-hazard framework. Earth-Science Reviews.	anthropogenic process; natural hazard interaction	No	Australia	Multiple		
21	T	MH	article	Greiving, S., 2006. Integrated risk assessment of multi-hazards: a new methodology. Special Paper-Geological Survey of Finland, 42, p.75.	risk assessment; technological hazards; vulnerability; natural hazards	No	Finland	Na		
22	T	MH	article	Grünthal, G., Thieken, A.H., Schwarz, J., Radtke, K.S., Smolka, A. and Merz, B., 2006. Comparative risk assessments for the city of Cologne–storms, floods, earthquakes. Natural Hazards, 38(1-2), pp.21-44.	risk assessment; storm; flood; earthquake	No	Germany	Storm; River Flooding; Earthquake		
23	T	C	article	Hao, Z. and Singh, V.P., 2016. Review of dependence modeling in hydrology and water resources. Progress in Physical Geography, 40(4), pp.549-578.	copula; entropy; extreme dependence; multivariate distribution; nonparametric method; parametric distribution; spatial dependence; temporal dependence; dependence modelling	Yes			Quant	Review
24	T	C	article	Hao, Z., Singh, V.P. and Hao, F., 2018. Compound Extremes in Hydroclimatology: A Review. Water (20734441), 10(6).	climate change; compound extremes; indicator; multivariate distribution; quantile regression	Yes			Quant	Review
25	T	MH&C	article	Hillier, J.K., Macdonald, N., Leckebusch, G.C. and Stavrinides, A., 2015. Interactions between apparently ‘primary’weather-driven hazards and their cost. Environmental Research Letters, 10(10), p.104003.	extreme weather; flood; insurance; interaction; risk; storm; atmospheric	Yes	United Kingdom	Extreme Wind; Drought; River Flooding	Qual	

ID	Sub-group	TS	Ref type	Citation	Keywords	Inter-relation	Studied Area	Hazards	Quant / Semi-quant/ Qual	Modelling method
26	T	MH	article	Jaimes, M.A., Reinoso, E. and Esteva, L., 2015. Risk analysis for structures exposed to several multi-hazard sources. Journal of Earthquake Engineering, 19(2), pp.297-312.	intensity; losses; multiple hazards; simultaneous hazards; correlated damage	No	Mexico	Earthquake; Extreme Wind; Tsunami; Landslide		
27	T	MH	conference proceeding	James, M., Reinoso, E., Esteva, L.; A method for the risk assessment of buildings due to multiple hazard sources and correlated failure modes; NCEE 2014 - 10th U.S. National Conference on Earthquake Engineering: Frontiers of Earthquake Engineering		No		Earthquake; Extreme Wind; Tsunami; Landslide		
28	T	MH	article	Kameshwar, S. and Padgett, J.E., 2014. Multi-hazard risk assessment of highway bridges subjected to earthquake and hurricane hazards. Engineering Structures, 78, pp.154-166.	earthquake; hurricane; metamodel metamodel; risk; multi-hazard	No	USA	Earthquake; Extreme Wind		
29	T	MH	article	Kappes, M. S., Margreth Keiler, and Thomas Glade. "From single-to multi-hazard risk analyses: a concept addressing emerging challenges." (2010): 351-356.	multi-hazard; methodology	No	France	Avalanche; Landslide; River Flooding; Earthquake		
30	T	MH&C	PhD Thesis	Kappes, M.S., 2011. Multi-hazard risk analyses: a concept and its implementation. na.		No	France	Avalanche; Landslide; River Flooding		
31	T	MH&C	article	Kappes, M.S., Keiler, M., von Elverfeldt, K. and Glade, T., 2012. Challenges of analyzing multi-hazard risk: a review. Natural Hazards, 64(2), pp.1925-1958.	state of the art; multi-hazard	No		Avalanche; Landslide; River Flooding		

ID	Sub-group	TS	Ref type	Citation	Keywords	Inter-relation	Studied Area	Hazards	Quant / Semi-quant/ Qual	Modelling method
32	T	MH	article	Kappes, M.S., Papathoma-Koehle, M. and Keiler, M., 2012. Assessing physical vulnerability for multi-hazards using an indicator-based methodology. Applied Geography, 32(2), pp.577-590.	decision-making; multi-hazard; physical vulnerability; vulnerability indicators	No	France	Avalanche; Landslide; River Flooding		
33	T	MH	article	Katsanos, E.I., Thöns, S. and Georgakis, C.T., 2016. Wind turbines and seismic hazard: a state-of-the-art review. Wind Energy, 19(11), pp.2113-2133.	dynamic analysis; earthquake strong ground motions; multi-hazard environment; seismic loading; soil-structure interaction; structural response; wind turbines	No		Earthquake		
34	T	MH	article	Komendantova, N., Scolobig, A., Garcia-Aristizabal, A., Monfort, D. and Fleming, K., 2016. Multi-risk approach and urban resilience. International Journal of Disaster Resilience in the Built Environment, 7(2), pp.114-132.	decision making; governance; interdependency; knowledge generation; urban resilience; multi-risk	No		Earthquake		
35	T	MH	article	Koudogbo, F.N., Duro, J., Rossi, L., Rudari, R. and Eddy, A., 2014, October. Multi-hazard risk analysis using the FP7 RASOR Platform. In Remote Sensing for Agriculture, Ecosystems, and Hydrology XVI (Vol. 9239, p. 92390J). International Society for Optics and Photonics.	multi-hazard; risk assessment; tandem-x global DEM	No	Italy, Haiti	Earthquake; Landslide; River Flooding; Extreme Wind		
36	T	MH	article	Kreibich, H., Bubeck, P., Kunz, M., Mahlke, H., Parolai, S., Khazai, B., Daniell, J., Lakes, T. and Schröter, K., 2014. A review of multiple natural hazards and risks in Germany. Natural Hazards, 74(3), pp.2279-2304.	risk analysis; earthquakes; extreme temperatures; floods; multi-risk approaches; risk management; storms; g Germany; past natural hazard events	No	Germany	Earthquake; Extreme Temperature; River Flooding; Extreme Wind		

ID	**Sub-group**	**TS**	**Ref type**	**Citation**	**Keywords**	**Inter-relation**	**Studied Area**	**Hazards**	**Quant / Semi-quant/ Qual**	**Modelling method**
37	T	MH&C	article	Kumasaki, M., King, M., Arai, M. and Yang, L., 2016. Anatomy of cascading natural disasters in Japan: Main modes and linkages. Natural Hazards, 80(3), pp.1425-1441.	cascading natural disaster; compounding; interaction patters; risk assessment; striking; undermining; blocking	Yes	Japan	Earthquake; Landslide; Extreme Temperature; Tsunami; Wildfire; Lightning	Qual	
38	T	MH	article	Kwag, S. and Gupta, A., 2017. Probabilistic risk assessment framework for structural systems under multiple hazards using Bayesian statistics. Nuclear Engineering and Design, 315, pp.20-34.	Bayesian inference; Bayesian networks; vulnerability beyond design basis; multi-hazard risk assessment	Yes	USA	River Flooding; Earthquake; Extreme Wind	S-Quant	Fault tree; Bayesian Network
39	T	C	report	Lavell, A., Oppenheimer, M., Diop, C., Hess, J., Lempert, R., Li, J., Muir-Wood, R. and Myeong, S., 2012. Climate change: new dimensions in disaster risk, exposure, vulnerability, and resilience.		No				
40	T	MH	article	Lee, K.H. and Rosowsky, D.V., 2006. Fragility analysis of woodframe buildings considering combined snow and earthquake loading. Structural Safety, 28(3), pp.289-303.	fragility; hazards; performance-based design; probability; shear wall; snow load; wood structures; earthquake	No	USA	Snowfall; Earthquake		
41	T	C	article	Leonard, M., Westra, S., Phatak, A., Lambert, M., van den Hurk, B., McInnes, K., Risbey, J., Schuster, S., Jakob, D. and Stafford-Smith, M., 2014. A compound event framework for understanding extreme impacts. Wiley Interdisciplinary Reviews: Climate Change, 5(1), pp.113-128.	compound event; extreme impact; hazards; modelling system; statistical dependencies	Yes	Australia(Melbourne, Brisbane)	River Flooding; Wildfire; Storm Surge	S-Quant	Fault tree; Bayesian Network

ID	Sub-group	TS	Ref type	Citation	Keywords	Inter-relation	Studied Area	Hazards	Quant / Semi-quant/ Qual	Modelling method
42	T	C	article	Littell, J.S., Peterson, D.L., Riley, K.L., Liu, Y. and Luce, C.H., 2016. A review of the relationships between drought and forest fire in the United States. Global change biology, 22(7), pp.2353-2369.	climate variability; drought; ecological drought; fire; water balance; climate change	Yes	USA	Drought; Wildfire	Qual	
43	T+I	MH	article	Liu, B., Siu, Y.L. and Mitchell, G., 2016. Hazard interaction analysis for multi-hazard risk assessment: a systematic classification based on hazard-forming environment. Natural Hazards and Earth System Sciences, 16(2), pp.629-642.	quant approach; multi-hazard	Yes	Several	River Flooding; Storm Surge; Landslide	S-Quant	Empirical counting
44	T	MH	article	Liu, B., Siu, Y.L. and Mitchell, G., 2017. A Quant model for estimating risk from multiple interacting natural hazards: an application to northeast Zhejiang, China. Stochastic Environmental Research and Risk Assessment, 31(6), pp.1319-1340.	hazard interaction; hazard-forming environment; multi-hazard risk modelling; Zhejiang; Bayesian network	Yes	China	River Flooding; Storm Surge; Landslide	S-Quant	Empirical counting
45	T	MH	article	Liu, Z., Nadim, F., Garcia-Aristizabal, A., Mignan, A., Fleming, K. and Luna, B.Q., 2015. A three-level framework for multi-risk assessment. Georisk: Assessment and Management of Risk for Engineered Systems and Geohazards, 9(2), pp.59-74.	Bayesian network; cascading hazards; time-variant vulnerability; multi-risk	Yes	Europe	Multiple	S-Quant	Bayesian Network
46	T	MH	article	Lozoya, J.P., Sarda, R. and Jiménez, J.A., 2011. A methodological framework for multi-hazard risk assessment in beaches. Environmental science & policy, 14(6), pp.685-696.	iczm; coastal hazards ; ecosystem services; beach risk	No	Spain	Storm Surge; Erosion; River Flooding		

ID	Sub-group	TS	Ref type	Citation	Keywords	Inter-relation	Studied Area	Hazards	Quant / Semi-quant/ Qual	Modelling method
47	T	MH	article	Lung, T., Lavalle, C., Hiederer, R., Dosio, A. and Bouwer, L.M., 2013. A multi-hazard regional level impact assessment for Europe combining indicators of climatic and non-climatic change. Global Environmental Change, 23(2), pp.522-536.	flood; forest fire; heat stress; indicator; vulnerability; climate change	No	Europe	Wildfire; River		
48	T	MH	article	Marzocchi, W., Garcia-Aristizabal, A., Gasparini, P., Mastellone, M.L. and Di Ruocco, A., 2012. Basic principles of multi-risk assessment: a case study in Italy. Natural hazards, 62(2), pp.551-573.	multi-risk assessment; hazards interaction; risk assessment; Casalnuovo	No	Italy	Volcanic Ash; Landslides; Flood; Earthquake		
49	T	MH	report	Mignan, A., 2013. D7. 2 MATRIX-CITY User Manual. New methodologies for multi-hazard and multi-risk assessment methods for Europe, Deliverable, 7, p.78.		Yes		Multiple	S-Quant	Bayesian Network
50	T	MH	article	Mignan, A., Wiemer, S. and Giardini, D., 2014. The quantification of low-probability–high-consequences events: part I. A generic multi-risk approach. Natural Hazards, 73(3), pp.1999-2022.	multi-hazard; multi-risk; extreme event; monte carlo; markov chain	Yes		Multiple	S-Quant	Markov Chain
51	T	MH	article	Mignan, A., Scolobig, A. and Sauron, A., 2016. Using reasoned imagination to learn about cascading hazards: a pilot study. Disaster Prevention and Management, 25(3), pp.329-344.	cascading hazards; reasoned imagination	Yes			Qual	
52	T	MH	article	Mills, B., Unrau, D., Pentelow, L. and Spring, K., 2010. Assessment of lightning-related damage and disruption in Canada. Natural hazards, 52(2), pp.481-499.	Canada; casualty; cost; damage; disruption; lightning; thunderstorm	No	Canada	Lightning		

ID	Sub-group	TS	Ref type	Citation	Keywords	Inter-relation	Studied Area	Hazards	Quant / Semi-quant/ Qual	Modelling method
53	T	C	article	Moftakhari, H.R., Salvadori, G., AghaKouchak, A., Sanders, B.F. and Matthew, R.A., 2017. Compounding effects of sea level rise and fluvial flooding. Proceedings of the National Academy of Sciences, 114(37), pp.9785-9790.	coastal flooding; compound extremes; copula; failure probability; sea level rise	Yes	USA	River Flooding; Storm Surge	Quant	Copula
54	T	MH	report	Nadim, F., Liu, Z., Garcia-Aristizabal, A., Woo, G., Aspinall, W., Fleming, K., Vangelsten, B.V. and van Gelder, P., 2013. Framework for multi-risk assessment. Deliverable D5, 2.		Yes		Earthquake; Landslide	S-Quant	Bayesian Network; Fault tree
55	T	MH	article	Orencio, P.M. and Fujii, M., 2014. A spatiotemporal approach for determining disaster-risk potential based on damage consequences of multiple hazard events. Journal of Risk Research, 17(7), pp.815-836.	geographic information system; Philippines; spatiotemporal approach; multi-risk assessment	No	Philippines	Multiple		
56	T	MH	article	Ouyang, M., 2014. Review on modeling and simulation of interdependent critical infrastructure systems. Reliability engineering & System safety, 121, pp.43-60.	critical infrastructure systems (ciss); interdependencies; empirical approach; agent system dynamics; economic theory network; resilience	NA				
57	T	MH	article	Papathoma-Köhle, M., Kappes, M., Keiler, M. and Glade, T., 2011. Physical vulnerability assessment for alpine hazards: state of the art and future needs. Natural Hazards, 58(2), pp.645-680.	debris flows; floods; landslides; rock falls; vulnerability; avalanches					

ID	Sub-group	TS	Ref type	Citation	Keywords	Inter-relation	Studied Area	Hazards	Quant / Semi-quant/ Qual	Modelling method
58	T	MH&C	article	Pescaroli, G. and Alexander, D. (2018) Understanding Compound, Interconnected, Interacting, and Cascading Risks: A Holistic Framework. Risk Analysis	compounding risk; critical infrastructure; interacting risk; interconnected risk; Sendai framework for disaster risk reduction; societal resilience; cascading risk	Yes			Qual	
59	T	C	article	Saleh, F., Ramaswamy, V., Wang, Y., Georgas, N., Blumberg, A. and Pullen, J., 2017. A multi-scale ensemble-based framework for forecasting compound coastal-riverine flooding: The Hackensack-Passaic watershed and Newark Bay. Advances in Water Resources, 110, pp.371-386.	ensembles; flood forecasting; GEFS; HEC-RAS 2-D; hydrodynamic modelling; SECOM; uncertainty; coastal urban estuary	Yes	USA	River Flooding; Storm Surge	Quant	Hydrodynamic model
60	T	C	article	Salvadori, G., Durante, F., De Michele, C., Bernardi, M. and Petrella, L., 2016. A multivariate copula-based framework for dealing with hazard scenarios and failure probabilities. Water Resources Research, 52(5), pp.3701-3721.	copulas; failure probability; risk assessment; scenario; multivariate	No		River Flooding		
61	T	MH	article	Schmidt, J., Matcham, I., Reese, S., King, A., Bell, R., Henderson, R., Smart, G., Cousins, J., Smith, W. and Heron, D., 2011. Quant multi-risk analysis for natural hazards: a framework for multi-risk modelling. Natural Hazards, 58(3), pp.1169-1192.	natural hazards; multi-risk modelling; quant risk analysis; Hawke's bay; New Zealand; earthquakes; wind storms; floods	No	New Zeland	Earthquakes; Extreme Wind; River Flooding		
62	T	MH	article	Selva, J., 2013. Long-term multi-risk assessment: statistical treatment of interaction among risks. Natural hazards, 67(2), pp.701-722.	multi-risk; multi-hazard	No	Italy	Earthquake; Tsunami; Volcanic Eruption		

ID	Sub-group	TS	Ref type	Citation	Keywords	Inter-relation	Studied Area	Hazards	Quant / Semi-quant/ Qual	Modelling method
63	T	MH	article	Steptoe, H., Jones, S.E.O. and Fox, H., 2018. Correlations between extreme atmospheric hazards and global teleconnections: Implications for multihazard resilience. Reviews of Geophysics, 56(1), pp.50-78.	ENSO; hazards drivers; NAO; atmospheric connections between hazards	No		Extreme Rainfall; Extreme Wind		
64	T+M	C	article	Bevacqua, E., Maraun, D., Hobæk Haff, I., Widmann, M. and Vrac, M., 2017. Multivariate statistical modelling of compound events via pair-copula constructions: analysis of floods in Ravenna (Italy). Hydrology and Earth System Sciences, 21(6), pp.2701-2723.	conceptual model; pair copula; compound event; meteorological predictors	Yes	Italy	River Flooding; Storm Surge	Quant	Vine copula
65	T	MH	article	Tierz, P., Woodhouse, M.J., Phillips, J.C., Sandri, L., Selva, J., Marzocchi, W. and Odbert, H.M., 2017. A Framework for Probabilistic Multi-Hazard Assessment of Rain-Triggered Lahars Using Bayesian Belief Networks. Frontiers in Earth Science, 5, p.73.	probabilistic hazard assessment; volcanic multi-hazard; lahar triggering; Bayesian belief network; somma-vesuvius	Yes	Italy	Extreme Rainfall; Landslide	S-Quant	Bayesian Network
66	T	MH	article	Tonini, R., Sandri, L. and Thompson, M.A., 2015. PyBetVH: A Python tool for probabilistic volcanic hazard assessment and for generation of Bayesian hazard curves and maps. Computers & Geosciences, 79, pp.38-46.	Bayesian event tree; graphical user interface; hazard curves; interactive visualization; probabilistic volcanic hazard assessment	No	New Zealand	Volcanic Eruption		
67	T	MH&C	book chapter	Van Asch, T. ed., 2014. Mountain risks: from prediction to management and governance. Springer Netherlands.		No	France	Landslde; River Flooding; Avalanche		

ID	**Sub-group**	**TS**	**Ref type**	**Citation**	**Keywords**	**Inter-relation**	**Studied Area**	**Hazards**	**Quant / Semi-quant/ Qual**	**Modelling method**
68	T	C	article	AghaKouchak, A., Huning, L.S., Chiang, F., Sadegh, M., Vahedifard, F., Mazdiyasni, O., Moftakhari, H. and Mallakpour, I., 2018. How do natural hazards cascade to cause disasters?.	climate change; environmental sciences; hydrology; policy	No	USA	Wildfires		
69	M		article	Caine, N., 1980. The rainfall intensity: duration control of shallow landslides and debris flows. Geografiska Annaler. Series A. Physical Geography, pp.23-27.	rainfall; landslide; relationship			Extreme Rainfall; Landslide	Quant	Linear regression
70	T	MH	article	Van Verseveld, H.C.W., Van Dongeren, A.R., Plant, N.G., Jäger, W.S. and den Heijer, C., 2015. Modelling multi-hazard hurricane damages on an urbanized coast with a Bayesian Network approach. Coastal Engineering, 103, pp.1-14.	hurricane sandy ; xbeach; probabilistic damage hazards; Bayesian network	Yes	USA	Extreme Waves; Storm Surge; Erosion	S-Quant	Bayesian Network
71	T	MH	article	Van Westen, C.J., 2013. Remote sensing and GIS for natural hazards assessment and disaster risk management. Treatise on geomorphology, 3, pp.259-298.	cyclones; damage assessment; drought; earthquakes; elements-at-risk; flooding; forest fires; geographic information systems; hazard assessment; landslides; mobile-gis; multi-hazards; remote sensing; risk assessment; risk management; spatial data; vulnerability assessment; community-based disaster risk management	No		Landslides		

ID	Sub-group	TS	Ref type	Citation	Keywords	Inter-relation	Studied Area	Hazards	Quant / Semi-quant/ Qual	Modelling method
72	T+I	MH&C	book chapter	van Westen, C.J., Greiving, S. and Dalezios, N.R., 2017. Environmental Hazards Methodologies for Risk Assessment and Management. Environmental hazards Methodologies for Risk Assessment and Management, pp.31-94.		Yes		Multiple	Qual	
73	T	MH	conference proceeding	Van Westen, C.J., Montoya, L., Boerboom, L. and Badilla Coto, E., 2002, September. Multi-hazard risk assessment using GIS in urban areas: a case study for the city of Turrialba, Costa Rica. In Proc. Regional workshop on Best Practise in Disaster Mitigation, Bali (pp. 120-136).		No	Costa Rica	Landslides		
74	T	C	article	Wahl, T., Jain, S., Bender, J., Meyers, S.D. and Luther, M.E., 2015. Increasing risk of compound flooding from storm surge and rainfall for major US cities. Nature Climate Change, 5(12), p.1093.	climate change; rainfall; risk; storm surge; USA; compound flooding	Yes	USA	Extreme Rainfall; Storm Surge	Quant	Rank correlation
75	T	MH	article	Xu, L., Meng, X. and Xu, X., 2014. Natural hazard chain research in China: A review. Natural hazards, 70(2), pp.1631-1659.	definition; hazard chain; mechanism; methodology; recognition; classification	Yes	China	Multiple	Qual	
76	M		article	Carey, L.D., Rutledge, S.A. and Petersen, W.A., 2003. The relationship between severe storm reports and cloud-to-ground lightning polarity in the contiguous United States from 1989 to 1998. Monthly weather review, 131(7), pp.1211-1228.	lightnings; severe storm; hailstorm; tornadoes	Yes	USA	Lightning	Quant	Linear regression

ID	Sub-group	TS	Ref type	Citation	Keywords	Inter-relation	Studied Area	Hazards	Quant / Semi-quant/ Qual	Modelling method
77	M		article	Catane, S.G., Abon, C.C., Saturay, R.M., Mendoza, E.P.P. and Futalan, K.M., 2012. Landslide-amplified flash floods—the June 2008 Panay Island flooding, Philippines. Geomorphology, 169, pp.55-63.	landslide dam; flash flood; hydrologic modelling; typhoon fengshen; Philippines		Alkan, Philippines	Extreme Rainfall ; Landslides; River Flooding	Quant	Hydrological model
78	T	C	article	Zscheischler, J. and Seneviratne, S.I., 2017. Dependence of drivers affects risks associated with compound events. Science advances, 3(6), p.e1700263.		Yes		Extreme Temperature; Drought	Quant	Linear correlation; Archimedean Copula
79	T	MH	article	Zuccaro, G., Cacace, F., Spence, R.J.S. and Baxter, P.J., 2008. Impact of explosive eruption scenarios at Vesuvius. Journal of Volcanology and Geothermal Research, 178(3), pp.416-453.	cumulative damage; impact scenarios; probabilistic model; sub-plinian eruption	Yes	Italy	Volcanic Eruption	S-Quant	Event tree
80	M		article	Costa, J.E. and Schuster, R.L., 1988. The formation and failure of natural dams. Geological society of America bulletin, 100(7), pp.1054-1068.	landslide; dams failure; floods		worldwide	Extreme Rainfall; Earthquake; Snow Melt; Landslide; River Flooding	Quant	Linear regression
81	M		article	Fischer, E.M. and Knutti, R., 2013. Robust projections of combined humidity and temperature extremes. Nature Climate Change, 3(2), pp.126-130.	humidity; temperature extreme; climate change	Yes	worldwide	Humidity; Extreme Temperature	Quant	Climate model
82	M		article	Geist, E.L. and Parsons, T., 2006. Probabilistic analysis of tsunami hazards. Natural Hazards, 37(3), pp.277-314.	tsunami; probabilistic hazard analysis; seismic hazard analysis; monte carlo; tide gauge; empirical; power-law		North American Pacific coast	Earthquake; Tsunami	Quant	Hydrodynamic model

ID	Sub-group	TS	Ref type	Citation	Keywords	Inter-relation	Studied Area	Hazards	Quant / Semi-quant/ Qual	Modelling method
83	M		article	Glade, T., Crozier, M. and Smith, P., 2000. Applying probability determination to refine landslide-triggering rainfall thresholds using an empirical" Antecedent Daily Rainfall Model". Pure and Applied Geophysics, 157(6-8), pp.1059-1079.	landslides; probabilistic threshold determination; rainfall threshold; critical water		New Zeland	Extreme Rainfall; Landslide	Quant	Logistic regression
84	M		article	Irish, J.L., Resio, D.T. and Ratcliff, J.J., 2008. The influence of storm size on hurricane surge. Journal of Physical Oceanography, 38(9), pp.2003-2013.	hurricane; storm surge; Katrina		Gulf of Mexico	Storm Surge; Extreme Wind	Quant	Atmospheric model
85	M		article	Johansson, B. and Chen, D., 2003. The influence of wind and topography on precipitation distribution in Sweden: Statistical analysis and modelling. International Journal of Climatology, 23(12), pp.1523-1535.	precipitation; orographic enhancement; regression analysis; topography; airflow; spatial distribution; Sweden	Yes	Sweden	Extreme Rainfall	Quant	Linear regression
86	M		article	Keefer, D.K., 1994. The importance of earthquake-induced landslides to long-term slope erosion and slope-failure hazards in seismically active regions. Geomorphology, 10(1-4), pp.265-284.	earthquake-induced landslides; erosion; slope failure		worldwide	Earthquake; Landslide	Quant	Linear regression
87	M		article	Keefer, D.K., 2002. Investigating landslides caused by earthquakes–a historical review. Surveys in geophysics, 23(6), pp.473-510.	debris flows; earthquakes; ground failure; historical landslides; landslides; landslide inventories; lateral spreads; liquefaction; review; rock falls; seismic slope stability; slope failure			Earthquake; Landslide	Quant	Linear regression

ID	Sub-group	TS	Ref type	Citation	Keywords	Inter-relation	Studied Area	Hazards	Quant / Semi-quant/ Qual	Modelling method
88	M		article	Klerk, W.J., Winsemius, H.C., van Verseveld, W.J., Bakker, A.M.R. and Diermanse, F.L.M., 2015. The co-incidence of storm surges and extreme discharges within the Rhine–Meuse Delta. Environmental Research Letters, 10(3), p.035005.	storm surge; flood; statistic dependency; model association	Yes	Rhine-Meuse delta	Storm Surge; River Flooding	Quant	Tail dependence
89	M		article	Lian, J.J., Xu, K. and Ma, C., 2013. Joint impact of rainfall and tidal level on flood risk in a coastal city with a complex river network: a case study of Fuzhou City, China. Hydrology and Earth System Sciences, 17(2), p.679.	flood risk; urban area; tidal; joint probabilities; copulas		China	River Flooding	Quant	Extreme value copula
90	M		article	Ma, T., Li, C., Lu, Z. and Bao, Q., 2015. Rainfall intensity–duration thresholds for the initiation of landslides in Zhejiang Province, China. Geomorphology, 245, pp.193-206.	shallow landslides; rainfall thresholds; terrain slope; soil properties; kriging method		Zhejiang Province, China	Extreme Rainfall ; Landslide	Quant	Linear regression
91	T+M	MH	article	Ming, X., Xu, W., Li, Y., Du, J., Liu, B. and Shi, P., 2015. Quant multi-hazard risk assessment with vulnerability surface and hazard joint return period. Stochastic environmental research and risk assessment, 29(1), pp.35-44.	joint probability distribution; multi-hazard; risk; vulnerability surface; copula	Yes	China	River Flooding; Extreme Wind; Cold Wave; Drought	Quant	Extreme value copula
92	M		report	Phan, L.T., Simiu, E., McInerney, M.A., Taylor, A.A., Glahn, B. and Powell, M.D., 2007. Methodology for development of design criteria for joint hurricane wind speed and storm surge events: Proof of concept. NIST Technical Note, 1482.			USA		Quant	Hydrodynamic model

ID	Sub-group	TS	Ref type	Citation	Keywords	Inter-relation	Studied Area	Hazards	Quant / Semi-quant/ Qual	Modelling method
93	M		article	Piepgrass, M.V., Krider, E.P. and Moore, C.B., 1982. Lightning and surface rainfall during Florida thunderstorms. Journal of Geophysical Research: Oceans, 87(C13), pp.11193-11201.	electrical phenomena; H_2O in the atmosphere (humidity);storms	Yes	Florida		Quant	Linear regression
94	M		article	Silvestro, F., Rebora, N., Rossi, L., Dolia, D., Gabellani, S., Pignone, F., Trasforini, E., Rudari, R., Angeli, S.D. and Masciulli, C., 2016. What if the 25 October 2011 event that struck Cinque Terre (Liguria) had happened in Genoa, Italy? Flooding scenarios, hazard mapping and damage estimation. Natural Hazards and Earth System Sciences, 16(8), pp.1737-1753.	mapping; flash-flood		Liguria, Italy	River Flooding	Quant	Atmosheric model; Hydrological model; Hydrodynamic model
95	M		article	Suppasri, A., Imamura, F. and Koshimura, S., 2012. Tsunamigenic ratio of the Pacific Ocean earthquakes and a proposal for a tsunami index. Natural Hazards and Earth System Sciences, 12(1), p.175.	tsunami; earthquake; ratio		Pacific Ocean	Tsunami	Quant	Power regression (non-linear regression)
96	M		article	Svensson, C. and Jones, D.A., 2004. Dependence between sea surge, river flow and precipitation in south and west Britain. Hydrology and Earth System Sciences Discussions, 8(5), pp.973-992.	Britain; dependence; sea surge; river flow; precipitation; mid-latitude cyclone; seasonality; time lag	Yes	South and west Britain	Storm Surge; River Flooding; Extreme Rainfall	Quant	Tail dependence
97	T+M	C	article	van den Hurk, B., van Meijgaard, E., de Valk, P., van Heeringen, K.J. and Gooijer, J., 2015. Analysis of a compounding surge and precipitation event in the Netherlands. Environmental Research Letters, 10(3), p.035001.	compounding events; coastal water management; flooding	Yes	Netherland	Storm Surge; Extreme Rainfall	Quant	Atmospheric model; Hydrological model; Polynomial Regression

ID	Sub-group	TS	Ref type	Citation	Keywords	Inter-relation	Studied Area	Hazards	Quant / Semi-quant/ Qual	Modelling method
98	M		article	Yang, X.C. and Zhang, Q.H., 2013. Joint probability distribution of winds and waves from wave simulation of 20 years (1989-2008) in Bohai Bay. Water Science and Engineering, 6(3), pp.296-307.	wind speed; wave simulation; joint probability distribution; copula function.	Yes	Bohai Bay (China)	Extreme Wind ; Extreme Wave	Quant	Extreme value copula
99	M		article	Zheng, F., Westra, S., Leonard, M. and Sisson, S.A., 2014. Modeling dependence between extreme rainfall and storm surge to estimate coastal flooding risk. Water Resources Research, 50(3), pp.2050-2071.	dependence; coastal flood risk; extreme values		Australia	Storm Surge; Extreme Rainfall	Quant	Extreme value copula; Conditional model
100	M		article	Tinti, S., Pagnoni, G. and Piatanesi, A., 2003. Simulation of tsunamis induced by volcanic activity in the Gulf of Naples (Italy). Natural Hazards and Earth System Science, 3(5), pp.311-320.	tsunami; volcanic eruption		Gulf of Naples	Volcanic Eruption; Tsunami	Quant	Hydrodynamic model
101	M		article	Mazas, F. and Hamm, L., 2017. An event-based approach for extreme joint probabilities of waves and sea levels. Coastal Engineering, 122, pp.44-59.	joint probabilities; event; extreme value copula; upper tail dependence coefficient; wave height; sea level; chi-plot		Britanny	Storm Surge; Extreme Wave	Quant	Extreme value copula
102	M		article	Iordanidou, V., Koutroulis, A.G. and Tsanis, I.K., 2016. Investigating the relationship of lightning activity and rainfall: A case study for Crete Island. Atmospheric Research, 172, pp.16-27.	correlation; clustering; precipitation; lightning	Yes	Crete, Greece	Lightning; Extreme Rainfall	Quant	Spatio-temporal correlation; Linear regression
103	M		article	Geist, E.L., Lynett, P.J. and Chaytor, J.D., 2009. Hydrodynamic modeling of tsunamis from the Currituck landslide. Marine Geology, 264(1-2), pp.41-52.	hydrodynamic; landslide; numerical model; runup; sensitivity analysis; tsunami		North Carolina; USA		Quant	Hydrodynamic model

ID	**Sub-group**	**TS**	**Ref type**	**Citation**	**Keywords**	**Inter-relation**	**Studied Area**	**Hazards**	**Quant / Semi-quant/ Qual**	**Modelling method**
104	M		article	Pelinovsky, E. and Poplavsky, A., 1996. Simplified model of tsunami generation by submarine landslides. Physics and Chemistry of the Earth, 21(1-2), pp.13-17.					Quant	Hydrodynamic model
105	M		article	Dutykh, D., Poncet, R. and Dias, F., 2011. The VOLNA code for the numerical modeling of tsunami waves: Generation, propagation and inundation. European Journal of Mechanics-B/Fluids, 30(6), pp.598-615.	finite volumes; run-down; run-up; shallow water equations; tsunami generation; tsunami waves		Japan		Quant	Hydrodynamic model
106	M		article	Masina, M., Lamberti, A. and Archetti, R., 2015. Coastal flooding: A copula based approach for estimating the joint probability of water levels and waves. Coastal Engineering, 97, pp.37-52.	coastal flooding; copula; probability of failure; Ravenna (Italy); storm surge; wave runup		Italy		Quant	Extreme value copula; Rank correlation coefficients
107	M		article	Trepanier, J.C., Needham, H.F., Elsner, J.B. and Jagger, T.H., 2015. Combining surge and wind risk from hurricanes using a copula model: an example from Galveston, Texas. The Professional Geographer, 67(1), pp.52-61.	copula; extreme winds; hurricanes; risk; storm surge		Texas; USA		Quant	Archimedean copula; Rank correlation coefficients
108	M		article	Tolman, H.L. and Chalikov, D., 1996. Source terms in a third-generation wind wave model. Journal of Physical Oceanography, 26(11), pp.2497-2518.					Quant	Hydrodynamic model
109	M		article	Booij, N., Holthuijsen, L.H. and Ris, R.C., 1997. The" SWAN" wave model for shallow water. In Coastal Engineering 1996 (pp. 668-676).			Australia		Quant	Hydrodynamic model

ID	Sub-group	TS	Ref type	Citation	Keywords	Inter-relation	Studied Area	Hazards	Quant / Semi-quant/ Qual	Modelling method
110	M		article	Quecedo, M., Pastor, M. and Herreros, M.I., 2004. Numerical modelling of impulse wave generated by fast landslides. International journal for numerical methods in engineering, 59(12), pp.1633-1656.	characteristic based galerkin; fractional step; incompressible; level set; navier-stokes; non-newtonian		Alaska; USA		Quant	Hydrodynamic model
111	M		conference proceeding	Luger, S. and Harris, R.L., 2010, September. Modelling tsunami generated by earthquakes and submarine slumps using MIKE-21. In International MIKE by DHI conference, South Africa, Paper (p. P017).	earthquake; mike 21; submarine slump; tsunami		Sumatra		Quant	Hydrodynamic model
112	M		article	Meunier, P., Hovius, N. and Haines, A.J., 2007. Regional patterns of earthquake-triggered landslides and their relation to ground motion. Geophysical Research Letters, 34(20).	earthquake-triggered; landslides; ground motion	Yes			Quant	Linear regression
113	M		article	Bunya, S., Dietrich, J.C., Westerink, J.J., Ebersole, B.A., Smith, J.M., Atkinson, J.H., Jensen, R., Resio, D.T., Luettich, R.A., Dawson, C. and Cardone, V.J., 2010. A high-resolution coupled riverine flow, tide, wind, wind wave, and storm surge model for southern Louisiana and Mississippi. Part I: Model development and validation. Monthly weather review, 138(2), pp.345-377.	coupled model; hydrodynamic model; hurricane		Gulf of Mexico		Quant	Hydrodynamic (wave) model; Atmospheric model
114	M		article	Price, C. and Federmesser, B., 2006. Lightning-rainfall relationships in Mediterranean winter thunderstorms. Geophysical research letters, 33(7).	lightning; rainfall; relationship; thunderstorm	Yes	South Mediterranean		Quant	Linear Regression

ID	Sub-group	TS	Ref type	Citation	Keywords	Inter-relation	Studied Area	Hazards	Quant / Semi-quant/ Qual	Modelling method
115	M		article	Koutroulis, A.G., Grillakis, M.G., Tsanis, I.K., Kotroni, V. and Lagouvardos, K., 2012. Lightning activity, rainfall and flash flooding–occasional or interrelated events? A case study in the island of Crete. Natural Hazards and Earth System Sciences, 12(4), pp.881-891.	Crete; flash flood; interrelated events; rainfall; lightning	Yes	South Mediterranean		Quant	Linear Regression
116	M		article	Hawkes, P.J., Gouldby, B.P., Tawn, J.A. and Owen, M.W., 2002. The joint probability of waves and water levels in coastal engineering design. Journal of hydraulic research, 40(3), pp.241-251.	sea surge; joint probability; extreme; engineering				Quant	Gaussian Copula
117	M		article	Dutfoy, A., Parey, S. and Roche, N., 2014. Multivariate extreme value theory-A tutorial with applications to hydrology and meteorology. Dependence Modeling, 2(1).	multivariate extreme value theory; joint extreme hazards; asymptotic independence		France		Quant	Joint tail model
118	M		article	Ledford, A.W. and Tawn, J.A., 1997. Modelling dependence within joint tail regions. Journal of the Royal Statistical Society: Series B (Statistical Methodology), 59(2), pp.475-499.	coefficient of tail dependence; componentwise maxima; extreme value theory; maximum likelihood; non-homogeneous Poisson process; asymptotic independence		United Kingdom		Quant	Joint tail model
119	T+M	MH	article	Bout, B., Lombardo, L., van Westen, C.J. and Jetten, V.G., 2018. Integration of two-phase solid fluid equations in a catchment model for flashfloods, debris flows and shallow slope failures. Environmental Modelling & Software, 105, pp.1-16.	debris flow; flash floods; openlisem; physically-based modelling; shallow landslides; spatial numerical modelling	Yes	Sicilia; Italy	River Flooding; Landslide	Quant	Hydrodynamic model

ID	Sub-group	TS	Ref type	Citation	Keywords	Inter-relation	Studied Area	Hazards	Quant / Semi-quant/ Qual	Modelling method
120	T+M	C	article	Kumbier, K., Cabral Carvalho, R., Vafeidis, A.T. and Woodroffe, C.D., 2018. Investigating compound flooding in an estuary using hydrodynamic modelling: a case study from the Shoalhaven River, Australia.	hydrodynamic model; compound flooding	Yes	Australia	River Flooding; Storm Surge	Quant	Hydrodynamic model
121	M		article	Yue, S., 2000. The Gumbel logistic model for representing a multivariate storm event. Advances in Water Resources, 24(2), pp.179-185.	conditional distribution; Gumbel distribution; joint; marginal distribution; probability distribution; storm amount; storm frequency analysis; storm peak; bivariate extreme value distribution		Japan		Quant	Multivariate extreme value model (Bivariate logistic model)
122	T+M	C	article	Hao, Z., Hao, F., Singh, V.P. and Ouyang, W., 2017. Quant risk assessment of the effects of drought on extreme temperature in eastern China. Journal of Geophysical Research: Atmospheres, 122(17), pp.9050-9059.	copula framework; drought impact; hot extremes; conditional probability of extreme temperature; drought and wet conditions; impact	Yes	China	Extreme Hot Temperature; Drought	Quant	Gaussian copula
123	M		conference proceeding	Mueller, B. and Seneviratne, S.I., 2012. Hot days induced by precipitation deficits at the global scale. Proceedings of the national academy of sciences, 109(31), pp.12398-12403.	hot day prediction; soil moisture temperature coupling; standardized precipitation index; temperature extremes	Yes	Globe		Quant	Quantile regression
124	M		article	Meng, L. and Shen, Y., 2014. On the relationship of soil moisture and extreme temperatures in East China. Earth Interactions, 18(1), pp.1-20.	soil moisture; heat waves; east china	Yes	China		Quant	Quantile regression

ID	Sub-group	TS	Ref type	Citation	Keywords	Inter-relation	Studied Area	Hazards	Quant / Semi-quant/ Qual	Modelling method
125	M		article	Dong, S., Gao, J., Li, X., Wei, Y. and Wang, L., 2015. A storm surge intensity classification based on extreme water level and concomitant wave height. Journal of Ocean University of China, 14(2), pp.237-244.	classification; distribution; intensity; joint return period; Poisson bi-variable Gumbel logistic; Poisson bi-variable log-normal distribution; storm surge		China		Quant	Multivariate extreme value model
126	M		article	Rueda, A., Camus, P., Tomás, A., Vitousek, S. and Méndez, F.J., 2016. A multivariate extreme wave and storm surge climate emulator based on weather patterns. Ocean Modelling, 104, pp.242-251.	joint probability; extremes; statistical downscaling		Spain		Quant	Gaussian copula
127	M		article	Bengtsson, L., 2016. Probability of combined high sea levels and large rains in Malmö, Sweden, southern Öresund. Hydrological Processes, 30(18), pp.3172-3183.	extreme events; conditional probability; frank's copula; seasonal distribution; urban environment	Yes	Sweden		Quant	Archimedean copula; Conditional model
128	M		article	Benestad, R.E. and Haugen, J.E., 2007. On complex extremes: flood hazards and combined high spring-time precipitation and temperature in Norway. Climatic Change, 85(3-4), pp.381-406.	extreme; joint probability; precipitation; flood	Yes	Norway		Quant	Empirical copula
129	T+M	C	article	Tencer, B., Weaver, A. and Zwiers, F., 2014. Joint occurrence of daily temperature and precipitation extreme events over Canada. Journal of Applied Meteorology and Climatology, 53(9), pp.2148-2162.	extreme; joint occurrence; temperature; precipitation	Yes	Canada		Quant	One tail chi square test
130	M		article	Hawkes, P.J., 2008. Joint probability analysis for estimation of extremes. Journal of Hydraulic Research, 46(S2), pp.246-256.	coast; dependence; extremes; flood risk; joint probability; river		South England; United Kingdom		Quant	Multivariate extreme value model

ID	Sub-group	TS	Ref type	Citation	Keywords	Inter-relation	Studied Area	Hazards	Quant / Semi-quant/ Qual	Modelling method
131	M		article	Coles, S.G. and Tawn, J.A., 1994. Statistical methods for multivariate extremes: an application to structural design. Applied Statistics, pp.1-48.	concomitants; extreme value theory; generalized extreme value distribution; generalized pareto distribution; multivariate extreme value distribution; multivariate ordering; point processes; reliability; sea-levels; waves		South England; United Kingdom		Quant	Multivariate extreme value model
132	M		article	Zheng, F., Leonard, M. and Westra, S., 2017. Application of the design variable method to estimate coastal flood risk. Journal of Flood Risk Management, 10(4), pp.522-534.	change; climate; flood risk; joint probability; uncertainty analysis		Australia		Quant	Multivariate extreme value model; point process
133	T+M	C	article	Zheng, F., Westra, S. and Sisson, S.A., 2013. Quantifying the dependence between extreme rainfall and storm surge in the coastal zone. Journal of Hydrology, 505, pp.172-187.	extreme rainfall; extreme storm surge; dependence; flood risk	Yes	Australia		Quant	Tail dependence
134	M		article	Torres, J.M., Bass, B., Irza, N., Fang, Z., Proft, J., Dawson, C., Kiani, M. and Bedient, P., 2015. Characterizing the hydraulic interactions of hurricane storm surge and rainfall–runoff for the Houston–Galveston region. Coastal Engineering, 106, pp.7-19.	hurricane; rainfall runoff; storm surge; barrier; distributed inland hydrology; unsteady riverine modelling; swan+adcirc	Yes	USA		Quant	Hydrological model; Hydrodynamic model
135	M		article	Xu, K., Ma, C., Lian, J. and Bin, L., 2014. Joint probability analysis of extreme precipitation and storm tide in a coastal city under changing environment. PloS one, 9(10), p.e109341.	joint probability; extreme; precipitation; coastal		China		Quant	Archimedean copula

ID	Sub-group	TS	Ref type	Citation	Keywords	Inter-relation	Studied Area	Hazards	Quant / Semi-quant/ Qual	Modelling method
136	T+M	C	article	Petroliagkis, T.I., 2018. Estimations of statistical dependence as joint return period modulator of compound events–Part 1: Storm surge and wave height. Natural Hazards and Earth System Sciences, 18(7), pp.1937-1955.	dependence; joint return period; compound event	Yes	Europe	Storm Surge; Extreme Wave	Quant	Tail dependence; Linear correlation
137	M		article	Silva-Araya, W.F., Santiago-Collazo, F.L., Gonzalez-Lopez, J. and Maldonado-Maldonado, J., 2018. Dynamic modeling of surface runoff and storm surge during hurricane and tropical storm events. Hydrology, 5(1), p.13.	tropical storm modelling; two-dimensional hydrologic models; ocean circulation models; coastal flooding; coastal hazards		USA		Quant	Hydrological model; Hydrodynamic model
138	I		report	Decker, K. and Brinkman, H., 2015. List of External Hazards to be Considered in ASAMPSA_E.						
139	M		article	Wang, J., Gao, W., Xu, S. and Yu, L., 2012. Evaluation of the combined risk of sea level rise, land subsidence, and storm surges on the coastal areas of Shanghai, China. Climatic change, 115(3-4), pp.537-558.	combined risk; coastal area; subsidence; storm surge; china		China		Quant	Hydrodynamic model
140	T+M	C	article	Serinaldi, F., 2016. Can we tell more than we can know? The limits of bivariate drought analyses in the United States. Stochastic environmental research and risk assessment, 30(6), pp.1691-1704.	bivariate frequency analysis; joint return periods; copula; uncertainty; joint extreme event; drought; temperature; precipitation deficit; moisture conditions	Yes	USA	Drought; Extreme Temperature	Quant	Gaussian copula

ID	**Sub-group**	**TS**	**Ref type**	**Citation**	**Keywords**	**Inter-relation**	**Studied Area**	**Hazards**	**Quant / Semi-quant/ Qual**	**Modelling method**
141	M		article	Couasnon, Anaïs, Antonia Sebastian, and Oswaldo Morales-Nápoles. "A Copula-Based Bayesian Network for Modeling Compound Flood Hazard from Riverine and Coastal Interactions at the Catchment Scale: An Application to the Houston Ship Channel, Texas." Water 10, no. 9 (2018): 1190.	flood risk; copula; compound events; multivariate; storm surge; spatial dependence; Bayesian network				Quant	Non Parametric Bayesian Network, Gaussian Copula
142	M		article	Ward, P.J., Couasnon, A., Eilander, D., Haigh, I.D., Hendry, A., Muis, S., Veldkamp, T.I., Winsemius, H.C. and Wahl, T., 2018. Dependence between high sea-level and high river discharge increases flood hazard in global deltas and estuaries. Environmental Research Letters, 13(8), p.084012.	coastal flooding; compound flood; flood; flood risk; river flooding				Quant	Rank correlation; extreme value copula; archimedean copula
143	M		article	Berg, P., Moseley, C. and Haerter, J.O., 2013. Strong increase in convective precipitation in response to higher temperatures. Nature Geoscience, 6(3), p.181.					Quant	Linear regression
144	M		article	Sadegh, M., Ragno, E. and AghaKouchak, A., 2017. Multivariate C opula A nalysis T oolbox (MvCAT): Describing dependence and underlying uncertainty using a B ayesian framework. Water Resources Research, 53(6), pp.5166-5183.					Quant	Archimedean Copula; Extreme value Copula; Gaussian Copula
145	M		report	Cooley, D., Thibaud, E., Castillo, F. and Wehner, M.F., 2017. A Nonparametric Method for Producing Isolines of Bivariate Exceedance Probabilities. arXiv preprint arXiv:1710.05248.	asymptotic independence; extreme values; hidden regular variation; multivariate; regular variation				Quant	Tail dependence; Multivariate extreme model

ID	Sub-group	TS	Ref type	Citation	Keywords	Inter-relation	Studied Area	Hazards	Quant / Semi-quant/ Qual	Modelling method
146	M		article	Malamud, B.D., Turcotte, D.L., Guzzetti, F. and Reichenbach, P., 2004. Landslide inventories and their statistical properties. Earth Surface Processes and Landforms, 29(6), pp.687-711.	landslides; earthquakes; erosion; natural hazards; frequency-size statistics; intensity scale			Extreme Rainfall; Earthquake; Snow Melt; Landslide	Quant	Linear regression

Appendix B: Hazard Interrelations Database

This appendix is a database of 70 references related to **Chapter 2** and consists of the following:

- **Table B1**. Interrelations Database Structure. Detailed metadata information describing **Table B2**
- **Table B2**. Interrelations Database. A subset of 70 of the references from **Table A1** consisting of 73 rows of information (due to different hazard combinations for two references) with 14 attributes (columns) for each reference, including citation information, studied region, hazard A and B type and category in the interrelationship that is quantified, modelling approach, family and model, interrelationship type.

Table B1: Interrelations Database Structure. Detailed metadata information describing Table B2.

Attributes	**Definition**
Reference	
Publication Year	
Studied Area	
Hazard A	
Hazard B	
Model approach	**Empirical:** Experience-based equations or distributions representing the behaviour of the interaction between two (or more) hazards. **Mechanistic:** based on physical process and mechanism that rule the considered system operation. **Stochastic:** based on samples of different variables with random behaviour not dependent on the previous state of those variable (the range of data can be bounded)
Model subgroup	Multivariate model; Copula; Dependence measure; Regression; Conceptual model; Physical model
Model	Logistic regression; Hydrodynamic model; Extreme value copula; Vine copula; Linear correlation; Rank correlation; Hydrological model; Archimedean copula; Climate model; Tail dependence; Power regression; Polynomial regression; Joint tail model; Multivariate extreme model; Gaussian copula; Quantile regression; Conditional extreme model; Empirical copula.
Interrelation type	Triggering; Change condition; Compound; Independent; Mutually exclusive

Table B2: Interrelations Database. A subset of 70 of the references from Table A1 consisting of 73 rows of information (due to different hazard combinations for two references) with 14 attributes (columns) for each reference, including citation information, studied region, hazard A and B type and category in the interrelationship that is quantified, modelling approach, family and model, interrelationship type. A detailed description of each column is given in Table A1.

Reference	Year	Studied Area	Hazard A	Hazard B	model approach	Model subgroup	Model	Interrelation type
Benestad, R.E. and Haugen, J.E., 2007. On complex extremes: flood hazards and combined high spring-time precipitation and temperature in Norway. Climatic Change, 85(3-4), pp.381-406.	2007	Norway	Rainfall	Extreme Temperature	Empirical	Copula	Empirical Copula	Compound
Bengtsson, L., 2016. Probability of combined high sea levels and large rains in Malmö, Sweden, southern Öresund. Hydrological Processes, 30(18), pp.3172-3183.	2016	Sweden	Storm Surge	Extreme Rainfall	Stochastic	Copula; Multivariate Model	Archimedean Copula; Conditional Model	Mutually Exclusive
Berg, P., Moseley, C. and Haerter, J.O., 2013. Strong increase in convective precipitation in response to higher temperatures. Nature Geoscience, 6(3), p.181.	2013	Germany	Temperature	Extreme Rainfall	Empirical	Regression	Linear Regression	Compound
Bevacqua, E., Maraun, D., Hobæk Haff, I., Widmann, M. and Vrac, M., 2017. Multivariate statistical modelling of compound events via pair-copula constructions: analysis of floods in Ravenna (Italy). Hydrology and Earth System Sciences, 21(6), pp.2701-2723.	2017	Italy	Storm Surge	River Flooding	Stochastic	Copula	Vine Copula	Compound

Reference	Year	Studied Area	Hazard A	Hazard B	model approach	Model subgroup	Model	Interrelation type
Booij, N., Holthuijsen, L.H. and Ris, R.C., 1997. The" SWAN" wave model for shallow water. In Coastal Engineering 1996 (pp. 668-676).	1997	Australia	Extreme Wind	Extreme Wave Height	Mechanistic	Physical Model	Hydrodynamic Model	Triggering
Bout, B., Lombardo, L., van Westen, C.J. and Jetten, V.G., 2018. Integration of two-phase solid fluid equations in a catchment model for flashfloods, debris flows and shallow slope failures. Environmental Modelling & Software, 105, pp.1-16.	2018	Sicilia	Extreme Rainfall	Landslide	Mechanistic	Physical Model	Hydrodynamic Model	Triggering
Bunya, S., Dietrich, J.C., Westerink, J.J., Ebersole, B.A., Smith, J.M., Atkinson, J.H., Jensen, R., Resio, D.T., Luettich, R.A., Dawson, C. and Cardone, V.J., 2010. A high-resolution coupled riverine flow, tide, wind, wind wave, and storm surge model for southern Louisiana and Mississippi. Part I: Model development and validation. Monthly weather review, 138(2), pp.345-377.	2010	Gulf Of Mexico	Extreme Wind	Storm Surge; Extreme Wave	Mechanistic	Physical Model	Hydrodynamic (Wave) Model; Atmospheric Model	Compound; Triggering

Reference	Year	Studied Area	Hazard A	Hazard B	model approach	Model subgroup	Model	Interrelation type
Caine, N., 1980. The rainfall intensity: duration control of shallow landslides and debris flows. Geografiska Annaler. Series A. Physical Geography, pp.23-27.	1980	World	Extreme Rainfall	Landslide	Empirical	Regression	Linear Regression	Triggering
Carey, L.D., Rutledge, S.A. and Petersen, W.A., 2003. The relationship between severe storm reports and cloud-to-ground lightning polarity in the contiguous United States from 1989 to 1998. Monthly weather review, 131(7), pp.1211-1228.	2003	USA	Lightning	Hail	Empirical	Regression	Linear Regression	Compound
Carey, L.D., Rutledge, S.A. and Petersen, W.A., 2003. The relationship between severe storm reports and cloud-to-ground lightning polarity in the contiguous United States from 1989 to 1998. Monthly weather review, 131(7), pp.1211-1228.	2004	USA	Lightning	Extreme Rainfall	Empirical	Regression	Linear Regression	Compound
Carey, L.D., Rutledge, S.A. and Petersen, W.A., 2003. The relationship between severe storm reports and cloud-to-ground lightning polarity in the contiguous United States from 1989 to 1998. Monthly weather review, 131(7), pp.1211-1228.	2005	USA	Lightning	Tornado	Empirical	Regression	Linear Regression	Compound

Reference	Year	Studied Area	Hazard A	Hazard B	model approach	Model subgroup	Model	Interrelation type
Catane, S.G., Abon, C.C., Saturay, R.M., Mendoza, E.P.P. and Futalan, K.M., 2012. Landslide-amplified flash floods—the June 2008 Panay Island flooding, Philippines. Geomorphology, 169, pp.55-63.	2012	Philippines	Landslide	River Flooding	Mechanistic	Conceptual Model	Hydrological Model	Change Condition
Coles, S.G. and Tawn, J.A., 1994. Statistical methods for multivariate extremes: an application to structural design. Applied Statistics, pp.1-48.	1994	South England	Storm Surge	Extreme Wave Height	Stochastic	Multivariate Model	Joint Tail Model	Compound
Cooley, D., Thibaud, E., Castillo, F. and Wehner, M.F., 2017. A Nonparametric Method for Producing Isolines of Bivariate Exceedance Probabilities. arXiv preprint arXiv:1710.05248.	2017	USA; Pakistan	Extreme Wind	Drought	Stochastic; Empirical	Dependence Measure; Multivariate Model	Tail Dependence; Multivariate Extreme Model	Compound
Costa, J.E. and Schuster, R.L., 1988. The formation and failure of natural dams. Geological society of America bulletin, 100(7), pp.1054-1068.	1988	World	Landslide	River Flooding	Empirical	Regression	Linear Regression	Triggering

Reference	Year	Studied Area	Hazard A	Hazard B	model approach	Model subgroup	Model	Interrelation type
Couasnon, Anaïs, Antonia Sebastian, and Oswaldo Morales-Nápoles. "A Copula-Based Bayesian Network for Modeling Compound Flood Hazard from Riverine and Coastal Interactions at the Catchment Scale: An Application to the Houston Ship Channel, Texas." Water 10, no. 9 (2018): 1190.	2018	USA	Storm Surge	River Flooding	Stochastic	Copula	Non Parametric Bayesian Network, Gaussian Copula	Compound
Dong, S., Gao, J., Li, X., Wei, Y. and Wang, L., 2015. A storm surge intensity classification based on extreme water level and concomitant wave height. Journal of Ocean University of China, 14(2), pp.237-244.	2015	China	Storm Surge	Extreme Wave Height	Stochastic	Multivariate Model	Parametric Model	Compound
Dutfoy, A., Parey, S. and Roche, N., 2014. Multivariate extreme value theory-A tutorial with applications to hydrology and meteorology. Dependence Modeling, 2(1).	2014	France	Extreme Temperature	Extreme Wind	Stochastic	Multivariate Model	Joint Tail Model	Mutually Exclusive
Dutykh, D., Poncet, R. and Dias, F., 2011. The VOLNA code for the numerical modeling of tsunami waves: Generation, propagation and inundation. European Journal of Mechanics-B/Fluids, 30(6), pp.598-615.	2011	Japan	Earthquake	Tsunami	Mechanistic	Physical Model	Hydrodynamic Model	Triggering

Reference	Year	Studied Area	Hazard A	Hazard B	model approach	Model subgroup	Model	Interrelation type
Fischer, E.M. and Knutti, R., 2013. Robust projections of combined humidity and temperature extremes. Nature Climate Change, 3(2), pp.126-130.	2013	World	Extreme Temperature	Drought	Mechanistic	Physical Model	Climate Model	Compound
Geist, E.L. and Parsons, T., 2006. Probabilistic analysis of tsunami hazards. Natural Hazards, 37(3), pp.277-314.	2006	North American Pacific Coast	Earthquake	Tsunami	Mechanistic/ Stochastic	Physical Model	Hydrodynamic Model	Triggering
Geist, E.L., Lynett, P.J. and Chaytor, J.D., 2009. Hydrodynamic modeling of tsunamis from the Currituck landslide. Marine Geology, 264(1-2), pp.41-52.	2009	North Carolina	Landslide	Tsunami	Mechanistic	Physical Model	Hydrodynamic Model	Triggering
Glade, T., Crozier, M. and Smith, P., 2000. Applying probability determination to refine landslide-triggering rainfall thresholds using an empirical" Antecedent Daily Rainfall Model". Pure and Applied Geophysics, 157(6-8), pp.1059-1079.	2000	New Zealand	Extreme Rainfall	Landslide	Empirical	Regression	Logistic Regression	Triggering
Hao, Z., Hao, F., Singh, V.P. and Ouyang, W., 2017. Quantitative risk assessment of the effects of drought on extreme temperature in eastern	2017	China	Drought	Extreme Temperature	Stochastic	Copula	Gaussian Copula	Compound

Reference	Year	Studied Area	Hazard A	Hazard B	model approach	Model subgroup	Model	Interrelation type
China. Journal of Geophysical Research: Atmospheres, 122(17), pp.9050-9059.								
Hawkes, P.J., 2008. Joint probability analysis for estimation of extremes. Journal of Hydraulic Research, 46(S2), pp.246-256.	2008	South England	Storm Surge	Extreme Wave Height	Stochastic	Multivariate Model	Parametric Model	Compound
Hawkes, P.J., Gouldby, B.P., Tawn, J.A. and Owen, M.W., 2002. The joint probability of waves and water levels in coastal engineering design. Journal of hydraulic research, 40(3), pp.241-251.	2002		Storm Surge	Extreme Wave Height	Stochastic	Copula	Gaussian Copula	Compound
Iordanidou, V., Koutroulis, A.G. and Tsanis, I.K., 2016. Investigating the relationship of lightning activity and rainfall: A case study for Crete Island. Atmospheric Research, 172, pp.16-27.	2016	Crete	Lightning	Extreme Rainfall	Empirical	Regression	Spatio-Temporal Correlation; Linear Regression	Compound
Irish, J.L., Resio, D.T. and Ratcliff, J.J., 2008. The influence of storm size on hurricane surge. Journal of Physical Oceanography, 38(9), pp.2003-2013.	2008	Gulf Of Mexico	Extreme Wind	Storm Surge	Mechanistic	Physical Model	Atmospheric Model	Triggering

Reference	Year	Studied Area	Hazard A	Hazard B	model approach	Model subgroup	Model	Interrelation type
Johansson, B. and Chen, D., 2003. The influence of wind and topography on precipitation distribution in Sweden: Statistical analysis and modelling. International Journal of Climatology, 23(12), pp.1523-1535.	2003	Sweden	Extreme Wind	Extreme Rainfall	Empirical	Regression	Linear Regression	Compound
Keefer, D.K., 1994. The importance of earthquake-induced landslides to long-term slope erosion and slope-failure hazards in seismically active regions. Geomorphology, 10(1-4), pp.265-284.	2002	World	Earthquake	Landslide	Empirical	Regression	Linear Regression	Triggering
Keefer, D.K., 2002. Investigating landslides caused by earthquakes–a historical review. Surveys in geophysics, 23(6), pp.473-510.	1994	World	Earthquake	Landslide	Empirical	Regression	Linear Regression	Triggering
Klerk, W.J., Winsemius, H.C., van Verseveld, W.J., Bakker, A.M.R. and Diermanse, F.L.M., 2015. The co-incidence of storm surges and extreme discharges within the Rhine–Meuse Delta. Environmental Research Letters, 10(3), p.035005.	2015	Netherland	Storm Surge	River Flooding	Empirical	Dependence Measure	Tail Dependence	Compound

Reference	Year	Studied Area	Hazard A	Hazard B	model approach	Model subgroup	Model	Interrelation type
Koutroulis, A.G., Grillakis, M.G., Tsanis, I.K., Kotroni, V. and Lagouvardos, K., 2012. Lightning activity, rainfall and flash flooding–occasional or interrelated events? A case study in the island of Crete. Natural Hazards and Earth System Sciences, 12(4), pp.881-891.	2013	South Mediterranean	Lightning	Extreme Rainfall	Empirical	Regression	Linear Regression	Compound
Kumbier, K., Cabral Carvalho, R., Vafeidis, A.T. and Woodroffe, C.D., 2018. Investigating compound flooding in an estuary using hydrodynamic modelling: a case study from the Shoalhaven River, Australia.	2018	Australia	River Flooding	Storm Surge	Mechanistic	Physical Model	Hydrodynamic Model	Change Condition; Compound
Ledford, A.W. and Tawn, J.A., 1997. Modelling dependence within joint tail regions. Journal of the Royal Statistical Society: Series B (Statistical Methodology), 59(2), pp.475-499.	1997	United Kingdom	Extreme Wind	Extreme Rainfall	Stochastic	Multivariate Model	Joint Tail Model	Compound
Lian, J.J., Xu, K. and Ma, C., 2013. Joint impact of rainfall and tidal level on flood risk in a coastal city with a complex river network: a case study of Fuzhou City, China. Hydrology and Earth System Sciences, 17(2), p.679.	2013	China	Tidal Level	River Flooding	Stochastic	Copula	Extreme Value Copula	Change Condition

Reference	Year	Studied Area	Hazard A	Hazard B	model approach	Model subgroup	Model	Interrelation type
Luger, S. and Harris, R.L., 2010, September. Modelling tsunami generated by earthquakes and submarine slumps using MIKE-21. In International MIKE by DHI conference, South Africa, Paper (p. P017).	2010	Sumatra	Earthquake	Tsunami	Mechanistic	Physical Model	Hydrodynamic Model	Triggering
Ma, T., Li, C., Lu, Z. and Bao, Q., 2015. Rainfall intensity–duration thresholds for the initiation of landslides in Zhejiang Province, China. Geomorphology, 245, pp.193-206.	2015	Zhejiang Province, China	Extreme Rainfall	Landslide	Empirical	Regression	Linear Regression	Triggering
Malamud, B.D., Turcotte, D.L., Guzzetti, F. and Reichenbach, P., 2004. Landslide inventories and their statistical properties. Earth Surface Processes and Landforms, 29(6), pp.687-711.	2004		Earthquake	Landslide	Empirical	Regression	Linear Regression	Triggering
Masina, M., Lamberti, A. and Archetti, R., 2015. Coastal flooding: A copula based approach for estimating the joint probability of water levels and waves. Coastal Engineering, 97, pp.37-52.	2015	Italy	Storm Surge	Extreme Wave Height	Stochastic; Empirical	Copula	Extreme Value Copula; Rank Correlation Coefficients	Compound
Mazas, F. and Hamm, L., 2017. An event-based approach for extreme joint probabilities of waves and sea levels. Coastal Engineering, 122, pp.44-59.	2017	Britany	Extreme Wave Height	Storm Surge	Stochastic	Copula	Extreme Value Copula	Compound

Reference	Year	Studied Area	Hazard A	Hazard B	model approach	Model subgroup	Model	Interrelation type
Meng, L. and Shen, Y., 2014. On the relationship of soil moisture and extreme temperatures in East China. Earth Interactions, 18(1), pp.1-20.	2014	China	Drought	Extreme Temperature	Empirical	Regression	Quantile Regression	Compound
Meunier, P., Hovius, N. and Haines, A.J., 2007. Regional patterns of earthquake-triggered landslides and their relation to ground motion. Geophysical Research Letters, 34(20).	2007		Earthquake	Landslide	Empirical	Regression	Linear Regression	Triggering
Ming, X., Xu, W., Li, Y., Du, J., Liu, B. and Shi, P., 2015. Quantitative multi-hazard risk assessment with vulnerability surface and hazard joint return period. Stochastic environmental research and risk assessment, 29(1), pp.35-44.	2015	Yangtse River Delta Region (YRD), China	Extreme Wind	Extreme Rainfall	Stochastic	Copula	Extreme Value Copula	Compound
Mueller, B. and Seneviratne, S.I., 2012. Hot days induced by precipitation deficits at the global scale. Proceedings of the national academy of sciences, 109(31), pp.12398-12403.	2012	World	Drought	Extreme Temperature	Empirical	Regression	Quantile Regression	Compound
Pelinovsky, E. and Poplavsky, A., 1996. Simplified model of tsunami generation by submarine landslides. Physics and Chemistry of the Earth, 21(1-2), pp.13-17.	1996		Landslide	Tsunami	Mechanistic	Physical Model	Hydrodynamic Model	Triggering

Reference	Year	Studied Area	Hazard A	Hazard B	model approach	Model subgroup	Model	Interrelation type
Petroliagkis, T.I., 2018. Estimations of statistical dependence as joint return period modulator of compound events–Part 1: Storm surge and wave height. Natural Hazards and Earth System Sciences, 18(7), pp.1937-1955.	2018	Europe	Storm Surge	Extreme Wave Height	Empirical	Dependence Measure	Tail Dependence; Linear Correlation	Compound
Phan, L.T., Simiu, E., McInerney, M.A., Taylor, A.A., Glahn, B. and Powell, M.D., 2007. Methodology for development of design criteria for joint hurricane wind speed and storm surge events: Proof of concept. NIST Technical Note, 1482.	2007	Florida	Storm Surge	Extreme Wind	Stochastic Input Mechanistic	Physical Model	Hydrodynamic Model	Compound
Piepgrass, M.V., Krider, E.P. and Moore, C.B., 1982. Lightning and surface rainfall during Florida thunderstorms. Journal of Geophysical Research: Oceans, 87(C13), pp.11193-11201.	1982	Florida	Lightning	Extreme Rainfall	Empirical	Regression	Linear Regression	Compound
Price, C. and Federmesser, B., 2006. Lightning-rainfall relationships in Mediterranean winter thunderstorms. Geophysical research letters, 33(7).	2006	South Mediterranean	Lightning	Extreme Rainfall	Empirical	Regression	Linear Regression	Compound

Reference	**Year**	**Studied Area**	**Hazard A**	**Hazard B**	**model approach**	**Model subgroup**	**Model**	**Interrelation type**
Quecedo, M., Pastor, M. and Herreros, M.I., 2004. Numerical modelling of impulse wave generated by fast landslides. International journal for numerical methods in engineering, 59(12), pp.1633-1656.	2004	Alaska	Landslide	Tsunami	Mechanistic	Physical Model	Hydrodynamic Model	Triggering
Rueda, A., Camus, P., Tomás, A., Vitousek, S. and Méndez, F.J., 2016. A multivariate extreme wave and storm surge climate emulator based on weather patterns. Ocean Modelling, 104, pp.242-251.	2016	Spain	Storm Surge	Extreme Wave Height	Stochastic	Copula	Gaussian Copula	Compound
Sadegh, M., Ragno, E. and AghaKouchak, A., 2017. Multivariate C opula A nalysis T oolbox (MvCAT): Describing dependence and underlying uncertainty using a B ayesian framework. Water Resources Research, 53(6), pp.5166-5183.	2017	USA	Extreme Low Precipitation	Soil Moisture	Stochastic	Copula	Archimedean Copula; Extreme Value Copula; Gaussian Copula	Compound
Serinaldi, F., 2016. Can we tell more than we can know? The limits of bivariate drought analyses in the United States. Stochastic environmental research and risk assessment, 30(6), pp.1691-1704.	2016	USA	Drought	Extreme Temperature	Stochastic	Copula	Gaussian Copula	Compound

Reference	**Year**	**Studied Area**	**Hazard A**	**Hazard B**	**model approach**	**Model subgroup**	**Model**	**Interrelation type**
Silva-Araya, W.F., Santiago-Collazo, F.L., Gonzalez-Lopez, J. and Maldonado-Maldonado, J., 2018. Dynamic modeling of surface runoff and storm surge during hurricane and tropical storm events. Hydrology, 5(1), p.13.	2018	USA	Storm Surge	River Flooding	Mechanistic	Physical Model	Hydrological Model; Hydrodynamic Model	Compound
Silvestro, F., Rebora, N., Rossi, L., Dolia, D., Gabellani, S., Pignone, F., Trasforini, E., Rudari, R., Angeli, S.D. and Masciulli, C., 2016. What if the 25 October 2011 event that struck Cinque Terre (Liguria) had happened in Genoa, Italy? Flooding scenarios, hazard mapping and damage estimation. Natural Hazards and Earth System Sciences, 16(8), pp.1737-1753.	2016	Liguria, Italy	Extreme Rainfall	River Flooding	Mechanistic	Physical Model	Atmosheric Model; Hydrological Model; Hydrodynamic Model	Triggering
Suppasri, A., Imamura, F. and Koshimura, S., 2012. Tsunamigenic ratio of the Pacific Ocean earthquakes and a proposal for a tsunami index. Natural Hazards and Earth System Sciences, 12(1), p.175.	2012	Pacific Ocean	Earthquake	Tsunami	Empirical	Regression	Power Regression (Non-Linear Regression)	Triggering
Svensson, C. and Jones, D.A., 2004. Dependence between Storm surge, river flow and precipitation in south and west Britain.	2004	South And West Britain	Storm Surge	River Flooding	Empirical	Dependence Measure	Tail Dependence	Compound

Reference	Year	Studied Area	Hazard A	Hazard B	model approach	Model subgroup	Model	Interrelation type
Hydrology and Earth System Sciences Discussions, 8(5), pp.973-992.								
Tencer, B., Weaver, A. and Zwiers, F., 2014. Joint occurrence of daily temperature and precipitation extreme events over Canada. Journal of Applied Meteorology and Climatology, 53(9), pp.2148-2162.	2014	Canada	Rainfall	Extreme Temperature	Empirical	Test	One Tail Chi Square Test	Variable
Tinti, S., Pagnoni, G. and Piatanesi, A., 2003. Simulation of tsunamis induced by volcanic activity in the Gulf of Naples (Italy). Natural Hazards and Earth System Science, 3(5), pp.311-320.	2003	Gulf Of Naples	Volcanic Eruption	Tsunami	Mechanistic	Physical Model	Hydrodynamic Model	Triggering
Tolman, H.L. and Chalikov, D., 1996. Source terms in a third-generation wind wave model. Journal of Physical Oceanography, 26(11), pp.2497-2518.	1996		Extreme Wind	Extreme Wave Height	Mechanistic	Physical Model	Hydrodynamic Model	Triggering
Torres, J.M., Bass, B., Irza, N., Fang, Z., Proft, J., Dawson, C., Kiani, M. and Bedient, P., 2015. Characterizing the hydraulic interactions of hurricane storm surge and rainfall–runoff for the	2015	USA	Storm Surge	River Flooding	Mechanistic	Physical Model	Hydrological Model; Hydrodynamic Model	Compound

Reference	Year	Studied Area	Hazard A	Hazard B	model approach	Model subgroup	Model	Interrelation type
Houston–Galveston region. Coastal Engineering, 106, pp.7-19.								
Trepanier, J.C., Needham, H.F., Elsner, J.B. and Jagger, T.H., 2015. Combining surge and wind risk from hurricanes using a copula model: an example from Galveston, Texas. The Professional Geographer, 67(1), pp.52-61.	2015	Texas	Storm Surge	Extreme Wind	Stochastic; Empirical	Copula	Archimedean Copula; Rank Correlation Coefficients	Compound
van den Hurk, B., van Meijgaard, E., de Valk, P., van Heeringen, K.J. and Gooijer, J., 2015. Analysis of a compounding surge and precipitation event in the Netherlands. Environmental Research Letters, 10(3), p.035001.	2015	Netherland	Storm Surge	River Flooding	Mechanistic	Physical Model	Atmospheric Model; Hydrological Model	Compound
van den Hurk, B., van Meijgaard, E., de Valk, P., van Heeringen, K.J. and Gooijer, J., 2015. Analysis of a compounding surge and precipitation event in the Netherlands. Environmental Research Letters, 10(3), p.035001.	2015	Netherland	Extreme Wind	Storm Surge	Empirical	Regression	Polynomial Regression	Triggering

Reference	Year	Studied Area	Hazard A	Hazard B	model approach	Model subgroup	Model	Interrelation type
Wang, J., Gao, W., Xu, S. and Yu, L., 2012. Evaluation of the combined risk of sea level rise, land subsidence, and storm surges on the coastal areas of Shanghai, China. Climatic change, 115(3-4), pp.537-558.	2012	China	Land Subsidience	Storm Surge	Mechanistic	Physical Model	Hydrodynamic Model	Independence
Ward, P.J., Couasnon, A., Eilander, D., Haigh, I.D., Hendry, A., Muis, S., Veldkamp, T.I., Winsemius, H.C. and Wahl, T., 2018. Dependence between high sea-level and high river discharge increases flood hazard in global deltas and estuaries. Environmental Research Letters, 13(8), p.084012.	2018	World	Storm Surge	River Flooding	Empirical; Stochastic	Dependence Measure; Copula	Rank Correlation; Extreme Value Copula; Archimedean Copula	Compound
Xu, K., Ma, C., Lian, J. and Bin, L., 2014. Joint probability analysis of extreme precipitation and storm tide in a coastal city under changing environment. PloS one, 9(10), p.e109341.	2014	China	Storm Surge	Extreme Rainfall	Stochastic	Copula	Archimedean Copula	Compound
Yang, X.C. and Zhang, Q.H., 2013. Joint probability distribution of winds and waves from wave simulation of 20 years (1989-2008) in Bohai Bay. Water Science and Engineering, 6(3), pp.296-307.	2013	Bohai Bay (China)	Extreme Wind	Extreme Wave Height	Stochastic	Copula	Extreme Value Copula	Triggering

Reference	**Year**	**Studied Area**	**Hazard A**	**Hazard B**	**model approach**	**Model subgroup**	**Model**	**Interrelation type**
Yue, S., 2000. The Gumbel logistic model for representing a multivariate storm event. Advances in Water Resources, 24(2), pp.179-185.	2000	Tokushima	Extreme Rainfall A (Storm Peak)	Extreme Rainfall B (Storm Amount)	Stochastic	Multivariate Model	Parametric Model (Bivariate Logistic Model)	Compound
Zheng, F., Leonard, M. and Westra, S., 2017. Application of the design variable method to estimate coastal flood risk. Journal of Flood Risk Management, 10(4), pp.522-534.	2017	Australia	Storm Surge	Extreme Rainfall	Stochastic	Multivariate Model	Parametric Model; Point Process	Compound
Zheng, F., Westra, S. and Sisson, S.A., 2013. Quantifying the dependence between extreme rainfall and storm surge in the coastal zone. Journal of Hydrology, 505, pp.172-187.	2013	Australia	Storm Surge	Extreme Rainfall	Empirical	Dependence Measure	Tail Dependence	Compound
Zheng, F., Westra, S., Leonard, M. and Sisson, S.A., 2014. Modeling dependence between extreme rainfall and storm surge to estimate coastal flooding risk. Water Resources Research, 50(3), pp.2050-2071.	2014	Australia	Extreme Rainfall	Storm Surge	Stochastic	Copula; Multivariate Model	Extreme Value Copula; Conditional Model	Compound

Appendix C: Historic Multi-hazard events catalogue

This appendix is a catalogue of 50 multi-hazard events related to the five multi-hazard networks (ground movement, convective storm, extratropical cyclone, compound dry, compound cold) presented in **Chapter 3**:

- **Table C1.** The 50 historic major multi-hazard events compiled in **Chapter 3.**
- **Table C2**. 32 sources used to build the historic major multi-hazard event catalogue. The sources are of five types: single hazard catalogue; catalogue of reported weather events; peer review articles, disaster database; multi-hazard catalogue.
- **Table C3.** Supporting literature used to build the historic major multi-hazard events catalogue.

Table C1: The 50 historic major multi-hazard events compiled in Chapter 3. N_{Haz} is the number of hazard reported within the event, N_{Inter} is the number of interrelation that might have occurred during the event according to the networks developed in Section 3.3. D is the duration of the events in days and Ref ID is the ID of the reference used to estimate the attributes of the multi-hazard event (references are displayed in Table C2 and Table C3).

MH Event	Event	Start Date	End date	Hazards	Impacted place	N_{Haz}	N_{Inter}	Spatial scale	D (days)	Source ID
Ground Motion	GM01 Lisbon Tsunami 1755	01/11/1755	01/11/1755	Earthquake, Tsunami	Portugal	2	3	Continental	0.1	1,2,5*
	GM02 Norway Landslide-Tsunami 1888	23/04/1888	23/04/1888	Landslide, Tsunami	Norway	2	1	Local	1	1*
	GM03 Folkestone Tsunami 1911	31/12/1911	31/12/1911	Landslide, Tsunami	England	2	3	Local	1	1,5
	GM04 Dogger Bank Earthquake 1931	07/06/1931	07/06/1931	Earthquake, Tsunami	England	2	3	Local	1	3,7
	GM05 Valais earthquake 1946	25/01/1946	26/01/1946	Earthquake, Landslide	Switzerland	2	6	Local	2	2*
	GM06 Vaiont Landslide 1963	09/10/1963	09/10/1963	Landslide, Tsunami	Italy	2	3	Local	1	13*
	GM-7 Arette Earthquake 1967	13/08/1967	13/08/1967	Earthquake, Landslide	France	2	6	Regional	1	3,13*
	GM08 Nice Tsunami 1979	16/10/1979	16/10/1979	Landslide, Tsunami	France	2	3	Regional	1	1,13*
	GM09 L'Aquila earthquake 2009	06/04/2009	09/04/2009	Earthquake, Landslide	Italy	2	6	Regional	4	13,18*
	GM10 Lorca earthquake 2011	05/11/2011	08/11/2011	Earthquake, Landslide	Spain	2	1	Regional	4	12,17*
Convective Storm	CS01 Lynmouth Flood 1952	15/08/1952	16/08/1952	Rain, Flood, Landslide	England	3	3	Local	2	14,15, 17*
	CS02 Lisbon Flood 1967	25/11/1967	26/11/1967	Rain, River Flood, Landslide	Portugal	3	3	Local	2	21*
	CS03 Cantabrian range Flood 1983	26/08/1983	27/08/1983	Rain, Landslides, flood	Spain	3	3	Regional	2	12,21
	CS04 Biescas Flood 1996	07/08/1996	07/08/1996	Rain, Flood, Landslide	Spain	3	3	Local	1	21*
	CS05 The Bracknell Storm 2000	07/05/2000	07/05/2000	Rain, Lightning, Hail	England	3	3	Local	0.1	29*
	CS06 Paris Convective storm 2001	06/07/2001	07/07/2001	Rain, Lightning, Landslides, Flood	France	3	4	Local	1	12,28
	CS07 Devon Convective storm 2008	29/10/2008	30/10/2008	Rain, Lightning, Hail, Flood	England	4	4	Local	2	29,31*
	CS08	28/06/2012	29/06/2012	Rain, Lightning, Hail, Landslide	England	3	3	Regional	1	10,29*

MH Event	Event	Start Date	End date	Hazards	Impacted place	N_{Haz}	N_{Inter}	Spatial scale	D (days)	Source ID
	Midlands Convective storm 2012									
	CS09 SW France Flood 2013	18/06/2013	20/06/2013	Rain, Flood, Landslide	France	3	3	Local	3	12,28
	CS10 SE England Flood 2016	15/09/2016	16/09/2016	Rain, Lightning, Landslides, Flood	England	4	4	Regional	1	30,31
Extratropical Cyclone	ETC01 Great Storm of 1987	15/10/1987	16/10/1987	Rain, Wind, River Flood	United Kingdom, France	2	1	Regional	2	14,17, 26*
	ETC02 Storm Angus 2016	19/11/2016	20/11/2016	Rain, Wind, Storm Surge, Waves	England, Wales	4	4	Regional	2	6,29,30
	ETC03 Storm Martin 1999	27/12/1999	27/12/1999	Wind, Storm surge ,Waves, Rainfall, Landslide, Soil moisture excess, River Flood	France, Switzerland, Italy	3	2	Multi-regional	1	14,26*
	ETC04 Storm Erwin 2005	07/01/2005	08/01/2005	Rain, Wind, River Flood	Denmark, Ireland, Norway, Sweden and United Kingdom	3	3	Multi-regional	2	17,26, 29
	ETC05 Storm Gero 2005	11/01/2005	12/01/2005	Wind, Storm surge, Waves	Ireland, United Kingdom	3	2	Regional	2	6,17,26
	ETC06 Storm Klaus 2009	24/01/2009	24/01/2009	Wind, Storm surge, Waves, Rain, River Flood, Landslides, Soil moisture excess	Spain, France, Italy	7	7	Regional	1	26,28*
	ETC07 Storm Xynthia 2010	28/02/2010	02/03/2010	Wind, Storm surge ,Waves	France, Spain, Portugal, United Kingdom	3	2	Multi-regional	3	14,26, 27
	ETC08 St Jude Storm 2013	28/10/2013	28/10/2013	Rain, Wind, River Flood	United Kingdom, France, Germany, Belgium, Ireland	3	2	Regional	1	26,29, 30
	ETC09 Storm Xaver 2013	05/12/2013	06/12/2013	Wind, Storm Surge, Waves, Landslides	United Kingdom, Belgium, Norway	4	4	Regional	2	6,26,29
	ETC10 Storm Desmond 2015	05/12/2015	06/12/2015	Rain, Wind, River Flood, Landslides, Soil moisture excess	England, Wales	5	6	Regional	2	29,30, 32
	CD01 Landes Wildfire 1949	19/08/1949	25/08/1949	Drought, Extreme hot temperature, Wildfire, Wind	France	4	6	Local	7	14*
	CD02 Europe Drought-Heatwave 1976	01/04/1976	30/08/1976	Drought, Extreme hot temperature	France, United Kingdom	2	3	Multi-regional	152	9,17,20,22,23

MH Event	Event	Start Date	End date	Hazards	Impacted place	N_{Haz}	N_{Inter}	Spatial scale	D (days)	Source ID
Compound Dry hazards	CD03 Europe Drought 1989-1991	01/03/1989	01/12/1990	Drought, Extreme hot temperature, Wildfire	France, Spain, Italy	3	5	Multi-Regional	641	20,22, 23
	CD04 Europe Heatwave 2003	01/06/2003	31/08/2003	Drought, Extreme hot temperature, Wildfire	France, United Kingdom, Spain, Portugal, Germany, Belgium	3	5	Continental	92	14,16, 17,22, 23,24, 28,29
	CD05 Iberian Heatwave 2005	01/07/2005	01/10/2005	Extreme hot temperature, Drought, Wildfire	Spain, Portugal	3	5	Multi-regional	93	23,24, 25*
	CD06 Europe Heatwave 2006	18/06/2006	28/08/2006	Extreme hot temperature, Drought	United Kingdom, France, Belgium, Germany, Netherland	2	3	Continental	72	17,23, 29*
	CD07 UK Drought 2011	01/01/2011	31/05/2011	Extreme hot temperature, Drought	France, England	2	3	Multi-regional	151	9,20,2 9
	CD08 UK Heatwave 2015	01/08/2015	02/08/2015	Extreme hot temperature, Wildfire	United Kingdom	2	3	Multi-regional	2	9,14,2 9
	CD09 Portugal Fire 2017	17/06/2017	18/06/2017	Drought, Extreme hot temperature, Wildfire, Wind	Portugal	4	5	Local	2	14,24, 25*
	CD10 UK-France Heatwave 2019	01/03/2019	01/09/2019	Drought, Extreme hot temperature, Wildfire	France, United Kingdom	3	5	Multi-Regional	185	9,14,2 5,29
Compound Cold hazards	CC01 UK-France Cold wave 1947	21/01/1947	03/03/1947	Extreme cold temperature, Snow, River Flooding	United Kingdom, France	3	3	Multi-regional	42	17,19*
	CC02 Europe Cold wave 1956	31/01/1956	29/02/1956	Extreme cold temperature, Extreme Snow	France, Switzerland, Germany, Spain	2	1	Continental	30	9,16,1 9*
	CC03 Europe Cold wave 1963	13/11/1962	06/03/1963	Extreme cold temperature, Extreme Snow, Extreme wind	France, United Kingdom, Belgium, Germany	3	2	Multi-regional	114	9,16,1 9
	CC04 France-Spain Cold wave 1971	23/12/1970	15/01/1971	Extreme cold, Extreme snow	France, Spain	2	1	Multi-regional	24	9,16,1 9
	CC05 France Snowstorm 1980	02/11/1980	13/11/1980	Extreme snow, Extreme cold	France	2	1	Regional	12	9,19
	CC06 France-Spain Cold wave 1985	04/01/1985	19/01/1985	Extreme cold temperature, Extreme snow	France, Spain	2	1	Multi-regional	16	9,14,1 6,19
	CC07 France Snowstorm 2005	14/02/2005	10/03/2005	Extreme cold, Extreme snow	France	2	1	Regional	25	9,19
	CC08	02/02/2009	06/02/2009	Extreme cold, Extreme snow	United Kingdom	2	1	Multi-regional	5	29*

MH Event	Event	Start Date	End date	Hazards	Impacted place	N_{Haz}	N_{Inter}	Spatial scale	D (days)	Source ID
	UK Snowstorm 2009									
	CC09 UK-France Snowstorm 2010	25/11/2010	26/12/2010	Extreme cold, Extreme snow, Extreme wind	United Kingdom, France	3	2	Multi-regional	32	9,14,29
	CC10 UK-France Cold wave 2018	26/02/2018	01/03/2018	Extreme cold, Extreme snow, Extreme wind	United Kingdom, France	3	2	Multi-regional	4	29*

Table C2: 32 sources used to build the historic major multi-hazard event catalogue. Sources are of five types: single hazard catalogue; catalogue of reported weather events; peer review articles, disaster database; multi-hazard catalogue. Data in these catalogues have different types: Online tabular database; Online event catalogue, tabular database;

ID	*Abbrev*	*Full name*	*Source type*	*Data type*	*Hazards*	*Area of interest*	*MH event*	*Period*	*Available info*	*link - reference*
1		NCEI Significant Earthquake Database	Single hazard catalogue	Online tabular database	Earthquakes, Tsunami	Global	GM	-2000-2021	Date, Location, Magnitude	https://www.ngdc.noaa.gov/hazard/earthqk.shtml
2		NCEI Tsunami database	Single hazard catalogue	Tabular database	Tsunami	Global	GM	-2000-2020	Date, Location, Magnitude	https://www.ngdc.noaa.gov/hazard/tsu_db.shtml
3	ECOS-09	Swiss Seismological Service Earthquake catalogue	Single hazard catalogue	Online event catalogue	Earthquakes	Switzerland	GM	250-2008	Date, Location, Magnitude	http://seismo.ethz.ch/en/home/
4	EMEC	EMEC Earthquake catalogue	Single hazard catalogue	Tabular with coordinates	Earthquakes	Europe	GM	1000-2006	Date, Location, Magnitude	http://emec.gfz-potsdam.de/pub/emec_data/emec_data_frame.html
5		SurgeWatch	Single hazard catalogue	Online event catalogue	Extreme wave, Storm surge	UK	ETC	1000-2018	Date, Location, Magnitude	https://www.surgewatch.org/
6		A catalogue of tsunamis reported in the UK	Single hazard catalogue	Event catalogue	Tsunami	UK	GM	1000-2018	Date, Location, Magnitude	http://nora.nerc.ac.uk/id/eprint/513298/
7		BGS Significant British Earthquakes	Single hazard catalogue	Online tabular database	Earthquakes	UK	GM	1382-	Date, Location, Magnitude	https://earthquakes.bgs.ac.uk/earthquakes/UKsignificant/index.html
8	BD Tsunamis	Inventaire historique des tsunamis en France	Single hazard catalogue	Event catalogue	Tsunami	France	GM	1564-2009	Date, Location, Magnitude	http://infoterre.brgm.fr/rapports/RP-61152-FR.pdf
9		Infoclimat.fr	Catalogue of reported weather events	Event catalogue	Extreme wind, Extreme rainfall, Lightning, Extreme hot temperature, Extreme cold temperature, Extreme snow, Drought	France	ETC - CD - CC - CS	1653-	Date, Location, Magnitude	Infoclimat.fr
10		Severe Hailstorms in the United Kingdom and Ireland: A Climatological Survey with Recent and Historical Case Studies	Peer review article	Journal article	Hail	UK	CS	1687-2012	Date, Location, Magnitude	Webb, J.D. and Elsom, D.M., 2016. Severe hailstorms in the United Kingdom and Ireland: a climatological survey with recent and historical case studies. Extreme Weather, pp.155-194.
11		Meteo France Tempetes	Catalogue of reported weather events	Online event catalogue	Extreme wind	France	ETC	1703-2018	Date, Location, Magnitude	http://tempetes.meteo.fr

ID	Abbrev	Full name	Source type	Data type	Hazards	Area of interest	MH event	Period	Available info	link - reference
12		Meteo France Pluie Extreme	Catalogue of reported weather events	Online event catalogue	Extreme rainfall, Riverine Flood	France	ETC -CS	1766-2018	Date, Location, Magnitude	http://pluiesextremes.meteo.fr
13	EQIL	Worldwide Database of Earthquake-Induced Landslide Inventories	multi-hazard catalogue	Tabular with coordinates	Earthquakes, Landslides	Global	GM	1812-2016	Date, Location, Magnitude	Tanyaş, H., van Westen, C. J., Allstadt, K. E., .*et al.*,(2017). Presentation and analysis of a worldwide database of earthquake-induced landslide inventories. J. of Geophys. Res.: Earth Surface, 122, 2015.
14	EM-DAT	Emergency Events Database	Disaster database	Tabular with coordinates	Extreme wind, Extreme rainfall, Lightning, Extreme hot temperature, Extreme cold temperature, Extreme snow, Drought, Flood, Earthquakes, Landslides, Tsunami	Global	GM - ETC - CD - CC - CS	1900-	Date, Location, Magnitude	https://public.emdat.be/
15		Extreme Rainfall and Flood Event Recognition (DEFRA)	Catalogue of reported hydrological events	Report	River flooding, Extreme rainfall	UK	ETC - CS	1900-2000	Date, Location, Magnitude	DEFRA and Environment Agency: Extreme Rainfall and Flood Event Recognition R&D Technical Report: FD2201., 2002.
16		Heat and cold waves in Spain	Peer review article	Journal article	Extreme hot temperature, Extreme cold temperature	Spain	CD - CD	1900-2013	Date, Location, Magnitude	Prats, J. M. C. and Notivoli, R. S.: Chapter 21 Heat and Cold Waves in Spain, , (January), 307–322, 2013
17		Great British Weather disasters	Book	Event catalogue	Extreme wind, Extreme rainfall, Lightning, Extreme hot temperature, Extreme cold temperature, Extreme snow, Drought, Flood, Landslide	UK	ETC - CD - CC - CS	1901-2008		Eden, P.: Great British Weather Disasters, Continuum., 2008.
18		An Open Repository of Earthquake-Triggered Ground-Failure Inventories	multi-hazard catalogue	Tabular with coordinates	Earthquakes, Landslides	Global	GM	1908-2016	Date, Location, Magnitude	https://www.sciencebase.gov/catalog/item/583f4114e4b04fc80e3c4a1a

ID	Abbrev	Full name	Source type	Data type	Hazards	Area of interest	MH event	Period	Available info	link - reference
19		Meteo France Grand Froids	Catalogue of reported weather events	Online event catalogue	Extreme cold temperature	France	CC	1947-2018	Date, Location, Magnitude	http://www.meteofrance.fr/prevoir-le-temps/meteo-et-sante/grands-froids#
20		The biggest drought events in Europe from 1950 to 2012	Peer review article	Journal article	Drought	Europe	CD	1950-2005	Date, Location, Magnitude	
21		Major Floods in Europe 1950-2005	Peer review article	Event catalogue	Extreme rainfall, Riverine Flood	Europe	ETC - CS	1950-2005	Date, Location, Magnitude	Barredo, J. I.: Major flood disasters in Europe: 1950-2005, Nat. Hazards, 42(1), 125–148, 2007.
22	GDFC	A Global Drought and Flood Catalogue from 1950 to 2016	Single hazard catalogue	Journal article; Tabular with coordinates	Drought, River Flooding	Global	ETC - CS - CD	1950-2016	Date, Location, Magnitude	http://hydrology.princeton.edu/data/hexg/GDFC/index.html
23	EDR	European Drought Reference	Single hazard catalogue	Online tabular database	Drought	Europe	CD	1959-2007	Date, Location, Magnitude	https://www.geo.uio.no/edc/droughtdb/#:~:text=The%20European%20Drought%20Reference%20(EDR,historical%20drought%20events%20in%20Europe.
24	PRFD	Portuguese Rural Fire Database	Single hazard catalogue	Journal article; Tabular with coordinates	Wildfire	Portugal	CD	1980-2005	Date, Location, Magnitude	
25	EFD	European Fire Database	Single hazard catalogue	Tabular database	Wildfire	Europe	CD	1980-2016	Date, Location, Magnitude	https://effis.jrc.ec.europa.eu/applications/data-and-services/
26	XWS	Extreme Wind Storm Catalogue	Single hazard catalogue	Online event catalogue	Extreme wind	Europe	ETC	1981-2013	Date, Location, Magnitude	http://www.europeanwindstorms.org/cgi-bin/storms/storms.cgi
27	DFO	Dartmooth flood database	Single hazard catalogue	Tabular with coordinates	River flooding	Global	ETC - CS	1985-	Date, Location, Magnitude	https://www.dartmouth.edu/~floods/Dataaccess.htm
28	CAT NAT	catastrophes naturelles CCR	Disaster database	Online event catalogue	Riverine Flood, Drought, Storm surge, Landslides, Extreme wind, Earthquakes	France	ETC - CS - CD	1989-	Date, Location	https://catastrophes-naturelles.ccr.fr/
29		Met Office past Weather events	Catalogue of reported weather events	Online event catalogue	Extreme wind, Extreme rainfall, Lightning, Extreme hot temperature, Extreme cold temperature, Extreme snow, Drought	UK	ETC - CD - CC - CS	1990-	Date, Location, Magnitude	https://www.metoffice.gov.uk/weather/learn-about/past-uk-weather-events

ID	Abbrev	Full name	Source type	Data type	Hazards	Area of interest	MH event	Period	Available info	link - reference
30		Historic Flood Warnings (Environmental Agency)	Single hazard catalogue	Tabular with coordinates	Riverine Flood	UK	ETC - CS	2006-	Date, Location, Magnitude	https://data.gov.uk/dataset/d4fb2591-f4dd-4e7f-9aaf-49af94437b36/historic-flood-warnings
31		Floodlist	Single hazard catalogue	Online event catalogue	Extreme rainfall, Riverine Flood	Global	ETC - CS	2007-	Date, Location, Magnitude	http://floodlist.com/
32	GLC	Global Landslide Catalog	Single hazard catalogue	Tabular with coordinates	Landslides	Global	ETC - CS	2007-2016	Date, Location	https://data.nasa.gov/Earth-Science/Global-Landslide-Catalog/h9d8-neg4

Table C3 Supporting literature used to build the historic major multi-hazard events catalogue (Table C1)

Full Name	*Hazards*	*Area of interest*	*MH Events*	*Reference*
Analysis of large fires in European Mediterranean landscapes: Lessons learned and perspectives	Wildfire	Mediterranean basin	CD04-CD05	San-Miguel-Ayanz, J., Moreno, J. M. and Camia, A.: Analysis of large fires in European Mediterranean landscapes: Lessons learned and perspectives, For. Ecol. Manage., 294, 11–22, 2013.
Atmospheric analysis of the cold late February and early March 2018 over the UK	Extreme cold temperature	UK	CC10	Greening, K. and Hodgson, A.: Atmospheric analysis of the cold late February and early March 2018 over the UK, Weather, 74(3), 79–85, 2019.
The great storm of 16 October 1987	Extreme cold temperature	UK	ETC01	Prichard, B.: The Great Storm of 16 October 1987, Weather, 67(10), 255–260, 2012.
The 1755 Lisbon earthquake	Earthquake, Tsunami	Portugal	GM01	Chester, D. K.: The 1755 Lisbon earthquake, Prog. Phys. Geogr., 25(3), 363–383, 2001.
Forest Fires In Portugal Case Study, June 18, 2017	Wildfire	Portugal	CD09	Radovanovic, M., Vyklyuk, Y., Stevancevic, M., Milenkovic, M., Jakovljevic, D., Petrovic, M., Malinovic-Milicevic, S., Vukovic, N., Vujko, A., Yamashkin, A., Sydor, P., Vukovic, D. and Skoda, M.: Forest fires in Portugal - case study, 18 june 2017, Therm. Sci., 23(1), 73–86, 2019.
La catastrophe de Biescas du 7 août 1996 ; analyse de la crue torrentielle du rio Aras dans les Pyrénées aragonaises (Espagne)	River flooding, Extreme rainfall, Landslides	Spain	CS06	Lajournade, P. C., Beaufrcre, C., Lalanne-Berdouticq, G. and Martignac, F.: La catastrophe de Biescas du 7 août 1996 ; analyse de la crue torrentielle du rio Aras dans les Pyrénées aragonaises (Espagne), Houille Blanche, 53(5–6), 128–137, 199
Landslides Induced by Historical and Recent Earthquakes in Central-Southern Apennines (Italy): A Tool for Intensity Assessment and Seismic Hazard	Landslides	Italy	GM09	Esposito, E., Guerrieri, L., Porfido, S., Vittori, E., Blumetti, A. M., Comerci, V., Michetti, A. M. and Serva, L.: Landslides Induced by Historical and Recent Earthquakes in Central-Southern Apennines (Italy): A Tool for Intensity Assessment and Seismic Hazard, in Landslide Science and Practice, pp. 295–303, Springer Berlin Heidelberg, Berlin, Heidelberg., 2013.
L'Incendie meurtrier dans la forêt des Landes en août 1949	Wildfire	France	CD01	Deville, J.: L'incendie meurtrier dans la forêt des Landes en août 1949, edited by Pompiers De France., 2009.

Full Name	Hazards	Area of interest	MH Events	Reference
Modelling of the 1888 Landslide Tsunami, Trondheim, Norway	landslides, Tsunami	Norway	GM02	Glimsdal, S., L'Heureux, J.-S., Harbitz, C. B. and Pedersen, G. K.: Modelling of the 1888 Landslide Tsunami, Trondheim, Norway, in Landslide Science and Practice, pp. 73–79, Springer Berlin Heidelberg, Berlin, Heidelberg., 2013
The 1946 magnitude 6.1 earthquake in the Valais: Site-effects as contributor to the damage	earthquake, Landslide	Switzerland	GM05	Fritsche, S. and Fäh, D.: The 1946 magnitude 6.1 earthquake in the Valais: Site-effects as contributor to the damage, Swiss J. Geosci., 102(3), 423–439, 2009
The 1963 Vaiont Landslide	Landslide	Italy	GM06	Genevois, R. and Ghirotti, M.: The 1963 Vaiont Landslide The 1963 Vaiont Landslide, G. di Geol. Appl., 1, 41–52, 2005
The 1979 Nice harbour catastrophe revisited: Trigger mechanism inferred from geotechnical measurements and numerical modelling	Tsunami	France	GM08	Dan, G., Sultan, N. and Savoye, B.: The 1979 Nice harbour catastrophe revisited: Trigger mechanism inferred from geotechnical measurements and numerical modelling, Mar. Geol., 245(1–4), 40–64, 2007.
The Lynmouth Flood of August 1952	River flooding, Extreme rainfall	UK	CS01	Dobbie, C. H.: The Lynmouth Flood of August 1952, 1953.
Exceptional hailstorm hits Ottery St Mary on 30 october 2008	Hail	UK	CS07	Grahame, N., Riddaway, B., Eadie, A., Hall, B. and McCallum, E.: Exceptional hailstorm hits Ottery St Mary on 30 october 2008, Weather, 64(10), 255–263, 2009.
The 1956 Cold Wave in Western Europe	Extreme cold temperature	Europe	CC02	Dizerens, C., Lenggenhager, S., Schwander, M., Buck, A. and Foffa, S.: The 1956 Cold Wave in Western Europe, Geogr. Bernensia, G92, 101–111, 2017.
Western European Snow of 1-2 February 2009	Extreme snow	Europe	CC08	Grumm, R. H.: Western European Snow of 1-2 February 2009., 2009
The impacts of the 28 June 2012 storms on UK road and rail transport	Lightning	UK	CS08	Jaroszweski, D., Hooper, E., Baker, C., Chapman, L. and Quinn, A.: The impacts of the 28 June 2012 storms on UK road and rail transport, Meteorol. Appl., 22(3), 470–476, 2015
An analysis of the July 2006 heatwave extent in Europe compared to the record year of 2003	Extreme hot temperature	Europe	CD06	Rebetez, M., Dupont, O. and Giroud, M.: An analysis of the July 2006 heatwave extent in Europe compared to the record year of 2003, Theor. Appl. Climatol., 95(1–2), 1–7, 2009
Le tremblement de terre d'Arette	Earthquake	France	GM07	Piolle, X.: Le tremblement de terre d'Arette, Rev. Geogr. Pyren. Sud. Ouest., 39(4), 369–396, 1968.

Full Name	*Hazards*	*Area of interest*	*MH Events*	*Reference*
Widespread landslides induced by the Mw 5.1 earthquake of 11 May 2011 in Lorca, SE Spain	Earthquake, Landslide	Spain	GM10	Alfaro, P., Delgado, J., García-Tortosa, F. J., Lenti, L., López, J. A., López-Casado, C. and Martino, S.: Widespread landslides induced by the Mw 5.1 earthquake of 11 May 2011 in Lorca, SE Spain, Eng. Geol., 137–138(May 2011), 40–52, 2012
The deadliest storm of the 20th century striking Portugal: Flood impacts and atmospheric circulation	River flooding, Extreme rainfall, Landslides	Portugal	CS02	Trigo, R. M., Ramos, C., Pereira, S. S., Ramos, A. M., Zêzere, J. L. and Liberato, M. L. R.: The deadliest storm of the 20th century striking Portugal: Flood impacts and atmospheric circulation, J. Hydrol., 541, 597–610, 2016.
The Bracknell hailstorm of 7 May 2000	Hail	UK	CS05	Pedgley, D. E.: The Bracknell storm, 7 May 2000, Weather, 58, 171–181, 2003
Three extreme storms over Europe in December 1999	Extreme wind	Europe	ETC03	Ulbrich, U., Fink, A. H., Klawa, M. and Pinto, J. G.: Three extreme storms over Europe in December 1999, Weather, 56(3), 70–80, 2001.
Klaus - An exceptional winter storm over northern Iberia and southern France	Extreme wind, River flooding, Extreme rainfall, soil moisture excess	Spain, France	ETC06	Liberato, M. L. R., Pinto, J. G., Trigo, I. F. and Trigo, R. M.: Klaus - An exceptional winter storm over northern Iberia and southern France, Weather, 66(12), 330–334, 2011.
Winter 1947 in the British isles	Extreme cold temperature, Extreme snow, Extreme wind, River flooding	UK	CC01	Booth, G.: Winter 1947 in the British isles, Weather, 62(3), 61–68, 2007
The European 2016/17 drought	Extreme hot temperature, Drought, Wildfire	Europe	CD09	García-Herrera, R., Garrido-Perez, J. M., Barriopedro, D., Ordóñez, C., Vicente-Serrano, S. M., Nieto, R., Gimeno, L., Sorí, R. and Yiou, P.: The European 2016/17 drought, J. Clim., 32(11), 3169–3187, 2019

Appendix D: Numerical data for quantitative multi-hazard approach

This appendix contains **Table D1** which summarizes 34 freely available datasets to study and model the five multi-hazard networks presented in **Chapter 3**.

Table D1: Freely available numerical datasets for hazard interrelation studies divided into three categories: model outputs, In-situ observations and remote sensing.

Datasets		1.1 Earthquake	1.2 Landslide	2.1 Lightning activity	2.2 Extreme rainfall	2.3 Extreme wind	2.4 Extreme hot air	2.5 Extreme cold air	2.6 Hail	2.7 Extreme snowfall	3.1 Storm surge	3.2 Extreme waves	3.3 River flooding	3.4 Tsunami	3.5 Drought	3.6 Soil moisture excess	4.1 Wildfire	Spatial form	Spatial resolution	Temporal coverage	Coverage	Timestep	Relevant MH Networks	Data publisher
Models (Climate reanalysis)	M1. ERA 5				×	×	×	×		×		×			×	×		Gridded	0.25°	1979-current	Global	hourly	ETC-CC-CD	ECMWF - EU
	M2. UERRA				×	×	×	×										Gridded	0.11° - 0.05°	1961-current	Europe	6-hourly; daily	ETC-CD-CS	ECMWF - EU
	M3. GTSR										×							Gridded	variable	1979-2014	Global	daily	ETC	Vrije Universiteit Amsterdam - NL
	M4. Paired time series of daily discharge and storm surge										×							Gridded	0.25 - variable	1980-2014	Global	daily	ETC	Vrije Universiteit Amsterdam - NL
	M5. EFAS												×		×	×		Gridded	5km	1991-current	Europe	daily	ETC-CS	Copernicus - EU
	M6.POLCOMS-WAM											×						Gridded	12km	1999-2008	UK	hourly	ETC	BODC - UK
	M7. CMEMS Ocean waves hindcasts											×						Gridded	0,083deg	2018-current	Global	3-hourly	ETC	CMEMS - EU
	I1. Significant Earthquakes database	×												×				Point observation	NA	-2150-current	Global	NA	GM	NCEI - USA
	I2. Earthquake catalogue	×																Point observation	NA	1000-2006	Global	NA	GM	GFZ - GER

Datasets		1.1 Earthquake	1.2 Landslide	2.1 Lightning activity	2.2 Extreme rainfall	2.3 Extreme wind	2.4 Extreme hot air	2.5 Extreme cold air	2.6 Hail	2.7 Extreme snowfall	3.1 Storm surge	3.2 Extreme waves	3.3 River flooding	3.4 Tsunami	3.5 Drought	3.6 Soil moisture excess	4.1 Wildfire	Spatial form	Spatial resolution	Temporal coverage	Coverage	Timestep	Relevant MH Networks	Data publisher
In-situ Observations	I3. Tsunami database													×				Point observation	NA	-2000-current	Global	NA	GM	NCEI - USA
	I4. EQIL Inventory	×	×															Point observation	NA	1812-2016	Global	NA	GM	University of Twente - NL
	I5. GLC		×															Point observation	NA	2007-2016	Global	NA	CS-ETC	NASA - USA
	I6. E-Obs				×		×	×										Gridded	0.1°	1950-current	Europe	daily	ETC-CC-CD	ECAD - EU
	I7. Hadley Centre observations datasets ISD				×	×	×	×		×								Point observation	NA	1931-current	Global	sub-daily	ETC-CC-CD-CS	Met Office - UK
	I8. Integrated Surface Database (ISD)				×	×	×	×		×								Point observation	NA	1901-current	Global	hourly	ETC-CC-CD-CS	NCEI - USA
	I9. GHNC - daily				×		×	×										Point observation	NA	1861-current	Global	daily	ETC-CC-CD	NCEI - USA
	I10. MIDAS Open: UK Land Surface Stations Data				×	×	×	×										Point observation	NA	1853-current	UK	hourly; daily	ETC-CC-CD-CS	Met Office - UK
	I11. GRDC												×					Point observation	NA	1806-current	Global	daily	ETC-CS	WMO

Datasets		1.1 Earthquake	1.2 Landslide	2.1 Lightning activity	2.2 Extreme rainfall	2.3 Extreme wind	2.4 Extreme hot air	2.5 Extreme cold air	2.6 Hail	2.7 Extreme snowfall	3.1 Storm surge	3.2 Extreme waves	3.3 River flooding	3.4 Tsunami	3.5 Drought	3.6 Soil moisture excess	4.1 Wildfire	Spatial form	Spatial resolution	Temporal coverage	Coverage	Timestep	Relevant MH Networks	Data publisher
In-situ Observations	I12. National river flow archive												×					Point observation	NA	1841-current	UK	daily	ETC-CS	CEH - UK
	I13. Base de donnée Hydrométrie												×					Point observation	NA	1920-current	France	hourly; daily	ETC-CS	SANDRE - FR
	I14. ISMN												×		×	×		Point observation	NA	1952-current	Global	hourly	ETC-CD	ESA - EU
	I15. GESLA										×							Point observation	NA	1848-2015	Global	hourly	ETC	BODC - UK
	I16. UK Tide Gauge Network										×							Point observation	NA	1915-current	UK	hourly	ETC	BODC - UK
	I17. JASL										×							Point observation	NA	1846-current	Global	hourly; daily	ETC	NCEI - USA
	I18. Wave data series											×						Point observation	NA	1954-current	UK	daily	ETC	BODC - UK
	I19. PRFD																×	Point observation	NA	1980-2005	Portugal		CD	AFN - Portugal
	I20. ESWD			×					×									Point observation	NA	2006-current	Europe	NA	CS	ESSL - EU

Datasets		1.1 Earthquake	1.2 Landslide	2.1 Lightning activity	2.2 Extreme rainfall	2.3 Extreme wind	2.4 Extreme hot air	2.5 Extreme cold air	2.6 Hail	2.7 Extreme snowfall	3.1 Storm surge	3.2 Extreme waves	3.3 River flooding	3.4 Tsunami	3.5 Drought	3.6 Soil moisture excess	4.1 Wildfire	Spatial form	Spatial resolution	Temporal coverage	Coverage	Timestep	Relevant MH Networks	Data publisher
Remote sensing (Satellites)	S1. ATDNet			×														Point observation	NA	2008-current	Europe	NA	CS	Met Office - UK
	S2. MSWEP				×													Gridded	0.25°	1979-2015	Global	3-hourly	CS-ETC	Princeton Climate Analytics - USA
	S3. NIMROD Database				×													Gridded	1km	2004-current	UK	5 minutes	CS	Met Office - UK
	S4. PERSIANN CSS				×													Gridded	0.04°	2003-current	Global	hourly; daily	CS-ETC	CHRS - USA
	S5. GPM IMERG				×													Gridded	0.1°	2000-current	Global	half-hourly	CS-ETC	NASA - USA
	S6. CCI						×	×							×	×	×	Gridded	25km - 0.25°	1978-current	Global	daily; monthly	CD	ESA - EU
	S7. EUSTACE						×	×										Gridded	0.25°	1995-2016	Global	daily	CD-CC	EU - EU

Appendix E: Comparing model abilities through tail dependence measures

Summary:

This appendix provides complementary results to **Chapter 4** by comparing the six bivariate models abilities through dependence measure estimation. To compare tail dependence measure estimates to reference values, the root-mean-square error (RMSE) is used. Results show that marginal distributions do not have a significant impact on the estimation of the tail dependence measures and that the JT-KDE model is the most flexible to estimate dependence measures without prior assumption.

E1. Tail dependence measures estimations

Tail dependence measures η and χ are estimated by each model. For copulas, these measures are related to the copula parameters. In our set of four copulas, two are asymptotically dependent (Gumbel and Galambos) with η=1 and two are asymptotically independent (normal and FGM) with χ=0.

For the nonparametric joint tail approach, the χ and η measures are estimated following the procedure used by Winter (2016). For the conditional model, both measures are estimated from the simulated points. Marginal distributions (X_1, X_2) are transformed into the uniform margins (U1, U2). The χ measure is estimated by calculating the probability $P(V > u|U > u)$ (**Eq. 4.4**). The η measure is estimated in two steps. First $\bar{\chi}(u)$ is estimated as (Coles *et al.*, 1999):

$$\bar{\chi}(u) = \frac{2\log\ P(U>u)}{\log P(U>u,V>u)} - 1 = \frac{2\log(1-u)}{\log\left(\chi(u)(1-u)\right)} - 1, \tag{E1}$$

for $0 \leq u \leq 1$ with u a sufficiently high threshold. Second, the η measure is estimated from $\bar{\chi}$ (**Eq. E1**).

To compare the estimated dependence measure to the reference value, the root-mean-square error (RMSE), a measure of efficiency that accounts for both the bias and variance of the estimates is used, similarly to Zheng *et al.* (2014). Similarly to the metrics used in **Section 4.3**, the RMSE is calculated from 100 realizations of the 60 datasets.

E2. Comparison of model abilities

The estimation of dependence measure is an important step in bivariate analysis (Coles *et al.*, 1999; Heffernan, 2000; Zheng *et al.*, 2013, 2014; Dutfoy *et al.*, 2014). Models have also been compared on their ability to estimate the dependence measures χ and η. Results arising from this comparison provide a different perspective on the abilities of each model. **Figure E1** shows the RMSE of the dependence measures estimations for each of the 60 synthetic datasets.

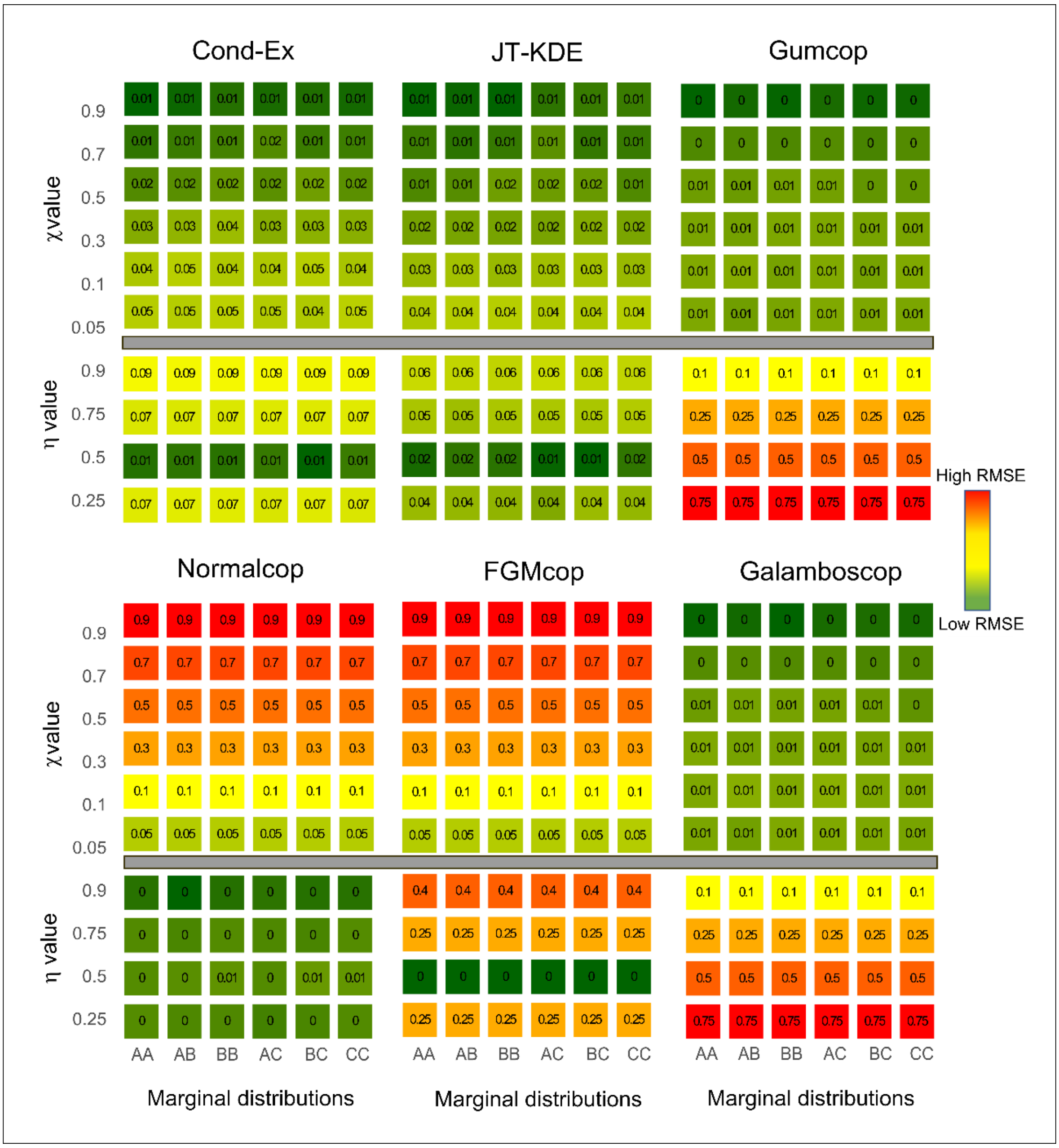

Figure E1: RMSE (root-mean-square error) of the estimated dependence measures to the reference for all 60 different datasets. Fitting capacities of each model are represented. Values in cells and colours represent the median RMSE from low (dark green) to high (red). The thickness of cell borders represent the 95% uncertainty around the median value

From **Fig. E1**, we observe the following:

- Marginal distributions do not have a significant impact on the accuracy of the estimation of these measures for the copulas.
- Marginal distributions have a small impact on the estimation of the dependence measures for the conditional extremes model and the joint-tail model, however, this impact is not as important as for the level curve estimation
- All copulas estimate very accurately the dependence measure within their operating range (AI for normal copula, near independence for FGM copula and AD for Gumbel and

Galambos copula). However, only the conditional extremes model and the joint-tail model can estimate both η and χ.

- The dependence measure estimator used in the joint-tail KDE approach offers slightly more accurate estimation for, in particular for η.
- Estimation performance of both joint tail KDE and condition extreme models decreases when approaching the interface between asymptotic dependence and asymptotic independence. The RMSE at χ=0.05 is close the 100% of the value of χ while the RMSE η =0.9 is at its highest for both Cond-EX and JT-KDE models. It is then hard to decipher with confidence the nature of the dependence in the asymptotic domain for low χ values and high η values.

Appendix F: Supplement to Evaluating the efficacy of bivariate extreme modelling approaches for multi-hazard scenarios (Chapter 4). Aloïs Tilloy *et al.*

Summary:

This appendix consists of a theoretical background on univariate and multivariate extreme value theory and on bivariate joint density. In **Appendix F1**, major theoretical concepts of multivariate extreme value theory are presented and the connections between these concepts is discussed. In **Appendix F2**, the joint density function of a bivariate distribution and its use for level curve comparison are presented

F1. Theoretical background on multivariate extreme values. Associated Section 4.2.1: Bivariate extreme dependence and Section 4.2.2: Bivariate models

F1.1 Univariate extreme value theory and regular variation

Extreme value analysis is a statistical approach for analysing extreme data values for a variable of interest. One of the earliest recorded mentions is by Fisher and Tippet (1928). Extreme value analysis was formalized into a statistical method by Gumbel (1958). It has been used extensively in the environmental sciences to overcome the limitations of empirical approaches (based on observed data) (e.g., Tiago de Oliveira, 1986; Bingham, 2007). Here we present three main concepts linked to univariate extreme value theory that can be extended to the bivariate case.

F1.1.1 Maximum domain of attraction and GEV

The first principle from which arises extreme value distributions is the *maximum domain of attraction*: let the random variables $x, \ldots, x_n$ be i.i.d. values, with distribution function F. Define $M_n = \max(x_1, \ldots, x_n)$ and suppose there exist sequences of normalizing constants $a_n > 0$, b_n such that (as $n \to \infty$) (Davison and Huser, 2015):

$$\mathrm{P}\left(\frac{M_n - b_n}{a_n} \leq z\right) = F^n(a_n z + b_n) \xrightarrow{d} G(z) \tag{F1.1}$$

where $\xrightarrow{d}$ denotes convergence in the distribution and G is a non-degenerate distribution function. Then G is an extreme value distribution and it is said that F belongs to the maximum domain of attraction of G. The constants a_n and b_n are called stabilizing constants. The possible G distributions are then summarized by the Generalized Extreme Value (GEV) distribution (Gümbel, 1958; Coles, 2001; Davison and Huser, 2015):

$$G(x) = P(X \leq x) = \exp\left(-\left(1 + \xi \frac{x-\mu}{\sigma}\right)^{-\frac{1}{\xi}}\right) \quad \text{(F1.2)}$$

for $1 + \xi \frac{x-\mu}{\sigma} > 0$, with

- $\mu \in (-\infty, \infty)$ the **location** parameter
- $\sigma \in [0, \infty)$ the **scale** parameter
- $\xi \in (-\infty, \infty)$ the **shape** parameter

The shape parameter ξ controls the heaviness of the tail. It means that the value of this parameter directly affects the estimation of the extremes. The Extreme Type Theorem gives three different families of limiting distributions depending on the sign of the shape parameter (Coles, 2001):

- $\xi = 0$, a Gumbel distribution with an exponential upper tail;
- $\xi > 0$, a Fréchet distribution with a heavy upper tail;
- $\xi < 0$, a reverse Weibull distribution with a light upper tail.

A threshold above which one value is considered as extreme can be set instead of selecting block maxima as extreme values. In that case, the distribution *G* of the exceedances above a high threshold *u* is a Generalized Pareto Distribution (GPD) (Davison and Smith, 1990) of the form:

$$G(x) = P(X \leq x | X > u) = 1 - \left(1 + \xi \frac{x-u}{\sigma_u}\right)^{-\frac{1}{\xi}} \quad \text{(F1.3)}$$

for $x > u$, with

- $\sigma_u \in [0, \infty)$ the **scale** parameter
- $\xi \in (-\infty, \infty)$ the **shape** parameter

The shape parameter ξ of the GPD is equivalent to the shape parameter of the corresponding GEV distribution. This shape parameter changes with the threshold level, which makes the choice of the threshold important(Bernardara *et al.*, 2014). The scale parameter for the GPD is also threshold-dependent.

F1.1.2 Max-stability

In the early years of extreme value statistics, Fréchet (1927) identified a functional equation, which he called the stability postulate that provides a mathematical basis for extrapolation and thus lies at the heart of the classical theory of extremes (Davison and Huser, 2015). His stability postulate is now referred to as *max-stability* (see **Eq. A4**). Max-stability is a property that is only satisfied by the three families of GEV: the Gumbel, Fréchet and Reverse Weibull families (Coles, 2001). A distribution *G* is then said to be max-stable if, for every $n > 0$, there exist constants $a_n > 0$ and b_n such that:

$$G^n(a_n z + b_n) = G(z) \tag{F1.4}$$

where $G^n(z)$ is the distribution function of M_n = max (x_1, ... ,x_n), with the x_i independent variables for a distribution G. This means that max-stability is satisfied by distributions for which the fact of taking sample maxima leads to the same distribution apart from changes of parameters (Coles, 2001). The maximum domain of attraction and the max-stability property allows one to model any sample maxima distribution with a GEV distribution.

F1.1.3 Regular variation

Another important concept linked to extreme value analysis is the theory of regularly varying functions. The link between this concept and extreme values has been mainly discussed by Resnick (1987). A regularly varying function is a function which behaves asymptotically like a power function. A function F is regularly varying at ∞ with index ρ, if for $x > 0$ (Resnick, 1987):

$$\lim_{t\to\infty} \frac{U(tx)}{U(t)} = x^{\rho} \tag{F1.5}$$

If $\rho = 0$, we call U a slowly varying function. Slowly varying functions are usually denoted by $\mathcal{L}(x)$The theory of regularly varying functions has links to many mathematical disciplines (Bingham *et al.*, 1987). Moreover, it has been used to understand and investigates maximum domains of attraction in extreme value theory (Bingham *et al.*, 1987; Resnick, 1987; De Haan and Resnick, 1996; Bingham, 2007).

F1.2 Multivariate extreme value statistics

Multivariate extreme value theory is an extension of univariate extreme value theory (Tiago de Oliveira, 1986; Resnick, 1987; Coles, 2001) and various properties of extreme value distributions are analogous in the multivariate framework. Here, the statistics of extremes in a multivariate context are formally presented building on the concepts introduced above (**Section F1.1**)

F1.2.1 Maximum domain of attraction and max stability

The maximum domain of attraction can be extended in the multivariate framework. Let the random variables ($X_{j,1}$, ...,$X_{j,d}$), where j=1,…,n, be a collection d-dimensional vectors of i.i.d. values with a joint distribution F. Define M_n = max ($X_{1,k}$, ... ,$X_{n,k}$) for k = 1,…,d and suppose there exist sequences of normalizing constants $a_{n,k} > 0$, $b_{n,k}$ for k= 1,…,d such that as $n \to \infty$ (Dutfoy *et al.*, 2014):

$$\mathrm{P}\left(\frac{M_{n,1}-b_{n,1}}{a_{n,1}} \le z_1, \dots, \frac{M_{n,d}-b_{n,d}}{a_{n,d}} \le z_n\right) = F^{n,d}\left(a_{n,d}z_d + b_{n,d}\right) \xrightarrow{d} G(z_1, \dots, z_d) \qquad \text{(F1.6)}$$

where $\xrightarrow{d}$ denotes convergence in the distribution and *G* is a distribution function with all non-degenerate marginals. Then the limiting distribution *G* is a Multivariate Extreme value distribution of dimension *d*, and *F* is said to be in the maximum domain of attraction of *G*. Each marginal

$$Z_k = \lim_{n\to\infty}\left(\frac{M_{n,k}-b_{n,k}}{a_{n,k}}\right) \qquad k = 1, \dots, d \qquad \text{(F1.7)}$$

follows a GEV distribution (**Section F1.1**) with parameters (μ_k, σ_k, ξ_k). In can also be shown that *G* must satisfy the max stability relation (Resnick, 1987; Tawn, 1988, 1990; Coles, 2001).

In practice, two steps are generally required to conduct a multivariate study:

(i) marginal distributions are usually estimated using the univariate extreme value methodology (**Section F1**);
(ii) the marginal distributions are then transformed to a common distribution, to handle the dependence structure using multivariate extreme value theory.

For reason of mathematical elegance and simplicity, but without loss of generality, marginal distributions are usually transformed to standard Fréchet distributions in multivariate extreme value analysis where $a_{n,k}$=k^{-1} and $b_{n,k}$ = 0 in (A7). This allows one to focus on the dependence structure between variables (Winter, 2016). From now on, we consider random variables *Z* = $(Z_1,\dots,Z_n)$ with common standard Fréchet margins.

F1.2.2 The exponent measure

The characterization of the dependence structure in the extremes is too complex to be summarized by a parametric family (Davison and Huser, 2015). However, the limiting distribution of *Z* with common Fréchet margins is a multivariate extreme value distribution *G* with $z \in \mathbb{R}^D$ and can be written as (Huser, 2013):

$$G(z) = \exp\{-V(z)\}, \qquad z > 0, \qquad \text{(F1.8)}$$

where *V(z)* is a Radon measure called the exponent measure, which contains all the information about dependence among the variables $Z = (Z_1, \dots, Z_n)$. The exponent measure can be interpreted as the approximate probability that at least one of the maxima $Z_{n,k}$ exceeds its threshold (Davison and Huser, 2015):

$$V(z) = D \int_{SD} \max\left(\frac{w}{z}\right) dH(w) \tag{F1.9}$$

with H a measure on the (D−1)-dimensional simplex $SD = w \in \mathbb{R}$. The measure dH is often called the spectral measure.

From the max-stability property with Fréchet margins, the exponent measure is regularly varying and homogeneous of order –1, meaning that:

$$V(tz) = \ t^{-1}V(z) \tag{F1.10}$$

Properties of the exponent measure, including its regular variation, play a central role when it comes to extrapolation in the upper tail of multivariate variables (Davidson and Huser, 2015). If a bivariate distribution is asymptotically independent, then the exponent measure $V(t) = 0$. The theory of regular variation also provides a framework for extrapolation in the upper tail and has been related to multivariate extreme value theory (Resnick, 1987, Cooley. *et al.* 2019).

F1.2.3 Multivariate and hidden regular variation

Results presented in Eqs. F1.7, F1.8 and F1.10 can be related to the concept of multivariate regular variation developed and presented by Resnick (Resnick, 1987, 2002). Multivariate variation on the cone $C = \ [0, \infty]^d - \{0\}$ can be defined as the following: suppose that Z is a d-dimensional random vector in $[0, \infty]^d$, then the distribution of Z is regularly varying (with unequal components) if there exist functions $b(t) \rightarrow \infty$, as $t \rightarrow \infty$ that, for a Radon measure v (i.e., finite on sets bounded away from zero) on C, we have the vague convergence which can be expressed as(Cooley *et al.*, 2019):

$$\lim_{t\to\infty} \left[tP\left(\frac{Z}{b(t)} \in A\right)\right] \rightarrow v\ (A) \tag{F1.11}$$

for any set $A \subset C$ and where $b(t)$ is a regularly varying function of some index $\alpha>0$ and v is a Radon measure on the cone $C = \ [0, \infty]^d - \{0\}$ which satisfies the homogeneous property

$$v(tA) = t^{-\alpha}\, v(A) \tag{F1.12}$$

for any scaler t and $A \subset C$. The limit measure $v(A)$ has a homogeneity property of order $-\alpha$. The coefficient α is the index of regular variation and $\alpha = {}^{1}/_{\xi}$ with ξ the shape parameter of the marginal distributions (see **Section F1.1**). With a standard Fréchet margins we have $\xi = 1$ and therefore $\alpha = 1$.

Multivariate extreme value and regular variation theory previously presented provide a rich theory for extremal dependence in the case of asymptotic dependence (Pickands, 1981; Das, 2009) but it is not able to distinguish between asymptotic independent and actual independence. Ledford and Tawn (1996; 1997) developed a dependence measure that can detect tail dependence in the asymptotic independence setting. The coefficient of tail dependence η measures the speed of decay toward independence at a high level (Davison and Huser, 2015). The coefficient η provides a better understanding of asymptotically independent behaviours and helped develop the concept of hidden regular variation.

Hidden regular variation is a property of the subfamily of distributions having both multivariate regular variation and asymptotic independence. (Resnick, 2002; Maulik and Resnick, 2005) Resnick (2002) Asymptotic independence is a degenerative case for multivariate extreme value theory (Cooley, 2019). The renormalizing sequence *b(t)* in Eq. F1.11 grows too rapidly. The latter is replaced by a lighter tailed normalizing sequence b^0. Hidden regular variation can therefore be expressed on the cone $C = (0, \infty]^d$ as:

$$\lim_{t\to\infty} \left[tP\left(\frac{Z}{b^0(t)} \in A\right)\right] \to v_0\,(A) \tag{F1.13}$$

for any set A bounded away from the axes, $A \subset C$, where b^0 is a regularly varying function and v is a Radon measure (i.e., finite on sets bounded away from zero) on the cone $C\ (0, \infty]^d$ which satisfies

$$v_0(tA) = t^{-1/\eta}\, v_0(A) \tag{F1.14}$$

for any scaler t and $A \subset C$. Here, η is the coefficient of tail dependence $\eta \in (0,1]$. A decreasing value of η corresponds to weaker dependence.

F1.3 Bivariate case

In the bivariate case, when $d = 2$, the exponent measure (**Section A2.2**) is expressed as:

$$V(z_1, z_2) = \int_0^1 \max\left(\frac{w}{z_1}, \frac{1-w}{z_2}\right) 2dH(w) \tag{F1.15}$$

with H an arbitrary distribution function on [0,1] satisfying the moment constraint

$$\int_0^1 \mathrm{w} dH(w) = 1/2 \tag{F1.16}$$

An alternative representation of equation incorporates the Pickands dependence function (Pickands, 1975), denoted by *A(w)*

$$V(z_1, z_2) = ({z_1}^{-1} + {z_2}^{-1})\, A(\frac{z_1}{z_1 + z_2}) \tag{F1.17}$$

where *A(w)* satisfies

$$A(w) = 2\int_0^1 \max\big((1-w)q, w(1-q)\big)\, dH(q) \tag{F1.18}$$

The Pickands dependence function $A(w)$ is a defined on the interval [0,1] and has the following properties: (i) $A(0) = A(1) = 1$, (ii) *A(w)* is convex and (iii) $A(w)$ is contained in a triangular region *A(w)* is usually used as a measure of the strength of dependence between two variables z_1 and z_2. The Pickands dependence function can be estimated parametrically through copula functions or with nonparametric estimators (Pickands, 1981; Capéraà *et al.*, 1997).

F1.3.1 Gumbel copula

The Gumbel copula (which is also an Archimedean copula) is one of the oldest extreme value copulas (Eschenburg, 2013). It is also referred to as the bivariate logistic model (with Gumbel margins) in the literature and was first introduced by Gumbel (1961):

$$C(u, v) = \exp\left\{-\left[(-\ln(u))^{\theta} + (-\ln(v))^{\theta}\right]^{1/\theta}\right\} \tag{F1.19}$$

with $\theta \in [1, \infty]$ the dependence parameter, *u* and *v* uniform marginal distributions, and ln the natural log and exp the exponential.

The Gumbel copula has been used widely in hydrology (Zhang and Singh, 2007; Salvadori and De Michele, 2010; Zheng *et al.*, 2013; Dung *et al.*, 2015) and coastal engineering (Yang and Zhang, 2013; Masina *et al.*, 2015; Mazas and Hamm, 2017). We will also use this copula in our simulation study as a reference for the asymptotic dependence case. Other important extreme value copulas include the Galambos copula which will be used alongside the Gumbel copula as asymptotically dependent models in our simulations (**Sect. 4.3**).

F1.3.2 Normal copula

The normal copula has been used in several hazard interrelation studies because of its flexibility (Rueda *et al.*, 2016; Serinaldi, 2016; Sadegh *et al.*, 2017). The normal copula is a single parameter copula with its parameter directly linked to the tail dependence coefficient η presented in **Sect. 2.2.** As showed by Ledford and Tawn (1997), the normal copula is suitable for the whole range of behaviour within the class of asymptotic independence (i.e. from sub-asymptotic positive to negative association). We use the normal copula as a reference for the asymptotic independence case; the normal copula is expressed as (Sadegh *et al.*, 2017):

$$C(u,v) = \int_{-\infty}^{\Phi^{-1}(u)} \int_{-\infty}^{\Phi^{-1}(v)} \frac{1}{2\pi\sqrt{1-\rho^2}} exp\left(\frac{2\rho xy - x^2 - y^2}{2(1-\rho^2)}\right) dxdy \tag{F1.20}$$

with $\Phi(.)$ the standard Gaussian distribution function and $\rho \in [-1, 1]$ the dependence parameter. The FGM copula exhibits near independent joint tail dependence behaviour, meaning that the coefficient of tail dependence is $\eta = 0.5$ (Ledford and Tawn, 1997).

F2. Level curve density. Associated Section: Section 2.3: Return Period in the bivariate framework and Section 3.2: Diagnostic tools

As mentioned in the main text, **Section 2.3** level curves are composed of an infinite set of bivariate values all corresponding to the same probability of exceedance. In the context of multi-hazards, events with very different properties (e.g., a storm with heavy rain and moderate wind vs. another storm with moderate rain and heavy wind) can have the same return period (Chebana and Ouarda, 2011; Volpi and Fiori, 2012; Sadegh *et al.*, 2018). One approach that has been implemented when using copula models is to use the density of the associated copula to weight (X_1,X_2) pairs on the curves (Volpi and Fiori, 2012). The joint density function of a copula is defined as (Volpi and Fiori, 2012):

$$f_{X_1,X_2}(x_1,x_2) = \frac{\partial^2 F_{X_1,X_2}(x_1,x_2)}{\partial x_1 \partial x_2}. \tag{F2.1}$$

It is then possible to identify a most-likely scenario (Gr̈aler *et al.*, 2013; Sadegh *et al.*, 2018) which is the coordinate of the level curve with the highest joint density (**Fig. F2.1**). Chebana and Ouarda (2011) proposed the decomposition of level curves into a naïve part (tail) and a proper part (central). Volpi and Fiori (2012) defined a level of probability to determine lower and upper limits of the proper part of the level curve. The most likely scenario and proper part of the level curve are shown in **Fig. F2.1,** respectively by the purple dot and the curve domain between blue diamonds along the level curve. The joint density probability function of copulas has also been used to estimate joint confidence intervals for level curves (Dung *et al.*, 2015; Zhang *et al.*, 2015; Serinaldi, 2016).

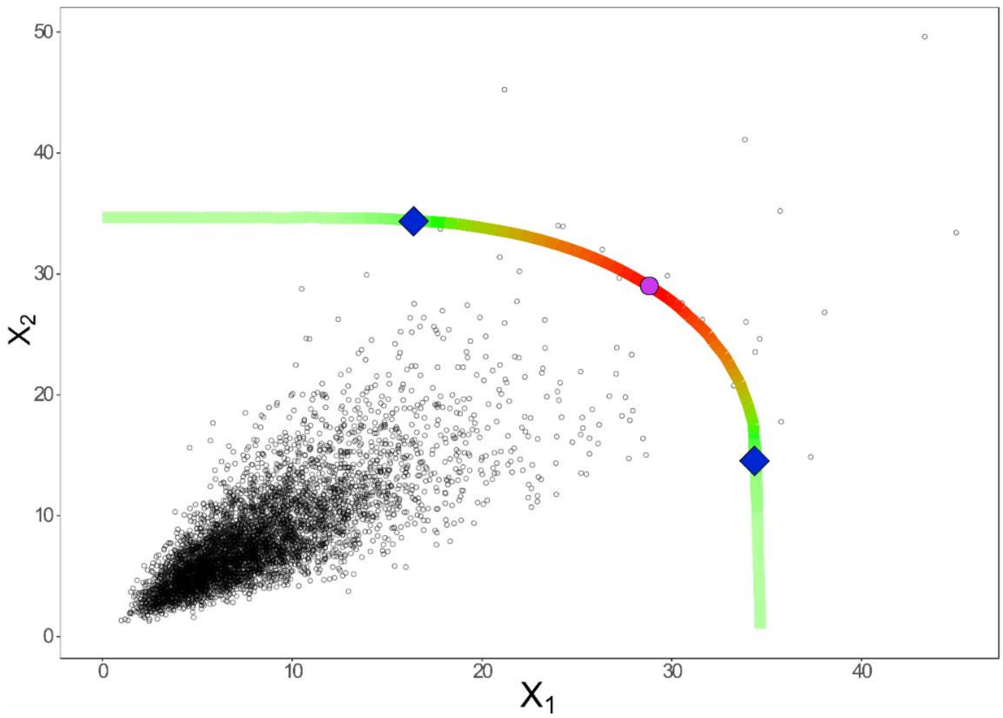

Figure F2.1: Level curve density from low (green) to high (red) for a probability of joint (X_1, X_2) exceedance p = 0.001 with its density (5000 realisations on a normal copula with log-normal distributions). The purple dot represents the most likely scenario while the two blue diamonds represent the upper and lower bound of the proper part of the curve with a 95% confidence level.

The level curve density can be estimated from parametric models (i.e., copula). However, it is also possible to estimate density with a kernel density estimator when enough data are available (main text, **Section4. 2.3.3**). For extreme low probability level curves as the ones we are interested in this study, there are few or no data. The simulation of extreme bivariate data with the conditional extremes model (main text, **Section 4.2.3.2**) overcomes this limitation, it is then possible to estimate the level curve density via a kernel density estimator.

Appendix F References

Bernardara, P., Mazas, F., Kergadallan, X. and Hamm, L.: A two-step framework for over-threshold modelling of environmental extremes, Nat. Hazards Earth Syst. Sci., 14(3), 635–647, 2014.

Bingham, N. H.: Regular variation and probability: The early years, J. Comput. Appl. Math., 200(1), 357–363, 2007.

Bingham, N. H., Goldie, C. M. and Teugels, J. L.: Regular variation, Cambridge University Press, Cambridge., 1987.

Capéraà, P., Fougères, A. L. and Genest, C.: A nonparametric estimation procedure for bivariate extreme value copulas, Biometrika, 84(3), 567–577, 1997.

Chebana, F. and Ouarda, T. B. M. J.: Multivariate quantiles in hydrological frequency analysis, Environmetrics, 22(1), 63–78, 2011.

Coles, S.: An Introduction to Statistical Modeling of Extreme Values, Springer London, London., 2001.

Cooley, D., Thibaud, E., Castillo, F. and Wehner, M. F.: A nonparametric method for producing isolines of bivariate exceedance probabilities, Extremes, 2019.

Das, B.: Conditional extreme value model and related topics, Cornell University., 2009.

Davison, A. C. and Huser, R.: Statistics of Extremes, Annu. Rev. Stat. Its Appl., 2(1), 203–235, 2015.

Davison, A. C. and Smith, R. L.: Models for Exceedances over High Thresholds, J. R. Stat. Soc. Ser. B, 52(3), 393–442, 1990.

Dung, N. V., Merz, B., Bárdossy, A. and Apel, H.: Handling uncertainty in bivariate quantile estimation - An application to flood hazard analysis in the Mekong Delta, J. Hydrol., 527, 704–717, 2015.

Dutfoy, A., Parey, S. and Roche, N.: Multivariate Extreme Value Theory - A Tutorial with Applications to Hydrology and Meteorology, Depend. Model., 2(1), 30–48, 2014.

Eschenburg, P.: Properties of extreme-value copulas, 2013.

Fisher, R. A. and Tippett, L. H. C.: Limiting forms of the frequency distribution of the largest or smallest member of a sample, Math. Proc. Cambridge Philos. Soc., 24(2), 180–190, 1928.

Gřaler, B., Van Den Berg, M. J., Vandenberghe, S., Petroselli, A., Grimaldi, S., De Baets, B. and Verhoest, N. E. C.: Multivariate return periods in hydrology: A critical and practical review focusing on synthetic design hydrograph estimation, Hydrol. Earth Syst. Sci., 17(4), 1281–1296, 2013.

Gumbel, E. J.: Bivariate Logistic Distributions, J. Am. Stat. Assoc., 56(294), 335–349, 1961.

Gümbel, E. J.: Statistics of extremes, Columbia U., New York, 1958.

de Haan, L.: On Regular Variation and Its Application to the Weak Convergence of Sample Extremes., 1970.

de Haan, L. and Resnick, S. I.: Limit theory for multivariate sample extremes, Zeitschrift für Wahrscheinlichkeitstheorie und Verwandte Gebiete, 40(4), 317–337, 1977.

De Haan, L. and Resnick, S.: Second-order regular variation and rates of convergence in extreme-value theory, Ann. Probab., 24(1), 97–124, 1996.

Huser, R.: Statistical Modeling and Inference for Spatio-Temporal Extremes, PhD thesis, EPFL, available at: https://infoscience. epfl.ch/record/188557?ln=en (Accessed 28 January 2020), 2013.

Ledford, A.: Statistics for near independence in multivariate extreme values, Biometrika, 83(1), 169–187, 1996.

Ledford, A. W. and Tawn, J. A.: Modelling Dependence within Joint Tail Regions, J. R. Stat. Soc. Ser. B (Statistical Methodol., 59(2), 475–499, 1997.

Masina, M., Lamberti, A. and Archetti, R.: Coastal flooding: A copula-based approach for estimating the joint probability of water levels and waves, Coast. Eng., 97, 37–52, 2015.

Maulik, K. and Resnick, S.: Characterizations and examples of hidden regular variation, Extremes, 7(1), 31–67, 2005.

Mazas, F. and Hamm, L.: An event-based approach for extreme joint probabilities of waves and sea levels, Coast. Eng., 122(February), 44–59, 2017.

Pickands, J.: Statistical Inference Using Extreme Order Statistics, Ann. Stat., 3(1), 119–131, 1975.

Pickands, J.: Multivariate extreme value distribution, in Proceedings 43th, Session of International Statistical Institution., 1981.

Resnick, S.: Hidden regular variation, second order regular variation and asymptotic independence, Extremes, 303–336, 2002.

Resnick, S. I.: Extreme Values, Regular Variation and Point Processes, Springer New York, New York, 1987.

Rueda, A., Camus, P., Tomás, A., Vitousek, S. and Méndez, F. J.: A multivariate extreme wave and storm surge climate emulator based on weather patterns, Ocean Model., 104, 242–251, 2016.

Sadegh, M., Ragno, E. and AghaKouchak, A.: Multivariate Copula Analysis Toolbox (MvCAT): Describing dependence and underlying uncertainty using a Bayesian framework, Water Resour. Res., 53(6), 5166–5183, 2017.

Sadegh, M., Moftakhari, H., Gupta, H. V., Ragno, E., Mazdiyasni, O., Sanders, B., Matthew, R. and AghaKouchak, A.: Multihazard Scenarios for Analysis of Compound Extreme Events, Geophys. Res. Lett., 45(11), 5470–5480, 2018.

Salvadori, G. and De Michele, C.: Multivariate multiparameter extreme value models and return periods: A copula approach, Water Resour. Res., 46(10), 2010.

Salvadori, G., Tomasicchio, G. R. and D'Alessandro, F.: Practical guidelines for multivariate analysis and design in coastal and offshore engineering, Coast. Eng., 88, 1–14, 2014.

Serinaldi, F.: Can we tell more than we can know? The limits of bivariate drought analyses in the United States, Stoch. Environ. Res. Risk Assess., 30(6), 1691–1704, 2016.

Tawn, J. A.: Bivariate extreme value theory: Models and estimation, Biometrika, 75(3), 397–415, 1988.

Tawn, J. A.: Modelling multivariate extreme value distributions, Biometrika, 77(2), 245–253, 1990.

Tiago de Oliveira, J.: Extreme values and meteorology, Theor. Appl. Climatol., 37(4), 184–193, 1986.

Volpi, E. and Fiori, A.: Design event selection in bivariate hydrological frequency analysis, Hydrol. Sci. J., 57(8), 1506–1515, 2012.

Winter, H. C.: Extreme Value Modelling of Heatwaves, Lancaster., 2016.

Yang, X. and Zhang, Q.: Joint probability distribution of winds and waves from wave simulation of 20 years (1989-2008) in Bohai Bay, Water Sci. Eng., 6(3), 296–307, 2013.

Zhang, L. and Singh, V. P.: Trivariate Flood Frequency Analysis Using the Gumbel–Hougaard Copula, J. Hydrol. Eng., 12(4), 431–439, 2007.

Zhang, Q., Xiao, M. and Singh, V. P.: Uncertainty evaluation of copula analysis of hydrological droughts in the East River basin, China, Glob. Planet. Change, 129, 1–9, 2015.

Zheng, F., Westra, S. and Sisson, S. A.: Quantifying the dependence between extreme rainfall and storm surge in the coastal zone, J. Hydrol., 505, 172–187, 2013.

Appendix G: Sensitivity Analysis of the spatiotemporal clustering procedure developed in Chapter 5.

Summary:

This Appendix G consists of a Sensitivity Analysis on the spatiotemporal clustering procedure for Compound Hazard Cluster Identification (CHCI) developed in **Chapter 5**. Parameters influencing the CHCI method are listed and a brief overview of sensibility analysis is provided. The Sensitivity Analysis is performed over one year of reanalysis data (2016) with the SRC (standardized regression coefficient). The SRC is a sensitivity index to assess the importance of each input parameter. For compound hazard cluster, the most dominant variable is the threshold for the sampling of extreme events.

G1. Introduction

In **Chapter 5**, a methodology is designed to identify single and compound hazard events over Great Britain. The Procedure developed involves numerous steps to go from raw ERA5 data of hourly maximum wind gust and hourly accumulated precipitation to compound wind rain clusters. Three main parameters influence the process and consequent results:

(i) the threshold selected to sample extreme events u

(ii) the ratio r of the spatiotemporal scaling parameter a and b

(iii) the density threshold μ

The neighbour parameter ε is not included here in the set of parameters that might influence the clustering process as it is set in a systematic manner (**Section 5.3.2**). The value of the parameter ultimately depends on the three other parameters. The limitations around the selection of these parameters are discussed in **Section 5.4.** In this appendix, a Sensitivity Analysis is conducted to understand the effect of the three aforementioned parameters (u, r, μ) on the output of the spatiotemporal clustering procedure (**Figure 5.4**). The Sensitivity Analysis is performed on a subsample of the datasets used in **Chapter 5**. One year of data (January-December 2016) is used to reduce computational time.

G2. Sensitivity Analysis

The idea behind Sensitivity Analysis is to change an input parameter X and assess if it produces a change in the output parameter Y. The measure of this change in Y allows determining the sensitivity of Y with respect to X (Nguyen and Reiter, 2015). A panoply of methods have been developed to conduct Sensitivity Analysis (See Hamby, 1994; Frey *et al.*, 2003; Nguyen and Reiter, 2015 for reviews). Here, a “statistical (or probabilistic) approach” is used. This type of approach is based on the generation of a sample of input vectors and associated outputs (Frey *et al.*, 2003). The three parameters of interest are sampled within given ranges. The extreme threshold u is set to 0.99 (99th percentile) in **Chapter 5**. In this SA, u varies between 0.95 and 0.99. The scaling parameters ratio takes three values: 2, 4, 8. Finally the density threshold μ takes four values between 5 and 30. The combination of these parameters creates a sample of 60 input parameter sets. The values retained for each parameter are displayed in **Table G1**.

Table G1: Values taken by the three input parameters in Sensitivity Analysis

Parameter	**Values**
Extreme threshold u	**0.99**; 0.98; 0.97; 0.96; 0.95
Scaling parameters ratio r	2; **4**; 8
Density threshold μ	5; **10**; 20; 30

The output variables of interest of this sensitivity analysis are the number of wind, rain and compound hazard clusters created. The clustering procedure illustrated in **Figure 5.4** is run for each of the 60 parameter sets, providing 60 output sets. To quantify the sensitivity of the three output in respect to u, r and μ, a sensitivity index is computed. Several sensitivity indices have been developed for statistical SA including: PEAR (Pearson product moment correlation coefficient), SPEA (Spearman coefficient), SRC (standardized regression coefficient), and SRRC (standardized rank regression coefficient) (Nguyen and Reiter, 2015). These indices are regression-based sensitivity indices that are suitable for linear trends.

Regression methods are often used in SA because of their relative simplicity and their low computational cost (Hamby, 1994; Nguyen and Reiter, 2015). Regression techniques build an approximate empirical model starting from a sample of the input $x= (x_1, \ldots, x_k)$ and output variable y. Such models can be written as (Bolado-Lavin and Badea, 2008):

$$y(x) = \beta_0 + \beta_1 x_1 + \cdots + \beta_k x_k + \varepsilon \qquad \text{(G1)}$$

Where $\varepsilon \sim N(0, \sigma^2)$ (normal distribution with null mean and variance σ^2) is a white noise and $\beta = (\beta_1, \ldots \beta_k)$ are the regression coefficients. **Equation G1** is a first-order polynomial regression and assumes the independence of each input. The regression parameters provide an estimate of the strength of the correlation between the inputs x and the output y. Regression techniques allow to create a sensitivity ranking based on the relative magnitude of each regression coefficient. To compare the magnitude of regression parameters, a standardization process is beneficial (Hamby, 1994).

One widely used sensitivity index based on the regression method is the SRC (standardized regression coefficient). This coefficient is expressed as follow (Saltelli *et al.*, 2004):

$$SRC_i = \beta_i \frac{\sigma_{xi}}{\sigma_y} \tag{G2}$$

where $i \in (1:k)$, β_i is the regression parameter of the variable x_i, σ_{xi} is the variance of variable x_i and σ_y is the variance of the output variable y. The influence of each input variables on the output is therefore comparable. The absolute value of the SRC represents a measure for parameter importance with higher SRC values indicating more influence on the model outcome, the sign of the SRC value indicates whether the model outcome increases or decreases as the value of the input factor changes (Menberg *et al.*, 2016). The reliability of the SRC depends on how well the linear regression model represents the output variable(Nguyen and Reiter, 2015). To assess how well the model fits the output, the coefficient of determination R^2, which indicates how much of the output variance σ_y can be explained by the variance of the linear model σ_x (Menberg *et al.*, 2016). R^2 is bounded between 0 and 1. Lower values indicate a poor fit of the model.

G3. Results

The Sensitivity Analysis is performed with the R package *sensitivity* (Iooss *et al.*, 2020) on three outputs: number of wind clusters N_w, number of rain cluster N_r and number of compound clusters N_c. The aim is to identify which input parameters are the most likely to influence the number of detected clusters, and therefore influence the results of the analysis developed in **Chapter 5**. Polynomial linear regression is computed regarding each of the three outputs. The regression coefficient of each variable has a p-value which tests the null hypothesis that the variable does not correlate with the output. For a p-value below a given significant level (e.g., 0.01), there is evidence to reject the null hypothesis that there is zero correlation between the input variable and the output. The results of the regression analysis for N_w, N_r and N_c are displayed in **Table G2**, **Table G3** and **Table G4**.

TableG2: Results for the regression analysis on the number of wind clusters N_w

Parameters	Regression coefficients	P-value	SRC	Rank
u	-7215.8	$3.84e^{-13}$***	-0.71 [-0.84,-0.54]	1
r	9.3	0.03*	0.16 [0.30,0.52]	3
μ	5.9	$2.31e^{-06}$***	0.39 [-0.84,-0.60]	2

R^2 = 0,92 | Significance Levels: 99.9% '***' 99% '**' 95% '*'

Table G2 have displayed the results of the regression analysis of the model $N_w = f(u, r, \mu)$. The coefficient of determination value is R^2 = 0.92, meaning that 92% of the variation in N_w is explained by the model. The p-values highlights if the relationship between u, r, μ and N_r is statistically significant. The scaling parameters ration r has a significant positive influence at a

95% level on the number of wind cluster according to the regression analysis. However, this influence remains weak compared to the one of u and μ. The extreme threshold u has a strong negative influence on the number of clusters, while the density threshold μ has a positive effect on N_{w}. (**Table G2**).

Table G3 Results for the regression analysis on the number of rain clusters N_r

Parameters	Regression coefficients	P-value	SRC	Rank
u	-13800.8	$<2e^{-16}$***	-0.59 [-0.69,-0.48]	2
r	2.7	0.58	0.02 [-0.06,0.10]	3
μ	-25.7	$<2e^{-16}$***	-0.75 [-0.84,-0.60]	1

R^2 = 0,66 | Significance Levels: 99.99% '***' 99.9% '**' 99% '*'

In **Table G3** are displayed the results of the regression analysis of the model $N_r = f(u, r, \mu)$. The coefficient of determination value is R^2 = 0.66, meaning that 66% of the variation in N_r is explained by the model. Despite being low, this value does not entirely disqualify the model. The p-values highlights if the relationship between u, r, μ and N_r are statistically significant. The scaling parameters ration r has an insignificant influence on the number of rain clusters according to the regression analysis. However, the extreme threshold and the density threshold both have a strong negative influence on the number of clusters, with the density threshold being the most important variable (**Table G2**).

Table G4 Results for the regression analysis on the number of compound clusters N_c

Parameters	Regression coefficients	P-value	SRC	Rank
u	$-1.15e^{+04}$	$<2e^{-16}$***	-0.92 [-0.99,-0.83]	1
r	-5.54	0,03*	-0.08 [-0.16,-0.01]	3
μ	-5.15	$1.06e^{-10}$***	-0.28 [-0.35,-0.20]	2

R^2 = 0,93 | Significance Levels: 99.99% '***' 99.9% '**' 99% '*'

In **Table G4** are displayed the results of the regression analysis of the model $N_c = f(u, r, \mu)$. The coefficient of determination value is R^2 = 0.93, meaning that 93% of the variation in N_c is explained by the model. The p-values highlights if the relationship between u, r, μ and Nc are statistically significant. The scaling parameters ration r has a significant positive influence at a 95% level on the number of compound clusters according to the regression analysis. However, the extreme threshold and the density threshold both have a negative influence on the number of clusters, with the extreme threshold being by far the most important variable (**Table G2**).

Figure G2 displays the absolute value of the SRC of the three input variables on the outcomes N_w, N_r and N_c. It indicates which variables are the most influent on the outcomes. The threshold parameter u has the most important influence on the N_w and N_c. The scaling parameter ratio r has low influence (insignificant for N_r) while the density threshold μ has the most important effect on N_r. It appears that Nr is not influenced by the same input parameters as Nw and Nc which are highly dominated by the value of the extreme threshold u. It is important to note that the linear regression models fitted on Nw and Nc both have a high R^2, while the one fitted on Nr has a low R^2, highlighting the difference between precipitation extremes and wind gust extremes.

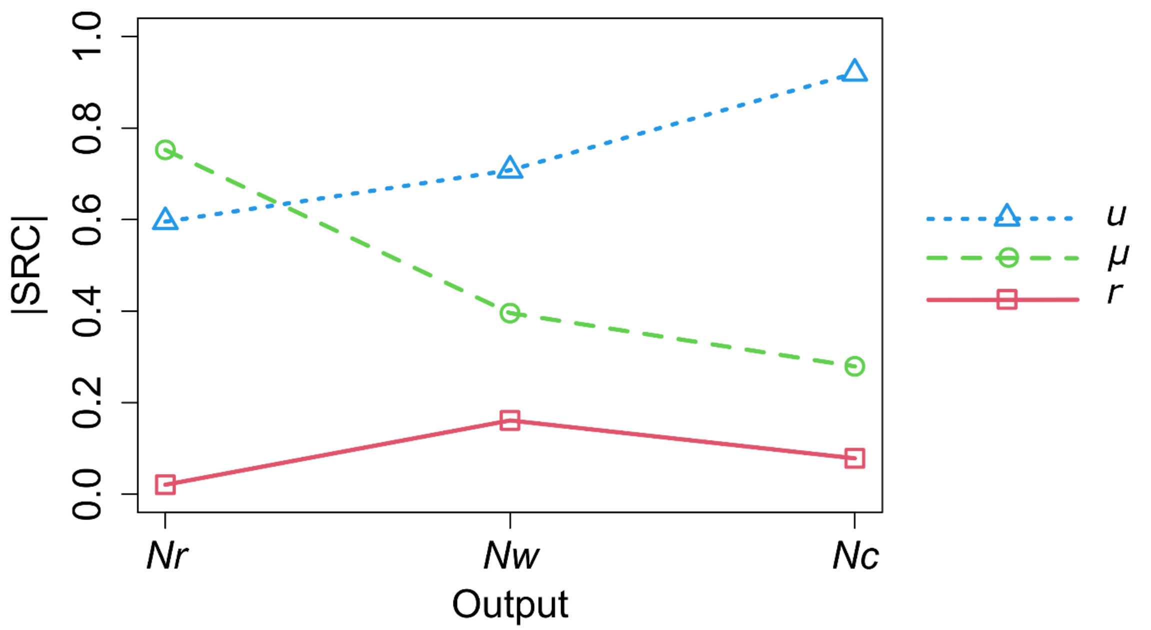

Figure G0.1: Results of the sensitivity analysis on the three output variables (*Nr, Nw, Nc*). *U* is the extreme threshold, *r* is the scaling parameter ration and μ is the density threshold. The absolute value of the standardized regression coefficient of each input variables is displayed for each output variable.

G4. Conclusion

In this appendix, variables that can influence the result of the spatiotemporal clustering procedure developed in **Chapter 5** have been identified and highlighted in **Figure 5.4.** The output variables retained to assess the influence of the procedure to the input variables are the number of rain, wind and compound hazard clusters created. These output variables are believed to have a significant influence on spatiotemporal attributes of clusters. A Sensitivity Analysis has been conducted on a sample of 60 combinations of the three input variables u, r and μ **(Table G1).** The Sensitivity Analysis was done over one year of reanalysis data (2016) with a regression-based approach. The SRC was used as a sensitivity index to assess the importance of each input parameter. For compound hazard cluster, the most dominant variable is the threshold for the sampling of extreme events which has a strong negative correlation with the number of clusters created, meaning that an increase of the threshold reduces the number of clusters. In **Chapter 5**, the highest value of *u* tested in the Sensitivity Analysis was selected (0.99). With the parameter set used in **Chapter 5**, 109 compound hazard clusters were identified for one year. The large size of the sample created justifies the use of a high threshold which is the main parameter influencing the number of clusters created.

Appendix G References

Bolado-Lavin, R. and Badea, A.: Review of Sensitivity Analysis Methods and Experience for Geological Disposal of Radioactive waste and Spent Nuclear Fuel., 2008.

Frey, C., Mokhtari, A. and Danish, T.: Evaluation of Selected Sensitivity Analysis Methods Based Upon Applications to Two Food Safety Process Risk Models, Washington D.C., 2003.

Hamby, D. M.: a Review of Techniques for Parameter Sensitivity, Environ. Monit. Assess. , 32©, 135–154, 1994.

Iooss, A. B., Veiga, S. Da, Janon, A., Pujol, G., Broto, B., Boumhaout, K., Delage, T., Amri, R. El, Fruth, J., Guillaume, J., Gratiet, L. Le, Lemaitre, P., Marrel, A., Mey-, A., Nelson, B. L., Oomen, R., Rakovec, O., Ramos, B., Roustant, O., Staum, J., Sueur, R., Touati, T., Weber, F. and Iooss, M. B.: Package ‘ sensitivity ,’ 2020.

Menberg, K., Heo, Y. and Choudhary, R.: Sensitivity analysis methods for building energy models: Comparing computational costs and extractable information, Energy Build., 133, 433–445, 2016.

Nguyen, A. T. and Reiter, S.: A performance comparison of sensitivity analysis methods for building energy models, Build. Simul., 8(6), 651–664, 2015.

Saltelli, A., Tarantola, S., Campolongo, F. and Ratto, M.: Sensitivity Analysis in Practice: A Guide to Assessing Scientific Models, John Wiley & Sons, Ltd, Chchester., 2004.

Appendix H: Complementary analysis of spatiotemporal features of compound wind-rain clusters

Summary:

This Appendix H consists of complementary analysis on spatiotemporal features of compound wind rain events in Great Britain and highlights how the database of compound hazard events created in **Chapter 5** can be further exploited. Herethe proportion of compound hazard events among wind and rain events is analysed with respect to the size and duration of these events. The two season spatial patterns regarding the occurrence of compound wind-rain events are discussed and spatial dependence of compound wind-rain occurrence between different sites are highlighted. Bivariate modelling is used to estimate return periods (estimated average time between event) of compound hazards events and highlight the influence of the intensity of extreme rainfall and extreme wind on the spatial and temporal scales of compound hazards events.

H1. Spatiotemporal features

Figure H1 shows the proportion of compound events amongst wind and rain events conditioned on the footprint (a) and duration (b) of events. For both rain and wind events, events with a greater footprint are more likely to be involved in a compound event. For example, when considering all footprint sizes, compound hazards events represent 20% of all rain events (**Figure H1**). For events with a footprint greater than 33% of the study area (i.e., regional and multi-regional), the share of compound event surges to 52%.

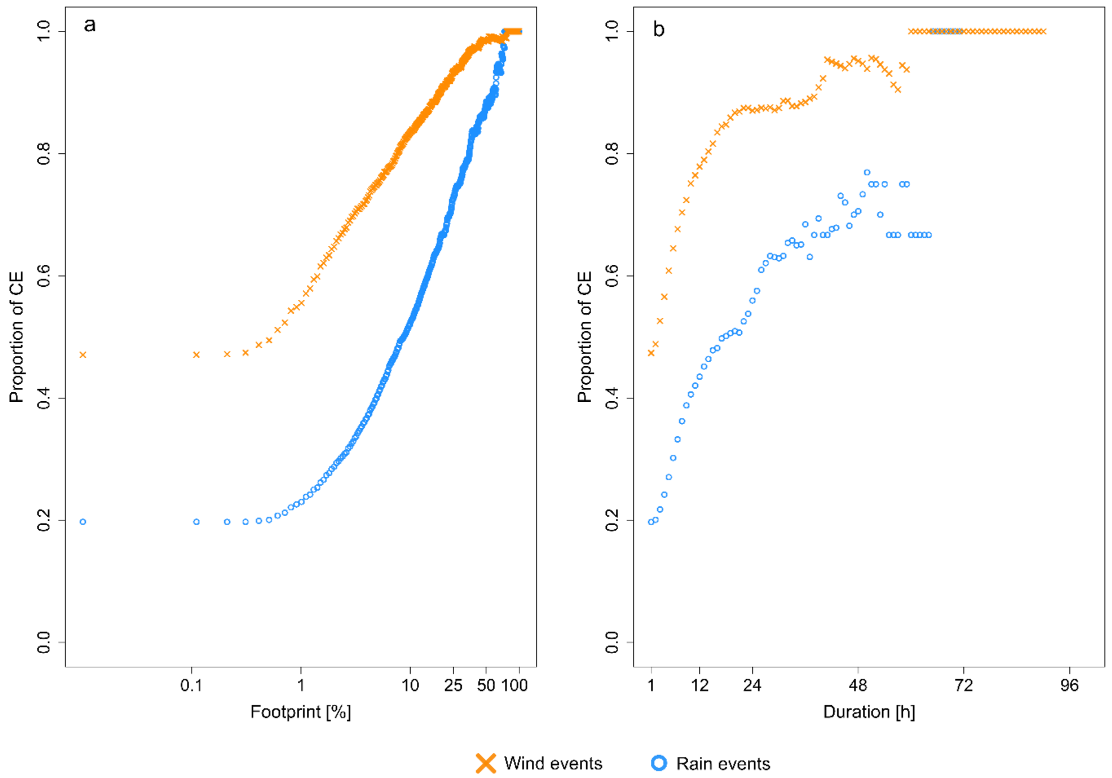

Figure H1: Proportion of Compound wind rain events among wind events (orange) and rain events (blue) depending on (a) spatial footprint (b) duration of the hazard events.

The seasonal patterns of compound wind-rain events have been discussed in **Section 5.3**. More than 80% of compound wind and precipitation events occur in the extended winter. In **Figure H2**, the frequency of compound events is displayed similarly to **Figure 5.13a**. However, in **Figure H2**, two maps are displayed, one for the extended winter and one for the extended summer. This division highlight two different patterns in terms of frequency of occurrence of compound wind-rain events. During the extended winter, there is a strong west-east pattern. This pattern is similar to the one observed by Blenkinsop *et al.* (2017) for daily rainfall accumulations, which are influenced by the prevailing direction of cyclonic weather systems and modified by orography, with western and northern areas being associated with orographically enhanced rainfall. In summer this pattern of compound wind rain events is replaced by a less well-defined north-south pattern. During summer, extreme hourly rainfall is less likely to be associated with such cyclonic systems and more probably a consequence of local-scale convection (or convection embedded within such systems) (Blenkinsop *et al.*, 2017).

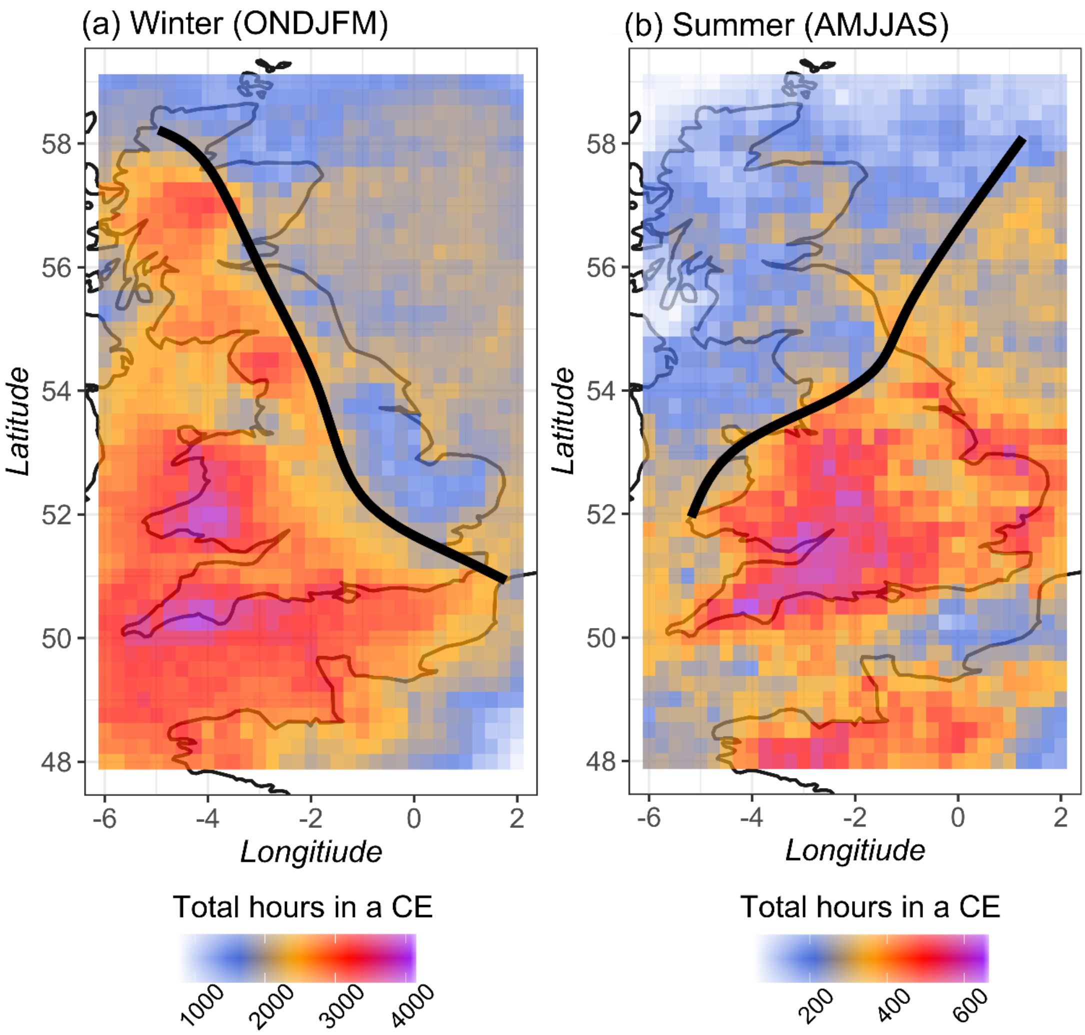

Figure H2: Total hours in a compound wind-rain event during (a) extended winter and (b) extended summer. Black lines are drawn manually to highlight the spatial patterns in compound wind-rain event occurrence.

The spatial dependence between different sites is investigated in **Figure H3. Figure H3** highlight the probability of each grid cell in the study area to be in a compound wind-rain event knowing that a given cell of reference is in a compound event (Ps). Four locations in Great Britain are taken as cells of reference: Cumbria, Sheffield, London and Glasgow. The spatial extent of compound wind-rain events is displayed with a different perspective from the one adopted in **Chapter 5**, highlighting that London is more likely to be in a large-scale event than Glasgow. Spatial dependences between places are also visible, for example, compound events occurrence in London is associated to compound events occurrence in South England while compound event occurring in Sheffield are more likely to develop over the Midlands and Wales.

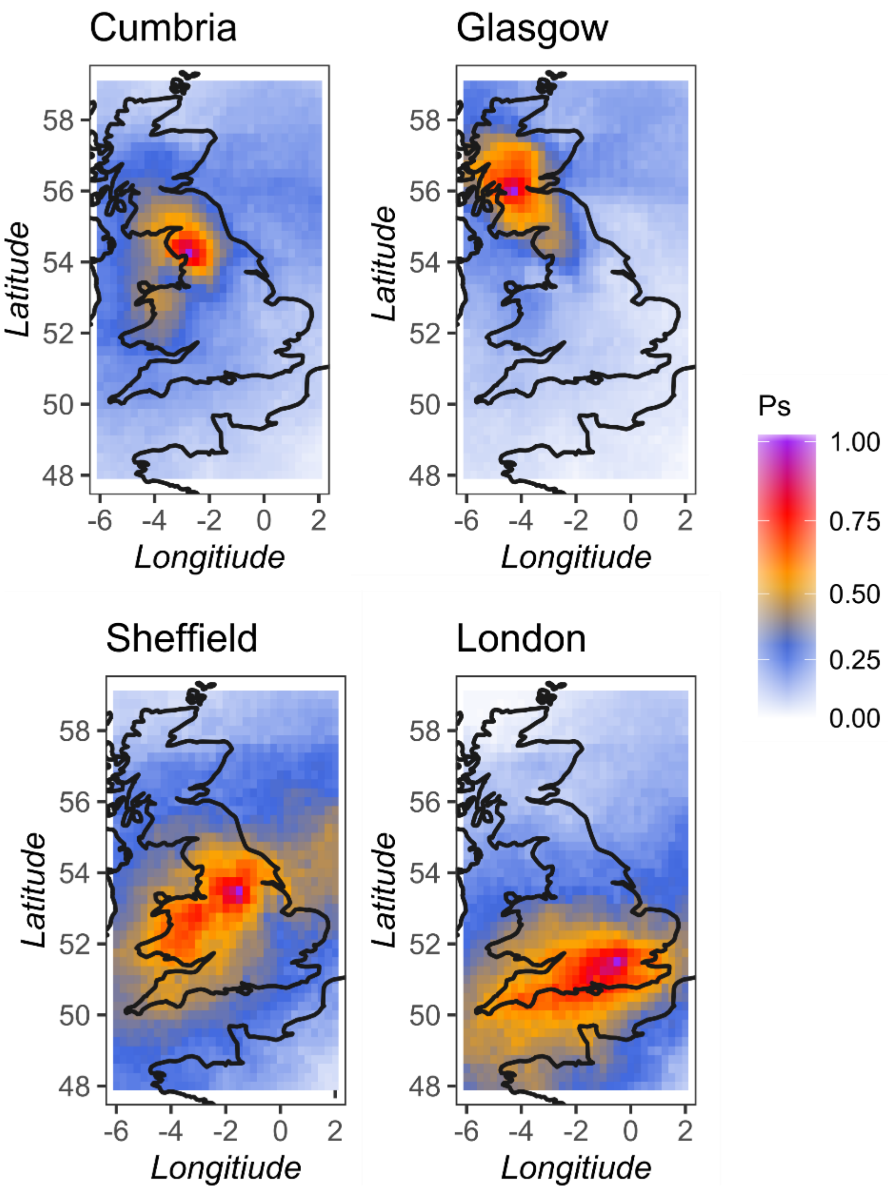

Figure H3: Spatial dependence of compound wind-rain occurrence between different sites. Ps is The probability of each grid cell in the study area to be in a compound wind-rain event knowing that a given cell of reference is in a compound event.

H2. Bivariate modelling

The concept of return period in a multivariate context has been widely discussed in the recent literature (Serinaldi, 2015; Gouldby *et al.*, 2017) (See **Chapter 4**). Nevertheless, a bivariate return period is expressed as a curve, named level curve (Volpi and Fiori, 2012; Bevacqua *et al.*, 2017). Here, the joint exceedance level curve is used to estimate a bivariate return period as it is commonly used in the literature and is relevant for practitioners (Hawkes, 2008; Mazas and Hamm, 2017). Let the random variables (X, Y) be vectors of i.i.d. values, the joint return period T of X and Y associated to the event ($X > x$ and $Y > y$) can be expressed as following (Mazas and Hamm, 2017):

$$T(x,y) = \frac{1}{\lambda_p P(X > x, Y > y)} \tag{H1}$$

With λ_p the mean number of events per year.

To estimate the extreme bivariate return period (e.g., 10 years,100 years), one can use bivariate extreme models. As there is no assumption here about the dependence between extreme wind and extreme rain within compound wind-rain events, a non-parametric approach is used, the joint tail KDE (kernel density estimation) approach, initially developed by (Cooley *et al.*, 2019). This approach combines a bivariate KDE to estimate bivariate the joint density below a threshold and multivariate extreme value theory to extrapolate in the joint tail of the bivariate distribution (see **Chapter 4**). However, in the joint tail, two variables can be either asymptotically independent or asymptotically dependent. The tail dependence is estimated with two measures χ and η (see **Chapter 4**). A value of η = 1 indicates asymptotic dependence, in which case the value of χ gives a measure of the strength of dependence. A limiting value of η less than 1 indicates asymptotic independence in which case χ is irrelevant and the value of η gives a measure of the strength of dependence (Coles *et al.*, 1999).

The intensity of rain and wind within a compound event is important to quantify the interrelation between these two hazards, and in particular, the nature of the dependence in the extremes. Bivariate extreme models can estimate the extremal dependence between two variables and therefore estimate joint return periods of events (**Chapter 4**). In this section, a bivariate extreme model is used to (i) evaluate the dependence structure between extreme rainfall and extreme wind gust in compound hazards events; (ii) extract set compound events with a return level greater than 1 year; (iii) examine the properties of major compound events.

To model the extremal dependence and the joint probability of wind and rain within a compound hazards event, the joint tail KDE model was used (see **Chapter 4**). The selection of this model has been driven by several factors: (i) its flexibility and relevance for the dependence structure of the compound hazards dataset; (ii) its relative simplicity and computational efficiency; (iii) its ability to estimate the return period of every event. The two tail dependence measures are estimated empirically and with the estimator presented in Winter (2016) which is derived from the joint-tail model of Ledford and Tawn (1997). The estimates with 95% CI bounds are displayed in **Table H1**. For more information about the two tail dependence measures, the reader can refer to **Section 4.2**.

Table H1: The two tail dependence estimates for the 4555 wind and rain accumulation couples. The empiric and model estimates of χ and η are displayed with a 95% confidence interval in brackets.

Tail dependence measure	Empiric estimate	JT.KDE estimate
χ	0.13 [-0.08,0.33]	0.1 [0.07,0.13]
η	0.58 [0.45,0.62]	0.54 [0.51,0.57]

Estimates from **Table H1** are used to characterize the nature of the tail dependence between *wa* and *ra* in compound hazards events. As η <<1, these two variables are considered as asymptotically independent and the value of η gives a measure of the strength of dependence (Coles *et al.*, 1999). Moreover, the value of η suggests a weak positive dependence. **Figure H4** is a scatterplot of *ra* and *wa* of the 4555 compound hazard events. A bivariate kernel density estimator is used to estimate the extreme level curve corresponding to a 1-year return period. This level curve is represented by a blue line in **Figure H4** and is used as a threshold to select the most intense compound hazards events over the 1979–2019 period. A total of 222 events exceeds the empiric 1-year return period threshold (coloured points in **Figure H4**) among the 4555 in the initial sample. The return period of the events is then estimated with the JT-KDE model. The most extreme events detected by our method over the period 1979–2019 occurred on January 7th and 8th 2005. It was the result of an extratropical cyclone named Erwin by the Free University of Berlin and mainly impacted Northern England and Scotland before causing important damages in Sweden and Baltic countries (Suursaar *et al.*, 2006). To give an order of magnitude, its wind-rain bivariate return period is estimated at more than 350 years by the JT-KDE model.

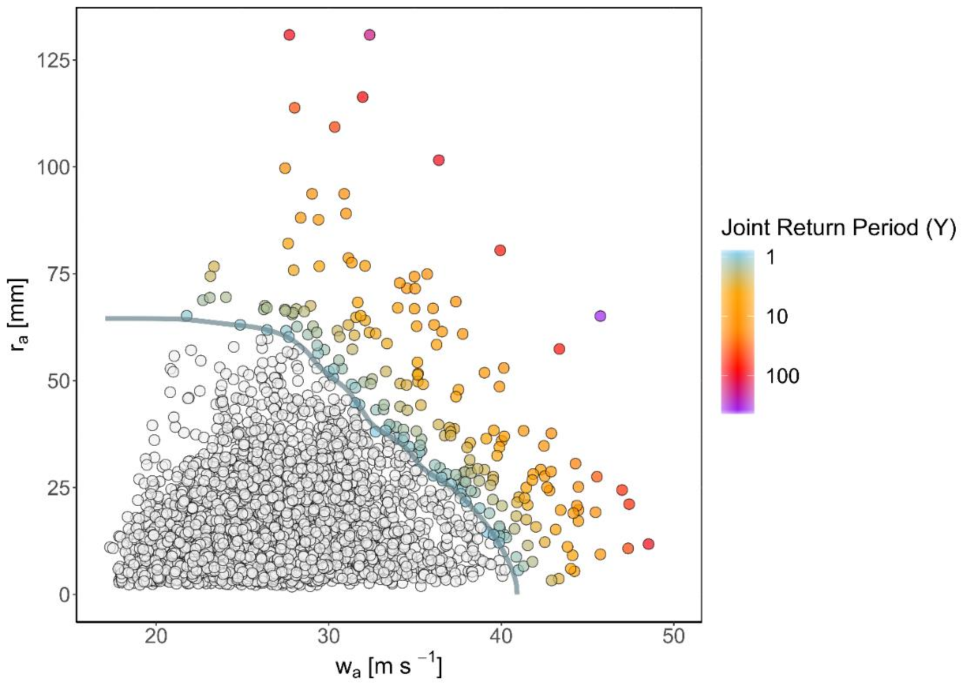

Figure H4: Scatter plot of wind accumulation (x-axis) and rain accumulation (y-axis) pairs of the 4555 compound hazards events identified with the CHCI methodology. The light blue line corresponds to a 1-year joint return period estimated with a kernel density estimator. This line is the threshold used to select major compound hazards events which are shown in colour. Colours of points above the blue line correspond to the return period.

While this sample of major events represents only 5% of the total number of events, it accounts for more than 35% of the total number of compound wind-rain event hours over Great Britain. This suggests that the most intense events in term of w_a and r_a last on average longer and have a larger footprint. This assumption is confirmed by **Figure H5**, which shows the spatial footprint and duration of the 4555 Compound wind-rain events detected and highlights the 222 major events sampled (**Figure H5**). While the relationship between joint return period, duration and footprint is not linear (most intense events are not the longest or the largest), **Figure H5** shows that major events occur in a different spatiotemporal interval than all events. Major events can occur on a small spatial scale (footprint < 1%), but their footprint is on average 5 times larger than the one of all compound wind-rain events. Major events also last at least 12 hours with an average duration of 40 hours. This suggests that the combined intensity of wind and rain in compound hazards events influences their duration and footprint size.

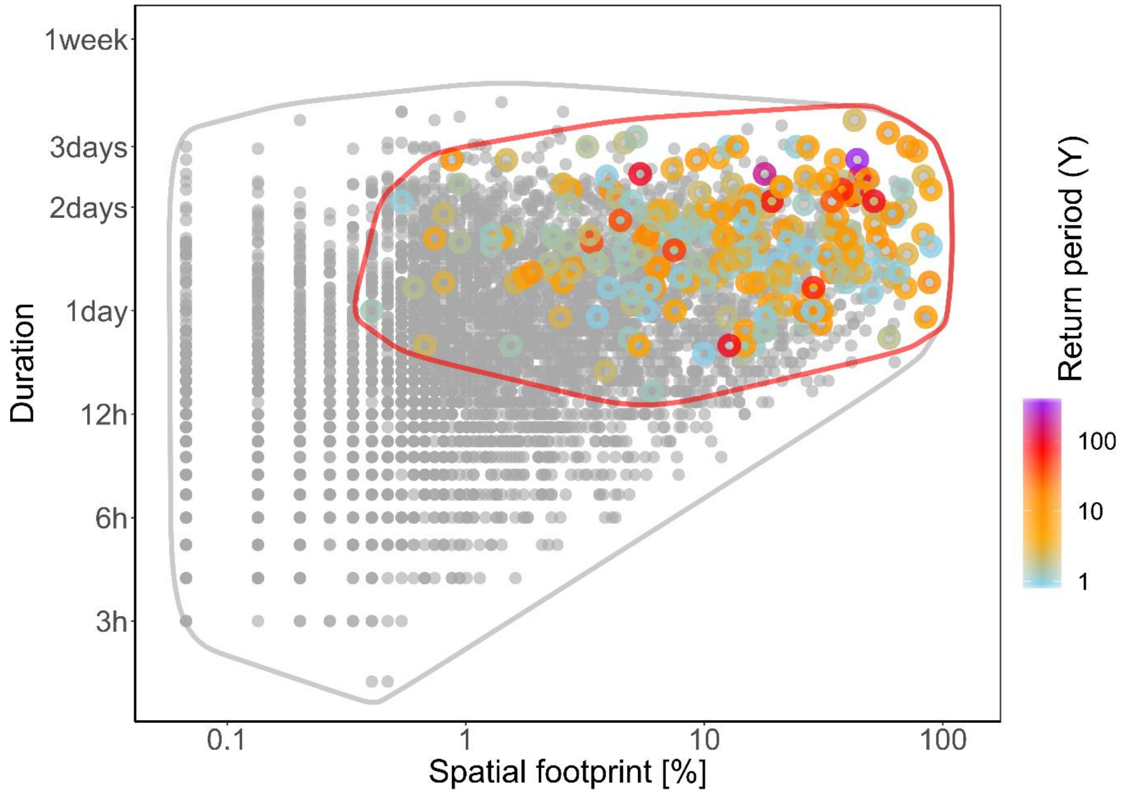

Figure H5: Duration and spatial footprint of the 4555 compound hazard events identified in the study. Grey points correspond to the whole population and coloured point correspond to the 222 major compound hazard events (with a bivariate return period greater than 1 year). Lines highlight the space-time contour of the whole population (grey) and the sample of major events (red).

Appendix H References

Blenkinsop, S., Lewis, E., Chan, S. C. and Fowler, H. J.: Quality-control of an hourly rainfall dataset and climatology of extremes for the UK, Int. J. Climatol., 37(2), 722–740, 2017.

Appendix I: Historic major wind or precipitation extreme events in Great Britain (1979-2019)

This appendix is a catalogue of 157 major wind or precipitation extreme events that occurred in Great Britain over the period 1979–2019. These events and their historic (Start date; end date) and spatial attributes (Region) are used to assess the ability of the method developed in **Chapter 5** to identify extreme events.

- **Table I1.** The 157 historic major multi-hazard events compiled in **Chapter 5.**

Table I1: The 157 historic major multi-hazard events compiled in Chapter 5. Regions are the 11 NUTS1 regions in Great Britain. The dominant hazard represents the primary hazard reported in sources and is used to associate the event to wind or rain clusters. Associated hazards are also displayed if mentioned in the sources.

ID	Year	Name	Start date	End date	Region	Dominant hazard	Associated hazards	Source
1	1979	Fastnet storm	1979-08-13	1979-08-14	South-West	Extreme wind		Eden,2008
2	1979		1979-12-04	1979-12-05	Scotland	Extreme wind		Eden,2008
3	1979		1979-12-14	1979-12-15	South-West	Extreme wind		Eden,2008
4	1979		1979-12-27	1979-12-28	All regions	Extreme rainfall	River flooding	Eden,2008
5	1980		1980-07-26	1980-07-26	South; Midlands; East	Extreme rainfall	River flooding	Eden,2008
6	1980		1980-08-07	1980-08-08	East; East-Midlands	Extreme rainfall	River flooding	Eden,2008
7	1981		1981-03-09	1981-03-10	Sout-West; East Midlands; West Midlands; Wales	Extreme rainfall	River flooding	Eden,2008
8	1981		1981-03-21	1981-03-23	Sout-West; East Midlands; West Midlands; Wales	Extreme rainfall	River flooding	Eden,2008
9	1981		1981-04-14	1981-04-14	South-East	Extreme rainfall	Lightning	Eden,2008
10	1981		1981-07-09	1981-07-09	South-East; London; South-West	Extreme rainfall	Lightning; River flooding	Eden,2008
11	1981		1981-08-05	1981-08-06	North-West; Midlands; London	Extreme rainfall	Lightning; River flooding	Eden,2008
12	1981		1981-12-13	1981-12-13	South-West	Extreme wind	Storm surge; extreme snow	Eden,2008
13	1982		1982-01-02	1982-01-08	Scotland; Yorkshire	Extreme rainfall	Soil moisture excess; River flooding	Eden,2008
14	1982		1982-03-03	1982-03-03	Scotland	Extreme wind		Eden,2008
15	1982		1982-06-21	1982-06-22	Yorkshire	Extreme rainfall	River flooding	Eden,2008
16	1982		1982-07-11	1982-07-12	South-West	Extreme rainfall	River flooding	Eden,2008
17	1982		1982-12-15	1982-12-20	All regions	Extreme wind		Eden,2008
18	1983		1983-01-31	1983-02-01	All regions	Extreme wind	Storm surge	Eden,2008
19	1983		1983-03-04	1983-03-06	Scotland	Extreme rainfall	River flooding	Eden,2008
20	1983		1983-05-27	1983-05-28	Scotland	Extreme rainfall	River flooding	Eden,2008
21	1983		1983-06-05	1983-06-05	South-West	Extreme rainfall	Hail, River flooding	Eden,2008
22	1983		1983-07-17	1983-07-17	North-West	Extreme rainfall	River flooding	Eden,2008
23	1983		1983-09-02	1983-09-05	All regions	Extreme wind		Eden,2008
24	1983		1983-12-20	1983-12-20	South-East; South-West	Extreme wind	Storm Surge	Eden,2008
25	1984		1984-07-23	1984-07-24	South-West	Extreme rainfall	River flooding	Eden,2008
26	1984		1984-10-18	1984-10-18	All regions	Extreme wind		Eden,2008
27	1984		1984-11-03	1984-11-03	Scotland; North-East	Extreme rainfall	River flooding	Eden,2008

ID	Year	Name	Start date	End date	Region	Dominant hazard	Associated hazards	Source
28	1986		1986-03-24	1986-03-24	Wales; West-Midlands	Extreme wind		Eden,2008
29	1986		1986-08-25	1986-08-26	South-West; Yorkshire; Midlands; Wales; North-West	Extreme rainfall	River flooding; Extreme wind	Eden,2008
30	1986		1986-12-29	1986-12-29	Wales	Extreme rainfall	River flooding	Eden,2008
31	1987		1987-03-27	1987-03-27	South-West; Wales	Extreme wind		Eden,2008
32	1987		1987-08-23	1987-08-23	North-West; East-Midlands; East; South-East	Extreme rainfall	River flooding	Eden,2008
33	1987		1987-10-09	1987-10-10	South-East	Extreme rainfall	River flooding	Eden,2008
34	1987	Great Storm of 1987	1987-10-15	1987-10-16	South-East; South-West	Extreme wind		Eden,2008; EM-DAT
35	1987		1987-10-18	1987-10-19	Wales	Extreme rainfall	River flooding	Eden,2008
36	1988		1988-02-09	1988-02-09	North-West; South West; Yorkshire	Extreme wind		Eden,2008
37	1988		1988-10-19	1988-10-19	North-West	Extreme rainfall	River flooding	Eden,2008
38	1989		1989-02-05	1989-02-06	Scotland	Extreme rainfall	River flooding	Eden,2008
39	1989		1989-02-13	1989-02-13	Scotland; North-East; North-West; Yorkshire	Extreme wind		Eden,2008
40	1989		1989-04-11	1989-04-11	Wales	Extreme wind		Eden,2008
41	1989		1989-05-19	1989-05-19	North-West; Yorkshire	Extreme rainfall	River flooding	Eden,2008
42	1989		1989-10-28	1989-10-28	South-West	Extreme wind		Eden,2008
43	1989		1989-12-14	1989-12-20	South-West	Extreme rainfall	Extreme wind; Storm surge	Eden,2008
44	1990	Burn's day storm	1990-01-25	1990-01-25	Wales; South-West; South-East; Yorkshire; London; East; Midlands; North-East; North-West	Extreme wind	Extreme rainfall; River flooding	Eden,2008; DFO
45	1990		1990-02-26	1990-02-26	North-West; Wales; Yorkshire	Extreme wind	Storm surge; Extreme rainfall; River flooding	Eden,2008; DFO
46	1990		1990-03-14	1990-03-15	Scotland	Extreme rainfall	River flooding	Eden,2008
47	1990		1990-10-28	1990-10-28	South-East; South-West	Extreme wind	Extreme rainfall; River flooding; Storm surge	Eden,2008; DFO
48	1991	Undine	1991-01-05	1991-01-05	Scotland; North-West; Wales	Extreme wind	Extreme rainfall	Eden,2008; EM-DAT; DFO
49	1991		1991-02-24	1991-03-01	North-East	Extreme rainfall	River flooding	DFO
50	1991		1991-09-27	1991-09-29	All regions	Extreme wind	Extreme rainfall	Eden,2008; DFO

ID	Year	Name	Start date	End date	Region	Dominant hazard	Associated hazards	Source
51	1991		1991-11-12	1991-11-12	South-West; West-Midlands	Extreme wind		Eden,2008
52	1991		1991-12-20	1991-12-21	North-West; Yorkshire	Extreme rainfall	River flooding	Eden,2008
53	1991		1991-12-31	1992-01-01	Scotland	Extreme wind		Eden,2008
54	1992		1992-03-31	1992-04-02	Scotland; North-East	Extreme rainfall	River flooding	Eden,2008; DFO
55	1992		1992-05-29	1992-05-31	London; East-Midlands; West-Midlands	Extreme rainfall	River flooding	Eden,2008
56	1992		1992-08-29	1992-08-31	All regions	Extreme wind	Extreme rainfall	Eden,2008
57	1992		1992-09-18	1992-09-23	South-West; West-Midlands; London	Extreme rainfall	River flooding	Eden,2008; DFO
58	1992		1992-11-29	1992-12-02	Wales; South-West	Extreme rainfall	River flooding	Eden,2008; DFO
59	1993		1993-01-16	1993-01-17	Scotland	Extreme wind	Storm surge; extreme snow	Eden,2008; DFO
60	1993		1993-01-23	1993-01-23	Scotland	Extreme rainfall		EM-DAT
61	1993		1993-02-21	1993-02-21	Scotland; North-West; North-East	Extreme wind	Storm surge	Eden,2008
62	1993		1993-06-09	1993-06-11	Wales; South-West; South-East	Extreme rainfall	River flooding	Eden,2008; DFO
63	1993		1993-12-09	1993-12-10	Wales; Midlands	Extreme wind		Eden,2008
64	1993		1993-12-30	1993-12-31	South-West	Extreme rainfall	River flooding	Eden,2008; DFO
65	1994		1994-01-23	1994-01-23	Scotland	Extreme wind		Eden,2008
66	1994		1994-04-01	1994-04-01	Wales; South-West	Extreme wind		Eden,2008
67	1994		1994-08-31	1994-09-01	East	Extreme rainfall	River flooding	Eden,2008
68	1994		1994-12-07	1994-12-12	Scotland	Extreme rainfall	River flooding	EM-DAT
69	1994		1994-12-26	1994-12-28	Wales	Extreme rainfall	River flooding	Eden,2008
70	1995		1995-01-17	1995-01-21	All regions	Extreme wind		Eden,2008
71	1995		1995-01-30	1995-01-31	North-West; Yorkshire	Extreme rainfall	River flooding; Landslides	Eden,2008
72	1995		1995-03-17	1995-03-17	Wales; Midlands; East	Extreme wind		Eden,2008
73	1996		1996-02-19	1996-02-20	East; Yorkshire; South-East	Extreme wind	Extreme snow; Storm surge	Eden,2008
74	1996		1996-05-19	1996-05-19	South-West	Extreme rainfall	Extreme wind	Eden,2008
75	1996	Lili	1996-10-27	1996-10-27	South-West; South-East; London; Scotland	Extreme wind		Eden,2008; EM-DAT
76	1997		1997-02-24	1997-02-24	England; Wales	Extreme wind	Storm surge	Eden,2008
77	1997		1997-05-17	1997-05-17	Midlands	Extreme rainfall	Hail; Extreme wind	Eden,2008
78	1997		1997-06-30	1997-07-01	Scotland	Extreme rainfall	River flooding	Eden,2008; EM-DAT
79	1997		1997-08-03	1997-08-04	South-West	Extreme rainfall	River flooding	Eden,2008

ID	Year	Name	Start date	End date	Region	Dominant hazard	Associated hazards	Source
80	1997		1997-08-13	1997-08-13	Scotland	Extreme wind		EM-DAT
81	1997		1997-08-19	1997-08-19	London; East-Midlands; West-Midlands	Extreme rainfall	River flooding; Landslides	Eden,2008
82	1997		1997-12-24	1997-12-24	All regions	Extreme wind		Eden,2008
83	1998	Désirée	1998-01-04	1998-01-04	South-West; Wales	Extreme wind	Storm surge	Eden,2008; EM-DAT
84	1998		1998-03-07	1998-03-08	Wales	Extreme rainfall	River flooding	DFO
85	1998		1998-04-08	1998-04-09	Wales, Midlands	Extreme rainfall	River flooding	Eden,2008; EM-DAT; DFO
86	1998		1998-06-13	1998-06-14	Scotland	Extreme rainfall	River flooding	DFO
87	1998		1998-10-24	1998-10-24	Wales, South-West; West-Midlands	Extreme rainfall	River flooding	Eden,2008; EM-DAT; DFO
88	1998		1998-12-26	1998-12-29	All regions	Extreme wind		Eden,2008
89	1999		1999-01-04	1999-01-05	North-West	Extreme rainfall	River flooding	Eden,2008
90	1999		1999-03-05	1999-03-06	Yorkshire	Extreme rainfall	River flooding	Eden,2008; EM-DAT; DFO
91	1999		1999-12-03	1999-12-03	Wales	Extreme wind		Eden,2008
92	1999		1999-12-24	1999-12-25	South-West; Wales	Extreme wind	Storm surge	Eden,2008; DFO
93	2000		2000-01-03	2000-01-03	Scotland	Extreme wind		Eden,2008
94	2000		2000-04-27	2000-04-27	Scotland	Extreme rainfall		EM-DAT
95	2000	Braknell storm	2000-05-07	2000-05-07	South-East	Extreme rainfall	River flooding	Met Office
96	2000		2000-07-04	2000-07-04	South-East	Extreme rainfall	River flooding	Eden,2008
97	2000		2000-10-11	2000-10-12	South-East	Extreme rainfall	River flooding	Eden,2008; EM-DAT; DFO
98	2000		2000-10-28	2000-10-29	Yorkshire	Extreme rainfall	River flooding	EM-DAT
99	2000		2000-10-30	2000-10-30	South-East; South-West; Wales	Extreme wind	Storm Surge	Eden,2008; DFO
100	2000		2000-11-30	2000-11-30	South-West; South-East	Extreme wind		EM-DAT
101	2000		2000-12-13	2000-12-14	England; Wales	Extreme wind		Eden,2008
102	2001		2001-02-09	2001-02-09	South-East; East	Extreme rainfall		EM-DAT
103	2001		2001-07-04	2001-07-04	Wales	Extreme rainfall	River flooding	Eden,2008
104	2001		2001-10-20	2001-10-21	Midlands; East	Extreme rainfall	River flooding	Eden,2008; EM-DAT; Met Office; DFO
105	2002	Jennifer	2002-01-28	2002-01-29	Scotland	Extreme wind		Eden,2008; EM-DAT

ID	Year	Name	Start date	End date	Region	Dominant hazard	Associated hazards	Source
106	2002		2002-02-01	2002-02-02	Wales; South-East; South-West	Extreme wind	Extreme rainfall; Storm surge; River flooding	Eden,2008
107	2002		2002-02-22	2002-02-22	Yorkshire	Extreme wind		Eden,2008
108	2002		2002-07-20	2002-07-20	North-West; Yorkshire; Scotland	Extreme rainfall		EM-DAT
109	2002		2002-07-30	2002-08-01	Yorkshire	Extreme rainfall	River flooding	Eden,2008; DFO
110	2002		2002-09-09	2002-09-09	South-West	Extreme rainfall	River flooding	Eden,2008
111	2002		2002-10-22	2002-10-25	Scotland	Extreme rainfall	River flooding	DFO
112	2002	Jeanett	2002-10-27	2002-10-27	South-West; South-East; London; Wales	Extreme wind		Eden,2008; EM-DAT
113	2002		2002-11-13	2002-11-14	Scotland; South-West	Extreme rainfall		Eden,2008; EM-DAT; DFO
114	2002		2002-12-27	2002-12-31	South-West; South-East; London; Wales	Extreme rainfall	River flooding	Eden,2008; DFO
115	2004		2004-02-01	2004-02-05	Wales; North-West	Extreme rainfall	River flooding	Eden,2008; DFO
116	2004		2004-03-20	2004-03-20	England; Wales	Extreme wind		Eden,2008
117	2004		2004-07-07	2004-07-08	East-Midlands; East	Extreme rainfall	River flooding; Lightnings	Eden,2008
118	2004	Boscastle disaster	2004-08-16	2004-08-16	South-West	Extreme rainfall	River flooding; Landslides	Eden,2008; EM-DAT; DFO
119	2005	Erwin	2005-01-06	2005-01-07	Scotland; North-West; North-East; Wales; Yorkshire	Extreme wind	Extreme rainfall; River flooding	Eden,2008; EM-DAT; DFO
120	2005	Gero	2005-01-11	2005-01-12	All regions	Extreme wind	Extreme rainfall; River flooding	Eden,2008; EM-DAT
121	2005		2005-06-19	2005-06-19	Wales; Midlands; North-West; Yorkshire	Extreme rainfall	Hail; River flooding	Eden,2008; Met Office; DFO
122	2005		2005-10-11	2005-10-12	North-West; Scotland; Wales	Extreme rainfall	River flooding	Eden,2008; DFO
123	2005		2005-11-11	2005-11-11	Wales	Extreme rainfall	River flooding	DFO
124	2006		2006-08-13	2006-08-13	London; South-West; South-East	Extreme rainfall	River flooding	Eden,2008
125	2006		2006-10-25	2006-10-25	Scotland	Extreme wind	Extreme rainfall; River flooding	Eden,2008; DFO
126	2007		2007-01-06	2007-01-10	North-West; Wales; Scotland	Extreme rainfall	River flooding	Eden,2008
127	2007	Kyrill	2007-01-18	2007-01-18	England; Wales	Extreme wind		Eden,2008; EM-DAT
128	2007		2007-06-15	2007-06-21	Nort-West; Wales; Yorkshire	Extreme rainfall	Broken Dam; River flooding	Eden,2008; EM-DAT; DFO
129	2007		2007-06-25	2007-07-03	All regions	Extreme rainfall		Eden,2008; EM-DAT; DFO

ID	Year	Name	Start date	End date	Region	Dominant hazard	Associated hazards	Source
130	2007		2007-07-19	2007-07-20	West-Midlands	Extreme rainfall	River flooding	Eden,2008; EM-DAT; DFO
131	2007		2007-11-08	2007-11-09	Scotland	Extreme wind	Storm surge	Eden,2008
132	2008		2008-01-18	2008-01-21	North-West; Wales; Scotland	Extreme rainfall	River flooding	Eden,2008; EM-DAT; DFO
133	2008	Johanna	2008-03-10	2008-03-10	All regions	Extreme rainfall	River flooding	EM-DAT
134	2008		2008-05-29	2008-05-29	South-West	Extreme rainfall	River flooding	Eden,2008
135	2008		2008-08-15	2008-08-16	North-West; West-Midlands; East-Midlands	Extreme rainfall	River flooding	DFO
136	2008		2008-09-06	2008-09-08	North-West; Wales; Yorkshire	Extreme rainfall	Rain	EM-DAT; DFO
137	2009	Cumbria flood	2009-11-19	2009-11-22	North-West	Extreme rainfall		EM-DAT; Met Office; DFO
138	2010	Xynthia	2010-02-28	2010-02-28	All regions	Extreme rainfall		EM-DAT
139	2010	Cornwall flood	2010-11-16	2010-11-17	South-West	Extreme rainfall	River flooding	DFO; Met Office
140	2012		2012-06-10	2012-06-11	All regions	Extreme rainfall		EM-DAT
141	2012		2012-06-23	2012-06-24	All regions	Extreme rainfall		EM-DAT
142	2012	Supercell	2012-06-28	2012-06-29	Midlands; Yorkshire	Extreme rainfall	Lightning; Hail	Met Office
143	2012		2012-09-23	2012-09-27	North-East; Yorkshire	Extreme rainfall	Extreme wind	EM-DAT; DFO
144	2012		2012-12-23	2012-12-23	South-West; Wales; Scotland	Extreme rainfall		EM-DAT
145	2013	Storm Christian	2013-10-27	2013-10-28	All regions	Extreme rainfall		EM-DAT
146	2013	Storm Xaver	2013-12-06	2013-12-07	Wales; Yorkshire; East; Midlands	Extreme wind	River flooding	EM-DAT; Met Office
147	2013		2013-12-23	2013-12-25	Midlands; South-West; Wales; Scotland	Extreme rainfall	Extreme wind	Met Office
148	2013	Storm Dirk	2013-12-26	2013-12-27	South-East	Extreme wind	River flooding	EM-DAT; Met Office
149	2013		2013-12-30	2013-12-31	All regions	Extreme wind		EM-DAT; Met Office
150	2014	Storm Ulla	2014-02-14	2014-02-15	All regions	Extreme wind	River flooding	EM-DAT
151	2014	Storm Berta	2014-08-10	2014-08-11	Scotland	Extreme rainfall	Extreme wind; River flooding	Met Office
152	2015	Storm Desmond	2015-12-04	2015-12-06	North-West	Extreme wind	River flooding	EM-DAT
153	2015		2015-12-26	2015-12-26	North-West; Yorkshire	Extreme rainfall		EM-DAT
154	2016	Storm Angus	2016-11-19	2016-11-22	South; London; Wales	Extreme rainfall	Extreme wind	Met Office
155	2017		2017-11-22	2017-11-26	Wales; North-West	Extreme rainfall		EM-DAT

ID	Year	Name	Start date	End date	Region	Dominant hazard	Associated hazards	Source
156	2018	Storm Eleanor	2018-01-02	2018-01-03	Midlands; Wales; Scotland	Extreme wind	Storm surge	EM-DAT
157	2018	Storm Hector	2018-06-13	2018-06-15	Scotland; Wales; North-West; Yorkshire	Extreme rainfall	Extreme wind; River flooding	Met Office